OPTOGENETICS: AN EMERGING APPROACH IN CARDIAC ELECTROPHYSIOLOGY

EDITED BY: Ming Lei and Christopher Huang
PUBLISHED IN: Frontiers in Physiology

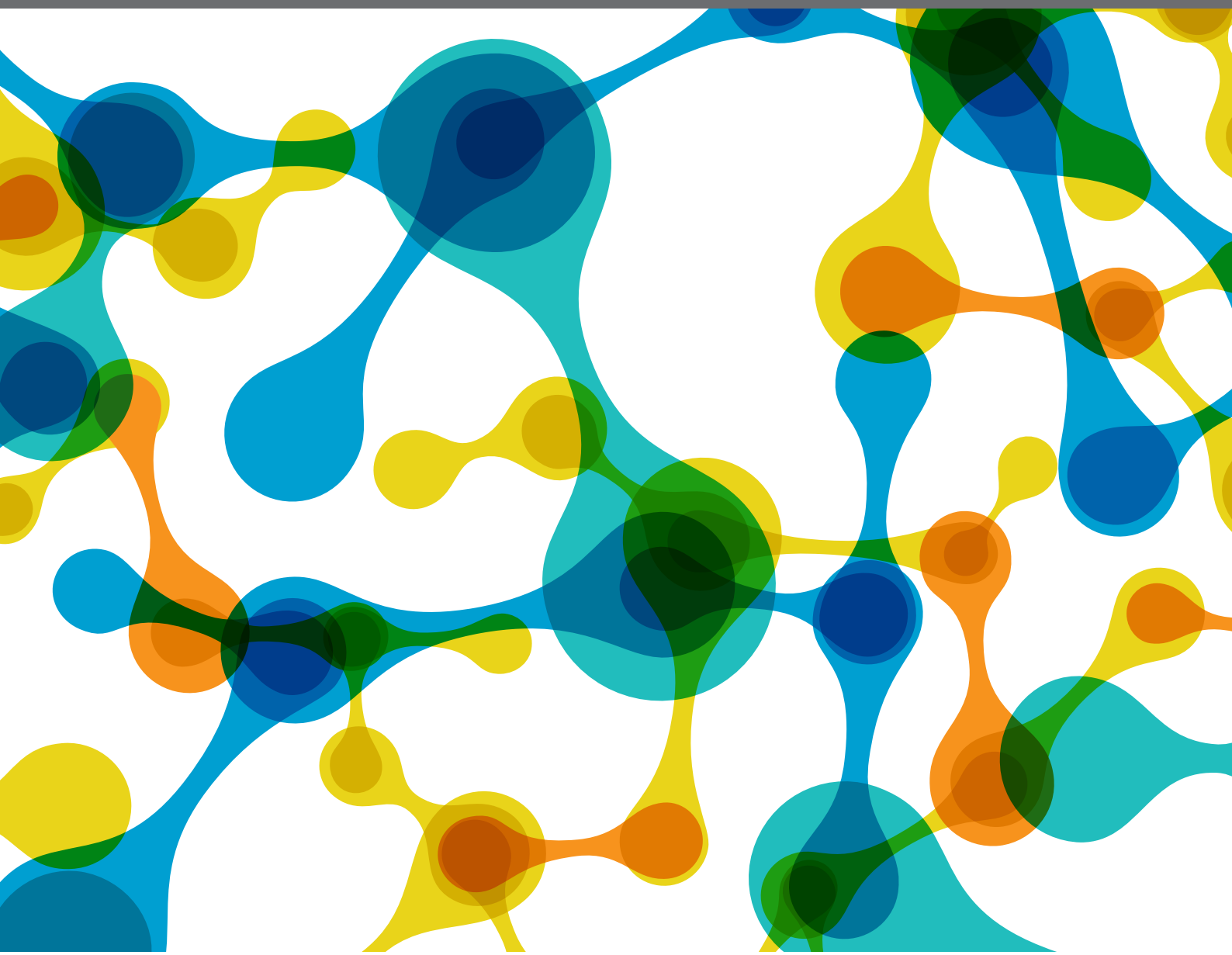

frontiers Research Topics

frontiers

ISSN 1664-8714
ISBN 978-2-88963-803-1
DOI 10.3389/978-2-88963-803-1

About Frontiers

Frontiers is more than just an open-access publisher of scholarly articles: it is a pioneering approach to the world of academia, radically improving the way scholarly research is managed. The grand vision of Frontiers is a world where all people have an equal opportunity to seek, share and generate knowledge. Frontiers provides immediate and permanent online open access to all its publications, but this alone is not enough to realize our grand goals.

Frontiers Journal Series

The Frontiers Journal Series is a multi-tier and interdisciplinary set of open-access, online journals, promising a paradigm shift from the current review, selection and dissemination processes in academic publishing. All Frontiers journals are driven by researchers for researchers; therefore, they constitute a service to the scholarly community. At the same time, the Frontiers Journal Series operates on a revolutionary invention, the tiered publishing system, initially addressing specific communities of scholars, and gradually climbing up to broader public understanding, thus serving the interests of the lay society, too.

Dedication to Quality

Each Frontiers article is a landmark of the highest quality, thanks to genuinely collaborative interactions between authors and review editors, who include some of the world's best academicians. Research must be certified by peers before entering a stream of knowledge that may eventually reach the public - and shape society; therefore, Frontiers only applies the most rigorous and unbiased reviews.
Frontiers revolutionizes research publishing by freely delivering the most outstanding research, evaluated with no bias from both the academic and social point of view. By applying the most advanced information technologies, Frontiers is catapulting scholarly publishing into a new generation.

What are Frontiers Research Topics?

Frontiers Research Topics are very popular trademarks of the Frontiers Journals Series: they are collections of at least ten articles, all centered on a particular subject. With their unique mix of varied contributions from Original Research to Review Articles, Frontiers Research Topics unify the most influential researchers, the latest key findings and historical advances in a hot research area! Find out more on how to host your own Frontiers Research Topic or contribute to one as an author by contacting the Frontiers Editorial Office: researchtopics@frontiersin.org

OPTOGENETICS: AN EMERGING APPROACH IN CARDIAC ELECTROPHYSIOLOGY

Topic Editors:
Ming Lei, University of Oxford, United Kingdom
Christopher Huang, University of Cambridge, United Kingdom

Citation: Lei, M., Huang, C., eds. (2020). Optogenetics: An Emerging Approach in Cardiac Electrophysiology. Lausanne: Frontiers Media SA.
doi: 10.3389/978-2-88963-803-1

Table of Contents

frontiers in Physiology

EDITORIAL
published: 28 April 2020
doi: 10.3389/fphys.2020.00414

Editorial: Optogenetics: An Emerging Approach in Cardiac Electrophysiology

Christopher L.-H. Huang[1,2]*, *Emily A. Ferenczi*[3] *and Ming Lei*[2,4]*

[1] Physiological Laboratory and Department of Biochemistry, University of Cambridge, Cambridge, United Kingdom, [2] Key Laboratory of Medical Electrophysiology of the Ministry of Education and Institute of Cardiovascular Research, Southwest Medical University, Luzhou, China, [3] Department of Neurology, Harvard Medical School, Massachusetts General Hospital and Brigham and Women's Hospital, Boston, MA, United States, [4] Department of Pharmacology, University of Oxford, Oxford, United Kingdom

Keywords: optogenetics, cardiac electrophysiology, cardiac arrhythmias, clinical translation, opsins

Editorial on the Research Topic

Optogenetics: An Emerging Approach in Cardiac Electrophysiology

Optogenetic techniques modulate excitable membranes through activation of photosensitive opsin proteins functioning as light-gated channels, transporters or receptors. Of the known, prokaryotic, algal or fungal, type I, and animal, type II, opsins, the type I opsins have been the most frequently used experimentally since they were first to be expressed in mammalian neurons in the early 2000s. Optogenetic approaches circumvent disadvantages of traditional, direct electrical stimulation, methods, such as tissue toxicity, and enhance cellular and spatial specificity of stimulus effects through genetic or developmental targeting.

These methods initially found neuroscience applications and these ranged widely from use in *in vitro* models to behaving animals, and in invertebrate through to mammalian systems (Boyden et al., 2005). They have more recently proved relevant to other excitable, particularly cardiac, tissues, in the latter case, particularly in fundamental scientific and translational studies of cardiac arrhythmogenesis (Bruegmann et al., 2016). Arrhythmias are the result of disruption of the normally orderly electrical excitation sequence initiating co-ordinated and effective atrial or ventricular contraction. They account for ∼3.7 million human deaths/year worldwide (Kuriachan et al., 2017). Their clinical management has often lagged progress in many other cardiological areas. This likely reflects our currently limited understanding of the physiological mechanisms that underly their initiation, maintenance or propagation (Huang, 2017; Lei et al., 2018; Huang et al., 2020).

Cardiac optogenetic approaches offer unprecedented opportunities and new exciting possibilities to resolving and intervening in such normal and diseased function. Optogenetic sensors can be incorporated into specific motifs and targeted at specific, tissue and cell types, and subcellular domains, and applied at high spatial and temporal resolution. This Research Topic

OPEN ACCESS

Edited and reviewed by:
Ruben Coronel,
University of Amsterdam, Netherlands

***Correspondence:**
Christopher L.-H. Huang
clh11@cam.ac.uk
Ming Lei
ming.lei@pharm.ox.ac.uk

Specialty section:
This article was submitted to Cardiac Electrophysiology, a section of the journal Frontiers in Physiology

Received: *16 March 2020*
Accepted: *06 April 2020*
Published: *28 April 2020*

Citation:
Huang CL-H, Ferenczi EA and Lei M (2020) Editorial: Optogenetics: An Emerging Approach in Cardiac Electrophysiology. Front. Physiol. 11:414. doi: 10.3389/fphys.2020.00414

collects articles focusing on optogenetic applications in cardiac electrophysiology. They particularly consider their ability to modify membrane voltage, intracellular Ca^{2+} and cellular signaling, and their potential for use in cardiac pacing, cardioversion, cell communication, in arrhythmia research (Boyle et al., 2018). Pioneering contributors in this cardiac field summarize underlying concepts, existing optogenetic tools and approaches, discussing their suitability for cardiac experimental studies and interventions. They then review examples of applications and situations where optogenetics have yielded new insights into and potential interventional approaches for cardiac physiology and cardiac disease.

Two background articles explore *available optogenetic approaches*, opsin proteins and their different ion conductances, kinetics, light sensitivity, and activation spectra, both in general, and bearing on cardiac applications (Ferenczi et al.; O'Shea et al.). These include the physical and practical background, and choices of opsin tools appropriate to the cellular physiology and experimental system in question (Deisseroth, 2015). Cardiac expression of the chosen optogenetic tool is variously achieved by coupling of "spark cells" at the single-cell level, construction of transgenic mice or *in vivo* introduction of adenoviral expression systems at the systems level. Adeno-associated viruses (AAVs) offer advantages in long-term, cardiac-specific gene expression. An article exploring optimal AAV serotypes (1, 6, or 9) reports preferential efficiency of AAV1/6 *in vitro* and AAV9 *in vivo* for cardiac optogenetic delivery (Ambrosi et al.). Optogenetic stimulation either activates or silences cellular excitation through membrane depolarization or hyperpolarization. Depolarizing, activated, cation-conducting channelrhodopsins (ChR) trigger cardiomyocyte action potentials; hyperpolarization by Cl^- pumps suppresses activity (Arrenberg et al., 2010). The activated photosensitive Cl^- channel, Guillardia theta ChR (GtACR1) silences neuronal action potential generation: microelectrode and *in vivo* optical whole heart recordings demonstrate depolarized cells as expected from the cardiac Cl^- Nernst potential, inhibiting re-excitation (Kopton et al.).

Optogenetic techniques promise to deliver *unique physiological insights* unobtainable from established procedures. At the cellular level, it could demonstrate, localize, and characterize electrical and Ca^{2+} transient activity in particular phenylethanolamine-N-methyl transferase (Pnmt)-derived cardiomyocyte subpopulations and their roles in localized adrenergic signaling (Fan et al.). At the whole heart level, optogenetic methods permitted temporally precise, acute, neuron-specific, parasympathetic stimulation in mice expressing ChR2 in their peripheral cholinergic neurons. This elicited sudden, dramatic but reversible heart rate reductions and atrioventricular conduction delays (Moreno et al.).

Optogenetic techniques can target and stably deliver perturbing light stimuli to *specific cell types* at the cellular, organ or whole organism levels, in different cardiac, sino-atrial nodal, atrial, ventricular regions, or the conducting tissues within or between them, permitting focussed study of the entire range of clinically important arrhythmic conditions. Thus, protocols combining optogenetic stimulation with dual cytosolic Ca^{2+}-membrane voltage optical mapping studied membrane potential, intracellular Ca^{2+} transients and pacemaker activity in a murine sino-atrial preparation (Dong et al.). Use of pseudo two-dimensional murine ventricular tissue slices profiled transmural and regional voltage and Ca^{2+} signaling gradients under stress produced by high frequency pacing, β-adrenergic stimulation or pathological, including hypertrophic, conditions (He et al.). We also include one report where the genetically-encoded sensor for altered cellular glutathione redox status, Grx1-roGFP2, provided readouts of cellular reactive oxygen species (Trautsch et al.). The latter modulate ryanodine receptor-mediated sarcoplasmic reticular Ca^{2+} release (Prosser et al., 2011) and phospholamban phosphorylation-regulated diastolic relaxation (Scotcher et al., 2016).

We complete the Research Topic by considering translational exploitations of optogenetic methods in *clinical cardiology*. These could achieve non-damaging optical control of excitation with high temporal and spatial resolution for sino-atrial pacemaking, or atrial or ventricular cardioversion. In contrast, normally used electrical shocks do not fully control the spatial extent and level of their resulting membrane potential changes. One article summarizes recent progress on optogenetic defibrillation and cardioversion, their underlying mechanisms and potential patient populations that might thus benefit (Sasse et al.). In channelrhodopsin-2 (ChR2) transgenic mice, a single 10–1,000 ms pulse at light intensities < 1.10 mW mm^{-2} sufficed to cardiovert fibrillating hearts into sinus rhythm. Optical mapping attributed this to both annihilating, excitation wave, collisions and propagation perturbations (Quiñonez Uribe et al.). Epicardial illumination terminated ventricular arrhythmias in explanted, hypokalaemic hearts expressing the light-driven proton pump ArchT, perfused with the K_{ATP} opener pinacidil. This was accompanied by hyperpolarization, more rapid action potential upstrokes but reduced conduction velocity implicating an enhanced electrical sink in terminating the arrhythmia. Such novel insights could improve our mechanistic understanding and treatment strategies for arrhythmia termination (Funken et al.).

AUTHOR CONTRIBUTIONS

EF surveyed and summarized all the contributions in this Research Topic and ML revised these, permitting CH to formulate the narrative underlying this Research Topic.

FUNDING

This work was funded by the Medical Research Council, UK (MR/M001288/1, CLHH; G10002647, G1002082, ML), Wellcome Trust, UK (105727/Z/14/Z,CLHH), British Heart Foundation, UK (BHF) (PG/19/59/34582, PG/14/79/31102, and PG/15/12/31280, and BHF Center for Research Excellence [CRE] at Cambridge, CLHH; PG/14/80/31106, PG/16/67/32340, PG/12/21/29473, PG/11/59/29004, and BHF CRE at Oxford, ML), National Natural Science Foundation of China (31171085, ML).

REFERENCES

Arrenberg, A. B., Stainier, D. Y. R., Baier, H., and Huisken, S. E. (2010). Optogenetic control of cardiac function. *Science* 330, 971–974. doi: 10.1126/science.1195929

Boyden, E. S., Zhang, F., Bamberg, E., Nagel, G., and Deisseroth, K. (2005). Millisecond-timescale, genetically targeted optical control of neural activity. *Nat. Neurosci.* 8, 1263–1268. doi: 10.1038/nn1525

Boyle, P. M., Karathanos, T. V., and Trayanova, N. A. (2018). Cardiac Optogenetics 2018. *JACC Clin. Electrophysiol.* 4, 155–167. doi: 10.1016/j.jacep.2017.12.006

Bruegmann, T., Boyle, P. M., Vogt, C. C., Karathanos, T. V., Arevalo, H. J., Fleischmann, B. K., et al. (2016). Optogenetic defibrillation terminates ventricular arrhythmia in mouse hearts and human simulations. *J. Clin. Invest.* 126, 3894–3904. doi: 10.1172/JCI88950

Deisseroth, K. (2015). Optogenetics: 10 years of microbial opsins in neuroscience. *Nat. Neurosci.* 18, 1213–1225. doi: 10.1038/nn.4091

Huang, C. L.-H. (2017). Murine electrophysiological models of cardiac arrhythmogenesis. *Physiol. Rev.* 97, 283–409.doi: 10.1152/physrev.00007.2016

Huang, C. L.-H., Wu, L., Jeevaratnam, K., and Lei, M. (2020). Update on antiarrhythmic drug pharmacology. *J Cardiovasc Electrophysiol* 31, 579–592. doi: 10.1111/jce.14347

Kuriachan, V., Sumner, G., and Mitchell, L. (2017). Sudden cardiac death. *Curr. Probl. Cardiol.* 40, 133–200. doi: 10.1016/j.cpcardiol.2015.01.002

Lei, M., Wu, L., Terrar, D. A., and Huang, C. L. H. (2018). Modernized classification of cardiac antiarrhythmic drugs. *Circulation* 138, 1879–1896. doi: 10.1161/CIRCULATIONAHA.118.035455

Prosser, B. L., Ward, C. W., and Lederer, W. J. (2011). X-ROS signaling: Rapid mechano-chemo transduction in heart. *Science* 333, 1440–1445. doi: 10.1126/science.1202768

Scotcher, J., Prysyazhna, O., Boguslavskyi, A., Kistamas, K., Hadgraft, N., Martin, E. D., et al. (2016). Disulfide-activated protein kinase G Iα regulates cardiac diastolic relaxation and fine-tunes the Frank-Starling response. *Nat. Commun.* 333, 1440–1445. doi: 10.1038/ncomms13187

Conflict of Interest: The authors declare that the research was conducted in the absence of any commercial or financial relationships that could be construed as a potential conflict of interest.

frontiers in Physiology

REVIEW
published: 11 September 2019
doi: 10.3389/fphys.2019.01096

Principles of Optogenetic Methods and Their Application to Cardiac Experimental Systems

*Emily A. Ferenczi[1], Xiaoqiu Tan[2] and Christopher L.-H. Huang[3,4]**

[1]Department of Neurology, Massachusetts General Hospital and Brigham and Women's Hospital, Harvard Medical School, Boston, MA, United States, [2]Key Laboratory of Medical Electrophysiology, Ministry of Education and Medical Electrophysiological Key Laboratory of Sichuan Province, Institute of Cardiovascular Research, Southwest Medical University, Luzhou, China, [3]Physiological Laboratory, University of Cambridge, Cambridge, United Kingdom, [4]Department of Biochemistry, University of Cambridge, Cambridge, United Kingdom

Optogenetic techniques permit studies of excitable tissue through genetically expressed light-gated microbial channels or pumps permitting transmembrane ion movement. Light activation of these proteins modulates cellular excitability with millisecond precision. This review summarizes optogenetic approaches, using examples from neurobiological applications, and then explores their application in cardiac electrophysiology. We review the *available opsins*, including depolarizing and hyperpolarizing variants, as well as modulators of G-protein coupled intracellular signaling. We discuss the biophysical properties that determine the ability of microbial opsins to evoke reliable, precise stimulation or silencing of electrophysiological activity. We also review *spectrally shifted* variants offering possibilities for enhanced depth of tissue penetration, combinatorial stimulation for targeting different cell subpopulations, or all-optical read-in and read-out studies. *Expression of the chosen optogenetic tool* in the cardiac cell of interest then requires, at the *single-cell level*, introduction of opsin-encoding genes by viral transduction, or coupling "spark cells" to primary cardiomyocytes or a stem-cell derived counterpart. At the *system-level*, this requires construction of transgenic mice expressing ChR2 in their cardiomyocytes, or *in vivo* injection (myocardial or systemic) of adenoviral expression systems. *Light delivery*, by laser or LED, with widespread or multipoint illumination, although relatively straightforward *in vitro* may be technically challenged by cardiac motion and light-scattering in biological tissue. *Physiological read outs* from cardiac optogenetic stimulation include single cell patch clamp recordings, multi-unit microarray recordings from cell monolayers or slices, and electrical recordings from isolated Langendorff perfused hearts. Optical readouts of specific cellular events, including ion transients, voltage changes or activity in biochemical signaling cascades, using small detecting molecules or genetically encoded sensors now offer powerful opportunities for all-optical control and monitoring of cellular activity. Use of optogenetics has expanded in cardiac physiology, mainly using optically controlled depolarizing ion channels to control heart rate and for optogenetic defibrillation. ChR2-expressing cardiomyocytes show normal baseline and active excitable membrane and Ca^{2+} signaling properties and are sensitive even to ~1 ms light pulses. They have been employed in studies of the intrinsic cardiac adrenergic system and of cardiac arrhythmic properties.

Keywords: optogenetics, cardiac electrophysiology, opsin selection, light delivery, physiological readout, channelrhodopsin, halorhodopsin, archaerhodopsin

OPEN ACCESS

Edited by:
T. Alexander Quinn, Dalhousie University, Canada

Reviewed by:
Franziska Schneider-Warme, University Heart Center Freiburg, Germany
Philipp Sasse, University of Bonn, Germany

***Correspondence:**
Christopher L.-H. Huang
clh11@cam.ac.uk

Specialty section:
This article was submitted to Cardiac Electrophysiology, a section of the journal Frontiers in Physiology

Received: *10 April 2019*
Accepted: *08 August 2019*
Published: *11 September 2019*

Citation:
Ferenczi EA, Tan X and Huang CL-H (2019) Principles of Optogenetic Methods and Their Application to Cardiac Experimental Systems. Front. Physiol. 10:1096. doi: 10.3389/fphys.2019.01096

INTRODUCTION

Optogenetics offers techniques to modulate the activity of excitable cells using light, in a genetically specified manner. The method harnesses microbial proteins, known as opsins, which are light-activated proteins (channels or pumps) that permit transmembrane movement of ions. There are two types of opsins: Type I (found in prokaryotes, algae, and fungi) and Type II (found in animals). The opsins used most commonly in optogenetics fall under the category of Type I opsins (although some Type II opsins are also used) and are referred to as rhodopsins, meaning that they contain both an opsin protein (with seven transmembrane domains) as well as a light-sensitive chromophore. When activated by light, opsins cause depolarization or hyperpolarization of the cell membrane, with resulting cellular excitation or silencing on a millisecond time scale. Opsins were first expressed in mammalian neurons in the mid-2000s; since then the optogenetic toolkit has vastly expanded to address a number of different experimental demands. Aided by the recent elucidation of the crystal structure of opsin proteins, opsin engineering has led to a wide array of available tools with different properties, including ion conductances, kinetics, light sensitivity, and activation spectra. Although initial applications of optogenetics were primarily within the field of neuroscience, the technique soon became relevant to other excitable tissues. In this review, we summarize existing optogenetic tools and approaches and discuss their suitability for cardiac experimental questions. We then review existing cardiac applications and discuss some recent examples in cardiac optogenetics that have yielded new insights into cardiac physiology and cardiac disease.

Any optogenetic experiment involves several practical considerations: first, the properties of the chosen opsin tool and whether it is suited to the cellular physiology of interest and the experimental application. This includes the direction of the ionic current, as well as the nature of the transported ion(s), in addition to the kinetics and temporal precision of the tool, the amplitude of the evoked current (which in turn depends on a number of factors described below), and its spectral properties. The next consideration is the ability to specifically target (usually anatomically and/or genetically) the cell type of interest and deliver light into the experimental system of interest in a stable and spatially precise manner. Finally, the read-out of the system will depend on the experimental question being addressed; for example, this might be an electrophysiological recording, or a physiological imaging technique or an organ-level or behavioral output (**Figure 1**).

Studies of cardiac arrhythmias have traditionally depended upon electrical stimulation, which has the advantage of being temporally precise, but also carries several disadvantages including toxicity to the tissue, lack of cellular or anatomic specificity of the stimulation due to the rapid spread of current from the electrode tip, and lack of flexibility in terms of duration of stimulation (Bruegmann et al., 2010). The advent of optogenetics now allows temporally precise bidirectional modulation of cellular activity (using depolarizing and hyperpolarizing tools) (**Figure 1A**) and improved cellular specificity *via* genetic or developmental targeting methods and spatial specificity through the use of patterned illumination. The combination of optogenetic tools with optical activity sensors (e.g., calcium or voltage sensors) has also permitted realization of the highly desired "all-optical read-in and read-out" approach (**Figure 1B**).

The first cardiac optogenetic experiments were published in 2010, when two groups demonstrated light-induced modulation of function in mouse (Bruegmann et al., 2010) and zebrafish cardiomyocytes (Arrenberg et al., 2010). Since then, this approach has been applied to a wide range of cardiac experimental and translational questions including mechanisms of arrhythmia generation to optical defibrillation, arrhythmia termination, and pacing (**Figure 1C**).

SELECTING AN OPSIN FOR CARDIAC OPTOGENETICS: DIRECTIONALITY, LIGHT SENSITIVITY, KINETICS, AND SPECTRAL PROPERTIES

Depolarizing Tools

The first depolarizing rhodopsin-based tool to be expressed in mammalian neurons utilized a multicomponent system, in which *Drosophila* photoreceptor genes (rhodopsin + arrestin + $G_q\alpha$, a combination known as "chARGe") were co-expressed in mammalian cultured hippocampal neurons (Zemelman et al., 2002). This system successfully drove light-activated neural firing and was the first proof-of-principle that rhodopsins could be used to modulate mammalian neural activity. One disadvantage of this multi-component system was its reliance on the exogenous delivery of retinal for rhodopsin photocycle function. In 2005, the first single-component microbial opsin, channelrhodopsin (ChR2), found in the algae *Chlamydomonas reinhardtii*, was expressed in mammalian neurons and elicited precise neural spiking in response to pulses of blue light (Boyden et al., 2005). In these early experiments, it was determined that sufficient retinal is present in vertebrate tissue for the ChR2 photocycle to function without the need for additional components. ChR2 is a non-selective cation channel, permeable to protons $\gg$ sodium ions > potassium ions $\gg$ calcium ions under physiological conditions (Deisseroth and Hegemann, 2017). When the channel pore is opened through a sequence of molecular changes that are initiated by photon absorption, the resulting net inward flow of positive ions results in a depolarizing photocurrent. This elicits an action potential when the excitable cell membrane reaches its firing threshold. Over the last 10 years, many naturally occurring depolarizing microbial rhodopsins have been found and genetically engineered mutant and chimeric rhodopsins have been developed, widely varying in terms of their channel kinetics, photocurrent magnitude, and spectral sensitivity (review: Deisseroth, 2015).

The ability of a depolarizing opsin to evoke precisely timed sequences of action potentials in response to pulses of light depends in part on the balance of two key properties – its light sensitivity and its channel kinetics, in combination with the

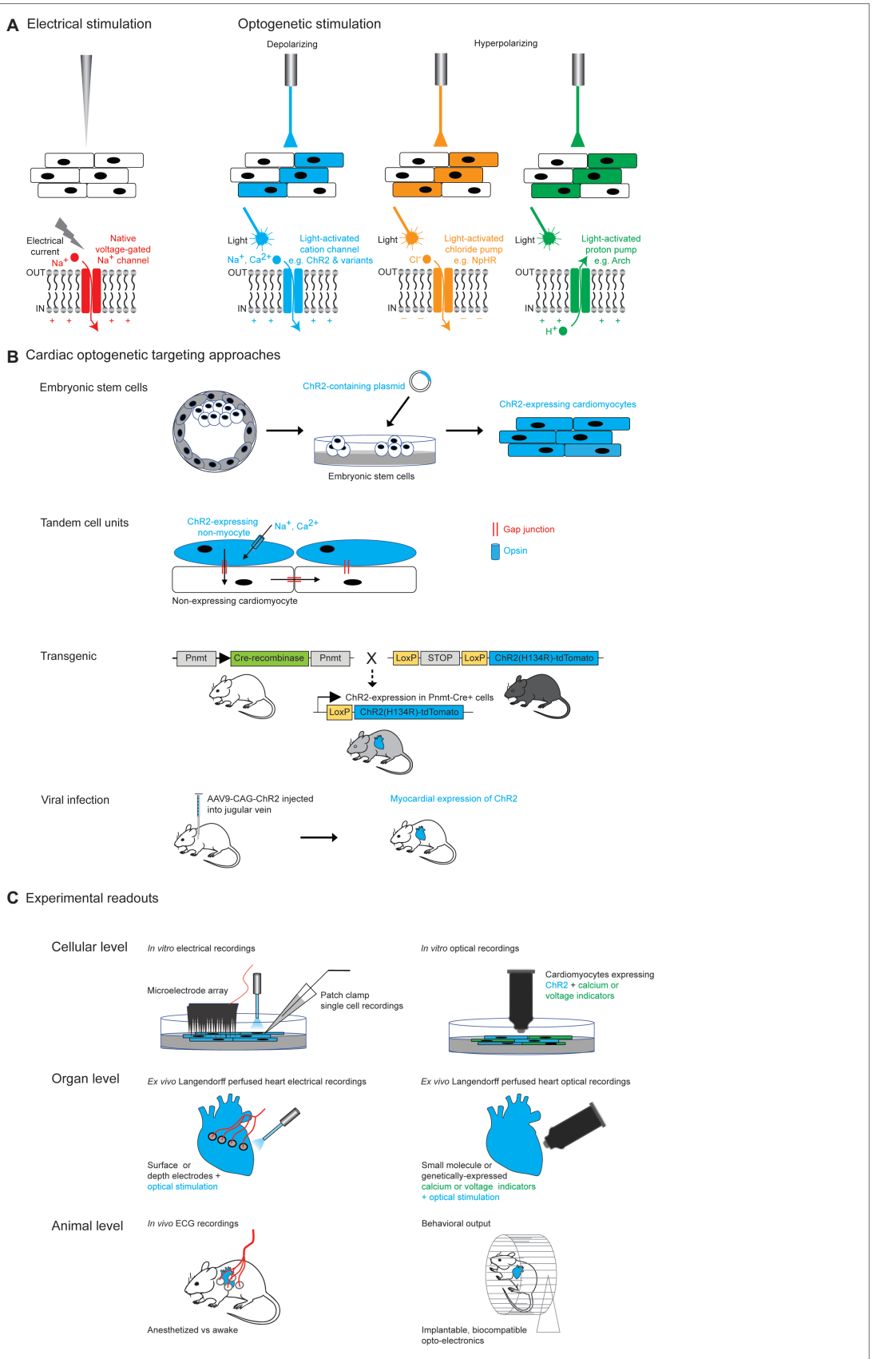

FIGURE 1 | Continued

FIGURE 1 | Optogenetic approaches in cardiac tissue. **(A)** Comparison of electrical and optogenetic stimulation paradigms, highlighting cellular specificity and bidirectionality of optogenetic techniques. **(B)** Examples of different methods of targeting opsins to cardiac tissue. Section on transgenic methods is adapted from Figure 1A from Wang et al. (2017). Section on viral infection describes the experimental approach used by Vogt et al. (2015). **(C)** Examples of different optogenetic read-outs for cardiac applications, ranging from *in vitro* to *in vivo* experimental set-ups.

physiological response of the cell to the photocurrent. The ability of a depolarizing rhodopsin to evoke precisely timed sequences of action potentials in response to pulses of light depends on the balance of several key properties. One is the photocurrent amplitude, which is in turn determined by light sensitivity (light intensity required to reach half maximal activation), the single-channel conductance, and the degree of channel expression in the cell membrane of interest. Other contributing factors include the channel kinetics as well as the cell's physiological response to the photocurrent. Rhodopsins with higher light sensitivity require a lower light intensity to reach maximal photocurrent amplitude, and thus may drive depolarization more readily across a range of light intensities or across a larger volume of tissue (Mattis et al., 2011). However, in order to generate sustained action potential spiking in response to a long train of light pulses, channels should close quickly after the end of a light pulse to avoid sustained membrane depolarization and refractoriness; the kinetics of channel closure are described by the tau-off (τ_{off}). In addition, the channels must have a low rate of desensitization and/or recover rapidly from the desensitized state. It has been demonstrated that there is a strong correlation between light sensitivity and τ_{off}, suggesting that the light sensitivity of a membrane-bound rhodopsin population is mainly accounted for by channel off-kinetics, although differences in single channel intrinsic light sensitivity and conductance may explain deviations from the curve (e.g., in the case of the stable-step function opsins, see below). Others have noted that this suggests a theoretical trade-off between light sensitivity (volume of tissue activation) and channel kinetics (spiking precision) (Mattis et al., 2011). Fast channelrhodopsin mutants, such as the ChETA (ChR2/E123T) variants) have accelerated τ_{off} but lower light sensitivity; they are thus able to produce very precise trains of action potentials but require higher light intensities to do so (Gunaydin et al., 2010; Berndt et al., 2011). In contrast, mutant channelrhodopsins which are highly light sensitive (e.g., C1V1 variants, CatCh) are able to generate an initial action potential with high reliability but have slower τ_{off}, higher plateau potentials, and thus a higher likelihood of spike failure over a train of light pulses. However, since light scatters within opaque tissue, opsins with higher light sensitivity may be more effective at generating spiking over a greater tissue volume (at increasing distance from the light source) (Broyles et al., 2018).

Newer highly light-sensitive bistable channelrhodopsin variants, known as "stable step function opsins" with τ_{off} of the order of ~30 min can provide stable subthreshold excitation over long time periods, even in the absence of ongoing light stimulation (Berndt et al., 2009; Yizhar et al., 2011b). Unlike the large photocurrents of fast opsins which drive precise action potentials, bistable variants instead produce small photocurrents that drive subthreshold depolarization, enhancing a cell's excitability by increasing its sensitivity to physiologic excitatory inputs. These can be used for experimental paradigms that require persistent subthreshold excitation in the absence of ongoing light stimulation (Yizhar et al., 2011b; Ferenczi et al., 2016). The bistable step function opsins are activated by a brief pulse of blue light, but can also be switched off in a temporally precise manner by longer wavelengths of light.

The most frequently used opsin in cardiac tissue to date is $ChR2_{HR}$ which is similar to the wild type ChR2 but has a point mutation that creates larger photocurrents at the expense of slightly slower τ_{off} (~20 ms). It is well expressed in cardiomyocytes and generates reliable action potentials in response to pulsed light (Bruegmann et al., 2010). However, when applying optogenetics to cardiac tissue, the specific properties of cardiomyocytes and non-myocytes should be considered. For example, for cardiomyocyte contraction, voltage-gated Ca^{2+} channels open secondary to an initial brief depolarizing input (e.g., from voltage-gated Na^{+} channel activation or an optogenetic depolarization), and the rise in intracellular Ca^{2+} through transmembrane influx and sarcoplasmic reticulum release generates the contractile force. A slow but sensitive opsin with large photocurrents and greater calcium ion permeability (such as CaTCh, Kleinlogel et al., 2011; Mattis et al., 2011; Bingen et al., 2014) may have the advantage of activating a larger volume of cardiac muscle, but risk leading to cellular calcium overload and could potentially be arrhythmogenic.

Hyperpolarizing Tools

The first hyperpolarizing optogenetic tool was derived from the salt-deprived *Natromonas pharaonis* halorhodopsin (NpHR) (Han and Boyden, 2007; Zhang et al., 2007; Gradinaru et al., 2008). NpHR is a chloride pump activated by yellow light, which generates an inward chloride current at the resting somatic neuronal membrane potential. Proton pumps activated by green light, such as Arch/eArch (from *Halorubrum sodomense*), ArchT (from *Halorubrum* strain TP009), eBR (from *Halobacterium*), and Mac (from *Leptosphaeria maculans*) also generate hyperpolarizing currents from outwardly directed proton pumping (Chow et al., 2010). More recently, light-activated outwardly directed sodium pumps have also been shown to drive hyperpolarization and silence neural activity (Sudo et al., 2013; Tsunoda et al., 2017). Genetic modification of these hyperpolarizing tools through the addition of endoplasmic reticulum export motifs and membrane trafficking signals (Gradinaru et al., 2008; Mattis et al., 2011) has led to enhanced surface membrane expression and larger photocurrents, which has improved their efficacy in driving cell silencing. However, light-activated pumps have several disadvantages in electrically excitable tissue. Since they are not driven by naturally occurring electrochemical gradients, they are energetically inefficient compared to the light activated ion channels, with only one ion pumped per proton. Similarly, the pumps are not limited by physiological ionic gradients and may therefore be more likely to generate supra-physiological photocurrents that could be harmful to cell viability or produce paradoxical

and unexpected cellular responses (Mattis et al., 2011; Ferenczi and Deisseroth, 2012). Therefore, over recent years, there has been a concerted effort to develop hyperpolarizing light activated ion channels through protein-structure guided channel engineering based on knowledge of the channelrhodopsin crystal structure (Kato et al., 2012; Wietek et al., 2014; Berndt and Deisseroth, 2015; Berndt et al., 2016). Through replacement of negatively charged amino acid residues within the channel pore of cation-selective channelrhodopsins, chloride-permeable variants with a negatively shifted reversal potential (~−60 mV in cultured mammalian neurons) can now be used for blue-light activated cellular silencing (iC1C2, iC++, ChloCs). Bistable highly light sensitive variants, analogous to the stable step function depolarizing opsins, SwiChR, SwiChR++, and SloChloC, have been engineered with off-kinetics of several seconds (in contrast to milliseconds for iC1C2), although the currents can be terminated rapidly by a pulse of red light when desired.

In 2015, naturally occurring anion-permeable light-activated ion channels (ACRs) were isolated from chlorophyte algae, *Guillardia theta* (GtACR1 and GtACR2) (Govorunova et al., 2015). Their crystal structures were also recently elucidated, opening many avenues for further understanding and modification of these channels (Kato et al., 2018; Kim et al., 2018). These chloride-permeable ion channels are characterized by their high intrinsic single-channel conductance, and as such have larger photocurrents and higher sensitivity than previously engineered variants and are able to efficiently silence neurons in culture. However, a major concern with both naturally occurring and engineered chloride channels is their tendency to induce antidromic spiking in axonal compartments, possibly as a result of differences in intracellular chloride concentration between the soma and the axon. Genetic modifications to improve membrane and somatic targeting have led to GtACR variants whose expression is restricted to the soma, allowing effective neuron silencing and decreased antidromic spiking in axons *in vivo* (Mahn et al., 2018). Despite these improvements, variability in intracellular chloride concentrations both within and between neurons remains a fundamental constraint of the chloride-permeable inhibitors. A more reliable and efficient form of inhibition would be through increased membrane permeability to potassium, and the search for a light-sensitive potassium channel still continues. Although no single-component potassium channel has yet been discovered or engineered, alternative strategies in which a plant photoreceptor LOV domain is fused to and controls a potassium channel (BLINK 1 and 2) has successfully been expressed in neurons to silence activity and modulate behavior in zebrafish and rodents (Alberio et al., 2018) and other two-component systems have been tested in cardiomyocytes (see below).

In cardiac optogenetics, Arrenberg et al. (2010) first used eNpHR in zebrafish hearts to drive myocardial cell hyperpolarization and cessation of myocardial contractions. Since then several groups have successfully suppressed cardiomyocyte activity using a variety of inhibitory optogenetic tools, including eNpHR (Abilez, 2012; Park et al., 2015b) and archaerhodopsin (Arch/ArchT) (Nussinovitch et al., 2014). Since then several groups have successfully suppressed cardiomyocyte activity using a variety of inhibitory optogenetic tools, including eNpHR (Abilez, 2012; Park et al., 2015b) and archaerhodopsin (Arch/ArchT) (Nussinovitch et al., 2014). ArchT-mediated cardiomyocyte hyperpolarization has also been used to terminate ventricular arrhythmias in the intact hearts of transgenic mice (Funken et al., 2019). As expected from the chloride reversal potential in cardiomyocytes, recent work (Kopton et al., 2017, 2018) has highlighted that cardiomyocytes in culture demonstrate excitation in response to light stimulation with both naturally occurring and engineered chloride channels. This can be explained by the fact that the reversal potential for chloride in the cardiomyocyte is more positive than the resting membrane potential, thus optically opening chloride channels tends to lead to membrane depolarization (Hiraoka, 1998). This property has been flexibly used in experimental preparations to allow either optical pacing of cardiac contractions in response to short pulses of light, or silencing of cardiomyocyte activity with prolonged activation through the induction of depolarization block (Kopton et al., 2018). Interestingly, other studies demonstrated an opposite effect on membrane potential, with ACRs eliciting large hyperpolarizing photocurrents with intracellular Cl^- concentrations adjusted by the patch pipette to 4 mM (Govorunova et al., 2016). The discrepancy between studies may be related to experimental preparations (e.g., intracellular chloride concentration) and developmental stage of the cardiomyocytes: the depolarizing effect was seen in cardiomyocytes isolated from rabbits age 9–10 weeks whereas hyperpolarization was seen in cultured neonatal rat cardiomyocytes. These findings also raise the importance of developing light-gated potassium channels, to more effectively stabilize the cardiac membrane potential at hyperpolarized resting potentials. Very recently, a two-component system consisting of a photo-activated adenylyl cyclase (PAC) fused to a small cyclic nucleotide-gated potassium channel (or split from each other by a self-cleaving 2A peptide), was expressed in cardiomyocytes and was found to reversibly silence cardiomyocyte activity *in vitro* and *in vivo* for tens of seconds (Bernal Sierra et al., 2018) (review: Entcheva, 2013).

G-protein Modulators/Cell Signaling Modulators

Optogenetic tools are not only limited to ion channels, but also encompass a range of light-sensitive proteins that modulate intracellular signaling *via* G-protein coupled pathways. These can be naturally occurring or genetically engineered proteins. An example of a naturally occurring G-protein modulating opsin is melanopsin, which has been used in both neuroscience and cardiac research to generate sustained Gq activation (Koizumi et al., 2013; Beiert et al., 2014). In addition, the Opto-XRs are a family of engineered G-protein modulating opsins which have been designed to flexibly couple to different downstream signaling pathways (Airan et al., 2009). The first Opto-XRs were light-sensitive adrenergic receptors (ARs), known as Opto-α1AR and Opto-β2AR. These were shown to differentially modulate Gq and Gs signaling, respectively, with opposing effects on neural activity. A number of other chimeric tools have since been developed, including light-sensitive opioid receptors (OMOR) (rat rhodopsin coupled to the intracellular portion of the μ-opioid

receptor) (Siuda et al., 2015), light-sensitive metabotropic glutamate receptors (melanopsin fused to intracellular components of mGluR6) (van Wyk et al., 2015), and light-sensitive serotonin receptors (melanopsin fused to intracellular loops of 5HT receptors) (McGregor et al., 2016). In cardiac physiology, a recent study has demonstrated the use of a jellyfish opsin (JellyOp) to activate Gs signaling in cardiomyocyte embryoid bodies and the intact heart (Makowka et al., 2019). An advantage of these tools is that for certain cell types (e.g., non-excitable cells such as glia) and synapses, they may provide a more physiological form of modulation, for example, mimicking natural neuromodulatory inputs. However, one disadvantage is that endogenous G-protein coupled pathways are dependent upon highly spatially localized machinery at the membrane for physiological propagation of the appropriate signal, which may not be in place with exogenous Opto-XR approaches. This has perhaps limited their widespread adoption over the last decade. Ongoing work is further refining and expanding this toolbox, which has promising translational applications, both for the understanding of intracellular signaling mechanisms as well as the development of pharmacologic therapeutic targets (Kato et al., 2012; Hegemann and Nagel, 2013; Deisseroth and Hegemann, 2017).

Spectral Properties of Opsins

Alongside kinetics and photocurrent magnitude, much genetic engineering of opsins has focused on spectral tuning. The absorption spectrum of opsins is determined by the molecular and electrostatic environment of the chromophore within the protein, and knowledge of the crystal structure has provided key information to allow spectral tuning (by changing the energy of the ground state or excited state) through the modification of key residues of the rhodopsin molecules. This can be achieved by exchanging residues interacting with the retinal Schiff-base (e.g., counterion residues) or residues that influence the polarity along the retinal polyene chain (Yan et al., 1995; Kato et al., 2012; Hegemann and Nagel, 2013; Deisseroth and Hegemann, 2017). Wild-type channelrhodopsin has a peak activation spectrum of 470 nm (blue light activated), but naturally occurring and engineered variants have now been developed to cover a wide range of the visible spectrum from being even more blue-shifted (Govorunova et al., 2013) to red-shifted (Zhang et al., 2008; Yizhar et al., 2011b; Lin et al., 2013; Klapoetke et al., 2014). The first of these red-shifted variants to be discovered, VChR1 is maximally activated by green light (~530 nm), but retains strong photocurrents in amber light (590 nm), a wavelength that produced no measurable depolarization in ChR2-expressing cells. Further engineering of opsin chimeras and targeted mutant variants has led to an array of red-shifted opsins with large photocurrents and fast off-kinetics [C1V1 variants, red-activatable ChR (ReaChR), Chrimson] (Yizhar et al., 2011b; Lin et al., 2013; Klapoetke et al., 2014; Gupta et al., 2019). Several blue-shifted rhodopsin variants have also been identified. For example, one variant from a freshwater green alga [*Scherffelia dubia* channelrhodopsin (sdChR)] was genetically modified to have a spectral activation peak of 460 nm (10 nm blue shifted relative to ChR2) as well as faster kinetics. This variant, known as CheRiff, was shown to have 9-fold higher light sensitivity than $ChR2_{HR}$ and had minimal optical cross-talk with red-shifted voltage indicators (Hochbaum et al., 2014). *Platymonas subcordiformis* ChR (PsChR) (Govorunova et al., 2013) and *Tetraselmis striata* ChR (TsChR) (Klapoetke et al., 2014) are the most blue-shifted variants identified to date, with a spectral activation peak of ~445 nm, but so far they have not been used widely in optogenetic applications. It is important to note that the newer red-shifted variants (e.g., Chrimson) have greater proton permeability than other ChR2 variants, and their use has been associated with pronounced intracellular acidification (Vierock et al., 2017).

A major advantage of red-shifted variants is the possibility of combinatorial stimulation experiments using both blue light and yellow or red light to activate different cell populations within the same anatomical area, or for all-optical read-in and read-out methods, in which stimulation is combined with imaging techniques. One limitation of the early red-shifted options was that despite their red-shifted shoulder many retained some activity within the blue light range (Venkatachalam and Cohen, 2014), making it challenging to spectrally segregate optogenetic stimulation at blue wavelengths. The most recent red-shifted mutant opsin, Chrimson-SA, which was spectrally tuned based on understanding of the crystal structure of Chrimson, addresses this issue, with maximal activation at 605 nm (20 nm further red-shifted than the original Chrimson) and much smaller photocurrents at the blue end of the spectrum (Oda et al., 2018). It may now be feasible to spectrally segregate optogenetic stimulation at blue and red wavelengths, although careful titration of expression levels and light intensities will be required. For imaging purposes (as will be discussed further in the "Optical read-out" section), it is possible to stimulate with ChR2 in the blue light range and image cellular activity with red-shifted calcium indicators [e.g., RCaMP, jRGECO1a; (Dana et al., 2016)]. Now with the most-red shifted Chrimson (Chrimson-SA), it may also be possible to stimulate at red wavelengths and image at blue wavelengths, although again, careful titration must be performed, and the appropriate controls included. Such spectral constraints also apply to the hyperpolarizing optogenetic tools (Wietek et al., 2017), which to date do not have such far red-shifted variants.

Another theoretical advantage of red-shifted spectra is volume and depth of tissue modulation. Since blue light is known to scatter more easily in opaque tissue such as the brain or cardiac tissue, red light has the potential to penetrate further with less scattering and thus may allow greater volume and depth of optogenetic modulation (Yizhar et al., 2011a,b), even through the intact skull (Lin et al., 2013).

TARGETING OPSINS TO CARDIAC TISSUE

Having chosen an optogenetic tool for a particular experiment, the next step is to express the tool in a cardiac cell of interest.

There are a variety of methods to target specific cardiomyocyte or non-myocyte cells either *in vitro* or *in vivo* which we discuss below (Ambrosi et al., 2014) (**Figure 1B**).

In vitro Targeting Methods

The first cardiac optogenetic study in mouse used developmental techniques with mouse embryonic stem cells (ESCs) to generate ChR2-expressing cardiomyocytes (Bruegmann et al., 2010). The ESCs were transfected with a plasmid encoding ChR2 using the β-actin promoter (CAG) to drive strong expression in cardiomyocytes. The ESC developed into embryoid bodies, within which cardiomyocytes were identified on the basis of their expression of the muscle specific protein α-actinin. Illumination of the embryoid bodies with pulsed blue light resulted in contraction of cells expressing ChR2. Bruegmann et al. (2010) also demonstrated that pulsed blue light could generate local electrical activity in a two-dimensional layer of purified ChR2-expressing ESC-derived cardiomyocytes, and that focal illumination at one site spread to other regions through the functional syncytium formed by the cell population. Prolonged illumination caused cessation of electrical activity, likely due to opsin-induced refractoriness of the illuminated area. Finally, in transgenic mice expressing ChR2-expressing ESCs, blue light illumination of the beating heart induced supraventricular or ventricular pacing depending on the site of illumination.

There have since been several additional reports of the use of embryonic stem cells to generate opsin-expressing cardiomyocytes. Beiert et al. (2014) transfected mouse embryonic stem cells with a plasmid containing a light-activated Gq-coupled receptor, melanopsin, to generate melanopsin-expressing cardiomyocytes in embryoid bodies (Beiert et al., 2014). Illumination with blue light resulted in faster beating of the embryoid bodies as well as irregular beating at high light intensities. Abilez et al. used lentiviral transfection of human-induced pluripotent stem cells (hiPSCs) to drive expression of both ChR2 as well as the first-generation inhibitory opsin, NpHR1.0 in hiPSC-derived cardiomyocytes to drive bidirectional control of cellular contractile activity (Abilez, 2012).

It is also possible to express optogenetic constructs in neonatal and adult primary ventricular cardiomyocytes using viral vector transduction (Ambrosi et al., 2015). Lentiviral vectors have been used to drive *in vitro* expression of ChR2 and NpHR in neonatal ventricular cardiomyocytes (Park et al., 2015b) and expression of channelrhodopsin variants such as CatCh in neonatal atrial cardiomyocytes (Bingen et al., 2014). Bernal Sierra et al. transduced cultured adult rabbit ventricular cardiomyocytes with an adenovirus vector containing a two-component cyclic nucleotide-activated potassium channel. These cells exhibited light-activated cardiomyocyte silencing for up to 5 days after isolation (Bernal Sierra et al., 2018).

At the single cell level, optical pacing has been accomplished in iPSc/ESC cardiomyocytes and both neonatal and adult cardiomyocytes. This is exemplified in tandem cell units (TCU) formed from non-excitable (e.g., HEK) cells (also known as "spark cells") transfected to express a light-sensitive ion channel (ChR2) coupled through gap junctions to excitable cardiomyocytes (CM) to form an optically controllable functional TCU (Jia et al., 2011). Dual whole-cell patch clamp experiments demonstrated that TCUs formed from ChR2-expressing HEK cells successfully established coupling with neonatal rat or adult canine cardiomyocytes. Optical stimulation of ChR2-expressing HEK cells paced the flanking myocytes. The use of gap junction blockers demonstrated a requirement for functional gap junctions in such optical pacing. Using these functional TCUs, it was possible for the first time to combine optical excitation and optical imaging to record light-triggered muscle contractions and high-resolution propagation maps of light-triggered electrical waves. The latter were quantitatively indistinguishable from electrically triggered waves. Thus, illumination with 470 nm light activates ChR2, resulting in an inward current and cell depolarization in the illuminated non-excitable cell. Ionic exchange *via* gap junctions leads to cardiomyocyte excitation, and the resulting action potentials are then conducted throughout the functional syncytium of coupled cardiomyocytes.

Nussinovitch et al. demonstrated a similar TCU approach but this time using co-culture of ESC-derived cardiomyocytes with fibroblasts which were genetically engineered to simultaneously express both ChR2 and the red-shifted inhibitory opsin, ArchT. With this approach, they were able to generate bidirectional modulation, driving optogenetic pacing using blue light and optogenetic suppression of activity with red light (Nussinovitch et al., 2014). The advantage of this technique is that non-myocyte adult cardiac cells, such as fibroblasts, can survive *in vitro* for longer periods of time than primary cardiomyocytes.

The interactions between non-myocyte cardiac cells and cardiomyocytes have also been studied using this approach. For example, one study investigated the functional coupling between cardiac macrophages and cardiomyocytes in the AV node of mice, using a co-culture preparation. They demonstrated that the two cell types are electrically coupled *via* connexin 43 gap junctions in the AV node and exhibit synchronous membrane depolarization (Hulsmans et al., 2017). This approach then formed the basis for *in vivo* investigation of the functional role of this coupling on AV node conduction using optogenetic techniques (see below).

In vivo and *ex vivo* Targeting Methods

An effective approach to generate opsin expression *in vivo* in a cell-type specific manner is through the generation of transgenic animals. This approach has been used to drive expression in both cardiomyocytes as well as cardiac non-myocytes. To date, optogenetic transgenic mice, zebrafish, and *Drosophila* have all been used in cardiac optogenetic experiments. One of the earliest cardiac optogenetic experiments was performed in transgenic zebrafish (Arrenberg et al., 2010). The Gal4/UAS genetic system was used to express the inhibitory NpHR or excitatory ChR2 in larval zebrafish cardiomyocytes. Illumination of the pacemaker region in the atrioventricular canal *in vivo* disrupted cardiac contractile activity and demonstrated that only a few cells (only three cells in some cases, 10–30 cells on average) were necessary for heart beat initiation.

In mice, several different cardiac transgenic models have been developed. One example is a transgenic mouse generated using the Cre-lox conditional genetic targeting system, in which mice expressing Cre-recombinase under the cardiac-specific α-myosin heavy chain (α-MyHC) promoter are crossed with mice which conditionally express $ChR2_{HR}$ on exposure to Cre-recombinase (Ai27D mice). The resulting offspring expresses $ChR2_{HR}$ specifically in cardiac tissues (Zaglia et al., 2015; Crocini et al., 2016; Scardigli et al., 2018). This approach has been used to investigate the propensity for cardiac tissue to generate focal ectopic electrical activity at different locations in the heart and under different physiological and pathological conditions, including cardiac ischaemia (Zaglia et al., 2015). It has also been used for temporally and spatially precise termination of ventricular arrhythmias under open loop and closed loop conditions (Crocini et al., 2016; Scardigli et al., 2018). Zaglia et al. (2015) also went one step further by driving ChR2 expression specifically in the Purkinje cell system, as opposed to expression throughout all cardiomyocytes. This was achieved by crossing connexin40-Cre mice with conditional ChR2-expressing mice, such that only the connexin-40 cells (present throughout the cardiac conducting system, including Purkinje cells and the atria) express ChR2. Using these two different genetic preparations, Zaglia et al. (2015) were able to compare the effects of optogenetic stimulation when applied to all cardiomyocytes versus when applied specifically to the conducting system. They found that the number of non-specifically targeted cardiomyocytes needed to initiate an ectopic focus was much greater (~1,300–1,800 cells) than the number of specifically targeted Purkinje fibers (~100 fibers).

Several studies have also reported on transgenic methods for optogenetic targeting of cardiac non-myocytes, such as sympathetic cardiac neurons, parasympathetic neurons, cardiac neuroendocrine cells, and cardiac macrophages. Cardiac sympathetic neurons were targeted by cross-breeding mice expressing Cre-recombinase under the catecholaminergic-specific promoter tyrosine hydroxylase (TH) with mice that express ChR2 in a Cre-dependent manner, resulting in mice that express ChR2 only in TH-expressing catecholaminergic cells. This transgenic model was used to study the specific role of cardiac sympathetic nerve activation on cardiac contraction and arrhythmia (Wengrowski et al., 2015; Prando et al., 2018). The role of parasympathetic input to the heart was studied in a similar manner, by crossing mice expressing Cre-recombinase under the choline acetyltransferase (ChAT) promoter (expressed by peripheral cholinergic parasympathetic neurons) with mice expressing Cre-dependent ChR2 (Moreno et al., 2019).

Another transgenic approach was used to drive ChR2 expression specifically in phenylethanolamine n-methyltransferase (*Pnmt*+) cells by crossing *Pnmt-Cre* mice with mice that express ChR2 in a Cre-dependent manner (Wang et al., 2017). The *Pnmt* gene encodes an enzyme converting noradrenaline to adrenaline, suggesting that early in development *Pnmt*+ cells may have neuroendocrine functions. In adult mice, these cells are predominantly located on the left side of the heart and have properties consistent with working cardiomyocytes. When illuminated with blue light, ChR2-expressing cardiomyocytes drove paced cardiac activity or generated arrhythmogenic activity, depending on the light-stimulation protocol, confirming that the activity of the subset of cardiomyocytes that have been *Pnmt*+ during development or underwent fusion with *Pnmt*+ cells was sufficient to control cardiac rhythm (**Figure 2A**). Light pulses delivered to the left atrium of a *PnmtCre/ChR2* (**Figure 2B**) but not wild-type *Pnmt*+/+ heart evoked ECG spikes (**Figure 2C**), with normal RR, PR, and QT intervals, and QRS duration (**Figure 2D**), a pacing effect not observed with pulsed right atrial or ventricular illumination (**Figure 2E**). Light pacing could be used to explore pro-arrhythmic properties under β-adrenergic stress using previously established stimulation protocols imposing extrasystolic stimuli progressively earlier after pacing trains of eight stimuli (S1) (**Figure 2F**), or burst pacing at variable (100–30 ms) or fixed (20 ms) cycle lengths (**Figure 2G**).

Similar approaches also been used to generate mice expressing hyperpolarizing optogenetic tools specifically in cardiomyocytes, by crossing *αMyHC-Cre* mice with mice that conditionally express ArchT on exposure to Cre-recombinase (Ai40D mice). This has been used to study hyperpolarization as a mechanism for ventricular arrhythmia termination (Funken et al., 2019).

Despite the flexibility of the Cre-LoxP systems, these approaches also have limitations, including leaky or incomplete Cre-recombination, which can result in off-target expression and compromise targeting specificity (Johnston et al., 2017). The non-inducible Cre-LoxP system also does not specify the cell type at the time of investigation, but rather highlights the developmental origin of Cre-positive cells or previous fusion events. To address some of these limitations, inducible Cre-LoxP expression systems have been developed to provide temporal control over the expression of Cre-recombinase and reduce leaky recombination events occurring early in development. This method was used to target cardiac macrophages (Hulsmans et al., 2017). In this study, mice expressing tamoxifen-inducible Cre driven by the *Cx3cr1* promoter (targeting cells of the mononuclear phagocytic lineage) were bred with mice expressing Cre-dependent ChR2, resulting in mice that express ChR2 specifically in AV node macrophages only after the administration of tamoxifen. This approach allowed the experimenters to causally assess the influence of AV node macrophage activation on atrial conduction *in vivo* and in a Langendorff-perfused heart preparation (Hulsmans et al., 2017). However, it is important to note the limitations of tamoxifen induction, which include variable induction strength across different tissues.

These studies represent the tip of the iceberg of genetically targeted cardiac cells. There are now a large number of cell specific promoters that may permit spatially constrained opsin expression in regions such as the sinus node, the atria, ventricles, conduction system, or progenitor cells. In addition, some genetic motifs may also permit subcellular targeting, for example, localizing the opsin to the plasma membrane, the sarcoplasmic reticulum or the mitochondria (Koopman et al., 2017). In parallel with the field of neuroscience, a number of groups have turned to viral vectors to drive opsin

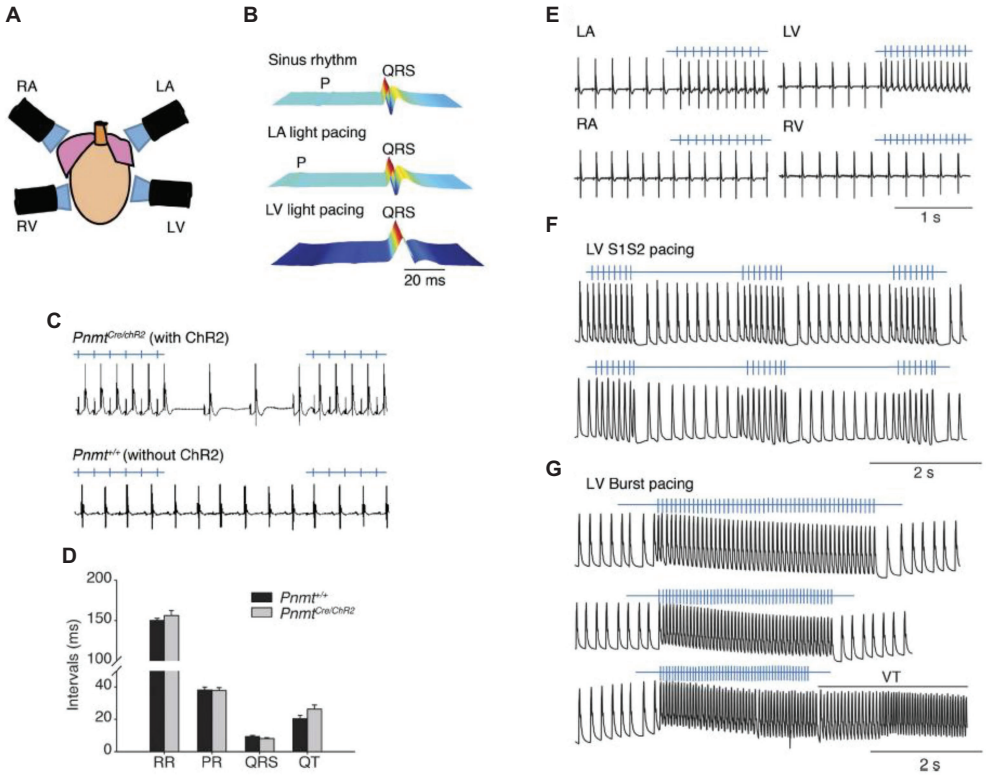

FIGURE 2 | Control of heart rhythm and investigation of pro-arrhythmic markers in a *Pnmt-Cre/ChR2* mouse model expressing channelrhodopsin 2 (ChR2) permitting selective optogenetic stimulation of PdCM cells expressing phenylethanolamine n-methyltransferase (*Pnmt*). **(A)** Light pacing localized to 4 different regions of the heart. **(B)** ECG recording of a *Pnmt-Cre/ChR2* heart in intrinsic sinus rhythm (top) and following pacing applied to the left atrium (middle) and left ventricle (bottom panel). "P" denotes P wave in the ECG. **(C)** Light pulses delivered to the left atria of a *Pnmt-Cre/ChR2* but not a wild-type *Pnmt*+/+ heart evoking ECG spikes in a 1:1 manner. **(D)** Similar RR interval, PR interval, QRS interval and QT interval in Pnmt-Cre/ChR2 and Pnmt+/+ hearts. **(E)** Comparison of ECG entrainment with light stimulation applied to the left and right, atria and ventricles in a Pnmt-Cre/ChR2 heart. **(F,G)** Monophasic action potential recordings in the left ventricle of a Pnmt-Cre/ChR2 heart during programmed light stimulation delivered to the left ventricle in a S1S2 **(F)** or burst pacing protocol **(G)** [From Figure 3 of Wang et al. (2017)].

expression in cardiomyocytes and cardiac non-myocytes. Viral vector delivery using adeno-associated virus (AAV) is desirable for their safety and for potential application in humans, in contrast to transgenic or developmental methods. A disadvantage is that this approach will necessarily result in a smaller proportion of opsin-expressing cardiomyocytes, compared to other techniques. Vogt et al. (2015) demonstrated that opsin expression through intracardiac delivery of a viral vector can indeed be sufficient to modulate cardiac activity, and the expression has been shown to persist for over 12 months (Bruegmann et al., 2016). The AAV9 serotype has been shown to have good tropism for cardiomyocytes (Inagaki et al., 2006; Pacak et al., 2006) therefore was chosen for the optogenetic construct. The AAV9-CAG-ChR2$_{HR}$-mCherry construct was injected systemically through the external jugular vein of wild-type mice. Expression of the fluorophore label, mCherry, was detectable after 4 weeks throughout the heart and evenly distributed across the ventricular wall. Dissociated ChR2-expressing cardiomyocytes showed robust inward photocurrents and action potential responses to short pulses of blue light. *In vivo*, blue light pulses could drive ventricular pacing (electrocardiographically recordable as broad QRS complexes without preceding P-waves) at 30–50 beats per minute above the resting heart rate in approximately three quarters of the tested hearts. Lack of *in vivo* optogenetic responses was likely the result of low construct expression, as demonstrated by lower mCherry fluorescent signal in the ventricles. The team calculated that the minimal percentage of expressing cells for optogenetic pacing was 30–40% and demonstrated as proof of principle that this percentage could be achieved through a systemic viral injection. One disadvantage of this method is off-target expression in other organs, for example, they also found mCherry-labeled muscle fibers in the diaphragm and a small number of hepatocytes. It may be possible to circumvent this with the use of cell-type specific promoters.

Viral vector delivery has also been used in other animal models. For example, one group used AAV2/9 to transfect cardiac sympathetic neurons in the left stellate ganglion of dogs with the hyperpolarizing tool ArchT (Yu et al., 2017). The authors demonstrated optogenetic suppression of myocardial-ischemia-induced ventricular arrhythmias in the dog heart, thus representing a first translational cardiac optogenetic application in a large, clinically relevant animal model.

LIGHT DELIVERY SYSTEMS

Light Scattering in Cardiac Tissue

For *in vitro* cell culture or monolayer preparations, light delivery is relatively straight forward. For neurons, the light power density (number of incident photons per unit time per unit area multiplied by individual photon energy) required to elicit an action potential by wild type ChR2 has been estimated at ~1–5 mW/mm^2 (Boyden et al., 2005), whereas in cultured myocytes, less than 1 mW/mm^2 is required for optical pacing (Bruegmann et al., 2010). The reporting of light power density for optogenetic experiments has been discussed in detail elsewhere (Yizhar et al., 2011a). However, in optogenetic experiments in intact *in vivo* or *ex vivo* systems, light-scattering by biological tissue limits the even delivery of light through the tissue volume. In the brain, experiments using coherent light of different wavelengths through an optical fiber demonstrated that light in the brain scatters in a spherical distribution, rather than the conical distribution seen in saline, with longer wavelengths scattering less than shorter wavelengths (Yizhar et al., 2011a). In cardiac tissue, similarly careful measurements have been performed to determine the degree of attenuation of blue light across the myocardium (Zaglia et al., 2015). Analysis of the beam intensity profile over different depths of tissue from the optical fiber confirmed that over 90% of the total light intensity remained within a myocardial volume that was approximately cylindrical in shape. The depth and width of the cylinder could be modulated by the applied light intensity and the diameter of the optical fiber (Zaglia et al., 2015). These measurements were used to shape the volume of illuminated cardiac tissue in order to determine the minimal cardiac volume required to generate ectopic foci of activity.

Mode of Light Delivery

Examples of light delivery systems can be found in published cardiac optogenetic experiments and recent reviews (Boyle et al., 2015, 2018a). Laser light is a commonly chosen light source for many applications, as the spectra can be closely matched to the activation peak of different opsins and the beams have low divergence and can be steered or patterned by mirrors or beam splitters on an optical table and coupled into optical fibers for high efficiency *in vivo* light delivery. Properties of lasers for optogenetics experiments are discussed in detail in earlier reviews (Yizhar et al., 2011a). However, LEDs have become increasingly attractive and lower cost light sources, with improvements in power output and spectral diversity over recent years. Disadvantages include their tendency to generate heat and the degree of divergence of LED beams, which lowers the coupling efficiency into optical fibers. Broadband light sources (e.g., arc lamp-based epifluorescence illuminators or light bulbs from video projectors (Arrenberg et al., 2010) can be coupled with shutters and spectral filters to generate spectrally flexible light sources. In *ex-vivo* preparations (e.g., Langendorff heart or *in situ* beating heart experiments), digital micromirror devices (DMDs) have also been used to generate user-defined light patterns to focus the light on different anatomical targets (Arrenberg et al., 2010; Scardigli et al., 2018).

For *in vivo* intracardiac light delivery, implantable microscopic inorganic LEDs (micro-ILEDs) either singly or as an array have been proposed. To overcome the issue of blue light scattering and increase the depth of light penetration, these micro-LEDs could be used in combination with red-light shifted opsins which tend to be less vulnerable to light scattering and achieve a greater penetration depth (such as C1V1 variants, ReaChR and Chrimson) (Yizhar et al., 2011b; Lin et al., 2013; Klapoetke et al., 2014; Boyle et al., 2015). The development of new biocompatible membranes has opened up the possibility for implantable, stretchable or injectable opto-electronic films or membranes (Kim et al., 2013; Liu et al., 2015) that could be applied to the epicardial or endocardial surface to provide widespread illumination across the myocardium or flexible multi-point illumination (Boyle et al., 2015). The development of new biocompatible membranes has opened up the possibility for implantable, stretchable or injectable opto-electronic films or membranes (Kim et al., 2013; Liu et al., 2015) that can be applied to the epicardial or endocardial surface to provide widespread illumination across the myocardium or flexible multi-point illumination (Boyle et al., 2015). Novel bio-optoelectronic devices have recently been developed to include soft biocompatible sensors and feedback systems for closed-loop control (Park et al., 2015a; Mickle et al., 2019). However, although these exciting advances have been demonstrated *in vivo* in the brain and other peripheral tissues (e.g., peripheral nerves, bladder), they have yet to be successfully applied to cardiac tissue for optical stimulation. Recently, a multi-LED probe was used for the first time to drive intramural optical stimulation of ChR2 in isolated murine hearts, demonstrating optical pacing as proof of principle (Ayub et al., 2018).

The use of two-photon illumination for optogenetic experiments in neurons is reviewed in detail elsewhere (Carrillo-Reid et al., 2017; Ronzitti et al., 2017; Alberio et al., 2018). Therefore here we will only briefly summarize its major advantages and challenges. Two-photon illumination allows for high spatial resolution stimulation in three dimensions, over a greater depth of penetration than traditional wide field one-photon illumination. In neuroscience, this has opened up new avenues for the investigation of the spatial complexity of neural activity and neural connectivity, for example allowing stimulation of multiple genetically defined individual neurons or their subcellular compartments such as axon terminals or dendrites (Packer et al., 2012). Several major technical challenges had to be overcome in order for two-photon optogenetics to be realized. These include the inherent low single channel conductivity and two-photon absorption properties of ChR2, such that with the small spot site of two-photon illumination, the degree of evoked membrane depolarization is insufficient to reach action potential threshold (Rickgauer and Tank, 2009). This has been addressed in several ways such as the use of chimeric opsins with enhanced two photon absorption (e.g., C1V1 variants) (Prakash et al., 2012) as well as adaptations of laser scanning techniques. By increasing the spot size (at the expense of axial resolution) in combination with laser scanning techniques to scan the two-photon spot rapidly over the surface of a single cell (~30 ms), it is possible to activate many rhodopsin

molecules almost simultaneously and drive sufficient membrane depolarization to cause action potential initiation. An additional challenge is to scale this up in order to stimulate many multiple individual neurons simultaneously. One way to perform this is move the scanning beam quickly through space (raster scan), to sequentially target several different cells (e.g., achieved using scanning galvanometer mirrors, or acoustic optic deflectors). However, this is a relatively slow approach, especially if the goal is to target tens to hundreds of neurons simultaneously. An alternative approach is to generate patterned light illumination to direct light to multiple cells at once. This can be achieved with a digital mirror microarray device or more recently, digital holographic methods using a spatial light modulator (Ronzitti et al., 2017; Yang and Yuste, 2018).

Two-photon optogenetics also helps to circumvent challenges of spectral combinatorial approaches. For example, it permits the spatial segregation of optogenetic stimulation light from optical imaging light, such that one population of cells could be modulated optogenetically at the same time that the activity of a different but spatially intermingled population of cells is monitored with genetically encoded fluorescent activity sensors [e.g., GCaMP (Packer et al., 2015; Ronzitti et al., 2017)]. This is done most reliably with minimal cross-talk between the spectral channels when blue-shifted opsins are combined with red-shifted activity sensors (Forli et al., 2018) (see "Optical read out" section below). In additional, two-photon stimulation has the further advantage of shifting the excitation light to the near-infrared end of the spectrum, allowing deeper penetration into tissue. Successful two-photon optogenetic stimulation has now been demonstrated with a wide panel of engineered depolarizing, hyperpolarizing, and bistable variants, further increasing the range of experimental possibilities (Prakash et al., 2012).

In cardiac experiments, two-photon stimulation thus presents an even greater challenge. It is unlikely that the small stimulation volumes generated by two photon techniques will be sufficient to pace the well-coupled syncytium of cardiomyocytes with low input resistance (from Kir2.1 potassium currents). So far, two photon approaches for optogenetic stimulation have not been shown to work in the heart, although they may be used for high resolution imaging purposes.

CARDIAC READOUTS

An essential component of any optogenetic experiment is to monitor the response of the experimental set-up to the applied optogenetic modulation, also known as a "read out." This can occur at many levels of the biological hierarchy – from single cell or tissue, to whole organ or organism responses (**Figure 1C**).

Electrophysiological Readouts

Electrical recordings represent a major type of readout of cellular and tissue response to stimulation. Depending on the experimental question, different readouts may focus on single cell activity using patch clamp electrophysiology (Bruegmann et al., 2010), multi-unit activity using micro-array recordings in cell monolayers or slices (Hofmann et al., 2010; Nussinovitch et al., 2014), whole organ activity in an *ex vivo* Langendorff preparation with depth or surface electrodes, or *in vivo* in an anesthetized or awake animal using ECG recordings (Bruegmann et al., 2010; Vogt et al., 2015; Wang et al., 2017). Electrical readouts have the advantage of high temporal resolution and for single cells provide a rich biophysical readout. However, for larger scale recordings in monolayers or whole organs, the spatial resolution and extent of electrical recordings are limited by the number and distribution of electrode contacts. Novel engineered electrodes and electrode arrays have attempted to overcome this limitation, such as grid electrodes and the new neuropixel probe which is of great interest to the neuroscience community (Steinmetz et al., 2018). However, this sampling limitation, along with the invasive nature of many types of electrical recordings, has also led to the development of alternative optical imaging approaches.

Optical Readouts

A major goal in both neuroscience and cardiac research is to non-invasively read out cellular activity at single cell resolution over a wide area. To this end, much effort has focused on developing "all-optical approaches" for simultaneous optogenetic stimulation and recording of cellular activity. For a detailed description of the range of such experimental approaches, please see comprehensive review by O'Shea et al. (2019). Great strides have been made in this direction with the development of new genetically encoded optical sensors (Koopman et al., 2017). These sensors produce a fluorescent signal in response to specific cellular events, such as ion transients, voltage changes, or activation of biochemical signaling cascades. These have been reviewed in depth elsewhere (e.g., (Entcheva and Bub, 2016; Koopman et al., 2017; Deo and Lavis, 2018) and so here we will simply summarize the major categories of sensors that have been used or are of potential use in cardiac optogenetics.

The most widely used ion sensors are calcium sensors, although magnesium, chloride, and hydrogen ion sensors have also been described. Calcium sensors can be divided into two broad types – calcium-sensitive dyes (small molecule calcium chelators) and the more recently developed genetically encoded calcium sensors (GECIs). All GECIs contain a calcium-binding domain fused to either a single or two fluorescent proteins (FRET-based fluorescence). The single fluorescent protein sensors, GCaMPs, are now widely used in neuroscience due to their high signal to noise ratio and fast kinetics; however, unlike the FRET-based sensors (e.g., cameleon), they do not provide a ratiometric signal which can result in confounds during myocardial cell contraction. Despite this, GCaMPs have been used to record calcium transients in cardiomyocytes *in vivo* (Tallini et al., 2006), even at subcellular resolution [e.g., nanosparks (Shang et al., 2014)]. Initially, the GCaMP sensors had predominantly green emission spectra due to their GFP-based fluorescence, but newer versions with red-shifted emission spectra, including RCaMPs, R-GECO (Dana et al., 2016), and near-infrared-GECO (NIR-GECO) (Qian et al., 2019) have now been developed, which are important for combination with optogenetic tools. Despite extensive work on spectral tuning of different opsins, most optogenetic tools retain at least some

activity in the blue end of the spectrum, making it difficult for them to be reliably combined with blue light-activated sensors. It is also important to note that there is potential cardiotoxicity from calcium indicators, for example, these have been shown to produce hypertrophy of the myocardium when used chronically (Yang et al., 2018) and various reports have suggested that GCaMPs may interfere with calcium channel dynamics, calcium buffering, and signaling (Steinmetz et al., 2017). To date, the field of cardiac optogenetics has largely opted to use the calcium-sensitive small molecule dyes. For example, Jia et al. (2011) first used the calcium dye Rhod-4 in a cardiac cell syncytium to image cardiomyocyte-mediated wave propagation triggered by optogenetic stimulation by ChR2. Recently, combinatorial viral constructs containing a blue light-activated opsin (in this case $ChETA_{TC}$) and red-shifted genetically encoded calcium indicators (R-GECO) have been successfully used for optical stimulation and recording in primary ventricular cardiomyocytes (Chang et al., 2017).

Another desirable readout is optical measurement of membrane voltage, as opposed to a surrogate cellular response such as calcium transients. To date, the most frequently used optical voltage sensors in cardiac optogenetics are red-shifted voltage sensitive dyes. These have been used to map action potential propagation as well as emergent properties such as excitation waves in cardiac tissue with high temporal resolution (Burton et al., 2015; Entcheva and Bub, 2016; Feola et al., 2017). The red-shifted dyes have excitation wavelengths of >600 nm, ensuring minimal concomitant activation of channelrhodopsin or other blue-spectrum opsins. This all-optical approach was first performed by Park et al. (2015b) who demonstrated bidirectional voltage responses across a cardiomyocyte monolayer in response to stimulation by ChR2 or silencing by the inhibitory opsin eNpHR3.0. For this, they used Pittsburgh-I (PGH1) which is a voltage-sensitive dye with spectral properties highly suited for combination with blue-light activated optogenetic tools (excitation peak 608 nm, emission peak 880 nm) (Salama et al., 2005). Since then, multiple groups have employed voltage-sensitive dye imaging techniques in the Langendorff perfused heart (Zaglia et al., 2015; Crocini et al., 2016). Voltage sensitive dyes can also be used in combination with other small-molecule dyes – for example, Wang et al. (2017) used both calcium- (rhod-2) and voltage-sensitive (RH237) dyes to map calcium and voltage changes across atrial and ventricular tissue in a Langendorff heart preparation. They thus confirmed that the spread of excitation in response to optogenetic stimulation of adrenergic Pnmt-derived cardiomyocytes was comparable to that produced by conventional electrical stimulation (Wang et al., 2017). Closed loop systems are highly desirable for interventional applications. Scardigli et al. (2018) were the first to devise an all-optical closed-loop system, expressing ChR2 in transgenic mouse hearts under the cardiomyocyte-specific promoter alpha-MyHC and imaging action potential propagation in Langendorff-perfused hearts with the red-shifted voltage-sensitive dye (di-4-ANBDQPQ) (Scardigli et al., 2018). Using real-time image analysis, they used voltage responses in the ventricles or atria to trigger optogenetic stimulation to restore ventricular responses after AV block or interrupt re-entrant circuit arrhythmias. Finally, a key advantage of such all optical approaches is the capability of observing and manipulating emerging properties of excitable tissues, such as excitation waves (Burton et al., 2015; Entcheva and Bub, 2016; Feola et al., 2017).

Genetically encoded voltage indicators (GEVIs) have also seen great improvement over recent years. There are several different types of GEVI, including voltage-sensing fluorescent proteins (VSFP) (FRET-based or single fluorescent proteins) as well as opsin-based sensors. The proton-pumping microbial opsins such as archaerhodopsin (Arch), *L. maculans* (MAC), and subsequently engineered non-pumping mutants, have an endogenous fluorescence that is modulated by changes in local membrane voltage thus permitting voltage sensing with optical resolution of single action potentials (Kralj et al., 2012; Gong et al., 2013; Maclaurin et al., 2013; Yang and St-Pierre, 2016). Much work focuses on continuing to improve VSFP and rhodopsin-based GEVIs in terms of signal to noise ratio, temporal resolution and toxicity/off-target effects. Only very recently was a red-shifted GEVI developed with bright enough fluorescence to enable voltage monitoring in combination with optogenetic stimulation (Yi et al., 2018). In the heart, VSFPs have been used to monitor membrane voltage and action potential propagation in cardiac myocytes *in vitro*, *in vivo*, and ex vivo (Liao et al., 2015) as well as in cardiac non-myocytes (Quinn et al., 2016).

Finally, there are a number of optical sensors designed to detect changes in activity in biochemical transduction cascades, for example, calmodulin-CAMKII/calcineurin, cAMP/PKA, and cGMP/PKG activity. These biological processes and thus their sensors act over a slower time course than ion and voltage sensors. A number of FRET-based and genetically encoded sensors are available and have been used in combination with optogenetic stimulation in neurons [e.g., (Harada et al., 2017); reviewed in (Spangler and Bruchas, 2017)] but to date have not yet been combined with optogenetics in cardiac tissue. These sensors will be particularly useful for studying and testing longer-term modulatory effects of cellular and subcellular optogenetic activation in specific cardiac cell types (Koopman et al., 2017).

EXAMPLES OF CARDIAC APPLICATIONS OF OPTOGENETIC TECHNIQUES

Emerging optogenetic techniques provide unprecedented opportunities to study cardiac physiology particularly with the capacity to deliver optogenetic control with spatiotemporal resolution and cell type specific precision. Over the last decade, there has been an explosion in the use of optogenetics in cardiac physiology, with applications ranging from investigating action potential propagation across cardiomyocyte monolayers to arrhythmia initiation and termination *in vivo*. Future endeavors, many of which are already in progress, fall under a wide range of areas.

In vitro Properties of ChR2-Expressing Cardiomyocytes

Single ChR2-expressing ventricular cardiomyocytes can be isolated from adult transgenic mice (generated from ChR2-expressing

embryonic stem cells) (Bruegmann et al., 2010). These have been used to characterize the biophysical effects of ChR2 activation by application of blue light. The ChR2-EYFP fusion protein was localized to the ventricular cardiomyocyte cell membrane and t-tubular system, and ChR2-expressing cells showed normal resting membrane potentials, membrane resistances, and action potential durations relative to controls. In both ventricular and atrial cardiomyocytes, light application induced typical ChR2 currents measured by patch clamp with decay time constants similar to those reported elsewhere (Nagel et al., 2005) (~20 ms) and shorter than typical cardiomyocyte refractory periods. Action potentials could be elicited with even ~1 ms duration light pulses. Brief pulses of light reliably evoked action potentials. The action potentials resulting from brief light stimulation were accompanied by Ca^{2+} transients. Prolonged light stimulation induced action potentials followed by prolonged depolarizations. Such longer light stimulations resulted in prolonged elevations in intracellular levels of Ca^{2+} (Bruegmann et al., 2010).

ChR2 has also been used for precise local stimulation in two-dimensional *in vitro* cultures. The ChR2-expressing, ESC-derived cardiomyocytes were plated on multi-electrode arrays, where they formed two-dimensional functional syncytia of synchronously beating cells whose activity could be followed through local field potentials. Evoked electrical activity elicited by pulsed illumination spread to other regions and moving the illumination site correspondingly shifted the initial pacemaker site. Prolonged local illumination suppressed electrical activity in the illuminated area while sparing spontaneous activity in the non-illuminated areas consistent with this producing a sustained depolarization that would cause a local Na^{+} channel refractoriness.

In vivo Electrophysiological Studies of ChR2-Murine Hearts

Illumination of ChR2 expressing cardiomyocytes permits introduction of novel stimulation patterns *in vitro* and *in vivo*, in investigations of physiological mechanisms involved in pacemaking or site-specific pro-arrhythmic effects of prolonged depolarizations and delayed afterdepolarizations. Thus, electrocardiographic studies of focal atrial ChR2 activation with pulsed blue illumination in anesthetized ChR2-EYFP expressing mice led to supraventricular pacing accompanied by prolonged (by ~50%) P-wave durations and PQ intervals (by ~20%) (Bruegmann et al., 2010). Ventricular illumination evoked ventricular extrasystolic beats with a delay of ~9 ms, prolonged QRS durations (by ~ 100%), and alterations in QRS waveforms that varied with the site of stimulation, reflecting action potential initiation at the level of the ventricular cardiomyocyte, rather than *via* the conducting pathways of the heart. An illumination area of 0.05 mm^2 (with a blue light intensity of 7.2 mW mm^{-2}), corresponding to ~50 epicardial myocytes in addition to cardiomyocytes in deeper layers, sufficed to induce pacing, but higher light intensities were required with smaller areas of stimulation. The latencies of electrocardiographic responses *in vivo* were similar to the observed delays from onset of illumination to action potential peak in cardiomyocytes *in vitro* (~10 ms). Finally, prolonged illumination likely leading to long-term ChR2 activation and sustained depolarizations in ventricular regions disturbed the regular pattern of sinus rhythm and generated spontaneous ventricular extra beats.

An alternative *in vivo* approach in genetically wild-type rats utilized adeno-associated virus (AAV) intramyocardial transgene delivery to express the *ChR2* transgene at one or more ventricular sites. Surface electrocardiographic measurements then revealed that focused blue light delivered *via* the optical fiber achieved efficient activation of the ventricle when applied at the apex (the site of ChR2-transgene delivery). It thus altered heart rates from a baseline sinus rhythm (~180 beats/min) to up to 300 beats/min during illumination. This did not occur when illumination was applied to remote myocardial areas in the same hearts or in animals injected with control AAV-CAG-GFP virus. Similar results were obtained in isolated perfused hearts. Other studies have demonstrated that ChR2 stimulation of cardiomyocytes is compatible with the use of long-wavelength voltage-sensitive dyes. These high resolution optical mapping studies confirmed that the ChR2-expressing cardiomyocytes were the source of pacemaker activity by demonstrating a shift in the site of the earliest ventricular activation – from the location of the conventional pacing electrode (at the side of the ventricles) to the site of ChR2-expression (at the apex) (Nussinovitch and Gepstein, 2015).

ANTI-ARRHYTHMIC INTERVENTIONS IN CHR2-MURINE HEARTS

Applications of optogenetic techniques have been explored for their localizable, potentially translationally important, anti-arrhythmic effects (Bingen et al., 2014; Bruegmann et al., 2016, 2018; Crocini et al., 2016; Nyns et al., 2017; Funken et al., 2019). Classical electrical cardioversion including implantable cardioverter defibrillator (ICD) applies generalized electrical discharges to the whole heart without reference to particular re-entrant conduction pathways. Its resulting shocks cause pain, myocardium damage, and chest muscle contractures, with accompanying psychological discomfort. Optical defibrillation has the potential to develop and test bespoke effective therapeutic stimulation using much lower energy. This may need to address challenges such as potentially being less consistent than electrical defibrillation, due to variability in optogenetic expression whether between subjects and within a single heart, concerns about translatability of the required gene therapy to humans. There are also the technical issues relating to heating from and cumbersome nature of the light source and other hardware difficulties.

At the level of *in vitro* cellular preparations, anti-arrhythmic effects of light were explored in neonatal rat atrial cardiomyocyte monolayers transduced with lentiviral vectors encoding light-activated Ca^{2+}-translocating channelrhodopsin (CatCh-eYFP) or with eYFP controls. Light pulses (duration 10 ms, wavelength 470 nm) then triggered action potentials only in the CatCh-expressing cultures. Burst pacing induced spiral waves rotating around functional cores, modeling atrial fibrillation. Optical and multi-electrode array (MEA) mapping assessed effects of prolonged (500 ms) light pulses activating CatCh. These

terminated re-entry in all CatCh-expressing cultures but none of the controls. This took place through a uniform depolarization depressing overall excitability (Bingen et al., 2014).

In adult Wistar rats, systemically delivered cardiotropic adeno-associated virus vectors encoding the red-activatable channelrhodopsin (ReaChR) produced its global cardiac, cardiomyocyte-restricted, and transgene expression. This permitted ReaChR-mediated depolarization and pacing. Ninety-seven percent of ventricular monomorphic and 57% of polymorphic ventricular tachycardias (VT) induced by burst pacing could then be terminated by single 470-nm light pulses (1,000 ms, 2.97 mW/mm^2) in Langendorff perfused hearts. This termination was preceded by prolongation of the action potential (by ~14 ms) and pharmacological interventions that shortened the action potential duration were observed to prevent arrhythmia termination (Nyns et al., 2017).

Epicardial optical stimulation through cardiac-expressed ChR2 also proved effective in terminating ventricular arrhythmias, whether in isolated perfused hearts from ChR2-transgenic or WT mice following adeno-associated virus-based ChR2 gene transfer. Illumination of the anteroseptal epicardium with blue light (470 nm) proved effective whether sustained ventricular arrhythmia was induced by electrical burst stimulation or S1-S2 protocols applied at the right ventricular base under conditions of reduced K^+ (2 mM) and the presence of the K_{ATP} channel activator pinacidil (100 μM). Thus, uniform light-induced depolarization proved effective for cardiac defibrillation. Explorations of light duration, intensity, and size of illuminated area indicated a requirement for illumination lasting for at least the duration of an entire VT cycle (~80 ms), over an area > 15 mm^2, and of intensity ~0.4–1 mW/mm^2, suggesting a requirement for a depolarization of a critical portion of myocardium. Such findings extended to experimental infarct-related ST-elevation associated arrhythmia, following left anterior descending coronary artery ligation. Sustained ventricular arrhythmia following forced electrical pacing was terminated by a single light pulse. Concordant findings emerged from WT hearts after adeno-associated virus induced ChR2 gene transfer (Bruegmann et al., 2016).

Further optogenetic and imaging techniques simultaneously mapped and controlled electrical activity in intact ChR2-expressing transgenic mouse hearts made to show monomorphic VTs with spatially demonstrable slowed re-entrant conduction. Application of spatially defined stimulation patterns demonstrated that in contrast to a *single point* and *single line* stimulation, triple-line pattern optical stimulation at 10 mW/mm^2 successfully achieved cardioversion, doing so while confining the irradiated epicardium with a reduction of total irradiation energy (0.25 and 1 mJ, respectively) (Crocini et al., 2016).

Optogenetic techniques also proved experimentally effective in termination of atrial tachyarrhythmias in intact *ex* and *in vivo* hearts from transgenic and wild-type mice, respectively. Isolated ChR2 and pro-arrhythmic connexin 40, Cx-40-Ala96Ser expressing murine hearts perfused with low K^+-Tyrode's solution and an atrial K_{ATP}-channel activator showed a pro-arrhythmic shortened atrial refractoriness and slowed atrial conduction. Atrial arrhythmia was terminated using epicardially focused blue light (470 nm, 0.4 mW/mm^2) likely acting by light-induced block of electrical activity. This optical effect was reproduced in wild-type mice made to express ChR2 *via* adeno-associated virus (AAV) delivery (Bruegmann et al., 2018).

Finally, optogenetic methods permitted explorations of temporally and spatially controlled cell type selective induction of hyperpolarization as an approach to ventricular arrhythmia termination. These utilized mice with a cardiomyocyte-specific expression of the light-driven proton pump ArchT. The isolated cardiomyocytes showed light-induced outward currents causing membrane hyperpolarization. Isolated perfused hearts in which ventricular arrhythmias were induced by electrical stimulation under conditions of low [K^+] and pinacidil showed a significant incidence of cardioversion upon illumination. *In situ* sharp electrode intracellular recordings showed an accompanying cardiomyocyte hyperpolarization. However, enhanced action potential upstroke rates upon illumination were accompanied by slowed conduction. Thus, the observed anti-arrhythmic effects might arise from accompanying increased electrical sink currents, suggestive of novel mechanisms by which the observed cardioversion took place. Such hypotheses might prompt further investigation and their possible application (Funken et al., 2019).

COMPUTATIONAL ANALYSES OF PRO- AND ANTI-ARRHYTHMIC INTERVENTIONS USING CHR2-MURINE HEARTS

Computational studies have assessed the efficacy of optogenetic termination of both atrial tachycardia (AT) and VT through targeting specific cardiac regions if this was applied to human hearts. One study attempted to terminate re-entrant AT following rapid pacing by optogenetic stimulation of channelrhodopsin-2 (ChR2) expressed through gene delivery. This employed three patient-specific computational models reconstructed from late gadolinium-enhanced MRI scans (Boyle et al., 2018b). It compared efficacies of distributed endocardial illumination by multi-optrode grids and targeted illumination of the identified critical isthmus. The latter involved considerably smaller illuminated areas and input powers. AT termination rates for distributed illumination were low (<5% for short, 1/10 ms and ~20% for longer, 100/1,000 ms pulses). Targeted illumination similarly achieved low outcomes for short (0% for 1/10 ms) pulses, but significantly better outcomes for longer stimuli (100 ms: 54% success; 1,000 ms: 90% success), exceeding the AT cycle length. Thus, targeted optogenetic stimulation based on analysis of AT morphology is a potential approach to atrial defibrillation. A computational exploration of optogenetic defibrillation for modeling infarct-related human VT suggested that red light illumination could terminate tachycardic episodes in diseased, ChR2-expressing hearts. This appeared to involve ChR2-mediated transmural depolarization of the myocardium inactivating voltage-dependent Na^+ channels in cardiomyocytes through the ventricular myocardial wall interrupting wavefront propagation (Bruegmann et al., 2016).

TRANSLATIONAL IMPLICATIONS OF OPTICAL PACING

Optogenetics offers potential alternatives to drug or electrotherapy for treating arrhythmia. Drug therapy for atrial fibrillation can have serious side effects even including proarrhythmic effects. Patients at risk from potentially fatal ventricular arrhythmias currently receive implantable defibrillators delivering electrical shocks terminating arrhythmias on demand. However, such electrical shock therapy is associated with discomfort and tissue damage.

Optical pacing is compatible with energy requirements that compare favorably with electric pacing and optical fibers may be more biocompatible than electrodes. Optical pacing could potentially simultaneously pace multiple sites with advantages for cardiac resynchronization therapy over biventricular electrical pacemakers (McAlister et al., 2007). Hypothetically, forced expression and subsequent activation of light-gated cation channels in cardiomyocytes might deliver a depolarizing force sufficient for atrial or ventricular defibrillation. There is also the possibility of utilizing optogenetic proteins generating hyperpolarizing current such as halorhodopsin or archaerhodopsin. Prolonged illumination producing sustained depolarization or hyperpolarization may successfully interrupt re-entrant electric activity thereby terminating arrhythmias. As indicated above, constant illumination of ChR2-expressing cardiomyocytes prolongs depolarization and refractoriness electrically silencing the illuminated areas (Bruegmann et al., 2010). However, such optogenetic approaches will require introduction of the ChR2 or other optogenetic probes either by a TCU approach (Jia et al., 2011) or through direct ChR2 cardiomyocyte expression (Bruegmann et al., 2010). They will involve establishing effective pacing strategies and stable pacemaker function without cell rejection or tumor formation. The clinical use of optical pacing may still be a distant prospect as it will need to establish superiority over existing implantable devices and surmounting technical challenges attached to using cardiac optogenetics *in vivo* (Sasse, 2011).

CONCLUSIONS

In conclusion, the use of optogenetics in cardiology research has greatly accelerated over the last decade since the technique was first demonstrated as a proof of principle in zebrafish and mouse cardiomyocytes (Arrenberg et al., 2010; Bruegmann et al., 2010). The versatility of different optogenetic tools now allows extensive modulation of the morphology, direction, duration, and location of cellular membrane potential responses, and cardiac computational modeling will be important for developing and testing hypotheses regarding the impact of these different types of stimulation on the cardiac cycle (Boyle et al., 2013; Entcheva and Bub, 2016). Features of optogenetic tools, such as their versatility, bidirectionality, and high temporal, spatial and genetic precision confer a number of advantages over traditional electrical stimulation techniques. They also lend themselves to all-optical read-in/read-out experimental approaches, to allow modulation and monitoring of large numbers of individual cells in a minimally invasive manner. To date, these approaches have been applied to single myocardial cells and cell pairs, myocardial monolayers in culture, *ex vivo* Langendorff perfused hearts as well as *in vivo* hearts under anesthesia. Experiments have addressed fundamental questions about the physiology of the cardiac action potential and the spread of electrical activity across the heart as well as disease-focused questions such as mechanisms of arrhythmia initiation, propagation, and termination.

Ongoing work that will be shared with the neuroscience community will be the continued development and expansion of the optogenetic tool kit, and major goals include the development of red-shifted opsin that lacks a shoulder in the blue end of the spectrum and a single-component light activated potassium channel.

Future cardiac directions will need to focus on further optimization of optogenetic tools specifically for myocardial cells such as modification of kinetics of depolarization/hyperpolarization to better suit the cardiac action potential and modulation of specific ion permeability to minimize off-target effects of non-physiologic changes in intracellular ion concentration. Other work will need to focus on improving genetic methods to specifically target different myocardial cell types and improving engineering approaches to permit chronic *in vivo* light delivery with flexible illumination patterns and its combination with read out methods such as optical recordings for closed-loop stimulation paradigms. Improvements in optoelectronic device engineering with low power LED arrays for long-duration, multi-site stimulation, closed loop sensing and implantable or injectable flexible electronics that can mold to and adapt with the mobile myocardium will be necessary for cardiac optogenetics to become relevant for clinical applications. Finally, basic science and translational applications will continue to expand, for example, to include investigation of not only cellular but also subcellular mechanisms underlying myocardial excitability, contractility, rhythm generation and spread, in physiological as well as pathological states.

AUTHOR CONTRIBUTIONS

All three authors contributed to this review as a whole, with EF leading on the sections covering the principles and techniques bearing on optogenetic methods and XT and CH those aspects bearing on their cardiac application. Repeated revisions of the text were performed by EF and CH.

FUNDING

Our work is funded by the Medical Research Council (MR/M001288/1), Wellcome Trust (105727/Z/14/Z), the British Heart Foundation (BHF) (PG/14/79/31102 and PG/15/12/31280), the BHF Centres of Research Excellent at Oxford and Cambridge (UK), and the Nature Science Foundation (grant no. 81670310) (China).

REFERENCES

Abilez, O. (2012). Cardiac optogenetics. In 34th Annual International Conference of the IEEE EMBS (San Diego, California), pp. 1386–1389.

Airan, R. D., Thompson, K. R., Fenno, L. E., Bernstein, H., and Deisseroth, K. (2009). Temporally precise in vivo control of intracellular signalling. *Nature* 458, 1025–1029. doi: 10.1038/nature07926

Alberio, L., Locarno, A., Saponaro, A., Romano, E., Bercier, V., Albadri, S., et al. (2018). A light-gated potassium channel for sustained neuronal inhibition. *Nat. Methods* 15, 969–976. doi: 10.1038/s41592-018-0186-9

Ambrosi, C. M., Boyle, P. M., Chen, K., Trayanova, N. A., and Entcheva, E. (2015). Optogenetics-enabled assessment of viral gene and cell therapy for restoration of cardiac excitability. *Sci. Rep.* 5:17350. doi: 10.1038/srep17350

Ambrosi, C. M., Klimas, A., Yu, J., and Entcheva, E. (2014). Cardiac applications of optogenetics. *Prog. Biophys. Mol. Biol.* 115, 294–304. doi: 10.1016/j.pbiomolbio.2014.07.001

Arrenberg, A. B., Stainier, D. Y. R., Baier, H., and Huisken, S. E. (2010). Optogenetic control of cardiac function. *Science* 330, 971–974. doi: 10.1126/science.1195929

Ayub, S., Ruther, P., Paul, O., Kohl, P., and Zgierski-Johnston, C. M. (2018). Invasive optical pacing in perfused, optogenetically modified mouse heart using stiff multi-LED optical probes. In Proceedings of the Annual International Conference of the IEEE Engineering in Medicine and Biology Society, EMBS, pp. 1–4.

Beiert, T., Bruegmann, T., and Sasse, P. (2014). Optogenetic activation of Gq signalling modulates pacemaker activity of cardiomyocytes. *Cardiovasc. Res.* 102, 507–516. doi: 10.1093/cvr/cvu046

Bernal Sierra, Y. A., Rost, B. R., Pofahl, M., Fernandes, A. M., Kopton, R. A., Moser, S., et al. (2018). Potassium channel-based optogenetic silencing. *Nat. Commun.* 9:4611. doi: 10.1038/s41467-018-07038-8

Berndt, A., and Deisseroth, K. (2015). Expanding the optogenetics toolkit. *Science* 349, 590–591. doi: 10.1126/science.aac7889

Berndt, A., Lee, S. Y., Wietek, J., Ramakrishnan, C., Steinberg, E. E., Rashid, A. J., et al. (2016). Structural foundations of optogenetics: determinants of channelrhodopsin ion selectivity. *Proc. Natl. Acad. Sci. USA* 113, 822–829. doi: 10.1073/pnas.1523341113

Berndt, A., Schoenenberger, P., Mattis, J., Tye, K. M., Deisseroth, K., Hegemann, P., et al. (2011). High-efficiency channelrhodopsins for fast neuronal stimulation at low light levels. *Proc. Natl. Acad. Sci. USA* 108, 7595–7600. doi: 10.1073/pnas.1017210108

Berndt, A., Yizhar, O., Gunaydin, L. A., Hegemann, P., and Deisseroth, K. (2009). Bi-stable neural state switches. *Nat. Neurosci.* 12, 229–234. doi: 10.1038/nn.2247

Bingen, B. O., Engels, M. C., Schalij, M. J., Jangsangthong, W., Neshati, Z., Feola, I., et al. (2014). Light-induced termination of spiral wave arrhythmias by optogenetic engineering of atrial cardiomyocytes. *Cardiovasc. Res.* 104, 194–205. doi: 10.1093/cvr/cvu179

Boyden, E. S., Zhang, F., Bamberg, E., Nagel, G., and Deisseroth, K. (2005). Millisecond-timescale, genetically targeted optical control of neural activity. *Nat. Neurosci.* 8, 1263–1268. doi: 10.1038/nn1525

Boyle, P. M., Karathanos, T. V., and Trayanova, N. A. (2015). "Beauty is a light in the heart": the transformative potential of optogenetics for clinical applications in cardiovascular medicine1. *Trends Cardiovasc. Med.* 25, 73–81. doi: 10.1016/j.tcm.2014.10.004

Boyle, P. M., Karathanos, T. V., and Trayanova, N. A. (2018a). Cardiac optogenetics: 2018. *JACC Clin. Electrophysiol.* 4, 155–167. doi: 10.1016/j.jacep.2017.12.006

Boyle, P. M., Murphy, M. J., Karathanos, T. V., Zahid, S., Blake, R. C., and Trayanova, N. A. (2018b). Termination of re-entrant atrial tachycardia via optogenetic stimulation with optimized spatial targeting: insights from computational models: optogenetic termination of atrial arrhythmia. *J. Physiol.* 596, 181–196. doi: 10.1113/jp275264

Boyle, P. M., Williams, J. C., Ambrosi, C. M., Entcheva, E., and Trayanova, N. A. (2013). A comprehensive multiscale framework for simulating optogenetics in the heart. *Nat. Commun.* 4:2370. doi: 10.1038/ncomms3370

Broyles, C., Robinson, P., and Daniels, M. (2018). Fluorescent, bioluminescent, and optogenetic approaches to study excitable physiology in the single cardiomyocyte. *Cell* 7:E51. doi: 10.3390/cells7060051

Bruegmann, T., Beiert, T., Vogt, C. C., Schrickel, J. W., and Sasse, P. (2018). Optogenetic termination of atrial fibrillation in mice. *Cardiovasc. Res.* 114, 713–723. doi: 10.1093/cvr/cvx250

Bruegmann, T., Boyle, P. M., Vogt, C. C., Karathanos, T. V., Arevalo, H. J., Fleischmann, B. K., et al. (2016). Optogenetic defibrillation terminates ventricular arrhythmia in mouse hearts and human simulations. *J. Clin. Invest.* 126, 3894–3904. doi: 10.1172/JCI88950

Bruegmann, T., Malan, D., Hesse, M., Beiert, T., Fuegemann, C. J., Fleischmann, B. K., et al. (2010). Optogenetic control of heart muscle in vitro and in vivo. *Nat. Methods* 7, 897–900. doi: 10.1038/nmeth.1512

Burton, R. A. B., Klimas, A., Ambrosi, C. M., Tomek, J., Corbett, A., Entcheva, E., et al. (2015). Optical control of excitation waves in cardiac tissue. *Nat. Photonics* 9, 813–816. doi: 10.1038/nphoton.2015.196

Carrillo-Reid, L., Yang, W., Kang Miller, J., Peterka, D. S., and Yuste, R. (2017). Imaging and optically manipulating neuronal ensembles. *Annu. Rev. Biophys.* 46, 271–293. doi: 10.1146/annurev-biophys-070816-033647

Chang, Y.-F., Broyles, C. N., Brook, F. A., Davies, M. J., Turtle, C. W., Nagai, T., et al. (2017). Non-invasive phenotyping and drug testing in single cardiomyocytes or beta-cells by calcium imaging and optogenetics. *PLoS One* 12:e0174181. doi: 10.1371/journal.pone.0174181

Chow, B. Y., Han, X., Dobry, A. S., Qian, X., Chuong, A. S., Li, M., et al. (2010). High-performance genetically targetable optical neural silencing by light-driven proton pumps. *Nature* 463, 98–102. doi: 10.1038/nature08652

Crocini, C., Ferrantini, C., Coppini, R., Scardigli, M., Yan, P., Loew, L. M., et al. (2016). Optogenetics design of mechanistically-based stimulation patterns for cardiac defibrillation. *Sci. Rep.* 6:35628. doi: 10.1038/srep35628

Dana, H., Mohar, B., Sun, Y., Narayan, S., Gordus, A., Hasseman, J. P., et al. (2016). Sensitive red protein calcium indicators for imaging neural activity. *elife* 5:e12727. doi: 10.7554/eLife.12727

Deisseroth, K. (2015). Optogenetics: 10 years of microbial opsins in neuroscience. *Nat. Neurosci.* 18, 1213–1225. doi: 10.1038/nn.4091

Deisseroth, K., and Hegemann, P. (2017). The form and function of channelrhodopsin. *Science* 357:eaan5544. doi: 10.1126/science.aan5544

Deo, C., and Lavis, L. D. (2018). Synthetic and genetically encoded fluorescent neural activity indicators. *Curr. Opin. Neurobiol.* 50, 101–108. doi: 10.1016/j.conb.2018.01.003

Entcheva, E. (2013). Cardiac optogenetics. *Am. J. Physiol. Heart Circ. Physiol.* 304, H1179–H1191. doi: 10.1152/ajpheart.00432.2012

Entcheva, E., and Bub, G. (2016). All-optical control of cardiac excitation: combined high-resolution optogenetic actuation and optical mapping: all-optical control of cardiac excitation. *J. Physiol.* 594, 2503–2510. doi: 10.1113/JP271559

Feola, I., Volkers, L., Majumder, R., Teplenin, A., Schalij, M. J., Panfilov, A. V., et al. (2017). Localized optogenetic targeting of rotors in atrial cardiomyocyte monolayers. *Circ. Arrhythm. Electrophysiol.* 10, pii: e005591. doi: 10.1161/CIRCEP.117.005591

Ferenczi, E., and Deisseroth, K. (2012). When the electricity (and the lights) go out: transient changes in excitability. *Nat. Neurosci.* 15, 1058–1060. doi: 10.1038/nn.3172

Ferenczi, E. A., Zalocusky, K. A., Liston, C., Grosenick, L., Warden, M. R., Amatya, D., et al. (2016). Prefrontal cortical regulation of brainwide circuit dynamics and reward-related behavior. *Science* 351, aac9698–aac9698. doi: 10.1126/science.aac9698

Forli, A., Vecchia, D., Binini, N., Succol, F., Bovetti, S., Moretti, C., et al. (2018). Two-photon bidirectional control and imaging of neuronal excitability with high spatial resolution in vivo. *Cell Rep.* 22, 3087–3098. doi: 10.1016/j.celrep.2018.02.063

Funken, M., Malan, D., Sasse, P., and Bruegmann, T. (2019). Optogenetic hyperpolarization of cardiomyocytes terminates ventricular arrhythmia. *Front. Physiol.* 10:498. doi: 10.3389/fphys.2019.00498

Gong, Y., Li, J. Z., and Schnitzer, M. J. (2013). Enhanced Archaerhodopsin fluorescent protein voltage indicators. *PLoS One* 8:e66959. doi: 10.1371/journal.pone.0066959

Govorunova, E. G., Cunha, S. R., Sineshchekov, O. A., and Spudich, J. L. (2016). Anion channelrhodopsins for inhibitory cardiac optogenetics. *Sci. Rep.* 6:33530. doi: 10.1038/srep33530

Govorunova, E. G., Sineshchekov, O. A., Janz, R., Liu, X., and Spudich, J. L. (2015). Natural light-gated anion channels: a family of microbial rhodopsins for advanced optogenetics. *Science* 349, 647–650. doi: 10.1126/science.aaa7484

Govorunova, E. G., Sineshchekov, O. A., Li, H., Janz, R., and Spudich, J. L. (2013). Characterization of a highly efficient blue-shifted channelrhodopsin from the marine alga *Platymonas subcordiformis*. *J. Biol. Chem.* 288, 29911–29922. doi: 10.1074/jbc.M113.505495

Gradinaru, V., Thompson, K. R., and Deisseroth, K. (2008). eNpHR: a natronomonas halorhodopsin enhanced for optogenetic applications. *Brain Cell Biol.* 36, 129–139. doi: 10.1007/s11068-008-9027-6

Gunaydin, L. A., Yizhar, O., Berndt, A., Sohal, V. S., Deisseroth, K., and Hegemann, P. (2010). Ultrafast optogenetic control. *Nat. Neurosci.* 13, 387–392. doi: 10.1038/nn.2495

Gupta, N., Bansal, H., and Roy, S. (2019). Theoretical optimization of high-frequency optogenetic spiking of red-shifted very fast-Chrimson-expressing neurons. *Neurophotonics* 6:025002. doi: 10.1117/1.NPh.6.2.025002.E

Han, X., and Boyden, E. S. (2007). Multiple-color optical activation, silencing, and desynchronization of neural activity, with single-spike temporal resolution. *PLoS One* 2:e299. doi: 10.1371/journal.pone.0000299

Harada, K., Ito, M., Wang, X., Tanaka, M., Wongso, D., Konno, A., et al. (2017). Red fluorescent protein-based cAMP indicator applicable to optogenetics and in vivo imaging. *Sci. Rep.* 7:7351. doi: 10.1038/s41598-017-07820-6

Hegemann, P., and Nagel, G. (2013). From channelrhodopsins to optogenetics: from channelrhodopsins to optogenetics. *EMBO Mol. Med.* 5, 173–176. doi: 10.1002/emmm.201202387

Hiraoka, M. (1998). Role of cardiac chloride currents in changes in action potential characteristics and arrhythmias. *Cardiovasc. Res.* 40, 23–33. doi: 10.1016/S0008-6363(98)00173-4

Hochbaum, D., Zhao, Y., Farhi, S., Klapoetke, N., Werley, C., Kapoor, V., et al. (2014). All-optical electrophysiology in mammalian neurons using engineered microbial rhodopsins. *Nat. Methods* 11, 825–833. doi: 10.1038/nmeth.3000

Hofmann, B., Maybeck, V., Eick, S., Meffert, S., Ingebrandt, S., Wood, P., et al. (2010). Light induced stimulation and delay of cardiac activity. *Lab Chip* 10, 2588–2596. doi: 10.1039/c003091k

Hulsmans, M., Clauss, S., Xiao, L., Aguirre, A. D., King, K. R., Hanley, A., et al. (2017). Macrophages facilitate electrical conduction in the heart. *Cell* 169, 510–522.e20. doi: 10.1016/j.cell.2017.03.050

Inagaki, K., Fuess, S., Storm, T. A., Gibson, G. A., McTiernan, C. F., Kay, M. A., et al. (2006). Robust systemic transduction with AAV9 vectors in mice: efficient global cardiac gene transfer superior to that of AAV8. *Mol. Ther.* 14, 45–53. doi: 10.1016/j.ymthe.2006.03.014

Jia, Z., Valiunas, V., Lu, Z., Bien, H., Liu, H., Wang, H.-Z., et al. (2011). Stimulating cardiac muscle by light: cardiac optogenetics by cell delivery. *Circ. Arrhythm. Electrophysiol.* 4, 753–760. doi: 10.1161/CIRCEP.111.964247

Johnston, C. M., Rog-Zielinska, E. A., Wülfers, E. M., Houwaart, T., Siedlecka, U., Naumann, A., et al. (2017). Optogenetic targeting of cardiac myocytes and non-myocytes: tools, challenges and utility. *Prog. Biophys. Mol. Biol.* 130, 140–149. doi: 10.1016/j.pbiomolbio.2017.09.014

Kato, H. E., Kim, Y. S., Paggi, J. M., Evans, K. E., Allen, W. E., Richardson, C., et al. (2018). Structural mechanisms of selectivity and gating in anion channelrhodopsins. *Nature* 561, 349–354. doi: 10.1038/s41586-018-0504-5

Kato, H. E., Zhang, F., Yizhar, O., Ramakrishnan, C., Nishizawa, T., Hirata, K., et al. (2012). Crystal structure of the channelrhodopsin light-gated cation channel. *Nature* 482, 369–374. doi: 10.1038/nature10870

Kim, Y. S., Kato, H. E., Yamashita, K., Ito, S., Inoue, K., Ramakrishnan, C., et al. (2018). Crystal structure of the natural anion-conducting channelrhodopsin GtACR1. *Nature* 561, 343–348. doi: 10.1038/s41586-018-0511-6

Kim, T., McCall, J. G., Jung, Y. H., Huang, X., Siuda, E. R., Li, Y., et al. (2013). Injectable, cellular-scale optoelectronics with applications for wireless optogenetics. *Science* 340, 211–216. doi: 10.1126/science.1232437

Klapoetke, N. C., Murata, Y., Kim, S. S., Pulver, S. R., Birdsey-Benson, A., Cho, Y. K., et al. (2014). Independent optical excitation of distinct neural populations. *Nat. Methods* 11, 338–346. doi: 10.1038/nmeth.2836

Kleinlogel, S., Feldbauer, K., Dempski, R. E., Fotis, H., Wood, P. G., Bamann, C., et al. (2011). Ultra light-sensitive and fast neuronal activation with the Ca2+-permeable channelrhodopsin CatCh. *Nat. Neurosci.* 14, 513–518. doi: 10.1038/nn.2776

Koizumi, A., Tanaka, K. F., and Yamanaka, A. (2013). The manipulation of neural and cellular activities by ectopic expression of melanopsin. *Neurosci. Res.* 75, 3–5. doi: 10.1016/j.neures.2012.07.010

Koopman, C. D., Zimmermann, W. H., Knöpfel, T., and de Boer, T. P. (2017). Cardiac optogenetics: using light to monitor cardiac physiology. *Basic Res. Cardiol.* 112:56. doi: 10.1007/s00395-017-0645-y

Kopton, R. A., Baillie, J. S., Rafferty, S. A., Moss, R., Zgierski-Johnston, C. M., Prykhozhij, S. V., et al. (2018). Cardiac electrophysiological effects of light-activated chloride channels. *Front. Physiol.* 9:1806. doi: 10.3389/fphys.2018.01806

Kopton, R., Rog-Zielinska, E., Siedlecka, U., Wietek, J., Hegemann, P., Kohl, P., et al. (2017). Optogenetic modulation of cardiomyocyte excitability. *Biophys. J.* 112:424a. doi: 10.1016/j.bpj.2016.11.2268

Kralj, J. M., Douglass, A. D., Hochbaum, D. R., Maclaurin, D., and Cohen, A. E. (2012). Optical recording of action potentials in mammalian neurons using a microbial rhodopsin. *Nat. Methods* 9, 90–95. doi: 10.1038/nmeth.1782

Liao, M. L. C., De Boer, T. P., Mutoh, H., Raad, N., Richter, C., Wagner, E., et al. (2015). Sensing cardiac electrical activity with a cardiac myocyte-targeted optogenetic voltage indicator. *Circ. Res.* 117, 401–412. doi: 10.1161/CIRCRESAHA.117.306143

Lin, J. Y., Knutsen, P. M., Muller, A., Kleinfeld, D., and Tsien, R. Y. (2013). ReaChR: a red-shifted variant of channelrhodopsin enables deep transcranial optogenetic excitation. *Nat. Neurosci.* 16, 1499–1508. doi: 10.1038/nn.3502

Liu, J., Fu, T.-M., Cheng, Z., Hong, G., Zhou, T., Jin, L., et al. (2015). Syringe-injectable electronics. *Nat. Nanotechnol.* 10, 629–636. doi: 10.1038/nnano.2015.115

Maclaurin, D., Venkatachalam, V., Lee, H., and Cohen, A. E. (2013). Mechanism of voltage-sensitive fluorescence in a microbial rhodopsin. *Proc. Natl. Acad. Sci. USA* 110, 5939–5944. doi: 10.1073/pnas.1215595110

Mahn, M., Gibor, L., Patil, P., Cohen-Kashi Malina, K., Oring, S., Printz, Y., et al. (2018). High-efficiency optogenetic silencing with soma-targeted anion-conducting channelrhodopsins. *Nat. Commun.* 9:4125. doi: 10.1038/s41467-018-06511-8

Makowka, P., Bruegmann, T., Dusend, V., Malan, D., Beiert, T., Hesse, M., et al. (2019). Optogenetic stimulation of G_s -signaling in the heart with high spatio-temporal precision. *Nat. Commun.* 10:1281. doi: 10.1038/s41467-019-09322-7

Mattis, J., Tye, K. M., Ferenczi, E. A., Ramakrishnan, C., O'Shea, D. J., Prakash, R., et al. (2011). Principles for applying optogenetic tools derived from direct comparative analysis of microbial opsins. *Nat. Methods* 9, 159–172. doi: 10.1038/nmeth.1808

McAlister, F. A., Ezekowitz, J., Hooton, N., Vandermeer, B., Spooner, C., Dryden, D. M., et al. (2007). Cardiac resynchronization therapy for patients with left ventricular systolic dysfunction: a systematic review. *JAMA* 297, 2502–2514. doi: 10.1001/jama.297.22.2502

McGregor, K. M., Bécamel, C., Marin, P., and Andrade, R. (2016). Using melanopsin to study G protein signaling in cortical neurons. *J. Neurophysiol.* 116, 1082–1092. doi: 10.1152/jn.00406.2016

Mickle, A. D., Won, S. M., Noh, K. N., Yoon, J., Meacham, K. W., Xue, Y., et al. (2019). A wireless closed-loop system for optogenetic peripheral neuromodulation. *Nature* 565, 361–365. doi: 10.1038/s41586-018-0823-6

Moreno, A., Endicott, K., Skancke, M., Dwyer, M. K., Brennan, J., Efimov, I. R., et al. (2019). Sudden heart rate reduction upon optogenetic release of acetylcholine from cardiac parasympathetic neurons in perfused hearts. *Front. Physiol.* 10:16. doi: 10.3389/fphys.2019.00016

Nagel, G., Brauner, M., Liewald, J. F., Adeishvili, N., Bamberg, E., and Gottschalk, A. (2005). Light activation of channelrhodopsin-2 in excitable cells of *Caenorhabditis elegans* triggers rapid behavioral responses. *Curr. Biol.* 15, 2279–2284. doi: 10.1016/j.cub.2005.11.032

Nussinovitch, U., and Gepstein, L. (2015). Optogenetics for in vivo cardiac pacing and resynchronization therapies. *Nat. Biotechnol.* 33, 750–754. doi: 10.1038/nbt.3268

Nussinovitch, U., Shinnawi, R., and Gepstein, L. (2014). Modulation of cardiac tissue electrophysiological properties with light-sensitive proteins. *Cardiovasc. Res.* 102, 176–187. doi: 10.1093/cvr/cvu037

Nyns, E. C. A., Kip, A., Bart, C. I., Plomp, J. J., Zeppenfeld, K., Schalij, M. J., et al. (2017). Optogenetic termination of ventricular arrhythmias in the whole heart: towards biological cardiac rhythm management. *Eur. Heart J.* 38, 2132–2136. doi: 10.1093/eurheartj/ehw574

O'Shea, C., Holmes, A. P., Winter, J., Correia, J., Ou, X., Dong, R., et al. (2019). Cardiac optogenetics and optical mapping – overcoming spectral congestion in all-optical cardiac electrophysiology. *Front. Physiol.* 10:182. doi: 10.3389/fphys.2019.00182

Oda, K., Vierock, J., Oishi, S., Rodriguez-Rozada, S., Taniguchi, R., Yamashita, K., et al. (2018). Crystal structure of the red light-activated channelrhodopsin Chrimson. *Nat. Commun.* 9:3949. doi: 10.1038/s41467-018-06421-9

Pacak, C. A., Mah, C. S., Thattaliyath, B. D., Conlon, T. J., Lewis, M. A., Cloutier, D. E., et al. (2006). Recombinant adeno-associated virus serotype

9 leads to preferential cardiac transduction in vivo. *Circ. Res.* 99, e3–e9. doi: 10.1161/01.RES.0000237661.18885.f6

Packer, A. M., Peterka, D. S., Hirtz, J. J., Prakash, R., Deisseroth, K., and Yuste, R. (2012). Two-photon optogenetics of dendritic spines and neural circuits. *Nat. Methods* 9, 1202–1205. doi: 10.1038/nmeth.2249

Packer, A. M., Russell, L. E., Dalgleish, H. W. P., and Häusser, M. (2015). Simultaneous all-optical manipulation and recording of neural circuit activity with cellular resolution in vivo. *Nat. Methods* 12, 140–146. doi: 10.1038/nmeth.3217

Park, S. A., Lee, S.-R., Tung, L., and Yue, D. T. (2015b). Optical mapping of optogenetically shaped cardiac action potentials. *Sci. Rep.* 4:6125. doi: 10.1038/srep06125

Park, S. I. L., Chung, H. U., Sundaram, S. S., Vogt, S. K., Samineni, V. K., Montana, M. C., et al. (2015a). Soft, stretchable, fully implantable miniaturized optoelectronic systems for wireless optogenetics. *Nat. Biotechnol.* 33, 1280–1286. doi: 10.1038/nbt.3415

Prakash, R., Yizhar, O., Grewe, B., Ramakrishnan, C., Wang, N., Goshen, I., et al. (2012). Two-photon optogenetic toolbox for fast inhibition, excitation and bistable modulation. *Nat. Methods* 9, 1171–1179. doi: 10.1038/nmeth.2215

Prando, V., Da Broi, F., Franzoso, M., Plazzo, A. P., Pianca, N., Francolini, M., et al. (2018). Dynamics of neuroeffector coupling at cardiac sympathetic synapses. *J. Physiol.* 596, 2055–2075. doi: 10.1113/JP275693

Qian, Y., Piatkevich, K. D., McLarney, B., Abdelfattah, A. S., Mehta, S., Murdock, M. H., et al. (2019). A genetically encoded near-infrared fluorescent calcium ion indicator. *Nat. Methods* 16, 171–174. doi: 10.1038/s41592-018-0294-6

Quinn, T. A., Camelliti, P., Rog-Zielinska, E. A., Siedlecka, U., Poggioli, T., O'Toole, E. T., et al. (2016). Electrotonic coupling of excitable and nonexcitable cells in the heart revealed by optogenetics. *Proc. Natl. Acad. Sci. USA* 113, 14852–14857. doi: 10.1073/pnas.1611184114

Rickgauer, J. P., and Tank, D. W. (2009). Two-photon excitation of channelrhodopsin-2 at saturation. *Proc. Natl. Acad. Sci. USA* 106, 15025–15030. doi: 10.1073/pnas.0907084106

Ronzitti, E., Conti, R., Zampini, V., Tanese, D., Foust, A. J., Klapoetke, N., et al. (2017). Submillisecond optogenetic control of neuronal firing with two-photon holographic photoactivation of Chronos. *J. Neurosci.* 37, 10679–10689. doi: 10.1523/JNEUROSCI.1246-17.2017

Salama, G., Choi, B. R., Azour, G., Lavasani, M., Tumbev, V., Salzberg, B. M., et al. (2005). Properties of new, long-wavelength, voltage-sensitive dyes in the heart. *J. Membr. Biol.* 208, 125–140. doi: 10.1007/s00232-005-0826-8

Sasse, P. (2011). Optical pacing of the heart: the long way to enlightenment. *Circ. Arrhythm. Electrophysiol.* 4, 598–600. doi: 10.1161/CIRCEP.111.965400

Scardigli, M., Müllenbroich, C., Margoni, E., Cannazzaro, S., Crocini, C., Ferrantini, C., et al. (2018). Real-time optical manipulation of cardiac conduction in intact hearts: real-time optical manipulation of cardiac conduction. *J. Physiol.* 596, 3841–3858. doi: 10.1113/JP276283

Shang, W., Lu, F., Sun, T., Xu, J., Li, L.-L., Wang, Y., et al. (2014). Imaging Ca^{2+} nanosparks in heart with a new targeted biosensor. *Circ. Res.* 114, 412–420. doi: 10.1161/CIRCRESAHA.114.302938

Siuda, E. R., Copits, B. A., Schmidt, M. J., Baird, M. A., Al-Hasani, R., Planer, W. J., et al. (2015). Spatiotemporal control of opioid signaling and behavior. *Neuron* 86, 923–935. doi: 10.1016/j.neuron.2015.03.066

Spangler, S. M., and Bruchas, M. R. (2017). Optogenetic approaches for dissecting neuromodulation and GPCR signaling in neural circuits. *Curr. Opin. Pharmacol.* 32, 56–70. doi: 10.1016/j.coph.2016.11.001

Steinmetz, N. A., Buetfering, C., Lecoq, J., Lee, C. R., Peters, A. J., Jacobs, E. A. K., et al. (2017). Aberrant cortical activity in multiple GCaMP6-expressing transgenic mouse lines. *Eneuro* 4:ENEURO.0207-17.2017. doi: 10.1523/ENEURO.0207-17.2017

Steinmetz, N. A., Koch, C., Harris, K. D., and Carandini, M. (2018). Challenges and opportunities for large-scale electrophysiology with Neuropixels probes. *Curr. Opin. Neurobiol.* 50, 92–100. doi: 10.1016/j.conb.2018.01.009

Sudo, Y., Okazaki, A., Ono, H., Yagasaki, J., Sugo, S., Kamiya, M., et al. (2013). A blue-shifted light-driven proton pump for neural silencing. *J. Biol. Chem.* 288, 20624–20632. doi: 10.1074/jbc.M113.475533

Tallini, Y. N., Ohkura, M., Choi, B.-R., Ji, G., Imoto, K., Doran, R., et al. (2006). Imaging cellular signals in the heart in vivo: cardiac expression of the high-signal Ca^{2+} indicator GCaMP2. *Proc. Natl. Acad. Sci. USA* 103, 4753–4758. doi: 10.1073/pnas.0509378103

Tsunoda, S. P., Prigge, M., Abe-Yoshizumi, R., Inoue, K., Kozaki, Y., Ishizuka, T., et al. (2017). Functional characterization of sodium-pumping rhodopsins with different pumping properties. *PLoS One* 12:e0179232. doi: 10.1371/journal.pone.0179232

van Wyk, M., Pielecka-Fortuna, J., Löwel, S., and Kleinlogel, S. (2015). Restoring the ON switch in blind retinas: opto-mGluR6, a next-generation, cell-tailored optogenetic tool. *PLoS Biol.* 13:e1002143. doi: 10.1371/journal.pbio.1002143

Venkatachalam, V., and Cohen, A. E. (2014). Imaging GFP-based reporters in neurons with multiwavelength optogenetic control. *Biophys. J.* 107, 1554–1563. doi: 10.1016/j.bpj.2014.08.020

Vierock, J., Grimm, C., Nitzan, N., and Hegemann, P. (2017). Molecular determinants of proton selectivity and gating in the red-light activated channelrhodopsin Chrimson. *Sci. Rep.* 7:9928. doi: 10.1038/s41598-017-09600-8

Vogt, C. C., Bruegmann, T., Malan, D., Ottersbach, A., Roell, W., Fleischmann, B. K., et al. (2015). Systemic gene transfer enables optogenetic pacing of mouse hearts. *Cardiovasc. Res.* 106, 338–343. doi: 10.1093/cvr/cvv004

Wang, Y., Lin, W. K., Crawford, W., Ni, H., Bolton, E. L., Khan, H., et al. (2017). Optogenetic control of heart rhythm by selective stimulation of cardiomyocytes derived from Pnmt+ cells in murine heart. *Sci. Rep.* 7:40687. doi: 10.1038/srep40687

Wengrowski, A. M., Wang, X., Tapa, S., Posnack, N. G., Mendelowitz, D., and Kay, M. W. (2015). Optogenetic release of norepinephrine from cardiac sympathetic neurons alters mechanical and electrical function. *Cardiovasc. Res.* 105, 143–150. doi: 10.1093/cvr/cvu258

Wietek, J., Rodriguez-Rozada, S., Tutas, J., Tenedini, F., Grimm, C., Oertner, T. G., et al. (2017). Anion-conducting channelrhodopsins with tuned spectra and modified kinetics engineered for optogenetic manipulation of behavior. *Sci. Rep.* 7:14957. doi: 10.1038/s41598-017-14330-y

Wietek, J., Wiegert, J. S., Adeishvili, N., Schneider, F., Watanabe, H., Tsunoda, S. P., et al. (2014). Conversion of channelrhodopsin into a light-gated chloride channel. *Science* 344, 409–412. doi: 10.1126/science.1249375

Yan, B., Spudich, J. L., Mazur, P., Vunnam, S., Derguini, F., and Nakanishi, K. (1995). Spectral tuning in bacteriorhodopsin in the absence of counterion and coplanarization effects. *J. Biol. Chem.* 270, 29668–29670. doi: 10.1074/jbc.270.50.29668

Yang, Y., Liu, N., He, Y., Liu, Y., Ge, L., Zou, L., et al. (2018). Improved calcium sensor GCaMP-X overcomes the calcium channel perturbations induced by the calmodulin in GCaMP. *Nat. Commun.* 9:1504. doi: 10.1038/s41467-018-03719-6

Yang, H. H., and St-Pierre, F. (2016). Genetically encoded voltage indicators: opportunities and challenges. *J. Neurosci.* 36, 9977–9989. doi: 10.1523/JNEUROSCI.1095-16.2016

Yang, W., and Yuste, R. (2018). Holographic imaging and photostimulation of neural activity. *Curr. Opin. Neurobiol.* 50, 211–221. doi: 10.1016/j.conb.2018.03.006

Yi, B., Kang, B. E., Lee, S., Braubach, S., and Baker, B. J. (2018). A dimeric fluorescent protein yields a bright, red-shifted GEVI capable of population signals in brain slice. *Sci. Rep.* 8:15199. doi: 10.1038/s41598-018-33297-y

Yizhar, O., Fenno, L. E., Davidson, T. J., Mogri, M., and Deisseroth, K. (2011b). Optogenetics in neural systems. *Neuron* 71, 9–34. doi: 10.1016/j.neuron.2011.06.004

Yizhar, O., Fenno, L. E., Prigge, M., Schneider, F., Davidson, T. J., O'Shea, D. J., et al. (2011a). Neocortical excitation/inhibition balance in information processing and social dysfunction. *Nature* 477, 171–178. doi: 10.1038/nature10360

Yu, L., Zhou, L., Cao, G., Po, S. S., Huang, B., Zhou, X., et al. (2017). Optogenetic modulation of cardiac sympathetic nerve activity to prevent ventricular arrhythmias. *J. Am. Coll. Cardiol.* 70, 2778–2790. doi: 10.1016/j.jacc.2017.09.1107

Zaglia, T., Pianca, N., Borile, G., Da Broi, F., Richter, C., Campione, M., et al. (2015). Optogenetic determination of the myocardial requirements for extrasystoles by cell type-specific targeting of ChannelRhodopsin-2. *Proc. Natl. Acad. Sci. USA* 112, E4495–E4504. doi: 10.1073/pnas.1509380112

Zemelman, B. V., Lee, G. A., Ng, M., and Miesenböck, G. (2002). Selective photostimulation of genetically chARGed neurons. *Neuron* 33, 15–22. doi: 10.1016/S0896-6273(01)00574-8

Zhang, F., Prigge, M., Beyrière, F., Tsunoda, S. P., Mattis, J., Yizhar, O., et al. (2008). Red-shifted optogenetic excitation: a tool for fast neural control derived from Volvox carteri. *Nat. Neurosci.* 11, 631–633. doi: 10.1038/nn.2120

Zhang, F., Wang, L.-P., Brauner, M., Liewald, J. F., Kay, K., Watzke, N., et al. (2007). Multimodal fast optical interrogation of neural circuitry. *Nature* 446, 633–639. doi: 10.1038/nature05744

Conflict of Interest Statement: The authors declare that the research was conducted in the absence of any commercial or financial relationships that could be construed as a potential conflict of interest.

frontiers in Physiology

MINI REVIEW
published: 06 June 2019
doi: 10.3389/fphys.2019.00675

Optogenetic Termination of Cardiac Arrhythmia: Mechanistic Enlightenment and Therapeutic Application?

Philipp Sasse[1], Maximilian Funken[1,2], Thomas Beiert[2] and Tobias Bruegmann[1,3,4,5]**

[1]*Institute of Physiology I, Medical Faculty, University of Bonn, Bonn, Germany,* [2]*Department of Internal Medicine II, University Hospital Bonn, University of Bonn, Bonn, Germany,* [3]*Research Training Group 1873, University of Bonn, Bonn, Germany,* [4]*Institute of Cardiovascular Physiology, University Medical Center, Georg August University Göttingen, Göttingen, Germany,* [5]*German Center for Cardiovascular Research (DZHK), Partner site Göttingen, Göttingen, Germany*

Optogenetic methods enable selective de- and hyperpolarization of cardiomyocytes expressing light-sensitive proteins within the myocardium. By using light, this technology provides very high spatial and temporal precision, which is in clear contrast to electrical stimulation. In addition, cardiomyocyte-specific expression would allow pain-free stimulation. In light of these intrinsic technical advantages, optogenetic methods provide an intriguing opportunity to understand and improve current strategies to terminate cardiac arrhythmia as well as for possible pain-free arrhythmia termination in patients in the future. In this review, we give a concise introduction to optogenetic stimulation of cardiomyocytes and the whole heart and summarize the recent progress on optogenetic defibrillation and cardioversion to terminate cardiac arrhythmia. Toward this aim, we specifically focus on the different mechanisms of optogenetic arrhythmia termination and how these might influence the prerequisites for success. Furthermore, we critically discuss the clinical perspectives and potential patient populations, which might benefit from optogenetic defibrillation devices.

Keywords: optogenetics, defibrillation, cardioversion, ventricular arrhythmia, ventricular tachycardia, ventricular fibrillation, atrial fibrillation, implantable cardioverter defibrillator

OPEN ACCESS

Edited by:
Christopher Huang, University of Cambridge, United Kingdom

Reviewed by:
Henggui Zhang, University of Manchester, United Kingdom
Leonardo Sacconi, University of Florence, Italy

****Correspondence:***
Philipp Sasse
philipp.sasse@uni-bonn.de
orcid.org/0000-0002-8502-9472
Tobias Bruegmann
tobias.bruegmann@med.uni-goettingen.de
orcid.org/0000-0002-6930-9634

Specialty section:
This article was submitted to Cardiac Electrophysiology, a section of the journal Frontiers in Physiology

Received: *22 February 2019*
Accepted: *13 May 2019*
Published: *06 June 2019*

Citation:
Sasse P, Funken M, Beiert T and Bruegmann T (2019) Optogenetic Termination of Cardiac Arrhythmia: Mechanistic Enlightenment and Therapeutic Application? Front. Physiol. 10:675. doi: 10.3389/fphys.2019.00675

INTRODUCTION

Optogenetic Tools Relevant to Cardiac Defibrillation

Optogenetics is a technology that employs light-sensitive proteins for the stimulation of cells and organs by illumination and can be used *in vitro* as well as *in vivo* (Hegemann and Nagel, 2013). Optogenetic stimulation provides unprecedented spatiotemporal resolution since light can be focused to specific regions using lenses or light fibers, and the exact time of activation and deactivation is defined by onset and duration of the illumination. Furthermore, by expressing optogenetic proteins under the control of cell type-specific promoters, the stimulation can be restricted to certain cell types of interest within an intact organ. The most frequently used optogenetic protein is Channelrhodopsin2 (ChR2), a light-gated, non-selective cation channel derived from green algae (Nagel et al., 2003). This protein with seven transmembrane domains contains all-trans-retinal as chromophore in which photon absorption leads to isomerization to the 13-cis form and subsequently opening of the channel pore, which mainly conducts Na^+

and K^+ ions. Fortunately, retinal as co-factor is already present in most mammalian tissues *in vivo* (Kane et al., 2005). Within excitable cells, ChR2 activation leads to inward currents and cell membrane depolarization, which allows contact-free control of the membrane potential. A myriad of different Channelrhodopsin variants have been created by amino acid exchanges, generating chimeric proteins or identifying new versions in other species in nature, which vary in their light sensitivity, wavelength specificity, and on- and off kinetics (Mattis et al., 2011). Besides channelrhodopsins, light-driven H^+ and Cl^- pumps from bacteria and fungi were used to export H^+ ions or import Cl^- ions, which leads to light-induced hyperpolarization and inhibition of electrical activity (Zhang et al., 2007; Mattis et al., 2011). New Cl^- selective ChR2 variants (Berndt et al., 2014; Wietek et al., 2014) as well as natural anion conducting light-gated channels (Govorunova et al., 2015) can also hyperpolarize some cell types; however, this depends strongly on the Nernst potential for Cl^-. In fact, in cardiomyocytes, light-induced activation of anion-conducting channels at resting membrane potential leads to depolarization as shown elegantly by Kopton et al. in this Research Topic article collection (Kopton et al., 2018). Recently, K^+ selective light-gated ion channels have been described for optogenetic silencing of electrical activity but with very slow off kinetics (Alberio et al., 2018; Bernal Sierra et al., 2018).

Optogenetic Pacing of Cardiomyocytes and Intact Hearts

Ever since its development, optogenetics has been used in the field of neuroscience to study basic neurophysiology and disease mechanisms by light-induced modulation of electrical activity in neurons (Adesnik, 2018). Our group has shown for the first time that optogenetics can be employed for light-based pacing of cardiomyocytes *in vitro* and of the atria and ventricles of transgenic mice *in vivo* (Bruegmann et al., 2010). Similarly, Arrenberg and colleagues demonstrated in embryonic zebrafish hearts light-induced hyperpolarization with a light-driven Cl^- pump to block excitation as well as ChR2-based pacing (Arrenberg et al., 2010). These publications laid the foundation for the field of cardiac optogenetics with subsequent publications focusing mainly on technological developments and optogenetic pacemaking (Jia et al., 2011; Abilez, 2012; Boyle et al., 2013; Nussinovitch et al., 2014; Zaglia et al., 2015; Klimas et al., 2016; Lapp et al., 2017; Rehnelt et al., 2017). In addition to direct pacing by light-induced depolarization, modulation of intrinsic pacemaking mechanisms and induction of arrhythmic beating were performed by optogenetic stimulation of the G_q or G_s protein-coupled receptors Melanopsin (Beiert et al., 2014) or Jellyfish opsin (Makowka et al., 2019), respectively. To be able to propose clinical applications of cardiac optogenetics, our group has demonstrated that systemic injection of adeno-associated viruses (AAV) results in ChR2 expression in the mouse heart, which is sufficient for optogenetic pacing (Vogt et al., 2015). The AAV ChR2 gene transfer strategy was extended to rats in order to suggest optogenetic cardiac resynchronization by multi-point illumination (Nussinovitch and Gepstein, 2015). Proving the ability to express ChR2 in wild-type hearts, these papers allowed for the first time a translational perspective for cardiac optogenetics. Because the potential application of optogenetic pacing of the heart has been reviewed extensively (Entcheva, 2013, 2014, 2015; Ambrosi et al., 2014; Boyle et al., 2014, 2015; Klimas and Entcheva, 2014) and optogenetics would probably provide only minor advantage over implantable electrical pacemakers, we will focus in this review on optogenetic termination of cardiac arrhythmia.

OPTOGENETIC TERMINATION OF CARDIAC ARRHYTHMIA

Cardiac Arrhythmia

Ventricular tachycardia (VT) and the subsequent degeneration into ventricular fibrillation (VF) are life-threatening arrhythmic states of the heart. These may result in a drop in cardiac output, reduction of arterial blood pressure, syncope, and often in sudden cardiac death. VT and VF occur after myocardial infarction, myocarditis, in patients with reduced ejection fraction, during electrolyte imbalance or because of side effects of drugs and mutations of cardiac ion channels. The primary therapy of these acutely life-threatening arrhythmias is defibrillation by an electric shock to resynchronize the heart. Atrial fibrillation (AF) represents the most common arrhythmia with growing incidence and is accompanied by an increase in morbidity and mortality despite being not acutely life-threatening (Lip et al., 2012). In early stages of AF, the first clinical aim is to restore sinus rhythm by cardioversion with external electrical shocks (Lip et al., 2012; Kirchhof et al., 2016).

Cardiac arrhythmias are usually initiated by an ectopic trigger and sustained by areas of slow conduction that promote the development of a so-called re-entry mechanism or the formation of rotors. Triggering occurs mainly during the diastole because of spontaneous opening of ion channels or Ca^{2+} release from intracellular stores. A re-entry mechanism is initiated, when the premature propagating wave front has to travel around a non-excitable region. Such regions can be non-excitable due to the anatomical structure (e.g., scar tissue) leading to re-entry wave fronts around the scar. Furthermore, electrophysiological heterogeneities such as partial refractory tissue (Wagner et al., 2015) can lead to cardiac electric rotors (Pandit and Jalife, 2013). A single macroscopic stable rotor (**Figure 1A**) or a re-entry wave front results in a monomorphic shape in the ECG. Additional rotors can be generated when waves traveling from the primary rotor encounter additional wavebreaks. This results in generation of highly periodic three-dimensional rotors that interact with each other in complex spatiotemporal patterns, which can be observed in the ECG as AF, polymorphic VT, or VF (Wagner et al., 2015).

Mechanisms of Electrical Defibrillation

Although the risk of VT can be reduced by pharmacological treatment or catheter-based ablation of pro-arrhythmogenic regions in the ventricles, ventricular arrhythmias often re-occur in patients resulting in a high risk of sudden cardiac death.

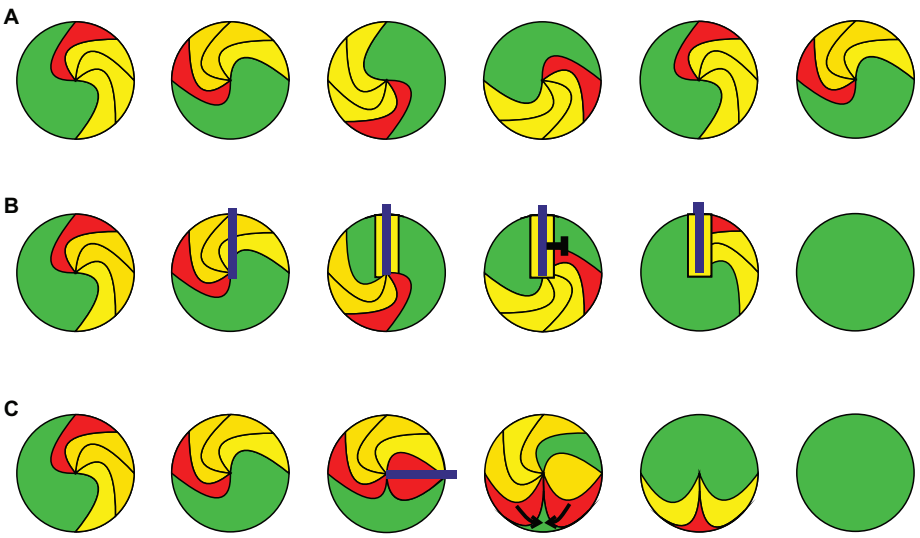

FIGURE 1 | Mechanisms of cardiac arrhythmia and optogenetic termination. The leading edge of the arrhythmic wave front is shown in red, the depolarized and refractory tissue in yellow, and the excitable gap in green. The illumination is displayed in blue. **(A)** A stable rotor of a cardiac arrhythmia is shown at different time points during one cycle around a phase singularity. **(B)** Example for optogenetic arrhythmia termination by conduction block. Sustained illumination starts within a depolarized area and keeps the surrounding area depolarized until the next arrhythmic wave front entering this region is blocked by refractory tissue. **(C)** Optogenetic arrhythmia termination by filling of the excitable gap. Brief illumination of the excitable gap generates a second excitation wave front, which travels toward the arrhythmic wave front until both are extinguished by their collision.

For this reason, patients with a propensity for VT/VF receive implantable cardiac defibrillators (ICD), which can terminate the arrhythmia by applying rapid antitachycardia pacing or finally by delivering a strong and painful electrical shock (Adgey et al., 2005). Even though the exact cellular mechanisms of defibrillation are still not fully understood, it was shown that it can be achieved by depolarization of a sufficient number of cells in accordance to the "critical mass theory." This model was developed in the early 1970s when Doug Zipes and colleagues demonstrated that injection of K^+ into the coronary arteries was able to defibrillate the canine heart (Zipes et al., 1975) probably by keeping cardiomyocytes depolarized and refractory and thereby block conduction. However, electrical shocks are restricted to few milliseconds and conduction block is unlikely to be sustained during electrical cardioversion or defibrillation. More likely, electrical shocks induce brief depolarization, which terminates arrhythmia by a mechanism called "filling of the excitable gap." The excitable gap is the excitable myocardium (**Figure 1A**, green) between the trailing edge of the bypassed and the leading edge of the next reentrant wave front (Kleber and Rudy, 2004) and can be activated by the electrical shock or by antitachycardia pacing protocols producing a second wave front which will collide with the arrhythmic wave front. The effectiveness of this mechanism has been documented in clinical trials (De Maria et al., 2017) and depends on the duration and location of the excitable gap relative to the pacing site, which is rather difficult to predict. The excitable gap can also be reduced by increasing the cardiac wavelength [conduction velocity × action potential duration (APD)]. This is considered to be one alternative mechanism of electrical defibrillation because it has been shown that electrical shocks can temporally increase APD (Dillon, 1991).

Interestingly, also hyperpolarized areas occur in the cardiac tissue during an electrical shock because of the presence of virtual anodes. In fact the hyperpolarized myocardium is even larger in extent than depolarized tissue, because of asymmetric non-monotonic influence of the electric shock on myocyte membrane potential (Nikolski et al., 2004; Dosdall et al., 2010). In consequence, cardiac excitation can be initiated *de novo* at the boundaries of a virtual anode potentially causing re-initiation of a re-entry mechanism and failure of defibrillation (Efimov et al., 1998). Mathematical modeling of the ventricles suggests that such re-initiation could be prevented if hyperpolarization is strong enough to recover all Na^+ channels from inactivation allowing the *de novo* excitations to travel fast enough through the virtual anode tissue to collide with the refractory tissue of depolarized areas (Cheng et al., 1998; Dosdall et al., 2010).

In vitro Experiments on Cardiomyocyte Monolayers Predict Optogenetic Defibrillation

The idea of optogenetic arrhythmia termination (Knollmann, 2010) was generated by our early experiments *in vitro*, which showed that continuous illumination prolongs APD and refractory period of ChR2 expressing cardiomyocytes. Specifically, high intensity illumination led to a constant membrane potential above −35 mV, which keeps Na^+ and Ca^{2+} channels inactivated. Consequently, we showed that in a monolayer of cardiomyocytes constant illumination was able to block electrical excitation and wave propagation into the illuminated region (Bruegmann et al., 2010), which led to the assumption that such conduction blocks can also be used to block arrhythmic wave fronts in the intact heart. This idea was supported by subsequent

in vitro experiments by others with cardiomyocyte monolayers: Bingen and colleagues were able to show that low light intensity illumination reduces the excitability, slows conduction, and thereby terminates rotor wave fronts in a monolayer of atrial neonatal rat cardiomyocytes (Bingen et al., 2014). Furthermore, the groups of Gil Bub and Emilia Entcheva demonstrated that specific illumination patterns can be used to inscribe excitation waves *in vitro* in cardiomyocyte monolayers to control the direction of conduction and to destabilize arrhythmic excitation patterns (Burton et al., 2015). The concept was extended by real time optogenetic manipulation of the core of spiral waves allowing their attraction, anchoring and unpinning ("spiral wave dragging") through controlled displacement of heterogeneities in atrial cardiomyocyte monolayers *in vitro* (Majumder et al., 2018). If these approaches using gentle modulation of cardiac arrhythmia patterns for self-extinction of planar waves in two-dimensional monolayers have an impact on scroll waves in the three-dimensional heart remains to be proven. Importantly, cores of scroll waves in the intact heart are represented as intramyocardial vortex filaments reaching from the epicardium to the endocardium, which has been recently visualized using high-resolution four-dimensional ultrasound-based strain imaging (Christoph et al., 2018). Thus "spiral wave dragging" of curved and non-perpendicular transmural vortex filaments with optogenetic approaches ("scroll wave dragging") seems to be very challenging because of the technical challenge to bend light rays with high temporal and spatial flexibility.

Optogenetic Defibrillation Using Conduction Block by Continuous Depolarization

One major advantage of optogenetic compared to electrical stimulation is the ability of constant depolarization by continuous illumination, which locks the illuminated region in absolute refractoriness and prevents (re-)excitation. Such conduction block would extinguish the arrhythmic wave front if conduction through the illuminated region was essential for arrhythmia maintenance (**Figure 1B**). However, in contrast to optogenetic pacing, which requires only epicardial excitation, effective conduction block would require sufficient epicardial illumination for transmural depolarization to inhibit mid-myocardial and endocardial wave propagation. About 6 years after establishing optogenetic pacing of mouse hearts, our group demonstrated optogenetic defibrillation in intact mouse hearts using constant illumination from the epicardial site, which terminated ventricular arrhythmia with a success rate of over 90% (Bruegmann et al., 2016). The main challenge was to find experimental conditions allowing stable ventricular arrhythmia without self-termination, which is difficult in the small mouse heart. We solved this by pharmacological opening of K_{ATP} channels to reduce APD and lowering the extracellular K^+ concentration to slow conduction, which both shorten the cardiac wavelength to fit into the small mouse heart (Bruegmann et al., 2018). For successful defibrillation, sufficient light intensity as well as size of illumination was important, suggesting that transmural depolarization of the whole myocardial wall is essential in concordance with the results from the critical mass theory (Zipes et al., 1975). Furthermore, computational simulations of an infarcted patient heart expressing ChR2 *in silico* by the group of Natalia Trajanova helped to understand that sufficient transmural depolarization, including endocardial depolarization, to keep Na^+ channels refractory is key to terminate a ventricular arrhythmia by epicardial illumination (Bruegmann et al., 2016). Similarly, experiments in ventricular slices from rat hearts (Watanabe et al., 2017) and in monolayers from neonatal rat cardiomyocytes revealed that arrhythmia termination in these two-dimensional systems requires illumination of one line spanning from the core region to the adjacent unexcitable parts (Feola et al., 2017). This would correlate to the required transmural depolarization in a three-dimensional heart to avoid endocardial wave front propagation. Our simulations showed that by epicardial illumination this condition can probably only be achieved using red light (669 nm) sensitive Channelrhodopsin variants because of the low penetrance of blue light (488 nm) in the thick human ventricular myocardium (Bruegmann et al., 2016).

Transmural depolarization to induce conduction block seems to be less challenging in the atria, because of the much thinner myocardial walls. In consequence, optogenetic cardioversion of atrial arrhythmia was successful in a ChR2 expressing mouse model heterozygous for an AF-promoting connexin 40/Gja5 mutation. This mouse line allowed induction of sustained AF episodes by intra-atrial electrical burst stimulation, which could be terminated by epicardial illumination (Bruegmann et al., 2018). Optogenetic AF termination was also proven in rats during muscarinic receptor stimulation to mimic vagal AF (Nyns et al., 2019). Because in both cases AF termination rates were highest at pulse duration >30 ms (Bruegmann et al., 2018) or >100 ms (Nyns et al., 2019), which is longer than the AF cycle time, it can be speculated that localized transmural conduction block and not filling of the excitable gap is the underlying mechanism.

Defibrillation Using Filling of the Excitable Gap by Optogenetic Pacing

In contrast to creating a conduction block by continuous transmural optogenetic depolarization, filling of the excitable gap requires only brief (~few ms) depolarization of epicardial cardiomyocytes above the action potential threshold. In consequence, required light energy (intensity × duration) would be much lower and similar to optogenetic cardiac pacemaking. This concept was proven by the group of Leonardo Sacconi using patterned light stimulation to terminate VT with one specific reentrant wave front (Crocini et al., 2016). The authors did not use constant illumination but repetitive short light pulses to confined regions, which eventually activate the excitable gap creating a new wave front that collides with the arrhythmic wave front (**Figure 1C**). However, similar to electrical antitachycardia pacing, successful defibrillation using localized stimulation requires to know the extent of the excitable gap in time and space, otherwise the local conduction block mechanism would be more effective. We have demonstrated this recently in optogenetic AF termination by comparing the

light intensities required for atrial pacing to those required for complete block of local electrical activity. AF termination efficacy was only ~50% using pacing light intensities, most likely because of random failure of stimulating the excitable gap. In contrast, application of higher light intensities, which are able to block electrical activity, terminated AF in all cases (Bruegmann et al., 2018).

The need for identification of the excitable gap in time and space can be circumvented using global pulsed illumination of the whole heart, which was shown in computer simulations on a human heart *in silico* (Karathanos et al., 2016). Furthermore, within this Research Topic article collection, Richter and colleagues showed experimentally on intact mouse hearts that indeed light pulses of low light intensity are sufficient for VT termination if ventricles are globally illuminated from all sites (Quinonez Uribe et al., 2018).

Because global homogeneous epicardial illumination of the human heart will be challenging, it will be important to compare defibrillation effectiveness by localized filling of the (previously identified) excitable gap using brief light pulses with localized conduction blocks by sustained illumination. Experimentally, this could be enabled by the recent development of an all-optical heart platform, combining epicardial voltage mapping with spatially defined optogenetic stimulation using a digital-mirror device in a closed-loop feedback system (Scardigli et al., 2018). Such a system would allow the on-line identification of reentrant wave fronts with excitable gaps and subsequent real-time illumination of the leading or trailing edge (**Figure 1**) as well as the rotor cores for potential "spiral/scroll wave dragging" (Majumder et al., 2018).

Defibrillation by Optogenetic Hyperpolarization

The interplay between de- and hyperpolarized areas during defibrillation as well as specific effects of hyperpolarization alone cannot be experimentally addressed by electrical shocks with non-controllable (virtual) anodes and cathodes. In contrast, optogenetic methods allow selective hyperpolarization using light-driven H^+ or Cl^- pumps. Within this Research Topic article collection, we report an optogenetic strategy to analyze the effects of hyperpolarization within the intact heart and to determine the potential mechanism for defibrillation (Funken et al., 2019). By expressing the light-inducible proton pump ArchaerhodopsinT in cardiomyocytes of transgenic mice, we were able to prove that hyperpolarization *per se* can terminate VA. Importantly, we identified a completely new VA termination mechanism by enhancing the electrical sink of the excitable gap presumably leading to conduction failure of high frequency wavelets with weak electrical source (source-sink mismatch). Unfortunately, the overall success rate was lower compared to conduction block by continuous depolarization with ChR2, which can be explained by the low efficiency of light-driven pumps as well as by simultaneous VA stabilizing mechanisms of hyperpolarization (increased Na^+ channel availability resulting in enhanced electrical source of the arrhythmic wave front). For future clinical perspectives, more effective optogenetic tools for hyperpolarization would be necessary. Unfortunately, the recently presented K^+ channel-based optogenetic approaches have very slow kinetics in the range of minutes (Alberio et al., 2018; Bernal Sierra et al., 2018). This would result in prolonged silencing of the ventricular activity even after defibrillation has occurred without reestablishment of blood circulation.

CLINICAL IMPLICATIONS OF OPTOGENETIC DEFIBRILLATION

Characteristics of Different Cardiac Arrhythmia Termination Mechanisms

In summary, we have identified two possible mechanisms for optogenetic termination of VA that can now be put into clinical context and be compared with current treatment strategies. (1) Optogenetic pacing to fill the excitable gap could be used for energy-reduced arrhythmia termination but requires either global illumination (Quinonez Uribe et al., 2018) or triggered localized illumination after mapping of the excitable gap by epicardial electrograms. (2) Generating a transmural conduction block by continuous optogenetic depolarization requires more light energy but only in predefined anatomical regions that are essential for arrhythmia re-entry (infarct border zone, area of slow conduction). Transmural depolarization must be facilitated using red light-sensitive channelrhodopsin variants such as the novel Chrimson mutants (Mager et al., 2018; Oda et al., 2018) because of the deeper tissue penetration. Also longer lasting Channelrhodopsin variants with 200–500 ms deactivation kinetics could be envisioned in which one or two brief light pulses would result in longer depolarization for low light energy conduction block and optogenetic defibrillation.

Clinical Perspectives of Implantable Optogenetic Defibrillators

Since publication of the first landmark-trials in the early 2000s (Moss et al., 2002; Bardy et al., 2005), implantation of an ICD has been a cornerstone in the treatment of patients with high risk for ventricular arrhythmia due to heart failure (Ponikowski et al., 2016), cardiac channelopathies, or previously survived sudden cardiac arrest (Priori et al., 2015). Upon detection of a potentially life-threatening ventricular arrhythmia, ICDs apply antitachycardia pacing protocols and subsequently high energy electrical shocks (up to 40 J) to terminate the arrhythmia. Electrical shocks are painful due to stimulation of nerve fibers and direct excitation of skeletal muscles and even low energy shocks for internal cardioversion of AF require sedation (Murgatroyd et al., 1995). Thus, inappropriate electrical shocks, which occur in 4–8% of patients, for example, due to false detection of supraventricular tachycardia (Tan et al., 2014; Kober et al., 2016), have a profound impact on the quality of life including anxiety, depression, and posttraumatic stress syndrome (Kamphuis et al., 2003). Furthermore, sub-studies of the SCD-HEFT trial (Poole et al., 2008) as well as a comparison of successful antitachycardia pacing with electrical shocks for arrhythmia termination (Sweeney et al., 2010) clearly

showed increased mortality in patients receiving inappropriate or appropriate ICD shocks. Implanted devices for early AF detection and termination with low energy electrical shocks have been clinically evaluated but were not tolerated because of pain during cardioversion (Geller et al., 2003).

Using specific virus capsids (Zacchigna et al., 2014) or promoters (Werfel et al., 2014) for selective expression of optogenetic actuator proteins in cardiomyocytes would allow in principle painless optogenetic defibrillation and cardioversion. Although yet not proven, it can be anticipated that optogenetic defibrillation by a few seconds of epicardial illumination is less harmful to the heart than electrical shocks. Moreover, sequential light pulses can be applied repetitively, as charging of capacitors to generate ICD electrical shocks is not required. The flexibility of using spatially and temporally shaped light patterns for defibrillation could also be used to minimize secondary pro-arrhythmic effects, which are discussed to be a major cause for electrical defibrillation failure (Charteris and Roth, 2011).

Technical Challenges Toward Optogenetic Arrhythmia Termination

Before optogenetic therapies can be suggested to patients, the proof-of-concept studies mentioned above have to be verified in preclinical large animal models with human-like anatomy and arrhythmia. Furthermore, long lasting virus-based gene transfer without immunological reactions against viruses or the non-human optogenetic proteins must be established. Toward this aim, we were able to prove that optogenetic defibrillation of VT and cardioversion of AF is also possible in wild-type mouse hearts after systemic injection of AAV (Bruegmann et al., 2016, 2018). Quite surprisingly for the episomal persisting, non-integrating AAV, we found that ChR2 expression was stable for periods of up to 15 months. Optogenetic defibrillation of VT was also confirmed in rats, at least for a period of up to 6 weeks after systemic AAV injection to express a red light-activated ChR2 variant (Nyns et al., 2017). As an alternative to systemic AAV injection, which might infect cells in other organs, gene painting by application of AAV in fibrin clots to the epicardium of the right atrium of rats was shown to result in very localized and highly effective gene transfer sufficient for optogenetic termination of AF (Nyns et al., 2019). Importantly, 4 weeks after gene painting, ~80% cardiomyocytes of the right atrium of immunosuppressed (rapamycin) rats expressed the ChR2 variant compared to only <40% of atrial myocytes >6 months after systemic AAV injection in mice (Bruegmann et al., 2016, 2018). However, long-term stable and transmural ChR2 expression in large animals without immunosuppression remains to be proven. Furthermore, because of the thick left ventricular wall of humans, it is questionable if epicardial gene painting results in sufficient transmural gene expression for optogenetic termination of VT/VF or if systemic or intracoronary infusion of AAV is better suited in this case.

Finally, sufficient transmural illumination must be achieved, e.g., by injectable cellular scale optoelectronics (Kim et al., 2013; Montgomery et al., 2015), LEDs in flexible biocompatible membranes (Xu et al., 2014), or μLED arrays (Gossler et al., 2014). Combining illumination systems with radio-frequency energy harvesters (Park et al., 2015) or with batteries will allow fully implantable illumination devices for chronic optogenetic stimulation of hearts *in vivo*. Recently, a hybrid system for automated AF detection and optogenetic cardioversion in anesthetized rats was described combining surface ECG leads, an external cardiac rhythm monitor, and an implanted atrial LED with a PDMS light guide (Nyns et al., 2019). Such an approach could be extended toward mechanistic investigations of AF-induced fibrotic remodeling of the atria *in vivo* ("AF begets AF") using fully implantable miniaturized bio-optoelectronic devices for closed-loop optogenetic control in freely moving rats *in vivo* (Mickle et al., 2019).

Patients Suited for Optogenetic Arrhythmia Termination

Most likely, first patients to benefit from painless and gentle optogenetic defibrillation would be those with recurrent episodes of electrical storm. Electrical storm is defined by three or more sustained episodes of VT/VF with appropriate ICD therapies within 24 h, and the incidence is ranging from 4 to 28% in ICD patients (Huang and Traub, 2008). Mortality is high, and therapeutic options are very limited including interventional catheter ablation from the endocardial or the epicardial side. VT recurrence rates following ablation of sustained VT are high, especially in patients with non-ischemic dilated cardiomyopathy (62 ± 4%) compared to those with ischemic cardiomyopathy (46 ± 4%, median follow-up of 6 years) (Kumar et al., 2016). Patients with ischemic cardiomyopathy typically have a more clearly defined subendocardial or transmural scar, which can be identified as anatomical substrate for re-entry mechanism and thus can be well targeted by endocardial ablation. Patients with non-ischemic dilated cardiomyopathy, however, often have a diffuse mid-myocardial and epicardial fibrosis and frequently require an epicardial ablation procedure (Kumar et al., 2016). Similar to the discussed transmural depolarization for optogenetic defibrillation, the generation of transmural lesions is a key factor for effective ablation, but this cannot always be achieved in the thick ventricular myocardium. In such patients, optogenetic defibrillation would be advantageous, given that transmural depolarization could be achieved with red-shifted optogenetics (see above).

In summary, patients suffering from frequent appropriate and inappropriate ICD shocks despite optimal medical therapy or with ineffective ablation due to diffuse fibrosis from non-ischemic dilated cardiomyopathy could benefit from implantable optogenetic defibrillation devices. Furthermore, an implantable optogenetic "atrioverter" to terminate AF on-demand might be useful to prevent or even revert AF-induced fibrotic remodeling of the atria ("AF begets AF") (Wijffels et al., 1995).

AUTHOR CONTRIBUTIONS

PS and TBr planned the manuscript. PS, MF, TBe, and TBr wrote the manuscript.

FUNDING

This work was supported by the German Research Foundation [313904155/SA1785/7-1, 380524518/SA1785/9-1, 214362475/GRK1873/2, and SPP 1926 Young Investigator Program (GO1011/11-1)]; the BONFOR Program, Medical Faculty, University of Bonn; and by the German Federal Ministry of Education and Research, funding program Photonics Research Germany, project BioPACE (13N14087). TBr was supported by the DZHK (German Centre for Cardiovascular Research). We also acknowledge support by the Open Access Publication Funds of the German Research Foundation and the Göttingen University.

REFERENCES

Abilez, O. J. (2012). Cardiac optogenetics. *Conf. Proc. IEEE Eng. Med. Biol. Soc.* 2012, 1386–1389. doi: 10.1109/EMBC.2012.6346197

Adesnik, H. (2018). Cell type-specific optogenetic dissection of brain rhythms. *Trends Neurosci.* 41, 122–124. doi: 10.1016/j.tins.2018.01.001

Adgey, A. A., Spence, M. S., and Walsh, S. J. (2005). Theory and practice of defibrillation: (2) defibrillation for ventricular fibrillation. *Heart* 91, 118–125. doi: 10.1136/hrt.2003.019927

Alberio, L., Locarno, A., Saponaro, A., Romano, E., Bercier, V., Albadri, S., et al. (2018). A light-gated potassium channel for sustained neuronal inhibition. *Nat. Methods* 15, 969–976. doi: 10.1038/s41592-018-0186-9

Ambrosi, C. M., Klimas, A., Yu, J., and Entcheva, E. (2014). Cardiac applications of optogenetics. *Prog. Biophys. Mol. Biol.* 115, 294–304. doi: 10.1016/j.pbiomolbio.2014.07.001

Arrenberg, A. B., Stainier, D. Y., Baier, H., and Huisken, J. (2010). Optogenetic control of cardiac function. *Science* 330, 971–974. doi: 10.1126/science.1195929

Bardy, G. H., Lee, K. L., Mark, D. B., Poole, J. E., Packer, D. L., Boineau, R., et al. (2005). Amiodarone or an implantable cardioverter-defibrillator for congestive heart failure. *N. Engl. J. Med.* 352, 225–237. doi: 10.1056/NEJMoa043399

Beiert, T., Bruegmann, T., and Sasse, P. (2014). Optogenetic activation of Gq signalling modulates pacemaker activity of cardiomyocytes. *Cardiovasc. Res.* 102, 507–516. Epub 2014/03/01. doi: 10.1093/cvr/cvu046

Bernal Sierra, Y. A., Rost, B. R., Pofahl, M., Fernandes, A. M., Kopton, R. A., Moser, S., et al. (2018). Potassium channel-based optogenetic silencing. *Nat. Commun.* 9:4611. doi: 10.1038/s41467-018-07038-8

Berndt, A., Lee, S. Y., Ramakrishnan, C., and Deisseroth, K. (2014). Structure-guided transformation of channelrhodopsin into a light-activated chloride channel. *Science* 344, 420–424. doi: 10.1126/science.1252367

Bingen, B. O., Engels, M. C., Schalij, M. J., Jangsangthong, W., Neshati, Z., Feola, I., et al. (2014). Light-induced termination of spiral wave arrhythmias by optogenetic engineering of atrial cardiomyocytes. *Cardiovasc. Res.* 104, 194–205. doi: 10.1093/cvr/cvu179

Boyle, P. M., Entcheva, E., and Trayanova, N. A. (2014). See the light: can optogenetics restore healthy heartbeats? And, if it can, is it really worth the effort? *Expert. Rev. Cardiovasc. Ther.* 12, 17–20. doi: 10.1586/14779072.2014.864951

Boyle, P. M., Karathanos, T. V., Entcheva, E., and Trayanova, N. A. (2015). Computational modeling of cardiac optogenetics: methodology overview & review of findings from simulations. *Comput. Biol. Med.* 65, 200–208. doi: 10.1016/j.compbiomed.2015.04.036

Boyle, P. M., Williams, J. C., Ambrosi, C. M., Entcheva, E., and Trayanova, N. A. (2013). A comprehensive multiscale framework for simulating optogenetics in the heart. *Nat. Commun.* 4:2370. doi: 10.1038/ncomms3370

Bruegmann, T., Beiert, T., Vogt, C. C., Schrickel, J. W., and Sasse, P. (2018). Optogenetic termination of atrial fibrillation in mice. *Cardiovasc. Res.* 114, 713–723. doi: 10.1093/cvr/cvx250

Bruegmann, T., Boyle, P. M., Vogt, C. C., Karathanos, T. V., Arevalo, H. J., Fleischmann, B. K., et al. (2016). Optogenetic defibrillation terminates ventricular arrhythmia in mouse hearts and human simulations. *J. Clin. Invest.* 126, 3894–3904. doi: 10.1172/JCI88950

Bruegmann, T., Malan, D., Hesse, M., Beiert, T., Fuegemann, C. J., Fleischmann, B. K., et al. (2010). Optogenetic control of heart muscle in vitro and in vivo. *Nat. Methods* 7, 897–900. doi: 10.1038/nmeth.1512

Burton, R. A., Klimas, A., Ambrosi, C. M., Tomek, J., Corbett, A., Entcheva, E., et al. (2015). Optical control of excitation waves in cardiac tissue. *Nat. Photonics* 9, 813–816. doi: 10.1038/nphoton.2015.196

Charteris, N. P., and Roth, B. J. (2011). How hyperpolarization and the recovery of excitability affect propagation through a virtual anode in the heart. *Comput. Math. Methods Med.* 2011:375059. doi: 10.1155/2011/375059

Cheng, Y., Van Wagoner, D. R., Mazgalev, T. N., Tchou, P. J., and Efimov, I. R. (1998). Voltage-sensitive dye RH421 increases contractility of cardiac muscle. *Can. J. Physiol. Pharmacol.* 76, 1146–1150. doi: 10.1139/y98-124

Christoph, J., Chebbok, M., Richter, C., Schroder-Schetelig, J., Bittihn, P., Stein, S., et al. (2018). Electromechanical vortex filaments during cardiac fibrillation. *Nature* 555, 667–672. Epub 2018/02/22. doi: 10.1038/nature26001

Crocini, C., Ferrantini, C., Coppini, R., Scardigli, M., Yan, P., Loew, L. M., et al. (2016). Optogenetics design of mechanistically-based stimulation patterns for cardiac defibrillation. *Sci. Rep.* 6:35628. doi: 10.1038/srep35628

De Maria, E., Giacopelli, D., Borghi, A., Modonesi, L., and Cappelli, S. (2017). Antitachycardia pacing programming in implantable cardioverter defibrillator: a systematic review. *World J. Cardiol.* 9, 429–436. doi: 10.4330/wjc.v9.i5.429

Dillon, S. M. (1991). Optical recordings in the rabbit heart show that defibrillation strength shocks prolong the duration of depolarization and the refractory period. *Circ. Res.* 69, 842–856. doi: 10.1161/01.RES.69.3.842

Dosdall, D. J., Fast, V. G., and Ideker, R. E. (2010). Mechanisms of defibrillation. *Annu. Rev. Biomed. Eng.* 12, 233–258. doi: 10.1146/annurev-bioeng-070909-105305

Efimov, I. R., Cheng, Y., Van Wagoner, D. R., Mazgalev, T., and Tchou, P. J. (1998). Virtual electrode-induced phase singularity: a basic mechanism of defibrillation failure. *Circ. Res.* 82, 918–925. doi: 10.1161/01.RES.82.8.918

Entcheva, E. (2013). Cardiac optogenetics. *Am. J. Physiol. Heart Circ. Physiol.* 304, H1179–H1191. doi: 10.1152/ajpheart.00432.2012

Entcheva, E. (2014). Fiat lux in understanding cardiac pacing, resynchronization and signalling by way of optogenetics. *Cardiovasc. Res.* 102, 342–343. doi: 10.1093/cvr/cvu109

Entcheva, E. (2015). A step closer to cardiac optogenetics in vivo. *Cardiovasc. Res.* 106, 180–181. doi: 10.1093/cvr/cvv116

Feola, I., Volkers, L., Majumder, R., Teplenin, A., Schalij, M. J., Panfilov, A. V., et al. (2017). Localized optogenetic targeting of rotors in atrial cardiomyocyte monolayers. *Circ. Arrhythm. Electrophysiol.* 10. doi: 10.1161/CIRCEP.117.005591

Funken, M., Malan, D., Sasse, P., and Bruegmann, T. (2019). Optogenetic hyperpolarization of cardiomyocytes terminates ventricular arrhythmia. *Front. Physiol.* 10:498. doi: 10.3389/fphys.2019.00498

Geller, J. C., Reek, S., Timmermans, C., Kayser, T., Tse, H. F., Wolpert, C., et al. (2003). Treatment of atrial fibrillation with an implantable atrial defibrillator--long term results. *Eur. Heart J.* 24, 2083–2089. doi: 10.1016/j.ehj.2003.09.033

Gossler, C., Bierbrauer, C., Moser, R., Kunzer, M., Holc, K., Pletschen, W., et al. (2014). GaN-based micro-LED arrays on flexible substrates for optical cochlear implants. *J. Phys. D. Appl. Phys.* 47:205401. doi: 10.1088/0022-3727/47/20/205401

Govorunova, E. G., Sineshchekov, O. A., Janz, R., Liu, X., and Spudich, J. L. (2015). NEUROSCIENCE. Natural light-gated anion channels: a family of microbial rhodopsins for advanced optogenetics. *Science* 349, 647–650. doi: 10.1126/science.aaa7484

Hegemann, P., and Nagel, G. (2013). From channelrhodopsins to optogenetics. *EMBO Mol. Med.* 5, 173–176. doi: 10.1002/emmm.201202387

Huang, D. T., and Traub, D. (2008). Recurrent ventricular arrhythmia storms in the age of implantable cardioverter defibrillator therapy: a comprehensive review. *Prog. Cardiovasc. Dis.* 51, 229–236. doi: 10.1016/j.pcad.2008.07.003

Jia, Z., Valiunas, V., Lu, Z., Bien, H., Liu, H., Wang, H. Z., et al. (2011). Stimulating cardiac muscle by light: cardiac optogenetics by cell delivery. *Circ. Arrhythm. Electrophysiol.* 4, 753–760. doi: 10.1161/CIRCEP.111.964247

Kamphuis, H. C. M., de Leeuw, J. R. J., Derksen, R., Hauer, R. N. W., and Winnubst, J. A. M. (2003). Implantable cardioverter defibrillator recipients: quality of life in recipients with and without ICD shock delivery - A prospective study. *Europace* 5, 381–389. doi: 10.1016/S1099-5129(03)00078-3

Kane, M. A., Chen, N., Sparks, S., and Napoli, J. L. (2005). Quantification of endogenous retinoic acid in limited biological samples by LC/MS/MS. *Biochem. J.* 388, 363–369. doi: 10.1042/BJ20041867

Karathanos, T. V., Bayer, J. D., Wang, D., Boyle, P. M., and Trayanova, N. A. (2016). Opsin spectral sensitivity determines the effectiveness of optogenetic termination of ventricular fibrillation in the human heart: a simulation study. *J. Physiol.* 594, 6879–6891. doi: 10.1113/JP271739

Kim, T. I., McCall, J. G., Jung, Y. H., Huang, X., Siuda, E. R., Li, Y., et al. (2013). Injectable, cellular-scale optoelectronics with applications for wireless optogenetics. *Science* 340, 211–216. doi: 10.1126/science.1232437

Kirchhof, P., Benussi, S., Kotecha, D., Ahlsson, A., Atar, D., Casadei, B., et al. (2016). 2016 ESC Guidelines for the management of atrial fibrillation developed in collaboration with EACTS. *Eur. Heart J.* 37, 2893–2962. doi: 10.1093/eurheartj/ehw210

Kleber, A. G., and Rudy, Y. (2004). Basic mechanisms of cardiac impulse propagation and associated arrhythmias. *Physiol. Rev.* 84, 431–488. doi: 10.1152/physrev.00025.2003

Klimas, A., Ambrosi, C. M., Yu, J., Williams, J. C., Bien, H., and Entcheva, E. (2016). OptoDyCE as an automated system for high-throughput all-optical dynamic cardiac electrophysiology. *Nat. Commun.* 7:11542. doi: 10.1038/ncomms11542

Klimas, A., and Entcheva, E. (2014). Toward microendoscopy-inspired cardiac optogenetics in vivo: technical overview and perspective. *J. Biomed. Opt.* 19:080701. doi: 10.1117/1.JBO.19.8.080701

Knollmann, B. C. (2010). Pacing lightly: optogenetics gets to the heart. *Nat. Methods* 7, 889–891. doi: 10.1038/nmeth1110-889

Kober, L., Thune, J. J., Nielsen, J. C., Haarbo, J., Videbaek, L., Korup, E., et al. (2016). Defibrillator implantation in patients with nonischemic systolic heart failure. *N. Engl. J. Med.* 375, 1221–1230. doi: 10.1056/NEJMoa1608029

Kopton, R. A., Baillie, J. S., Rafferty, S. A., Moss, R., Zgierski-Johnston, C. M., Prykhozhij, S. V., et al. (2018). Cardiac electrophysiological effects of light-activated chloride channels. *Front. Physiol.* 9:1806. doi: 10.3389/fphys.2018.01806

Kumar, S., Romero, J., Mehta, N. K., Fujii, A., Kapur, S., Baldinger, S. H., et al. (2016). Long-term outcomes after catheter ablation of ventricular tachycardia in patients with and without structural heart disease. *Heart Rhythm.* 13, 1957–1963. doi: 10.1016/j.hrthm.2016.07.001

Lapp, H., Bruegmann, T., Malan, D., Friedrichs, S., Kilgus, C., Heidsieck, A., et al. (2017). Frequency-dependent drug screening using optogenetic stimulation of human iPSC-derived cardiomyocytes. *Sci. Rep.* 7:9629. doi: 10.1038/s41598-017-09760-7

Lip, G. Y., Tse, H. F., and Lane, D. A. (2012). Atrial fibrillation. *Lancet* 379, 648–661. doi: 10.1016/S0140-6736(11)61514-6

Mager, T., Lopez de la Morena, D., Senn, V., Schlotte, J., D Errico, A., Feldbauer, K., et al. (2018). High frequency neural spiking and auditory signaling by ultrafast red-shifted optogenetics. *Nat. Commun.* 9:1750. doi: 10.1038/s41467-018-04146-3

Majumder, R., Feola, I., Teplenin, A. S., de Vries, A. A., Panfilov, A. V., and Pijnappels, D. A. (2018). Optogenetics enables real-time spatiotemporal control over spiral wave dynamics in an excitable cardiac system. *elife* 7. Epub 2018/09/28. doi: 10.7554/eLife.41076

Makowka, P., Bruegmann, T., Dusend, V., Malan, D., Beiert, T., Hesse, M., et al. (2019). Optogenetic stimulation of Gs-signaling in the heart with high spatio-temporal precision. *Nat. Commun.* 10:1281. Epub 2019/03/22. doi: 10.1038/s41467-019-09322-7

Mattis, J., Tye, K. M., Ferenczi, E. A., Ramakrishnan, C., O'Shea, D. J., Prakash, R., et al. (2011). Principles for applying optogenetic tools derived from direct comparative analysis of microbial opsins. *Nat. Methods* 9, 159–172. doi: 10.1038/nmeth.1808

Mickle, A. D., Won, S. M., Noh, K. N., Yoon, J., Meacham, K. W., Xue, Y., et al. (2019). A wireless closed-loop system for optogenetic peripheral neuromodulation. *Nature* 565, 361–365. Epub 2019/01/04. doi: 10.1038/s41586-018-0823-6

Montgomery, K. L., Yeh, A. J., Ho, J. S., Tsao, V., Mohan Iyer, S., Grosenick, L., et al. (2015). Wirelessly powered, fully internal optogenetics for brain, spinal and peripheral circuits in mice. *Nat. Methods* 12, 969–974. doi: 10.1038/nmeth.3536

Moss, A. J., Zareba, W., Hall, W. J., Klein, H., Wilber, D. J., Cannom, D. S., et al. (2002). Prophylactic implantation of a defibrillator in patients with myocardial infarction and reduced ejection fraction. *N. Engl. J. Med.* 346, 877–883. doi: 10.1056/NEJMoa013474

Murgatroyd, F. D., Slade, A. K., Sopher, S. M., Rowland, E., Ward, D. E., and Camm, A. J. (1995). Efficacy and tolerability of transvenous low energy cardioversion of paroxysmal atrial fibrillation in humans. *J. Am. Coll. Cardiol.* 25, 1347–1353.

Nagel, G., Szellas, T., Huhn, W., Kateriya, S., Adeishvili, N., Berthold, P., et al. (2003). Channelrhodopsin-2, a directly light-gated cation-selective membrane channel. *Proc. Natl. Acad. Sci. USA* 100, 13940–13945. doi: 10.1073/pnas.1936192100

Nikolski, V. P., Sambelashvili, A. T., Krinsky, V. I., and Efimov, I. R. (2004). Effects of electroporation on optically recorded transmembrane potential responses to high-intensity electrical shocks. *Am. J. Physiol. Heart Circ. Physiol.* 286, H412–H418. doi: 10.1152/ajpheart.00689.2003

Nussinovitch, U., and Gepstein, L. (2015). Optogenetics for in vivo cardiac pacing and resynchronization therapies. *Nat. Biotechnol.* 33, 750–754. doi: 10.1038/nbt.3268

Nussinovitch, U., Shinnawi, R., and Gepstein, L. (2014). Modulation of cardiac tissue electrophysiological properties with light-sensitive proteins. *Cardiovasc. Res.* 102, 176–187. doi: 10.1093/cvr/cvu037

Nyns, E. C. A., Kip, A., Bart, C. I., Plomp, J. J., Zeppenfeld, K., Schalij, M. J., et al. (2017). Optogenetic termination of ventricular arrhythmias in the whole heart: towards biological cardiac rhythm management. *Eur. Heart J.* 38, 2132–2136. doi: 10.1093/eurheartj/ehw574

Nyns, E. C. A., Poelma, R. H., Volkers, L., Plomp, J. J., Bart, C. I., Kip, A. M., et al. (2019). An automated hybrid bioelectronic system for autogenous restoration of sinus rhythm in atrial fibrillation. *Sci. Transl. Med.* 11. Epub 2019/03/01. doi: 10.1126/scitranslmed.aau6447

Oda, K., Vierock, J., Oishi, S., Rodriguez-Rozada, S., Taniguchi, R., Yamashita, K., et al. (2018). Crystal structure of the red light-activated channelrhodopsin Chrimson. *Nat. Commun.* 9:3949. doi: 10.1038/s41467-018-06421-9

Pandit, S. V., and Jalife, J. (2013). Rotors and the dynamics of cardiac fibrillation. *Circ. Res.* 112, 849–862. doi: 10.1161/CIRCRESAHA.111.300158

Park, S. I., Brenner, D. S., Shin, G., Morgan, C. D., Copits, B. A., Chung, H. U., et al. (2015). Soft, stretchable, fully implantable miniaturized optoelectronic systems for wireless optogenetics. *Nat. Biotechnol.* 33, 1280–1286. doi: 10.1038/nbt.3415

Ponikowski, P., Voors, A. A., Anker, S. D., Bueno, H., Cleland, J. G. F., Coats, A. J. S., et al. (2016). 2016 ESC Guidelines for the diagnosis and treatment of acute and chronic heart failure: the task force for the diagnosis and treatment of acute and chronic heart failure of the European society of cardiology (ESC) developed with the special contribution of the heart failure association (HFA) of the ESC. *Eur. Heart J.* 37, 2129–2200. doi: 10.1093/eurheartj/ehw128

Poole, J. E., Johnson, G. W., Hellkamp, A. S., Anderson, J., Callans, D. J., Raitt, M. H., et al. (2008). Prognostic importance of defibrillator shocks in patients with heart failure. *N. Engl. J. Med.* 359, 1009–1017. doi: 10.1056/NEJMoa071098

Priori, S. G., Blomstrom-Lundqvist, C., Mazzanti, A., Blom, N., Borggrefe, M., Camm, J., et al. (2015). 2015 ESC Guidelines for the management of patients with ventricular arrhythmias and the prevention of sudden cardiac death: the task force for the management of patients with ventricular arrhythmias and the prevention of sudden cardiac death of the European society of cardiology (ESC). Endorsed by: association for European paediatric and congenital cardiology (AEPC). *Eur. Heart J.* 36, 2793–2867. doi: 10.1093/eurheartj/ehv316

Quinonez Uribe, R. A., Luther, S., Diaz-Maue, L., and Richter, C. (2018). Energy-reduced arrhythmia termination using global photostimulation in optogenetic murine hearts. *Front. Physiol.* 9:1651. doi: 10.3389/fphys.2018.01651

Rehnelt, S., Malan, D., Juhasz, K., Wolters, B., Doerr, L., Beckler, M., et al. (2017). Frequency-dependent multi-well cardiotoxicity screening enabled by optogenetic stimulation. *Int. J. Mol. Sci.* 18. doi: 10.3390/ijms18122634

Scardigli, M., Mullenbroich, C., Margoni, E., Cannazzaro, S., Crocini, C., Ferrantini, C., et al. (2018). Real-time optical manipulation of cardiac conduction in intact hearts. *J. Physiol.* 596, 3841–3858. Epub 2018/07/11. doi: 10.1113/JP276283

Sweeney, M. O., Sherfesee, L., DeGroot, P. J., Wathen, M. S., and Wilkoff, B. L. (2010). Differences in effects of electrical therapy type for ventricular arrhythmias on mortality in implantable cardioverter-defibrillator patients. *Heart Rhythm.* 7, 353–360. doi: 10.1016/j.hrthm.2009.11.027

Tan, V. H., Wilton, S. B., Kuriachan, V., Sumner, G. L., and Exner, D. V. (2014). Impact of programming strategies aimed at reducing nonessential implantable cardioverter defibrillator therapies on mortality: a systematic review and meta-analysis. *Circ. Arrhythm. Electrophysiol.* 7, 164–170. doi: 10.1161/CIRCEP.113.001217

Vogt, C. C., Bruegmann, T., Malan, D., Ottersbach, A., Roell, W., Fleischmann, B. K., et al. (2015). Systemic gene transfer enables optogenetic pacing of mouse hearts. *Cardiovasc. Res.* 106, 338–343. doi: 10.1093/cvr/cvv004

Wagner, S., Maier, L. S., and Bers, D. M. (2015). Role of sodium and calcium dysregulation in tachyarrhythmias in sudden cardiac death. *Circ. Res.* 116, 1956–1970. doi: 10.1161/CIRCRESAHA.116.304678

Watanabe, M., Feola, I., Majumder, R., Jangsangthong, W., Teplenin, A. S., Ypey, D. L., et al. (2017). Optogenetic manipulation of anatomical re-entry by light-guided generation of a reversible local conduction block. *Cardiovasc. Res.* 113, 354–366. doi: 10.1093/cvr/cvx003

Werfel, S., Jungmann, A., Lehmann, L., Ksienzyk, J., Bekeredjian, R., Kaya, Z., et al. (2014). Rapid and highly efficient inducible cardiac gene knockout in adult mice using AAV-mediated expression of Cre recombinase. *Cardiovasc. Res.* 104, 15–23. doi: 10.1093/cvr/cvu174

Wietek, J., Wiegert, J. S., Adeishvili, N., Schneider, F., Watanabe, H., Tsunoda, S. P., et al. (2014). Conversion of channelrhodopsin into a light-gated chloride channel. *Science* 344, 409–412. doi: 10.1126/science.1249375

Wijffels, M. C., Kirchhof, C. J., Dorland, R., and Allessie, M. A. (1995). Atrial fibrillation begets atrial fibrillation. A study in awake chronically instrumented goats. *Circulation* 92, 1954–1968. doi: 10.1161/01.CIR.92.7.1954

Xu, L., Gutbrod, S. R., Bonifas, A. P., Su, Y., Sulkin, M. S., Lu, N., et al. (2014). 3D multifunctional integumentary membranes for spatiotemporal cardiac measurements and stimulation across the entire epicardium. *Nat. Commun.* 5:3329. doi: 10.1038/ncomms4329

Zacchigna, S., Zentilin, L., and Giacca, M. (2014). Adeno-associated virus vectors as therapeutic and investigational tools in the cardiovascular system. *Circ. Res.* 114, 1827–1846. doi: 10.1161/CIRCRESAHA.114.302331

Zaglia, T., Pianca, N., Borile, G., Da Broi, F., Richter, C., Campione, M., et al. (2015). Optogenetic determination of the myocardial requirements for extrasystoles by cell type-specific targeting of ChannelRhodopsin-2. *Proc. Natl. Acad. Sci. USA* 112, E4495–E4504. doi: 10.1073/pnas.1509380112

Zhang, F., Wang, L. P., Brauner, M., Liewald, J. F., Kay, K., Watzke, N., et al. (2007). Multimodal fast optical interrogation of neural circuitry. *Nature* 446, 633–639. doi: 10.1038/nature05744

Zipes, D. P., Fischer, J., King, R. M., Ad, N., and Jolly, W. W. (1975). Termination of ventricular fibrillation in dogs by depolarizing a critical amount of myocardium. *Am. J. Cardiol.* 36, 37–44. doi: 10.1016/0002-9149(75)90865-6

Conflict of Interest Statement: The authors declare that the research was conducted in the absence of any commercial or financial relationships that could be construed as a potential conflict of interest.

frontiers in Physiology

BRIEF RESEARCH REPORT
published: 24 April 2019
doi: 10.3389/fphys.2019.00498

Optogenetic Hyperpolarization of Cardiomyocytes Terminates Ventricular Arrhythmia

Maximilian Funken[1,2], Daniela Malan[1], Philipp Sasse[1] and Tobias Bruegmann[1,3,4,5]**

[1] Institute of Physiology I, Medical Faculty, University of Bonn, Bonn, Germany, [2] Department of Internal Medicine II, University Hospital Bonn, University of Bonn, Bonn, Germany, [3] Research Training Group 1873, University of Bonn, Bonn, Germany, [4] Institute of Cardiovascular Physiology, University Medical Center, Georg-August-University Göttingen, Göttingen, Germany, [5] DZHK (German Research Centre for Cardiovascular Research), Partner Site Göttingen, Göttingen, Germany

Cardiac defibrillation to terminate lethal ventricular arrhythmia (VA) is currently performed by applying high energy electrical shocks. In cardiac tissue, electrical shocks induce simultaneously de- and hyperpolarized areas and only depolarized areas are considered to be responsible for VA termination. Because electrical shocks do not allow proper control over spatial extent and level of membrane potential changes, the effects of hyperpolarization have not been explored in the intact heart. In contrast, optogenetic methods allow cell type-selective induction of de- and hyperpolarization with unprecedented temporal and spatial control. To investigate effects of cardiomyocyte hyperpolarization on VA termination, we generated a mouse line with cardiomyocyte-specific expression of the light-driven proton pump ArchT. Isolated cardiomyocytes showed light-induced outward currents and hyperpolarization. Free-running VA were evoked by electrical stimulation of explanted hearts perfused with low K^+ and the K_{ATP} channel opener Pinacidil. Optogenetic hyperpolarization was induced by epicardial illumination, which terminated VA with an average efficacy of ∼55%. This value was significantly higher compared to control hearts without illumination or ArchT expression (p = 0.0007). Intracellular recordings with sharp electrodes within the intact heart revealed hyperpolarization and faster action potential upstroke upon illumination, which should fasten conduction. However, conduction speed was lower during illumination suggesting enhanced electrical sink by hyperpolarization underlying VA termination. Thus, selective hyperpolarization in cardiomyocytes is able to terminate VA with a completely new mechanism of increased electrical sink. These novel insights could improve our mechanistic understanding and treatment strategies of VA termination.

Keywords: optogenetics, archaerhodopsin, ventricular arrhythmia, defibrillation, hyperpolarization, electrophysiology, ventricular tachycardia, ventricular fibrillation

OPEN ACCESS

Edited by:
Ming Lei,
University of Oxford, United Kingdom

Reviewed by:
Emilia Entcheva,
George Washington University, United States
Teun P. de Boer,
Utrecht University, Netherlands

****Correspondence:***
Philipp Sasse
philipp.sasse@uni-bonn.de
Tobias Bruegmann
tobias.bruegmann@med.uni-goettingen.de

Specialty section:
This article was submitted to Cardiac Electrophysiology, a section of the journal Frontiers in Physiology

Received: *22 January 2019*
Accepted: *08 April 2019*
Published: *24 April 2019*

Citation:
Funken M, Malan D, Sasse P and Bruegmann T (2019) Optogenetic Hyperpolarization of Cardiomyocytes Terminates Ventricular Arrhythmia. Front. Physiol. 10:498. doi: 10.3389/fphys.2019.00498

Abbreviations: aMHC, α-myosin-heavy-chain; AP, action potential; APD, action potential duration; ArchT, archaerhodopsin from Halorubrum strain TP009; VA, ventricular arrhythmia.

INTRODUCTION

Electrical shocks are the only acute life-saving treatment option for patients with ventricular tachycardia or ventricular fibrillation (ventricular arrhythmia, VA) and subsequent loss of cardiac output (Moss et al., 1996). Electrical shocks consist of one mono- or biphasic electrical field stimulation with high energy applied from external or implanted cardiac defibrillators in order to terminate the underlying high frequency activation and restore sinus rhythm. Due to the anisotropic architecture of the heart with different electrical properties of the intracellular versus the extracellular compartment (Clerc, 1976; Corbin and Scher, 1977; Roberts et al., 1979), the electrical stimulation induces simultaneously de- and hyperpolarized areas (Roth, 1994). These so-called virtual electrodes (Wikswo et al., 1995) consist of a virtual cathode with depolarization in a dog bone shape (Akar et al., 2001) and a perpendicular virtual anode with hyperpolarization parallel to the fiber orientation (Knisley, 1995; Neunlist and Tung, 1995; Sambelashvili et al., 2003) which can be even larger than the virtual cathode (Nikolski et al., 2004). For decades successful defibrillation has only been attributed to the depolarized tissue while the hyperpolarization is considered to generate new wavefronts by a anode-break mechanism (Cranefield et al., 1957) or create a phase singularity which can trigger a new excitation and generate a new arrhythmic wavefront (Efimov et al., 1998; Roth, 1998; Charteris and Roth, 2011). However, the specific effects of hyperpolarization in the intact heart could not be addressed experimentally so far because it is impossible to predict or control the extent of the virtual electrodes induced by electrical field stimulation.

Optogenetic stimulation enables selective hyperpolarization with light within an intact organ in a cell type of interest expressing light-inducible pumps (Wiegert et al., 2017). To analyze the effects of selective hyperpolarization in the intact heart, we expressed the light-driven proton pump archaerhodopsin from the Halorubrum sodomense strain TP009 (ArchT) (Han et al., 2011) selectively in cardiomyocytes in a transgenic animal model. ArchT transports H^+ outside of the cell upon illumination with green light with a peak wavelength of ∼550 nm leading to hyperpolarization of the cell-membrane (Mattis et al., 2012). The cellular buffer capacity prevents the cells from alkalosis if ArchT is activated only for a few seconds (Chow et al., 2010; Mahn et al., 2016). Importantly being an unidirectional outward pump, ArchT induces hyperpolarization without a reversal potential, which is an advantage over optogenetic Cl^- or K^+ conducting ion channels, which are ineffective or even depolarizing at membrane potentials close or below their reversal potential, respectively (Govorunova et al., 2015; Alberio et al., 2018; Bernal Sierra et al., 2018). Specifically, the recently identified Cl^- selective channelrhodopsin variants are not suited because the high intracellular Cl^- concentration results in light-induced depolarization in cardiomyocytes as elegantly described by Kopton et al. (2018) in this focused issue. Importantly, optogenetic hyperpolarization of cardiomyocytes has been used before *in vitro* by co-culture with ArchT-expressing fibroblasts (Nussinovitch et al., 2014) and in ArchT-expressing human induced pluripotent stem cell-derived cardiomyocytes (Quach et al., 2018).

Thus in this project, we aimed to detect the effects of sole hyperpolarization in the intact heart and to decipher a potential role in termination of VA by using ArchT expression in cardiomyocytes.

MATERIALS AND METHODS

An expanded Methods section is available in **Supplementary Material** online. All animal experiments were performed in accordance to the European Guideline for animal experiments 2010/63/EU. Ethical approval for animal experiments was not required because experiments were exclusively performed *ex vivo* on isolated hearts and transgenic animals did not show any pathological phenotype (as assessed by standardized score sheets for animal welfare). Mice were sacrificed by cervical dislocation.

Mouse Model, Expression Analysis, and Patch Clamp

Transgenic mice were generated by crossbreeding αMHC-Cre (Agah et al., 1997) with Ai40D mice, which express ArchT in fusion to eGFP after Cre-mediated excision of a floxed stop cassette (Daigle et al., 2018). Light-induced outward currents and their impact on membrane potential and action potentials (AP) were determined using whole cell patch-clamp recordings (Bruegmann et al., 2010; Vogt et al., 2015). ArchT was activated through the objective with green light (520 nm).

Optogenetic Defibrillation

Free-running sustained VA were induced by epicardial burst (50 Hz) or S1-S2 electrical stimulation (2 ms, 1–10 mA) of explanted hearts perfused with Tyrode solution containing 2 mM K^+ and the K_{ATP}-channel activator Pinazidil (100 μM) as reported previously (Bruegmann et al., 2016). The anterior ventricular wall was illuminated with a macroscope with green light (525 nm). Efficacy of optogenetic VA termination were analyzed with a 11 s long protocol with 4 light pulses (see **Supplementary Figure 1B**) and compared to spontaneous VA termination in control groups within the exact same time window.

Sharp Electrode Measurements in Intact Hearts

Cardiomyocytes' AP were recorded in explanted hearts perfused with Tyrode solution containing 2 mM K^+, 100 μM Pinacidil, as well as Blebbistatin (10 μM) and 2,3-Butanedione monoxime (7.5 mM) to inhibit contractions. Microelectrodes (filled with 3 M KCl, 60 – 120 MΩ,) were penetrated with a fast piezo actuator (5–10 μm steps) until stable resting membrane potential < -60 mV was obtained. Hearts were electrically paced using silver chloride electrodes placed < 3 mm from the recording site. For each recording site, AP upstroke velocity and conduction time were normalized to maximal values.

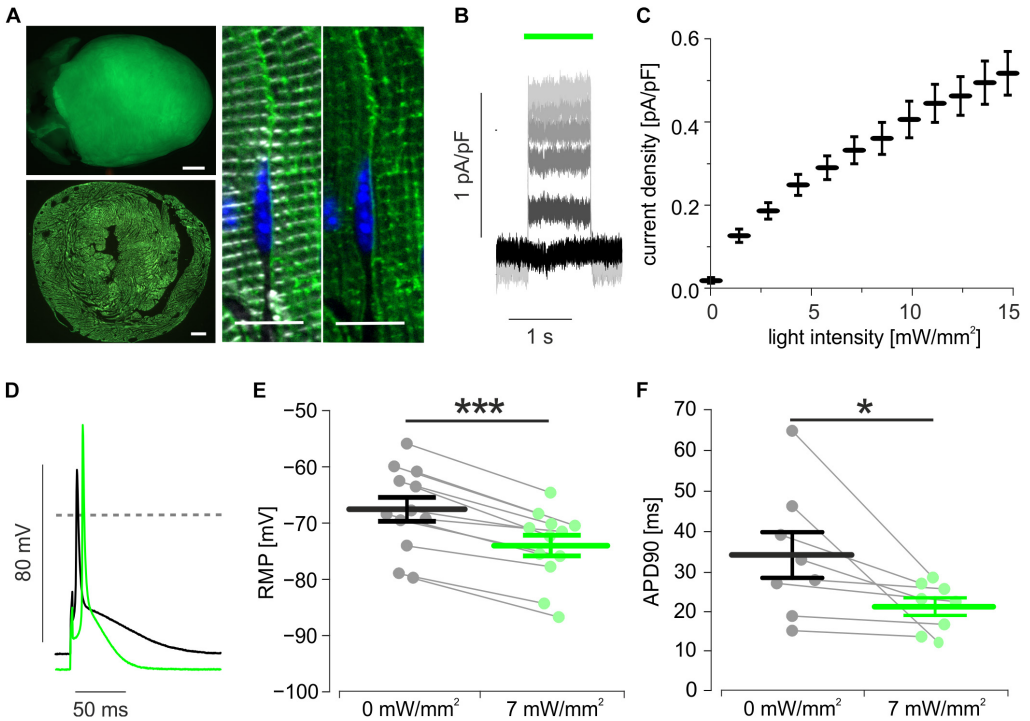

FIGURE 1 | Expression and function of ArchT in isolated cardiomyocytes. **(A)** eGFP fluorescence (green) of an ArchT-eGFP expressing mouse heart (**A**, top, bar = 1 mm), of a ventricular section (**A**, low, bar = 500 μm), and in α-actinin (white) positive cardiomyocytes (**A**, right, bar = 10 μm, nuclear staining in blue). **(B)** Representative traces of outward currents induced by illumination (green bar) with increasing light-intensities (from black to light gray: 0, 3, 6, 8, 10, 14 mW/mm^2). **(C)** Statistical analysis of light intensity to current density relationship (n = 14 cells). **(D)** Representative AP before (black) and during illumination (green, 7 mW/mm^2). **(E,F)** Statistical analysis of light-induced changes in resting membrane potential (**E**, $p < 0.0001$, n = 12 cells) and AP duration (**F**, $p = 0.039$, n = 8 cells) using two-sided paired students t-test. *$p < 0.05$; ***$p < 0.001$.

Statistics

Data are shown as mean ± s.e.m. Statistical analyses were performed using GraphPad Prism with the one-way ANOVA Kruskal–Wallis and Dunn's multiple comparison post-test for VA termination rates, two-sided paired students t-test for patch clamp experiments and a 2-way-ANOVA repeated measurements test for sharp electrode experiments. A p-value <0.05 was considered statistically significant.

RESULTS

Transgenic mice expressing ArchT-eGFP showed bright eGFP fluorescence signals on the epicardial surface which were homogenously distributed throughout the whole myocardial wall and were restricted to the plasma membrane and t-tubulus invaginations of cardiomyocytes (**Figure 1A**). Single cell dissociation revealed 97.4 ± 0.2% (n = 4) eGFP positive cardiomyocytes, which showed green (520 nm) light-evoked outward currents (**Figure 1B**) with current density depending almost linearly on the light intensity (**Figure 1C**). During current clamp recording of stimulated AP, illumination (7 mW/mm^2) led to hyperpolarization by 6.5 ± 0.7 mV (**Figures 1D,E**) and AP duration (APD) shortening by 24.3 ± 5.8% (**Figures 1D,F**).

To assess the effects of hyperpolarization on arrhythmia termination, hearts were explanted and perfused retrogradely in the Langendorff configuration (**Supplementary Figure 1A**). To obtain free-running sustained VA in the small mouse heart, extracellular K^+ concentration was reduced to 2 mM and the K_{ATP} channel opener Pinacidil was applied in order to decrease the cardiac wavelength by conduction slowing and AP shortening (Bruegmann et al., 2016, 2018). Electrical burst or S1 S2 stimulation protocols evoked VA consisting of ventricular tachycardia including Torsade-de-Pointe like arrhythmia (**Figure 2A**) and ventricular fibrillation. Illumination (525 nm, 1 s) of the anterior ventricular surface (24 mm^2) terminated VA inconsistently in some but not during all attempts (**Figure 2A**). For exact determination of optogenetic VA termination efficacy, we performed a precisely timed four light pulse protocol (**Supplementary Figure 1B**). VA termination rates were determined in the same 11 s long time window in all hearts. This yielded an average VA termination success rate of 53 ± 2% for optogenetic hyperpolarization of ArchT expressing hearts. Importantly, VA termination rate was significantly lower in control non-illuminated and/or non-ArchT expressing hearts, which showed spontaneous VA termination rates <30% (**Figure 2B**).

To gain insights into the mechanism underlying hyperpolarization-induced VA termination, we recorded AP

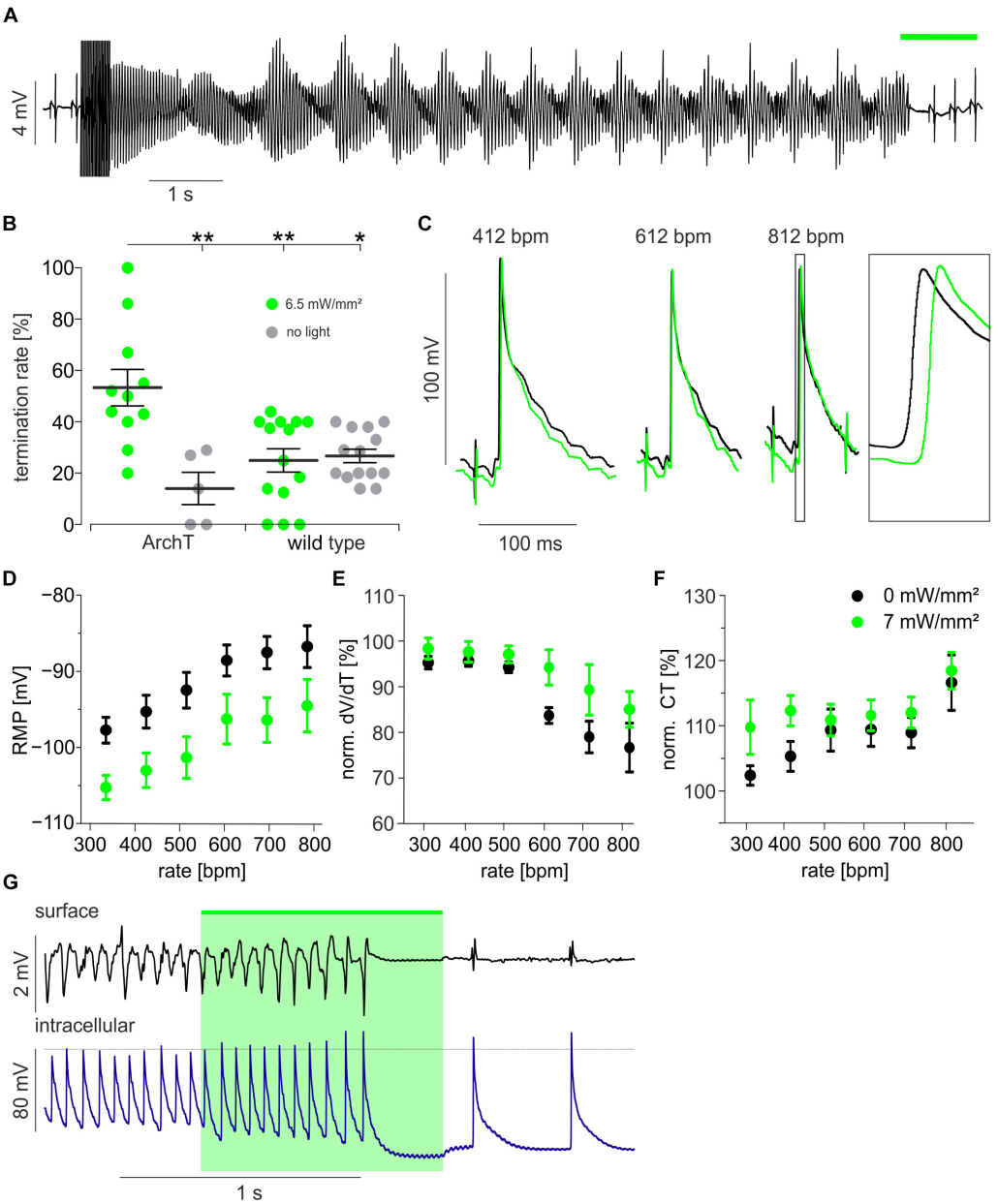

FIGURE 2 | Optogenetic defibrillation by light-induced hyperpolarization. **(A)** Representative example of a Torsade-de-pointe like ventricular arrhythmia induced by electrical burst stimulation and terminated by illumination (**green bar**, 3.4 mW/mm^2) of the ventricular surface (24 mm^2). **(B)** Statistical analysis of termination rates in ArchT expressing (n = 11 and 5) and wild type mice (n = 14) with (green) and without (gray) illumination (see section "Materials and Methods" and **Supplementary Figure 1B**) using the one-way ANOVA Kruskal–Wallis test with Dunn's multiple comparison post-test (*$p < 0.05$; **$p < 0.01$). **(C–F)** Sharp electrode measurements within the illuminated region of the intact heart during electrical pacing from a distant site (see **Supplementary Figure 1C**): Original traces of AP recorded while pacing with 412, 612, and 812 bpm before (black) and during illumination (green, 6.5 mW/mm^2, 24 mm^2) **(C)**. Analysis of resting membrane potential (RMP) (**D**, n = 4, $p < 0.0001$), max. AP upstroke velocity (dV/dt) (**E**, n = 4 – 10, $p < 0.0001$) and conduction time (CT) from the electrical stimulus to the AP generation (**F**, n = 4 – 10, $p = 0.01$) before (black) and during illumination (green) (two-way ANOVA repeated measurements test, p-values are indicating the influence of light). **(G)** Cardiac surface electrogram and simultaneous intracellular membrane potential recording during a ventricular arrhythmia episode with termination by light (green, 6.5 mW/mm^2, 24 mm^2).*$p < 0.05$; **$p < 0.01$.

from cardiomyocytes (**Supplementary Figure 1C**) by impaling sharp microelectrodes within the illuminated (6.5 mW/mm^2) area of intact hearts. Because of the high frequency of VA, we tried to mimic this situation by electrical pacing up to 812 bpm (**Figure 2C**). Pacing at higher heart rates increased the resting membrane potential and epicardial illumination reduced resting membrane potential similarly at all heart rates (**Figure 2D**). Interestingly, AP upstroke velocity was reduced

at heart rates >600 bpm indicating relative refractoriness through reduced Na^+ channel recovery from inactivation due to the depolarized resting membrane potential. This effect was partly reverted by light-induced hyperpolarization (**Figure 2E**). Light-induced restoration of Na^+ channel availability at high heart rates *per se* should result in faster conduction of the electrical excitation wave through the ventricles. However, when analyzing the conduction time between the electrical pacing site and the AP initiation at the recording site, we observed the opposite effect: At all beating rates this parameter was larger during illumination indicating slower electrical conduction or a longer path length during illumination and the effect was most prominent at slow pacing rates (**Figure 2F**). This might be explained by an increased electrical sink upon light-induced hyperpolarization, resulting in slower AP conduction from cell to cell. Importantly during an episode of free-running VA, we observed light-induced hyperpolarization and shortening of APD which was accompanied with a decrease in VA complexity from polymorphic to almost monomorphic VA finally resulting in VA termination (**Figure 2G**). Thus, we conclude that the increased electrical sink is the most likely mechanism underlying hyperpolarization-induced VA termination in our model.

DISCUSSION

Using optogenetic stimulation, we were able to selectively induce hyperpolarization within the intact heart and to demonstrate that hyperpolarization *per se* can terminate VA. In general, VA are triggered by an ectopic premature ventricular excitation and maintained by a short cardiac wavelength (conduction velocity * APD), which can be reduced by several additive mechanisms: The fast VA rate leads to (1) depolarization of the resting membrane potential (**Figure 2D**). In consequence, subthreshold depolarization can speed up propagation by bringing cells closer to the excitation threshold, which was shown elegantly by low dose optogenetic depolarization in a two dimensional monolayer of cardiomyocytes (Burton et al., 2015). However, further depolarization is eventually lowering Na^+ channel availability resulting in (2) slow AP upstroke, and (3) reduced conduction velocity. Furthermore Ca^{2+} channels are inactivated leading to (4) shorter APD. Using sharp electrode experiments, we could confirm the effects (1), (2), and (3) at high pacing rates.

We found that optogenetic hyperpolarization reduces APD (**Figure 1F**), which would rather stabilize VA but could explain the reduction in complexity from polymorphic VA into VT (**Figure 2G**). In line with Na^+ recovery by hyperpolarization, we observed faster AP upstroke velocities upon illumination, but this effect was not strong enough to decrease conduction time, e.g., by fasten conduction velocity. In contrast, the delay between the distant electrical pacing and AP generation was prolonged during illumination (**Figure 2F**) which can be explained by (A) delayed AP initiation at the pacing site, (B) lower conduction velocity between stimulation and the recording site, or (C) a different longer conduction pathway from the stimulation to the recording electrode. Importantly, all three effects would be indicators for an increased electrical sink pulling the resting membrane potential away from the excitation threshold (Burton et al., 2015). In consequence, hyperpolarized resting cardiomyocytes require more inward current from electrical pacing (A) or from the activated neighbor cardiomyocytes (B) to be depolarized above the AP threshold, which is important to maintain the arrhythmic wavefront. Unfortunately, using only one sharp electrode does not allow direct investigation of altered conduction pathways (C) by optogenetic hyperpolarization, however, solving this by combining non-transparent multi-electrode recording or spectrally overlapping voltage mapping with ArchT stimulation is technically challenging. We therefore conclude that the hyperpolarization-induced increase in electrical sink is the main mechanism terminating the VA episodes in our model, in which we have obtained stable VA using low K^+ concentrations and APD shortening by opening K_{ATP} channels.

Compared to continuous optogenetic depolarization using Channelrhodopsin 2 with an efficacy >95% (Bruegmann et al., 2016), VA termination by ArchT-induced hyperpolarization had a much lower and variable efficacy of ∼55%. This can be explained by parallel pro-arrhythmic effects of ArchT activation such as shorter APD reducing the cardiac wavelength or Na^+ channel restoration, which would increase the electrical source of the leading wavefront. Furthermore the low pumping rate of ArchT limits the amount of light induced outward current and hyperpolarization (Mahn et al., 2016) and we had to restrict light intensity to 6.5 mW/mm^2 to avoid cellular damage.

Importantly, the low efficacy excludes optogenetic hyperpolarization from any translational outlook, at least using the ineffective proton pump ArchT. Further development of effective and fast optogenetic K^+-selective channels could allow better insights into the efficacy of VA termination by increasing electrical sink. Selective hyperpolarization as well as combined optogenetic de- and hyperpolarization using spectrally separated optogenetic proteins will lead to a better understanding of VA maintenance and termination mechanisms and might improve current treatment strategies by electrical shocks and antiarrhythmic drugs.

CONCLUSION

Cardiomyocyte-specific expression of the light-inducible proton pump ArchT allowed to investigate the effects of isolated hyperpolarization in the intact heart. Thereby we were able to demonstrate that hyperpolarization *per se* can terminate VA with an increased electrical sink being the most probable mechanism.

ETHICS STATEMENT

Animal breeding and handling were performed in accordance to the European Guideline for animal experiments 2010/63/EU. Ethical approval for animal experiments was not required because experiments were exclusively performed *ex vivo* on isolated hearts and transgenic animals did not show any

pathological phenotype (as assessed by standardized score sheets for animal welfare).

AUTHOR CONTRIBUTIONS

TB and PS designed the study. MF, DM, PS, and TB performed the experiments. MF, DM, and TB analyzed the data. MF, PS, and TB prepared the manuscript.

FUNDING

This work was supported by the German Research Foundation [315402240/SA1785/8-1, 313904155/SA1785/7-1, 380524518/SA1785/9-1, 214362475/GRK1873/2, and SPP 1926 Young Investigator Program (GO1011/11-1)], the BONFOR Program, Medical Faculty, University of Bonn, by the German Federal Ministry of Education and Research, funding program Photonics Research Germany, project BioPACE (13N14087) and TB was supported by the DZHK (German Centre for Cardiovascular Research). We also acknowledge support by the Open Access Publication Funds of the German Research Foundation and the Göttingen University.

ACKNOWLEDGMENTS

The authors thank Frank Holst for his technical assistance, Dr. Dagmar Wachten (University of Bonn, Germany) for providing with the αMHC Cre mice, and the Jackson Laboratory (ME, United States) for providing with the Ai40D mice.

SUPPLEMENTARY MATERIAL

The Supplementary Material for this article can be found online at: https://www.frontiersin.org/articles/10.3389/fphys.2019.00498/full#supplementary-material

REFERENCES

Agah, R., Frenkel, P. A., French, B. A., Michael, L. H., Overbeek, P. A., and Schneider, M. D. (1997). Gene recombination in postmitotic cells. Targeted expression of Cre recombinase provokes cardiac-restricted, site-specific rearrangement in adult ventricular muscle *in vivo*. *J. Clin. Invest.* 100, 169–179. doi: 10.1172/JCI119509

Akar, F. G., Roth, B. J., and Rosenbaum, D. S. (2001). Optical measurement of cell-to-cell coupling in intact heart using subthreshold electrical stimulation. *Am. J. Physiol. Heart Circ. Physiol.* 281, H533–H542.

Alberio, L., Locarno, A., Saponaro, A., Romano, E., Bercier, V., Albadri, S., et al. (2018). A light-gated potassium channel for sustained neuronal inhibition. *Nat. Methods* 15, 969–976. doi: 10.1038/s41592-018-0186-9

Bernal Sierra, Y. A., Rost, B. R., Pofahl, M., Fernandes, A. M., Kopton, R. A., Moser, S., et al. (2018). Potassium channel-based optogenetic silencing. *Nat. Commun.* 9:4611. doi: 10.1038/s41467-018-07038-8

Bruegmann, T., Beiert, T., Vogt, C. C., Schrickel, J. W., and Sasse, P. (2018). Optogenetic termination of atrial fibrillation in mice. *Cardiovasc. Res.* 114, 713–723. doi: 10.1093/cvr/cvx250

Bruegmann, T., Boyle, P. M., Vogt, C. C., Karathanos, T. V., Arevalo, H. J., Fleischmann, B. K., et al. (2016). Optogenetic defibrillation terminates ventricular arrhythmia in mouse hearts and human simulations. *J. Clin. Invest.* 126, 3894–3904. doi: 10.1172/JCI88950

Bruegmann, T., Malan, D., Hesse, M., Beiert, T., Fuegemann, C. J., Fleischmann, B. K., et al. (2010). Optogenetic control of heart muscle *in vitro* and *in vivo*. *Nat. Methods* 7, 897–900. doi: 10.1038/nmeth.1512

Burton, R. A., Klimas, A., Ambrosi, C. M., Tomek, J., Corbett, A., Entcheva, E., et al. (2015). Optical control of excitation waves in cardiac tissue. *Nat. Photonics* 9, 813–816. doi: 10.1038/nphoton.2015.196

Charteris, N. P., and Roth, B. J. (2011). How hyperpolarization and the recovery of excitability affect propagation through a virtual anode in the heart. *Comput. Math. Methods Med.* 2011:375059. doi: 10.1155/2011/375059

Chow, B. Y., Han, X., Dobry, A. S., Qian, X., Chuong, A. S., Li, M., et al. (2010). High-performance genetically targetable optical neural silencing by light-driven proton pumps. *Nature* 463, 98–102. doi: 10.1038/nature08652

Clerc, L. (1976). Directional differences of impulse spread in trabecular muscle from mammalian heart. *J. Physiol.* 255, 335–346. doi: 10.1113/jphysiol.1976.sp011283

Corbin, L. V. II, and Scher, A. M. (1977). The canine heart as an electrocardiographic generator. Dependence on cardiac cell orientation. *Circ. Res.* 41, 58–67. doi: 10.1161/01.res.41.1.58

Cranefield, P. F., Hoffman, B. F., and Siebens, A. A. (1957). Anodal excitation of cardiac muscle. *Am. J. Physiol.* 190, 383–390. doi: 10.1152/ajplegacy.1957.190.2.383

Daigle, T. L., Madisen, L., Hage, T. A., Valley, M. T., Knoblich, U., Larsen, R. S., et al. (2018). A suite of transgenic driver and reporter mouse lines with enhanced brain-cell-type targeting and functionality. *Cell* 174, 465.e22–480.e22. doi: 10.1016/j.cell.2018.06.035

Efimov, I. R., Cheng, Y., Van Wagoner, D. R., Mazgalev, T., and Tchou, P. J. (1998). Virtual electrode-induced phase singularity: a basic mechanism of defibrillation failure. *Circ. Res.* 82, 918–925. doi: 10.1161/01.res.82.8.918

Govorunova, E. G., Sineshchekov, O. A., Janz, R., Liu, X., and Spudich, J. L. (2015). NEUROSCIENCE. Natural light-gated anion channels: a family of microbial rhodopsins for advanced optogenetics. *Science* 349, 647–650. doi: 10.1126/science.aaa7484

Han, X., Chow, B. Y., Zhou, H., Klapoetke, N. C., Chuong, A., Rajimehr, R., et al. (2011). A high-light sensitivity optical neural silencer: development and application to optogenetic control of non-human primate cortex. *Front. Syst. Neurosci.* 5:18. doi: 10.3389/fnsys.2011.00018

Knisley, S. B. (1995). Transmembrane voltage changes during unipolar stimulation of rabbit ventricle. *Circ. Res.* 77, 1229–1239. doi: 10.1161/01.res.77.6.1229

Kopton, R. A., Baillie, J. S., Rafferty, S. A., Moss, R., Zgierski-Johnston, C. M., Prykhozhij, S. V., et al. (2018). Cardiac electrophysiological effects of light-activated chloride channels. *Front. Physiol.* 9:1806. doi: 10.3389/fphys.2018.01806

Mahn, M., Prigge, M., Ron, S., Levy, R., and Yizhar, O. (2016). Biophysical constraints of optogenetic inhibition at presynaptic terminals. *Nat. Neurosci.* 19, 554–556. doi: 10.1038/nn.4266

Mattis, J., Tye, K. M., Ferenczi, E. A., Ramakrishnan, C., O'Shea, D. J., Prakash, R., et al. (2012). Principles for applying optogenetic tools derived from direct comparative analysis of microbial opsins. *Nat. Methods* 9, 159–172. doi: 10.1038/nmeth.1808

Moss, A. J., Hall, W. J., Cannom, D. S., Daubert, J. P., Higgins, S. L., Klein, H., et al. (1996). Improved survival with an implanted defibrillator in patients with coronary disease at high risk for ventricular arrhythmia. Multicenter automatic defibrillator implantation trial investigators. *N. Engl. J. Med.* 335, 1933–1940. doi: 10.1056/NEJM199612263352601

Neunlist, M., and Tung, L. (1995). Spatial distribution of cardiac transmembrane potentials around an extracellular electrode: dependence on fiber orientation. *Biophys. J.* 68, 2310–2322. doi: 10.1016/S0006-3495(95)80413-3

Nikolski, V. P., Sambelashvili, A. T., Krinsky, V. I., and Efimov, I. R. (2004). Effects of electroporation on optically recorded transmembrane potential responses

to high-intensity electrical shocks. *Am. J. Physiol. Heart Circ. Physiol.* 286, H412–H418. doi: 10.1152/ajpheart.00689.2003

Nussinovitch, U., Shinnawi, R., and Gepstein, L. (2014). Modulation of cardiac tissue electrophysiological properties with light-sensitive proteins. *Cardiovasc. Res.* 102, 176–187. doi: 10.1093/cvr/cvu037

Quach, B., Krogh-Madsen, T., Entcheva, E., and Christini, D. J. (2018). Light-activated dynamic clamp using iPSC-derived cardiomyocytes. *Biophys. J.* 115, 2206–2217. doi: 10.1016/j.bpj.2018.10.018

Roberts, D. E., Hersh, L. T., and Scher, A. M. (1979). Influence of cardiac fiber orientation on wavefront voltage, conduction velocity, and tissue resistivity in the dog. *Circ. Res.* 44, 701–712. doi: 10.1161/01.res.44.5.701

Roth, B. J. (1994). Mechanisms for electrical stimulation of excitable tissue. *Crit. Rev. Biomed. Eng.* 22, 253–305.

Roth, B. J. (1998). The pinwheel experiment revisited. *J. Theor. Biol.* 190, 389–393. doi: 10.1006/jtbi.1997.0565

Sambelashvili, A. T., Nikolski, V. P., and Efimov, I. R. (2003). Nonlinear effects in subthreshold virtual electrode polarization. *Am. J. Physiol. Heart Circ. Physiol.* 284, H2368–H2374. doi: 10.1152/ajpheart.00988.2002

Vogt, C. C., Bruegmann, T., Malan, D., Ottersbach, A., Roell, W., Fleischmann, B. K., et al. (2015). Systemic gene transfer enables optogenetic pacing of mouse hearts. *Cardiovasc. Res.* 106, 338–343. doi: 10.1093/cvr/cvv004

Wiegert, J. S., Mahn, M., Prigge, M., Printz, Y., and Yizhar, O. (2017). Silencing neurons: tools, applications, and experimental constraints. *Neuron* 95, 504–529. doi: 10.1016/j.neuron.2017.06.050

Wikswo, J. P. Jr., Lin, S. F., and Abbas, R. A. (1995). Virtual electrodes in cardiac tissue: a common mechanism for anodal and cathodal stimulation. *Biophys. J.* 69, 2195–2210. doi: 10.1016/S0006-3495(95)80115-3

Conflict of Interest Statement: The authors declare that the research was conducted in the absence of any commercial or financial relationships that could be construed as a potential conflict of interest.

frontiers in Physiology

PROTOCOLS
published: 06 August 2019
doi: 10.3389/fphys.2019.00954

A Protocol for Dual Calcium-Voltage Optical Mapping in Murine Sinoatrial Preparation With Optogenetic Pacing

Ruirui Dong[1†], Razik Mu-u-min[2†], Alastair J. M. Reith[2†], Christopher O'Shea[3†], Shicheng He[1], Kaizhong Duan[2], Kun Kou[1], Alexander Grassam-Rowe[2], Xiaoqiu Tan[1], Davor Pavlovic[3‡], Xianhong Ou[1‡] and Ming Lei[1,2*‡]*

[1]Key Laboratory of Medical Electrophysiology of Ministry of Education and Medical Electrophysiological Key Laboratory of Sichuan Province, Institute of Cardiovascular Research, Southwest Medical University, Luzhou, China, [2]Department of Pharmacology, University of Oxford, Oxford, United Kingdom, [3]Institute for Cardiovascular Sciences, University of Birmingham, Birmingham, United Kingdom

OPEN ACCESS

Edited by:
Bas J. Boukens,
University of Amsterdam,
Netherlands

Reviewed by:
Robert Alan Rose,
University of Calgary, Canada
Vincent Portero,
Academic Medical Center,
Netherlands

***Correspondence:**
Xianhong Ou
oxh8081@swmu.edu.cn
Ming Lei
ming.lei@pharm.ox.ac.uk

†Joint first authors
‡Joint senior authors

Specialty section:
This article was submitted to Cardiac Electrophysiology, a section of the journal Frontiers in Physiology

Received: 15 December 2018
Accepted: 09 July 2019
Published: 06 August 2019

Citation:
Dong R, Mu-u-min R, Reith AJM, O'Shea C, He S, Duan K, Kou K, Grassam-Rowe A, Tan X, Pavlovic D, Ou X and Lei M (2019) A Protocol for Dual Calcium-Voltage Optical Mapping in Murine Sinoatrial Preparation With Optogenetic Pacing. Front. Physiol. 10:954. doi: 10.3389/fphys.2019.00954

Among the animal models for studying the molecular basis of atrial and sinoatrial node (SAN) biology and disease, the mouse is a widely used species due to its feasibility for genetic modifications in genes encoding ion channels or calcium handling and signaling proteins in the heart. It is therefore highly valuable to develop robust methodologies for studying SAN and atrial electrophysiological function in this species. Here, we describe a protocol for performing dual calcium-voltage optical mapping on mouse sinoatrial preparation (SAP), in combination with an optogenetic approach, for studying SAP membrane potential, intracellular Ca^{2+} transients, and pacemaker activity. The protocol includes the details for preparing the intact SAP, robust tissue dual-dye loading, light-programmed pacing, and high-resolution optical mapping. Our protocol provides an example of use of the combination of optogenetic and optical mapping techniques for investigating SAP membrane potential and intracellular Ca^{2+} transients and pacemaker activity with high temporal and spatial resolution in specific cardiac tissues. Thus, our protocol provides a useful tool for studying SAP physiology and pathophysiology in mice.

Keywords: sinoatrial preparation, optogenetic pacing, optical mapping, murine heart, Ca^{2+} transient

INTRODUCTION

The heartbeat begins in the sinoatrial node (SAN) arising in a subset of nodal cells that display a spontaneous diastolic depolarization (Bleeker et al., 1980). Unique to such automaticity of the SAN, pacemaker cells possess "membrane clock" contributions by several membrane currents including the funny current, I_f, carried by hyperpolarization-activated cyclic nucleotide-gated (HCN) channels. I_f is initiated specifically at the initial phase of the diastolic depolarization, following the deactivation of outward delayed rectifier K^+ current, and triggering the activation of inward currents. Inward currents include Na^+-dependent background current; the T- and L-type Ca^{2+} currents, I_{CaT} and I_{CaL}; and possibly, sustained inward current, I_{st} (Lei et al., 2018). However, more recently, intracellular signaling involving the sarcoplasmic reticulum (SR) Ca^{2+} stores and the cellular cAMP levels and consequent phosphorylation of their signaling proteins have also been implicated in a "Ca^{2+} clock" contributing to diastolic depolarization (Lei et al., 2018). Whereby, spontaneous RyR2-mediated Ca^{2+} release may enhance electrogenic effects of the Na^+-Ca^{2+} exchanger

in late diastolic depolarization (Lei et al., 2018). These SR calcium release events may be triggered by calcium-induced calcium release following the activation of $Ca_{V1.3}$ calcium channels (Torrente et al., 2016). The relative importance of both the "membrane clock" and "Ca^{2+} clock" in pacemaker function remains controversial.

On the other hand, sinus node dysfunction (SND) associated with abnormal impulse formation or propagation in the SAN affects ≈1 in 600 cardiac patients aged >65 years and is responsible for ≈50% of the 1 million permanent pacemaker implants per year worldwide (de Marneffe et al., 1993). Although SND occurs most commonly in elderly patients in the absence of clinically apparent accompanying cardiac disease (de Marneffe et al., 1993), its pathogenesis is unclear. The development of novel pharmacological therapies to cure these patients relies on the thorough understanding of both normal physiology and pathophysiology of the SAN and atria.

Among the animal models for studying the basic molecular mechanisms of the SAN and atrial biology and disease, mice are widely used due to their feasibility for modifications in the expression of different genes that encode ion channels or calcium handling proteins. It is therefore highly valuable to develop robust methodologies and techniques for studying SAN and atrial electrophysiological properties.

Recent advances in the technique of optogenetics provide an unprecedented opportunity for defining specific cell-type function in a highly complex multicellular system. The technique has enabled control over the activity of one specific cell type while leaving others unaltered, with high temporal resolution and cellular precision. Since the first demonstrations of utility in mammalian neurons in 2005 (Boyden et al., 2005), optogenetics has spurred immense research activity in neuroscience and has extended to the cardiac field over the past few years (Entcheva, 2013; Nussinovitch and Gepstein, 2015; Boyle et al., 2018). We recently deployed a cell-type specific optogenetic approach to study the properties of $Pnmt^+$ cell-derived cardiomyocytes in the murine heart (Wang et al., 2017). Additionally, optical mapping using fluorescent dyes provides exciting opportunities for high spatio-temporal study of cellular electrophysiological events, including Ca^{2+} dynamics of the heart (Wang et al., 2017; Wen et al., 2018). The combination of these two technologies therefore allows development of unprecedented platforms for studying physiological events (e.g., voltage and Ca^{2+} signals) in a selective manner at high spatio-temporal resolution (O'Shea et al., 2019b).

In this manuscript, we describe a detailed protocol for the use of optogenetic and optical mapping techniques for investigating membrane potential and intracellular Ca^{2+} transients and pacemaker activity with high temporal and spatial resolution in sinoatrial preparations (SAPs). The protocol can be a powerful tool for studying SAP physiology and pathophysiology using the mouse as a model system.

METHODS AND MATERIALS

Animals

Pnmt-cre mice used in this study are as described previously (Wang et al., 2017). Animals used were <6 months old. Pnmt-cre/ChR2 mice exhibit cell-type specific expression of ChR2 by crossing B6.Cg-*Gt (ROSA)26Sor*$^{tm27.1(CAG-COP4H134R/tdTomato)\ Hze}$/J strain (Stock no. 012567, Jackson Labs) with a Cre transgenic strain under the control of a *Pnmt* promoter (Wang et al., 2017). Channelrhodopsin 2 (ChR2) was specifically introduced into murine cells expressing the *Phenylethanolamine n-methyltransferase* (*Pnmt*) gene, which encodes for the enzyme responsible for conversion of noradrenaline to adrenaline. The murine model led to the identification of a distinctive class of Pnmt-expressing neuroendocrine cells and their descendants (i.e., $Pnmt^+$ cell-derived cardiomyocytes) within the heart (Wang et al., 2017).

All procedures have been approved by Institutional Animals Ethics Committees at Southwest Medical University, Luzhou, China or Department of Pharmacology at University of Oxford, UK and the national guidelines under which the institution operates. All mice used in this study were maintained in a pathogen-free facility at Southwest Medical University or University of Oxford. Mice were given *ad libitum* access to food and water. The authors confirm that they have taken all steps to minimize the animals' pain and suffering.

Materials and Equipment

Table 1 shows the details of materials and buffers.

Figure 1 shows the optical imaging system for light stimulation of ChR2 light-sensitive channels and optical recording.

The tissues were paced through the activation of ChR2 light-sensitive channels. This was achieved by the delivery of 470 nm blue light pulses (13–14 ms pulse width) generated by OptoFlash (Cairn Research, Faversham, UK). Pulses were triggered by a 1,401 digitizer and Spike 2 software (Cambridge Electronic Design). Approximate blue light intensity was measured with a 818-ST2 Wand Detector connected to a 843-R power meter (both Newport Corporation, CA, USA), and we estimate an average irradiance in our experiments of 0.1–0.3 mW/mm^2 based on an approximate distance of 1–2 cm between Sylgard and liquid light guide (Oriel instruments Model No. 77525).

TABLE 1 | Details of materials and buffers.

Chemical and catalogue reference	Supplier
NaCl (SLBS2340V)	Sigma-Aldrich, St Louis, MO, USA
$NaHCO_3$ (SLBX3605)	Sigma-Aldrich
NaH_2PO_4 (BCBW9042)	Sigma-Aldrich
KCl (SLBS5003)	Sigma-Aldrich
$MgCl_2$ (BCBS6841V)	Sigma-Aldrich
$CaCl_2$ (SLBK1794V)	Sigma-Aldrich
Glucose (SLBT4811V)	Sigma-Aldrich
HEPES (W1122DO10)	Sangon biological Shanghai, China
2,3-butanedione monoxime (BDM) (29297)	Sigma-Aldrich
Blebbistatin (SLBV5564)	Tocris Bioscience Minneapolis, MN, USA
Voltage-sensitive dye RH237 (1971387)	Thermo Fisher Scientific, Waltham, MA, USA
Calcium indicator Rhod-2 AM (1890519)	Invitrogen, Carlsbad, CA, USA
Dimethyl sulfoxide (DMSO) (RNBT7442)	Sigma-Aldrich
Heparin Sodium (H51021209)	Chengdu Haitong Pharmaceutical Co. Ltd. Chengdu, China
Avertin (2,2,2-tribromoethanol)	Sigma-Aldrich Poole, Dorset, UK
Pluronic F127 (1899021)	Invitrogen, Carlsbad, CA, USA

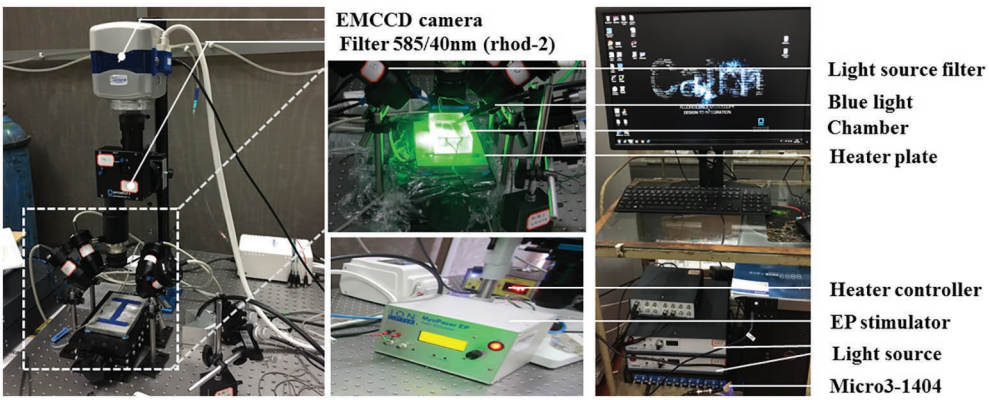

FIGURE 1 | The optical imaging system. Two green (a peak wavelength of 530 nm) and two red (a peak wavelength of 627 nm) LED lights (Cairn Research, Faversham, Kent, UK) were placed around the chamber so as to uniformly illuminate the SAP. The green LEDs were fitted with excitation bandpass filters (S555/25X, Chroma Technology GmbH, Germany), and the red LEDs were fitted with excitation bandpass filters (HQ640/50, Chroma Technology GmbH, Germany) to efficiently select the best excitation wavelength range for Rhod-2 AM and Di-4-ANBDQPQ, respectively. A multi-bandpass emission filter (ET595/50 + 700LP, Chroma Technology GmbH, Germany) was placed in front of the camera lens to avoid bleed-through of the excitation light and to selectively let the fluorescence emission pass through. A multi-stream light switcher (Cairn Research, Faversham, Kent, UK) was set up to automatically switch between the red and green LED lights in accordance with the frame rate of the camera. Signal recording using this setup is in such a way that one frame data recorded will have only the red light turned on (thereby recording voltage signal alone) and the next frame data recorded will have only the green light turned on (thereby recording CaT signal alone), and the process is repeated until the desired number of frames are recorded.

Buffer Compositions

Physiological Salt Solution

Freshly prepared physiological salt solution (PSS) containing in mM: NaCl 119, $NaHCO_3$ 25, NaH_2PO_4 1.0, KCl 4.7, $MgCl_2$ 1.2, $CaCl_2$ 1.35, and glucose 10; equilibrated with 95% O_2/5% CO_2 at 37°C, pH = 7.35.

Dye Loading Solution

Calcium indicator Rhod-2 AM (Invitrogen, Carlsbad, CA, USA) was dissolved in dimethyl sulfoxide (DMSO, Sigma-Aldrich, St. Louis, MO, USA) to prepare a stock concentration of 10 mg/ml (8.9 mM). The voltage indicator stock was prepared by dissolving Di-4-ANBDQPQ (University of Connecticut Health Center) in ethanol to obtain a stock concentration of 29 mM. To avoid repeated freezing and thawing, both stocks were stored in 50 µl aliquots at −20°C. For working concentrations of Rhod-2 AM dye loading solution, 15 µl Rhod-2 AM stock solution was mixed with 15 µl Pluronic F-127 (20% solution in DMSO, Invitrogen, Carlsbad, CA, USA) and then dissolved in 15 ml PSS (10 µM final concentration). Similarly, 5.2 µl of Di-4-ANBDQPQ stock was mixed with 15 µl Pluronic F-127 and then dissolved in 15 ml PSS to form a working concentration of Di-4-ANBDQPQ dye loading solution (10 µM final concentration). The working dye loading solutions were prepared on the day of the experiment.

Blebbistatin Physiological Salt Solution

Excitation-contraction uncoupler blebbistatin (Invitrogen, Carlsbad, CA, USA) was dissolved in in DMSO (Sigma-Aldrich, St. Louis, MO, USA) to make up 10 mM stock solution. To avoid repeated freezing and thawing, aliquots of 15 µl were stored at −20°C. A 10 µl of 10 mM stock blebbistatin solution was added to 15 ml PSS to make blebbistatin PSS solution (10 µM final concentration).

Preparation and Equipment

1. Dissection set-up includes stereomicroscope, dissection chamber filled with Sylgard gel, oxygenation device, LED light source, and surgical instruments.
2. The optical mapping system was set up as detailed below:

A custom-designed system equipped with an EMCCD camera (Evolve 128, Photometrics, Tucson, AZ, USA) was used (see **Figure 1**). Two green (to excite Ca^{2+} sensitive dye Rhod-2 AM; a peak wavelength of 530 nm) and two red (to excite the voltage sensitive dye Di-4-ANBDQPQ; a peak wavelength of 627 nm) LED lights (Cairn Research, Faversham, UK) were placed around the imaging chamber so as to uniformly illuminate the SAP. The green LEDs (peak wavelength = 530 nm) were fitted with excitation bandpass filters (S555/25X, Chroma Technology GmbH, Germany), and the red LEDs (peak wavelength = 627 nm) were fitted with excitation bandpass filters (HQ640/50, Chroma Technology GmbH, Germany) to efficiently select optimal excitation wavelength range for Rhod-2 AM and Di-4-ANBDQPQ, respectively. A multi-bandpass emission filter (ET595/50 + 700LP, Chroma Technology GmbH, Germany) was placed in front of the camera lens to avoid bleed-through of the excitation light and to selectively let the fluorescence emission to pass through. CaT (calcium transient) and transmembrane potential (V_m) measurements were taken at high resolution (128 × 128 pixels; pixel size 66 × 66 µm) at a rate of 520 frames/s.

PROTOCOL

Harvest the Mouse Heart and Prepare the Sinoatrial Preparation (30 min)

The steps for preparation of the SAP are outlined in **Figure 2** and as described previously (Liu et al., 2007; Hao et al., 2011; Sharpe et al., 2016). The details are as follows:

1. Non-recovery terminal general anesthesia was induced by injection of an overdose of 1.2% Avertin solution (0.5–0.8 ml i.p., 2,2,2-tribromoethanol, Sigma-Aldrich, Poole, Dorset, UK), followed by intraperitoneal injection with heparin (200 units).
2. Following sacrifice *via* cervical dislocation, the heart was rapidly excised and placed in warmed (37°C) and oxygenated (95% O_2 + 5% CO_2 gas) PSS solution in a dissection chamber.
3. The heart was gently pressed with the tips of fingers to push the blood out of heart. Fresh oxygenated PSS was then added for further dissection.
4. SAP containing two atria and the SAN region was dissected after clearing off the lung, thymus, ventricles, and connective tissues (**Figure 2B**).
5. The right atrium was opened from atrioventricular (AV) junction to expose the intercaval region containing the SAN, following which left atrium was opened to expose the left atrial endocardium. As the pacemaker cells are widely distributed throughout the entire region located between the superior (SVC) and inferior vena cava (IVC) and between the crista terminalis and intra-atrial septum (Glukhov et al., 2010), the SAP contains the SAN and the two atria intact.
6. The SAP was pinned onto a small rectangular piece of Sylgard gel by using fine insect pins. All dissection steps were performed in a dissection chamber with oxygenated PSS solution under a stereomicroscope.

Dual Dye Loading of the Sinoatrial Preparation (25 min)

7. A 50 ml falcon tube was filled with 15 ml of the Rhod-2 AM dye loading solution.
8. The Sylgard gel (with SAP attached) was then dropped into the falcon tube.
9. The SAP-containing falcon tube was placed in a 36°C water bath. The solution was oxygenated constantly by gently bubbling with 95% O_2/5% CO_2 (Note: heavy bubbling can lead to the formation of foam due to the presence of Pluronic F-127 in the solution. This can lead to the suboptimal dye loading). The SAP was incubated in the dye loading solution for 15 min.
10. Dual dye loading of the SAP was performed by incubating the SAP in Rhod-2 AM dye loading solution as detailed above (points 7–9), following which the Sylgard gel with SAP attached was transferred into a new 50 ml falcon tube containing 10 μM Di-4-ANBDQPQ dye loading solution. Incubation with Di-4-ANBDQPQ was performed for 10 min at 36°C and constantly bubbled with 95% O_2/5% CO_2.

Optical Mapping (30 min)

11. The imaging chamber was filled with 15 ml of blebbistatin PSS solution and was placed directly under the camera. The recording chamber was heated up to 36°C by a heating plate.
12. The Sylgard (with SAP attached) was removed from the falcon tube and pinned down in the imaging chamber. The sample was placed between the two field-stimulation electrodes. (Note: Removing the SAP from the Sylgard and pinning down directly in the chamber cause further damage to the SAP. Therefore, pinning down the Sylgard with the intact

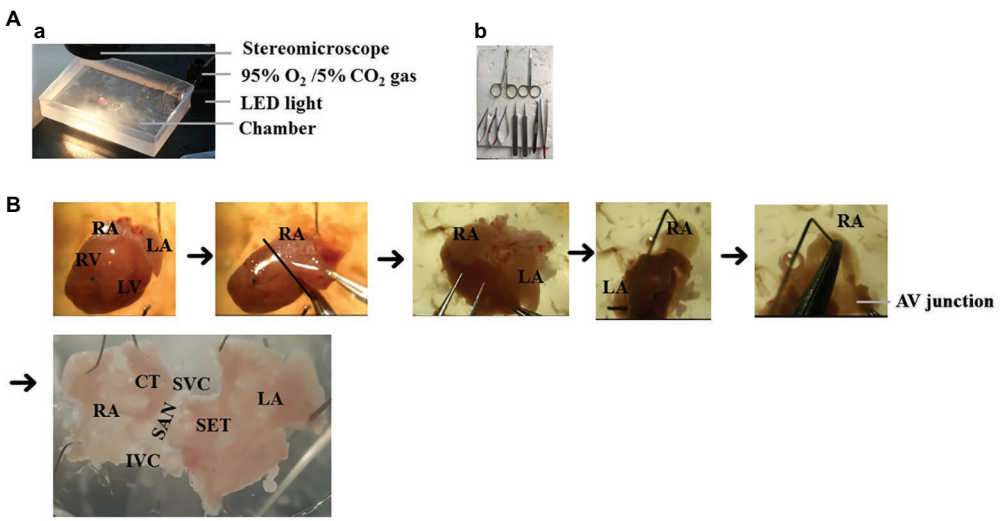

FIGURE 2 | The isolation of mouse SAP. **(A)** The setup of dissection. **(a)** The dissection was performed under the stereomicroscope and oxygenated PSS solution. **(b)** Surgical instruments. **(B)** The preparation of SAP. RA, right atrium; LA, left atrium; RV, right ventricle; LV, left ventricle; SAN, sinoatrial node; AV junction, atrioventricular junction, SET = septum, SVC = superior vena cava, IVC = inferior vena cava, CT = crista terminalis.

tissue is recommended). The blebbistatin PSS solution was bubbled in the imaging chamber with 95% O_2/5% CO_2 gas.

13. Imaging was performed after cessation of motion by blebbistatin. Imaging used the EMCCD camera controlled by the acquisition software Metamorph (Molecular Devices). During image recordings, the excitation lights were turned on, and bubbling was temporarily stopped (to avoid distortion of the signals due to bubbles and motion of the solution). Since Pnmt$^+$ cell-derived cardiomyocytes (PdCMs) express channelrhodopsin-2 (ChR2), they can be excited by exposure to 470 nm blue light. The stimulation protocol was then run, and baseline calcium transient or action potential recordings were taken. Recordings were taken again after stimulating the left atrium using blue light (pacing intervals: 150–160 ms, pulse duration: 13–14 ms, intensity: 1,992 mA). The frame rate of these recordings was 0.52 kHz.
14. For dual dye imaging, a multistream light switcher (Cairn Research, Faversham, Kent, UK) was set up to automatically switch between the red (627 nm) and green (530 nm) LED lights according to the frame rate of the camera. Signal recording using this setup was performed, so that one frame of the data was recorded under red light illumination (thereby recording V_m signal alone), and the next frame was recorded under green light illumination (thereby recording CaT signal alone) and so forth until the desired number of frames was recorded. This resulted in an interlaced signal containing alternate frames of CaT and V_m signals. The interlaced signal was separated into CaT and voltage signal using ImageJ and saved as separate files. Due to the signals being interposed, the frame rate recording was 0.26 kHz.

Analysis

15. The saved image files were loaded, processed, and analyzed using the optical mapping analysis software ElectroMap (developed by Dr. Pavlovic's group, https://github.com/CXO531/ElectroMap; O'Shea et al., 2019a).
16. Images were pre-processed by applying a 4 × 4 pixel Gaussian spatial filter (standard deviation = 1.5), a Top-Hat baseline correction (kernel size = 100 ms), and a third order Savitzky-Golay temporal filter. A window size of 40 ms before transient peak to 100 ms after transient peak was used. Action potential duration (APD) and CaT duration (CaD) were measured at the desired repolarization/decay percentage at each pixel across the tissue, as measured from time of maximum upstroke velocity (maximum dF/dt).
17. For assessment of local conduction velocities, activation maps were generated using time of depolarization midpoint. Conduction velocity across the SAP was then quantified using a multi-vector polynomial method (Bayly et al., 1998) with a local window size of 5 × 5 pixels.
18. To further assess conduction across the entire SAP, we used activation curve analysis, where the percentage of tissue activated was plotted as a function of time (O'Shea et al., 2019a).

Representative Results

A typical example of an SAP Ca^{2+} transient activation map reconstructed from spontaneous sinus rhythmic Ca^{2+} transients (by Rhod-2 AM) recorded with the optical mapping system is shown in **Figure 3A** for a SAP. The early activation point is located within the intercaval region near to where the SAN is located. However, as shown in **Figure 3B,** the calcium activation pattern and atrial conduction changed after stimulating with blue light (interval: 150 ms; duration: 13 ms; intensity: 1,992 mA; pulses per train: 50). The leading pacemaker site was shifted to the location of left atrium, suggesting that PdCMs were activated earlier than the SAN pacemaker cells. This is consistent with our previous report that PdCM cells predominantly localized to the left atrium and left ventricle, and the heart rate was controlled by stimulating PdCMs selectively with blue light (Wang et al., 2017). We hypothesize that PdCM cells overexpressing ChR2 may be a viable site for spatially-targeted optical pacing when sinus node pacemaker cells are dysfunctional. Further

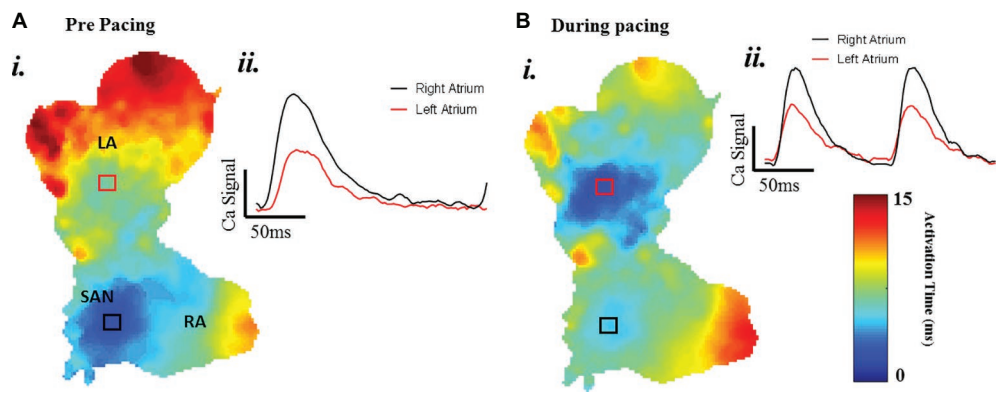

FIGURE 3 | The change of atrial conduction in optogenetic mice during after blue light stimulation. Maps produced by mapping the midpoint time of the CaT rise. **(A)** Ca^{2+} transient activation map during intrinsic pacing, before optical pacing. **(B)** Ca^{2+} transient activation map during optical pacing with blue (470 nm) light pulses.

investigation is required. **Figure 4** shows representative V_m and CaT maps and voltage and calcium traces from different regions of the SAP, illustrating the robustness of this preparation for murine research. We monitored the "rundown" of the V_m and CaT signals for up to 4 h – the average signal "rundown" is less than 25%. Our experiment usually finished within 3 h from the beginning of Langendorff perfusion of the heart. We again observe augmentation of the activation pattern induced by optical pacing, shown by both the voltage (**Figure 4**, upper panel) and calcium (**Figure 4**, lower panel) activation maps. Activation maps were produced by mapping the midpoint time of the AP/CaT rise.

We found that optogenetic pacing of a SAP can shift the activation point to the left, creating a new leading pacemaker site or "neonode." Activation patterns in the SAP were plotted using ElectroMap (O'Shea et al., 2019a), with the midpoint of the upstroke of the calcium transient used as a pixel-by-pixel readout of tissue activation. The earliest-activating pixel—discarding outliers—was designated the activation point for that tissue. The earliest activation point before pacing was always in the nodal region. Optogenetic pacing of PdCMs can move this activation point to the left (**Figure 5**), establishing a new leading pacemaker site toward the left atrium. This change in the location of the leading pacemaker is reversible upon cessation of pacing (**Figures 5A**,**E**). Left shift of the leading pacemaker occurred in four of seven SAPs (**Figure 5D**). One leftward deviation appears more upward relative to the SVC-IVC axis—this is due to contortion of the tissue. Although no leading pacemaker shift occurred in three SAPs, all seven SAPs were successfully paced by blue light: with a decrease in mean cycle length from 264.3 ± 42.7 ms before optogenetic pacing to 159.2 ± 1.4 ms during ($p < 0.02$). Mean cycle length after pacing was 281.9 ± 48.9 ms—not significantly different from before ($p = 0.63$). Therefore, we can always successfully and reversibly pace PdCMs using selective ChR2 overexpression. The variability in pacemaker shift observed (**Figure 5D**) is consistent with the variable distribution of murine PdCMs across both the SAN region and the left atrium (Ni et al., 2017; Wang et al., 2017). In summary, we report the possibility of using optogenetic pacing of PdCMs to establish novel left-shifted leading pacemaker sites in the murine heart.

To study the effects of optogenetic pacing on overall conduction, we utilized activation curve analysis where the percentage of tissue activated is plotted as a function of time (O'Shea et al., 2019a). Optogenetic pacing of PdCMs augments conduction in the SAP—producing a left shift of the activation curve (**Figure 6A**). This is most noticeable in the first few milliseconds of tissue activation (**Figure 6A**, inset). During optogenetic pacing, the rate of tissue activation is initially very rapid (**Figure 6B**, inset), otherwise, there are no major alterations to tissue activation rate (**Figure 6B**). Optogenetic pacing reduces the time to 5% tissue activation from 1.59 ± 0.24 to 0.88 ± 0.17 ms ($p = 0.03$),

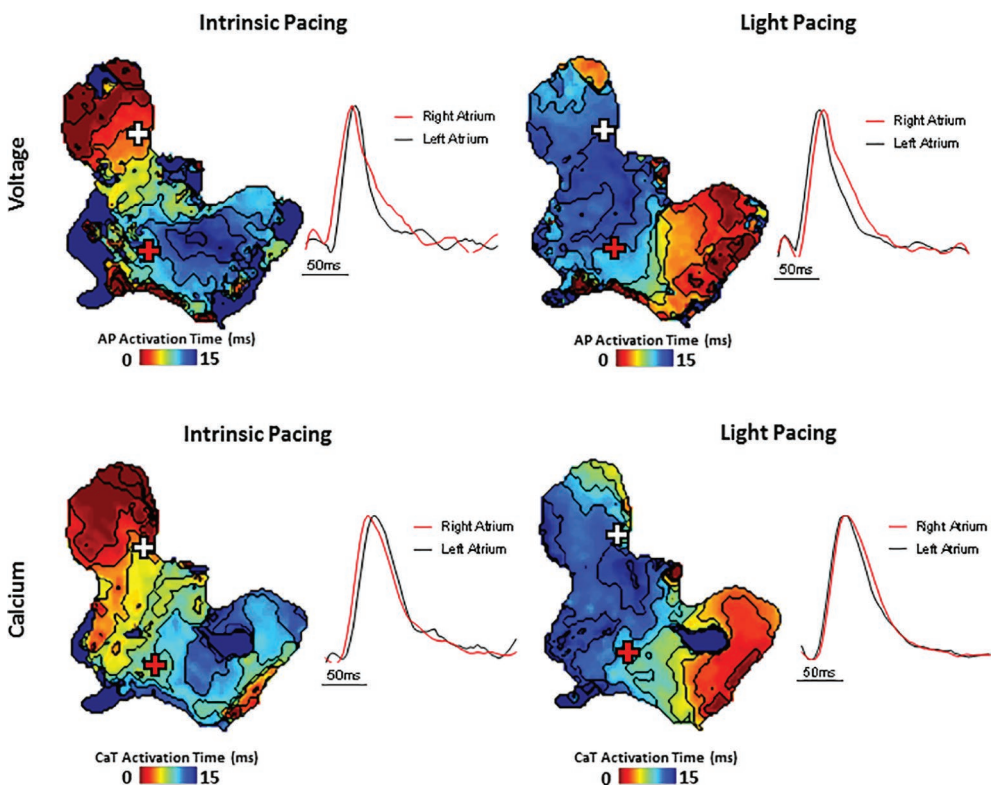

FIGURE 4 | Simultaneous voltage (top panels) and Ca^{2+} transient (bottom panels) activation maps reconstructed from spontaneous sinus rhythmic (left panels) and light paced (right panels) SAP. Maps were produced by mapping the midpoint time of the voltage and CaT rise with examples of voltage and Ca^{2+} transient traces from indicated regions of the preparation (white and red cross).

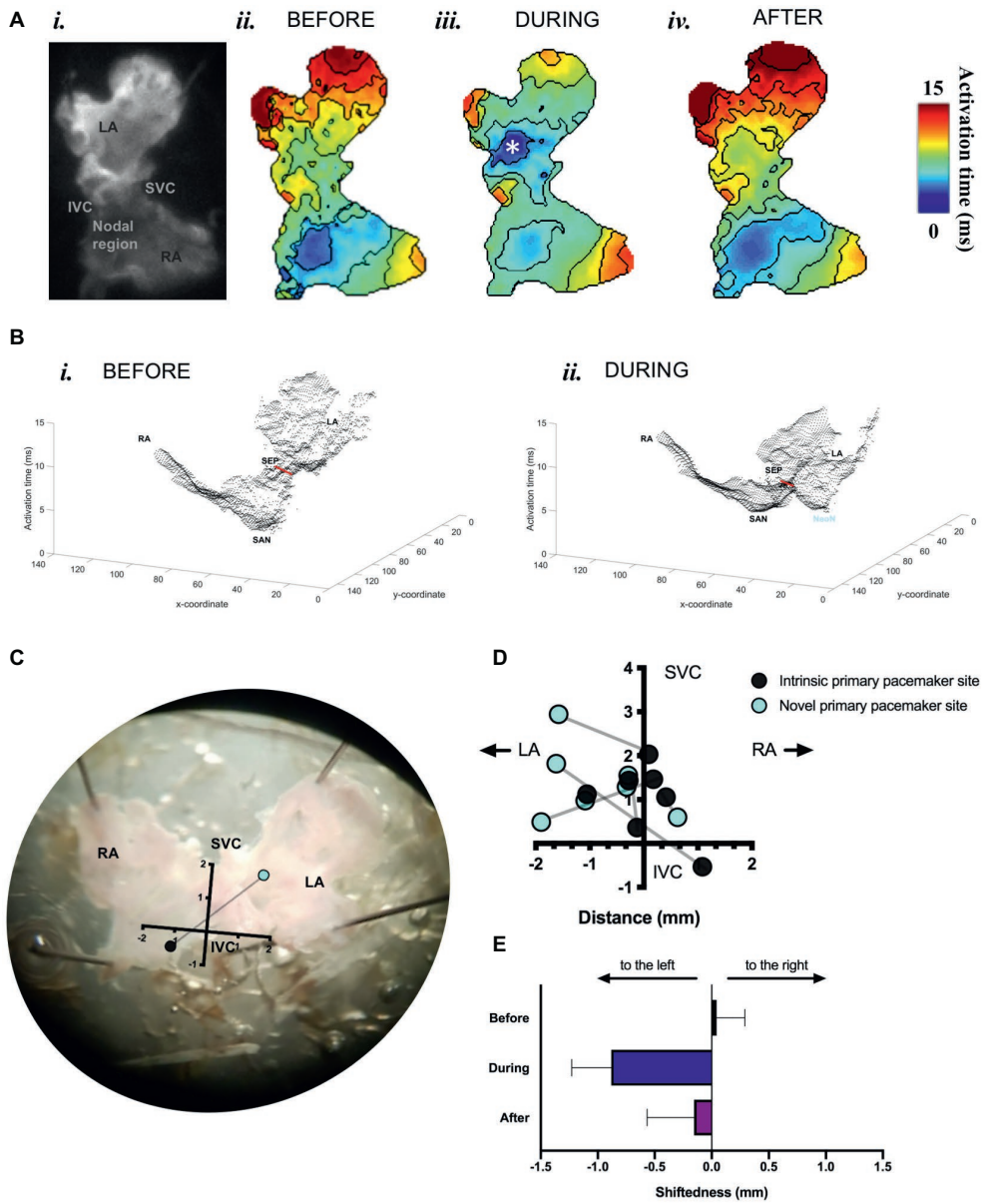

FIGURE 5 | Mapping of activation in SAPs under sinus rhythm and under optogenetic pacing. **(A)** (*i*) Representative SAP—camera view. (*ii*) Activation map for this SAP before optogenetic pacing. (*iii*) Activation map during pacing (note formation of "neonode", white asterisk). (*iv*) Activation map after pacing. Activation maps are calculated from Ca^{2+} transients. Fifty pacing spikes given, at 6.67 Hz. Contours drawn at 1/frame rate of the EMCCD. Scale bar, right. **(B)** 3-D graphical rendering of activation maps (*i*) before pacing, (*ii*) during pacing. SVC-IVC axis in red. Activation time on z-axis. **(C)** Representative SAP—microscope view. Pacemaker shift overlaid. SVC-IVC axis shown. Distances in mm. **(D)** SVC-IVC axis with relative pacemaker shifts plotted (n = 7). **(E)** Mean change in "shiftedness." LA, left atrium; RA, right atrium; SAN, sinoatrial node; SVC, superior vena cava; IVC, inferior vena cava; SEP, septum; NeoN, neonode.

the time to 10% tissue activation from 2.40 ± 0.25 to 1.46 ± 0.26 ms (p = 0.02), and the time to 20% tissue activation from 3.91 ± 0.52 to 2.27 ± 0.33 ms (p = 0.02) (**Figure 6C**), but at all points ≥30% tissue activation, there is no significant difference in activation time (**Figures 6A,B**).

We also wanted to explore whether the normal conduction pathways in the tissue remained intact during optogenetic pacing. Using ElectroMap, we computed local conduction velocities using the multi-vector method (Bayly et al., 1998) with a 5 × 5-pixel grid size. The magnitude of conduction velocity vectors (**Figure 6D**) did not change significantly with optogenetic pacing from 26.9 ± 3.3 before to 28.6 ± 2.5 cm/s during pacing (p = 0.34), and there were no major changes in the directionality of conduction vectors either (**Figure 6E**). In summary, we report the possibility of establishing a novel left-shifted leading pacemaker site, with only minimal, controlled disturbance to normal tissue activation rate, and little or no disturbance to the pathways along which conduction normally propagates.

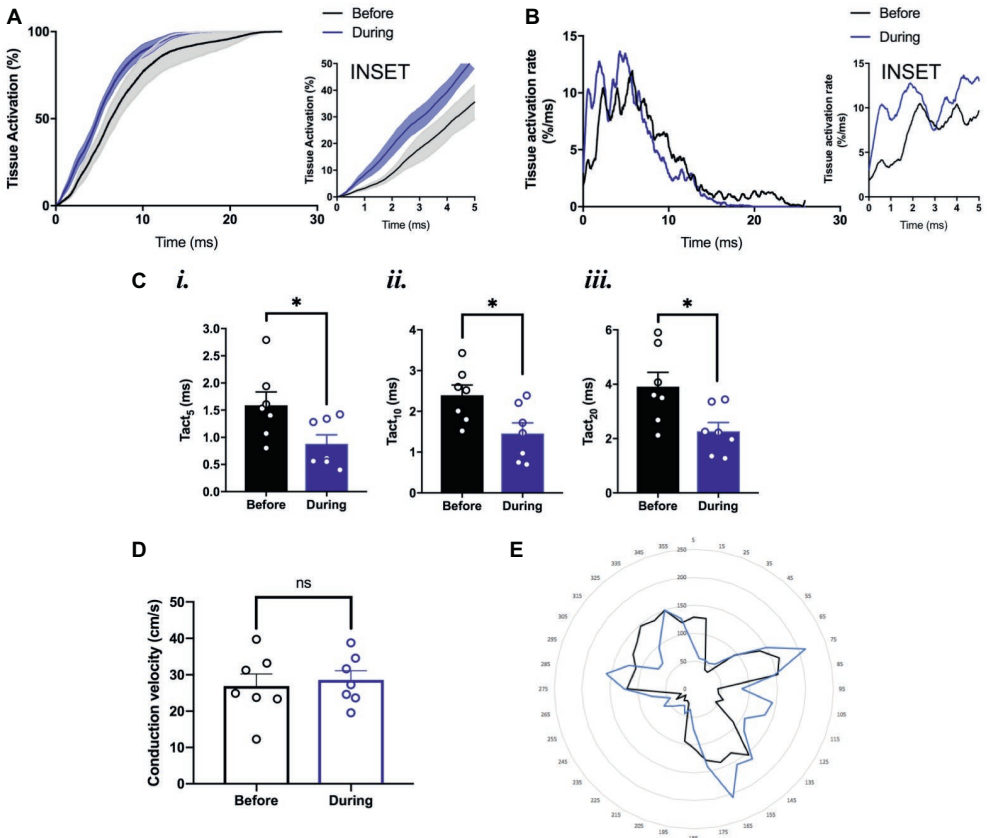

FIGURE 6 | Conduction pattern in the tissue under sinus rhythm and during optogenetic pacing. **(A)** Grouped activation curve showing mean % tissue activated over the time elapsed during a Ca^{2+} transient. SEM denoted by shading. Inset: zoomed section of first 5 ms. **(B)** Rate of change of % tissue activation plotted against time. Inset as above. **(C)** (*i*) Time to 5% tissue activation. (*ii*) Time to 10% tissue activation. (*iii*) Time to 20% tissue activation. **(D)** Mean magnitude of local conduction vectors. **(A–D)** $n = 7$ throughout. **(E)** Representative radar plot, showing local conduction vector directionalities. Angles binned into groups of 10°—so $0° \leq x < 10°$ becomes 5°, $10° \leq x <°20°$ becomes 15°, and so on. Concentric circles represent increasing frequency of vectors at that angle.

We found small alterations to calcium cycling in our tissues, but for the most part, there was no significant change in the characteristics of calcium transient rise time, calcium transient duration to 50% of the decay (CaD50), and calcium transient duration to 75% of the decay (CaD75) with optogenetic pacing. We measured the rise time, calcium transient duration to 50% of the decay (CaD50), and calcium transient duration to 75% of the decay (CaD75) as illustrated in **Figure 7A**. Rise time is a measure of upstroke duration, calculated between 10 and 90% of time to peak, which minimizes analytical uncertainty (Choi and Salama, 2000; Jaimes et al., 2016). We used a mixed-effects model, with Tukey's *post hoc* tests where required, to examine whether there were any significant effects of optogenetic pacing. For rise time, there was a significant overall effect of optogenetic pacing ($p < 0.0001$). *Post hoc* testing revealed that there was no significant effect of pacing on rise time in the right atrium or in the neonodal regions—but in the left atrium, rise time fell from 17.21 ± 0.94 ms before pacing to 15.24 ± 1.14 ms during pacing ($p < 0.002$) and rose again after pacing to 18.60 ± 1.00 ms ($p < 0.05$, during vs. after) and in the nodal region, rise time fell from 17.48 ± 1.03 to 15.24 ± 1.14 ms ($p < 0.03$) and rose again after pacing to 18.44 ± 0.95 ms ($p = 0.02$, during vs. after). In both regions, there was no significant difference between the before and after conditions (left atrium: $p = 0.39$; nodal region: $p = 0.61$)—so the reduction in rise time with optogenetic pacing is reversible upon cessation of pacing (**Figure 7B**). There was no overall significant effect of optogenetic pacing on either CaD50 ($p = 0.15$) or CaD75 ($p = 0.34$; **Figures 7C,D**). In summary, rise time is shorter in the left atrium and in the SAN region during optogenetic pacing, and this is a reversible change. Otherwise, calcium handling in the murine SAP appears to be only marginally affected.

DISCUSSION

The success in obtaining high quality V_m and Ca^{2+} mapping results in SAPs requires several important technical considerations, including high consumption of oxygen and high sensitivity to temperature and pH of the nodal tissue. Furthermore, the dense arrangement of nodal cells combined with the significant presence of connective tissue makes it hard for a Ca^{2+} dye to reach to the nodal and atrial cells. The critical steps include as follows:

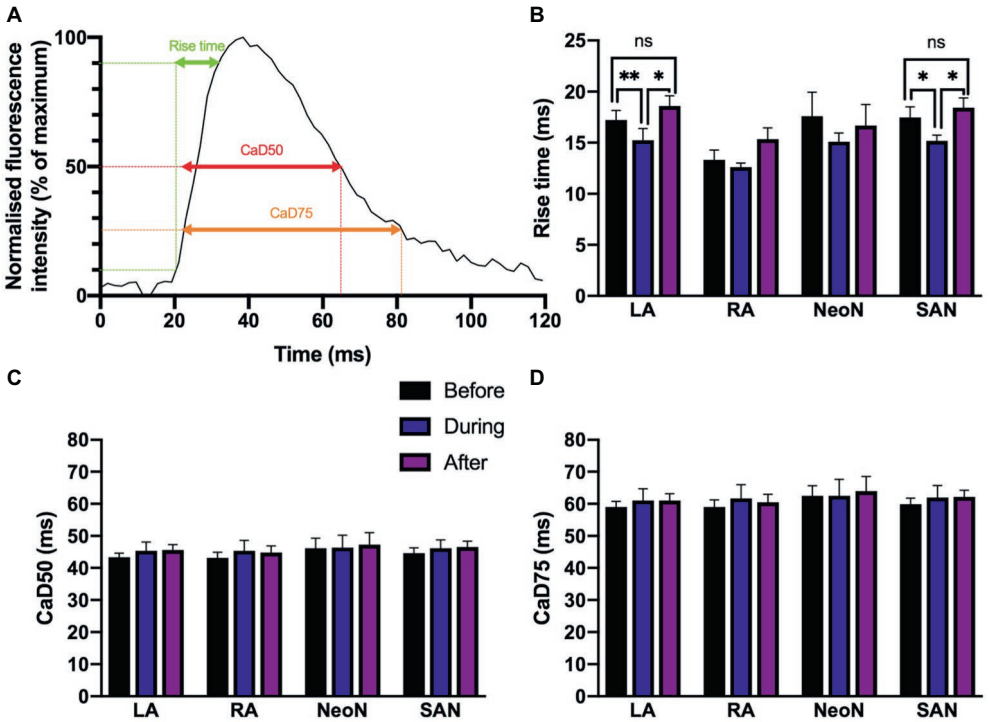

FIGURE 7 | (A) Characteristics of Ca^{2+} transients recorded from different regions under sinus rhythm and optogenetic pacing. Representative Ca^{2+} transient illustrating rise time; CaD50 (Ca^{2+} transient duration to 50% of the decay); and CaD75 (Ca^{2+} transient duration to 75% of the decay). CaD50 and CaD75 are calculated from max. dF/dt (max. upstroke) as detailed in the protocol. **(B)** Mean rise time, before (n = 7), during (n = 7), and after (n = 6) optogenetic pacing. Key at center. Grouping is by region: LA, left atrium; RA, right atrium; NeoN, neonodal region (n = 4); SAN, nodal region. **(C)** Mean CaD50 values, no overall significant effect of optogenetic pacing. **(D)** Mean CaD75 values, no overall significant effect of optogenetic pacing.

Tissue Preparation

Intact SAPs were micro-dissected as described previously (Ju et al., 2015). The SAN region was identified from anatomical landmarks, including the superior vena cava, the crista terminalis, and the interatrial septum. The tissue needs to be oxygenated constantly. At this point, temperature is not critical.

Dye Loading

The Ca^{2+}-sensitive dye used to load the SAP tissue was Rhod-2 AM, a dye in the acetoxymethyl ester form. Esterification of the fluorescent molecule (Rhod-2 AM) results in an uncharged molecule that can permeate cell membranes and chelate cytosolic Ca^{2+}. A 100-fold increase in the molecule's fluorescence intensity results from Ca^{2+} chelation (Choi and Salama, 2000). The voltage sensitive dye used was Di-4-ANBDQPQ, due to its favorable spectral properties for use with Rhod-2 AM. In our experiments, dye loading was carried out by incubating the tissue in a solution consisting of Pluronic F-127 dissolved in DMSO. Pluronic F-127 was incorporated into the dye loading solution to better disperse the dye into the physiological solution. Dye loading was observed to be generally better in younger mice than old, which may be related to connective tissue making up a smaller volume of the node.

The SAP's repetitive contractions may have disrupted dye loading and/or aided the leaking of the dye out from the tissue, making it a challenge to optimize dye loading conditions. A fluorescent dye that diffuses across the cell membrane well can also exit from the cytoplasm at a high rate. Reagents like probenecid help prevent this to an extent. Combining these with optimized temperatures, timings and oxygen supply are necessary for effective loading of the tissue with dye.

Optical Imaging

During imaging, motion artifacts caused disruption in the measurement of optical signals. Hence, to reduce contraction of the tissue, blebbistatin was used. Blebbistatin is an inhibitor of the adenosine triphosphatases associated with class II isoforms of myosin (Allingham et al., 2005). This compound has been identified as an effective excitation-contraction uncoupler, and previous investigators have used it at several different concentrations (Fedorov et al., 2007). The use of blebbistatin at 10 μM appeared to effectively abolish any motion artifact due to contraction of the SAP without harming SAP.

$Pnmt^{+}$ Cell-Derived Cardiomyocytes (PdCMs) and Biopacemaking Strategies

The advent of cardiac optogenetics has facilitated the identification of a new cardiomyocyte subpopulation in the murine heart, phenylethanolamine-N-methyl transferase $Pnmt^{+}$-derived cardiomyocytes (PdCMs; Wang et al., 2017). Through selective

manipulation of these cells using optogenetics, our study demonstrated how optogenetics can be used to target specific cardiomyocyte subpopulations, overcoming many of the issues associated with traditional electrophysiological techniques. Selectively stimulating PdCMs with rhythmic blue (470 nm) light pulses was sufficient to maintain sinus rhythm in murine atria, supporting previous observations from whole heart studies (Wang et al., 2017). It has also been found previously that the left atrium alone – dissected out– can be paced by light (Wang et al., 2017), but a capacity to optogenetically control the SAP has not been tested before.

The observation that a "neonode" is typically set up toward the left is consistent with previous findings that PdCMs occupy a left-sided distribution in murine heart (Wang et al., 2017). We therefore assessed the effect of pacing on left atrial activation. Optogenetic pacing of PdCMs leads to alterations in the conduction pattern across murine atria. We found (**Figure 5**) that optogenetic pacing of Pnmt-cre/Ai27D SAPs can often set up new sites of earliest activation ("neonodes") toward the left of the tissue. Our proof-of-principle studies clearly demonstrate feasibility of optogenetic control of heart rate *via* the specific cell population. Indeed, in four of seven SAPs, we observed "neonode" formation, with the leading pacemaker shifting toward the left atrium. Lack of leftward shift in three of seven preparations may be due to the heterogeneity in cell numbers and clustering of the Pnmt cells in the SAPs, thus altering sink-source properties of the myocardium. While the physiological consequences of the studies presented here (specifically using Pnmt cells) are not immediately clear, application of such approaches is of interest to the community and may lead to important findings on the consequences of the spatial shift in the leading pacemaker.

As recently reviewed by Boyle et al. (2018), initial work in this area assessed possibility to override the intrinsic pacing frequency of a beating heart using optical stimuli. Bruegmann et al. (2010) explored this question in a preclinical model by generating ChR^{2+} transgenic mice. They showed in an open-chest configuration that pulses of light from a focused light source could be used to maintain ventricular activation at rates faster than intrinsic sinus rhythm. Light-induced wavefronts were initiated from different parts of the heart (e.g., atrial or ventricular sites). Remarkably, the authors found that 1:1 capture could be maintained when the illuminated area was small (0.05 mm^2, ∼50 myocytes), suggesting that optogenetic pacing *via* a small population of cells is possible and robust. Several recent studies also provided evidence for the development of optogenetic defibrillating device for termination of tachyarrhythmias (Nyns et al., 2016; Bruegmann et al., 2017). Bruegmann et al. (2017) reported optogenetic termination of atrial tachyarrhythmia in intact hearts from transgenic as well as wild-type mice *ex* and *in vivo*. Thus, they suggested that their report could lay the foundation for the development of implantable devices for pain-free termination of AF. Nyns et al. (2016) demonstrated that forced expression of a light-gated depolarizing ion channel (ReaChR) in the adult rat heart allows contact- and shock-free termination of VTs through brief local illumination of the ventricular surface, i.e., without relying on conventional drugs, tissue ablation, or electroshocks. Both mono- and polymorphic VTs could be terminated in an effective and repetitive manner by a light-induced electrical current driven by natural electrochemical gradients, providing proof-of-concept for biological arrhythmia termination. Our study also provides proof-of-concept evidence supporting the development of light-based pacing devices targeted to a particular cellular population.

Limitations of the Protocol

There are a number of possible limitations in this protocol including: (1) possibility of injury during the dissection of the preparation; (2) effectiveness of dye loading may vary between preparations, thereby affecting the results; and (3) partial uncoupling (reduction in conductance) due to the use of blebbistatin, which could increase the regional differences in Ca^{2+} dynamics in SAPs.

Conclusions and Future Directions

Here, we have described a detailed protocol for dual optical mapping of murine SAPs with optogenetic pacing. Combination of high-resolution optical imaging with cell-specific optogenetic stimulation allows unique spatial control and study of electrophysiology of the SAP, not possible with traditional direct or field electrode techniques. In the present protocol, we have demonstrated this principle with PdCMs; however, the protocol can be valuable for any mouse models that cell specifically express opsins such as ChR2 within the sinoatrial region of the heart. Therefore, such an approach represents a powerful tool for enhanced electrophysiological understanding of supraventricular physiology and pathophysiology.

Future improvements may focus on exploring dual dye imaging and improved image processing software. Higher resolution and novel optical imaging modalities for 3D optical mapping are also important future directions of optical mapping.

ETHICS STATEMENT

Pnmt-Cre mice used in this study are as described in our previous paper (Wang et al., 2017). Animals used were <6 months old, 20–25 g. All procedures including animal subjects have been approved by Institutional Animals Ethics Committees at Southwest Medical University, Luzhou, China or Department of Pharmacology at University of Oxford and the national guidelines under which the institution operates. All mice used in this study were maintained in a pathogen-free facility at Southwest Medical University or University of Oxford. Mice were given *ad libitum* access to food and water. The authors confirm that they have taken all steps to minimize the animals' pain and suffering. Our work complies with the journal policy and regulations.

AUTHOR CONTRIBUTIONS

RD, RM, AR, and SH performed the experiments and produced the data. CO'S, AR, and DP analysed the results.

AG-R, KD, XT, and KK assisted with data processing and manuscript preparation. ML and XO drafted the manuscript with the assistance of RM, DP, and AR. ML revised the manuscript with the assistance of CO'S, DP, RM, AR, and AG-R.

FUNDING

This study was supported by Medical Research Council (G10002647, G1002082, ML), British Heart Foundation (PG/14/80/31106, PG/16/67/32340, PG/12/21/29473, PG/11/59/29004 ML; PG/17/55/33087, RG/17/15/33106, FS/19/16/34169, FS/19/12/34204 DP), BHF Centre of Research Excellence, Oxford (ML) grants, EPSRC (L016346 DP), National Natural Science Foundation of China (Nos. 81700308 and 31871181).

ACKNOWLEDGMENTS

We thank Dr. Leslie M. Loew at University of Connecticut for providing Di-4-ANBDQPQ.

REFERENCES

Allingham, J. S., Smith, R., and Rayment, I. (2005). The structural basis of blebbistatin inhibition and specificity for myosin II. *Nat. Struct. Mol. Biol.* 12, 378–379. doi: 10.1038/nsmb908

Bayly, P. V., KenKnight, B. H., Rogers, J. M., Hillsley, R. E., Ideker, R. E., and Smith, W. M. (1998). Estimation of conduction velocity vector fields from epicardial mapping data. *I.E.E.E. Trans. Biomed. Eng.* 45, 563–571. doi: 10.1109/10.668746

Bleeker, W. K., Mackaay, A. J., Masson Pevet, M., Bouman, L. N., and Becker, A. E. (1980). Functional and morphological organization of the rabbit sinus node. *Circ. Res.* 46, 11–22. doi: 10.1161/01.RES.46.1.11

Boyden, E. S., Zhang, F., Bamberg, E., Nagel, G., and Deisseroth, K. (2005). Millisecond-timescale, genetically targeted optical control of neural activity. *Nat. Neurosci.* 8, 1263–1268. doi: 10.1038/nn1525

Boyle, P. M., Karathanos, T. V., and Trayanova, N. A. (2018). Cardiac optogenetics: 2018. *JACC Clin. Electrophysiol.* 4, 155–167. doi: 10.1016/j.jacep.2017.12.006

Bruegmann, T., Beiert, T., Vogt, C. C., Schrickel, J. W., and Sasse, P. (2017). Optogenetic termination of atrial fibrillation in mice. *Cardiovasc. Res.* 114, 713–723. doi: 10.1093/cvr/cvx250

Bruegmann, T., Malan, D., Hesse, M., Beiert, T., Fuegemann, C. J., Fleischmann, B. K., et al. (2010). Optogenetic control of heart muscle in vitro and in vivo. *Nat. Methods* 7, 897–900. doi: 10.1038/nmeth.1512

Choi, B. R., and Salama, G. (2000). Simultaneous maps of optical action potentials and calcium transients in Guinea-pig hearts: mechanisms underlying concordant alternans. *J. Physiol.* 529, 171–188. doi: 10.1111/j.1469-7793.2000.00171.x

de Marneffe, M., Gregoire, J. M., Waterschoot, P., and Kestemont, M. P. (1993). The sinus node function: normal and pathological. *Eur. Heart J.* 14, 649–654. doi: 10.1093/eurheartj/14.5.649

Entcheva, E. (2013). Cardiac optogenetics. *Am. J. Physiol. Heart Circ. Physiol.* 304, H1179–H1191. doi: 10.1152/ajpheart.00432.2012

Fedorov, V. V., Lozinsky, I. T., Sosunov, E. A., Anyukhovsky, E. P., Rosen, M. R., Balke, C. W., et al. (2007). Application of blebbistatin as an excitation-contraction uncoupler for electrophysiologic study of rat and rabbit hearts. *Heart Rhythm* 4, 619–626. doi: 10.1016/j.hrthm.2006.12.047

Glukhov, A. V., Fedorov, V. V., Anderson, M. E., Mohler, P. J., and Efimov, I. R. (2010). Functional anatomy of the murine sinus node: high-resolution optical mapping of ankyrin-B heterozygous mice. *Am. J. Physiol. Heart Circ. Physiol.* 299, H482–H491. doi: 10.1152/ajpheart.00756.2009

Hao, X., Zhang, Y., Zhang, X., Nirmalan, M., Davis, L., Dobrzynski, H., et al. (2011). TGF-b1 mediated fibrosis and ion channel remodeling are key mechanisms producing the sinus node dysfunction associated with SCN5A deficiency and aging. *Circ. Arrhythm. Electrophysiol.* 4, 397–406. doi: 10.1161/CIRCEP.110.960807

Jaimes, R. 3rd, Walton, R. D., Pasdois, P., Bernus, O., Efimov, I. R., and Kay, M. W. (2016). A technical review of optical mapping of intracellular calcium within myocardial tissue. *Am. J. Physiol. Heart Circ. Physiol.* 310, H1388–H1401. doi: 10.1152/ajpheart.00665.2015

Ju, Y. K., Lee, B. H., Trajanovska, S., Hao, G., Allen, D. G., Lei, M., et al. (2015). The involvement of TRPC3 channels in sinoatrial arrhythmias. *Front. Physiol.* 6:86. doi: 10.3389/fphys.2015.00086

Lei, M., Wu, L., Terrar, D. A., and Huang, C. L. H. (2018). Modernized classification of cardiac antiarrhythmic drugs. *Circulation* 138, 1879–1896. doi: 10.1161/CIRCULATIONAHA.118.035455

Liu, J., Dobrzynski, H., Yanni, J., Boyett, M. R., and Lei, M. (2007). Organisation of the mouse sinoatrial node: structure and expression of HCN channels. *Cardiovasc. Res.* 73, 729–738. doi: 10.1016/j.cardiores.2006.11.016

Ni, H., Wang, Y., Crawford, W., Zhang, S., Cheng, L., Zhang, H., et al. (2017). Three-dimensional image reconstruction of distribution of Pnmt$^+$ cell-derived cells in murine heart. *Sci. Data* 4, 170134.

Nussinovitch, U., and Gepstein, L. (2015). Optogenetics for in vivo cardiac pacing and resynchronization therapies. *Nat. Biotechnol.* 33, 750–754. doi: 10.1038/nbt.3268

Nyns, E. C. A., Kip, A., Bart, C. I., Plomp, J. J., Zeppenfeld, K., Schalij, M. J., et al. (2016). Optogenetic termination of ventricular arrhythmias in the whole heart: towards biological cardiac rhythm management. *Eur. Heart J.* 38, 2132–2136. doi: 10.1093/eurheartj/ehw574

O'Shea, C., Holmes, A. P., Winter, J., Correia, J., Ou, X., Dong, R., et al. (2019b). Cardiac Optogenetics and Optical Mapping – Overcoming Spectral Congestion in All-Optical Cardiac Electrophysiology. *Front. Physiol.* 10, 1–14.

O'Shea, C., Holmes, A. P., Yu, T. Y., Winter, J., Wells, S. P., Correia, J., et al. (2019a). ElectroMap: high-throughput open-source software for analysis and mapping of cardiac electrophysiology. *Sci. Rep.* 9, 1389. doi: 10.1038/s41598-018-38263-2

Sharpe, E. J., St Clair, J. R., and Proenza, C. (2016). Methods for the isolation, culture, and functional characterization of sinoatrial node myocytes from adult mice. *J. Vis. Exp.* 116:54555. doi: 10.3791/54555

Torrente, A. G., Barrere, C., Nargeot, J., Mangoni, M. E., Mesirca, P., Rizzetto, R., et al. (2016). L-type Cav1.3 channels regulate ryanodine receptor-dependent Ca2+ release during sino-atrial node pacemaker activity. *Cardiovasc. Res.* 109, 451–461. doi: 10.1093/cvr/cvw006

Wang, Y., Lin, W. K., Crawford, W., Ni, H., Bolton, E. L., Khan, H., et al. (2017). Optogenetic control of heart rhythm by selective stimulation of cardiomyocytes derived from Pnmt+ cells in murine heart. *Sci. Rep.* 7, 40687. doi: 10.1038/s41598-017-18302-0

Wen, Q., Gandhi, K., Capel, R. A., Hao, G., O'Shea, C., Neagu, G., et al. (2018). Transverse cardiac slicing and optical imaging for analysis of transmural gradients in membrane potential and Ca^{2+} transients in murine heart. *J. Physiol.* 596, 3951–3965. doi: 10.1113/JP276239

Conflict of Interest Statement: The authors declare that the research was conducted in the absence of any commercial or financial relationships that could be construed as a potential conflict of interest.

frontiers in Physiology

MINI REVIEW
published: 10 July 2019
doi: 10.3389/fphys.2019.00713

Pnmt-Derived Cardiomyocytes: Anatomical Localization, Function, and Future Perspectives

Xuehui Fan[1†], Tianyi Sun[2†], William Crawford[2], Xiaoqiu Tan[1], Xianhong Ou[1], Derek A. Terrar[2], Steven N. Ebert[3] and Ming Lei[1,2]*

[1]Key Laboratory of Medical Electrophysiology, Ministry of Education and Medical Electrophysiological Key Laboratory of Sichuan Province, Collaborative Innovation Center for Prevention of Cardiovascular Diseases, Institute of Cardiovascular Research, Southwest Medical University, Luzhou, China, [2]Department of Pharmacology, University of Oxford, Oxford, United Kingdom, [3]Burnett School of Biomedical Sciences, College of Medicine, University of Central Florida, Orlando, FL, United States

In this mini-review, we provide an overview of phenylethanolamine-N-methyl transferase (Pnmt)-derived cardiomyocytes (PdCMs), a recently discovered cardiomyocyte subpopulation. We discuss their anatomical localization, physiological characteristics, possible function, and future perspectives. Their unique distribution in the heart, electrical activity, Ca^{2+} transient properties, and potential role in localized adrenergic signaling are discussed.

Keywords: optogenetics, Pnmt-derived cardiomyocytes, heart, Pnmt, catecholamines

OPEN ACCESS

Edited by:
Antonius Baartscheer, University of Amsterdam, Netherlands

Reviewed by:
Gudrun Antoons, Maastricht University, Netherlands
Christopher George, Swansea University, United Kingdom
Marcella Rocchetti, University of Milano-Bicocca, Italy

***Correspondence:**
Ming Lei
ming.lei@pharm.ox.ac.uk

[†]Joint first authors

Specialty section:
This article was submitted to Cardiac Electrophysiology, a section of the journal Frontiers in Physiology

Received: *08 December 2018*
Accepted: *21 May 2019*
Published: *10 July 2019*

Citation:
Fan X, Sun T, Crawford W, Tan X, Ou X, Terrar DA, Ebert SN and Lei M (2019) Pnmt-Derived Cardiomyocytes: Anatomical Localization, Function, and Future Perspectives. Front. Physiol. 10:713. doi: 10.3389/fphys.2019.00713

INTRODUCTION

The advent of cardiac optogenetics has facilitated the identification of a new cardiomyocyte subpopulation in the murine heart, phenylethanolamine-N-methyl transferase (Pnmt)-derived cardiomyocytes (PdCMs) (Wang et al., 2017). Through selective manipulation of these cells using optogenetics, our study demonstrated how this technique can be used to target specific cardiac cellular subpopulations, overcoming many of the issues associated with traditional electrophysiological techniques. In addition, combining optogenetics with electrophysiology, voltage imaging, and Ca^{2+} imaging allows for elucidation of specific cell functions *in vivo*. In this mini-review, we will discuss the anatomical localization, physiological characteristics, possible function, and future perspectives of PdCMs.

EARLY STUDIES OF CATECHOLAMINES IN THE HEART

Catecholamines are endogenous signaling molecules such as dopamine, noradrenaline (norepinephrine), and adrenaline (epinephrine). These molecules are typically synthesized in neurons at the site of their release, both at neuronal terminals and in cell bodies. The detection of catecholamines in the heart dates back to the late 1960s by Ignarro and Shideman, who demonstrated their production by cells other than sympathetic neurons (Ignarro and Shideman, 1968a,b,c). They determined the time of appearance and concentration of dopa (DA), dopamine, norepinephrine, and epinephrine in developing chick hearts, demonstrating the presence of catecholamines during the early days of the development. Embryonic hearts were also noted to take up tritium-labeled norepinephrine (H^5-NE) and epinephrine (H^3-E) during the development (Ignarro and Shideman, 1968b). The presence of catecholamine biosynthetic enzymes, including tyrosine hydroxylase, dopa decarboxylase, dopamine β-oxidase,

and Pnmt were also confirmed in chick embryonic hearts (Ignarro and Shideman, 1968c). Furthermore, catecholamine metabolism enzymes including catechol-O-methyl transferase (COMT) and monoamine oxidase (MAO) expression were also detected in the embryonic and developing chick heart. These enzymes were first detected in the embryonic developing heart on the fourth day, and increased thereafter until the 10th day when their activities plateaued. Activities of COMT and MAO increased on the 15th and 16th days and attained maximal values by the 19th day. Both enzymes subsequently exhibited sharp declines in their activities (to 13 and 40% of maximal values, respectively), reaching minimal values on the second and third days after hatching. This study therefore demonstrated the presence of catecholamines, their biosynthetic enzymes, and catecholamine transporters in the heart, although it did not determine their cellular origin.

ADRENERGIC CELLS AND INTRINSIC CARDIAC ADRENERGIC CELLS

Subsequent studies from numerous groups have established the existence of adrenergic cells in the heart (Ziegler et al., 2002; Owji et al., 2013). Adrenergic cells are present in both peripheral tissues (e.g., the adrenal medulla) and the central nervous system (e.g., the ventrolateral medulla) (Ziegler et al., 2002; Owji et al., 2013). Their primary role is mediating sympathetic responses to potentially stressful stimuli. These cells are characterized by their expression of Pnmt, the enzyme responsible for the final step in the adrenergic biosynthetic pathway, converting norepinephrine to epinephrine. The expression level of Pnmt in adrenergic cells within adrenal medulla is much higher than those in the brain and other tissues (Ziegler et al., 2002; Owji et al., 2013). Intriguingly, similar adrenergic cells have been identified in the heart of both developing and mature adults, and have been termed "Intrinsic Cardiac Adrenergic" (ICA) cells (Ebert et al., 1996, 2004; Huang et al., 1996, 2005; Ebert and Thompson, 2001; Osuala et al., 2011). ICA cells are present across all four chambers of the developing heart, but are primarily concentrated on the left side of the heart by adulthood, located predominantly in the left atrium and specific regions of the left ventricle (Owji et al., 2013). Such early expression of *Pnmt* is believed to denote a mesodermal origin of adrenergic cells in the heart (Ebert et al., 1996; Huang et al., 1996). Somewhat later in development, neural crest-derived (NCD) cells invade the heart and also appear to contribute neuroendocrine functions (Owji et al., 2013). These cells contain *Pnmt* mRNA and produce epinephrine (Ebert et al., 1996; Huang et al., 1996). *In vitro* experiments demonstrate the ability of these cells to increase the contraction rates of neonatal rat cardiomyocytes in culture. These Pnmt-positive cells have also been identified in human fetal hearts before sympathetic innervation of the heart occurs (Huang et al., 1996). However, the physiological role of these neuroendocrine cells within the heart is still poorly understood.

OPTOGENETIC ILLUMINATION OF PNMT-DERIVED CARDIOMYOCYTES

We recently developed a novel optogenetic mouse model with conditional cell-type expression of ChR2 by using *Pnmt* as a prompter gene (Wang et al., 2017). In this study, we crossed Pnmt-Cre mice with Ai27D mice (Stock No. 012567, Jackson Labs) expressing an improved channelrhodopsin-2/tdTomato fusion protein. Following exposure to Cre recombinase in PdCMs, the offspring mice were used in optogenetic studies with rapid depolarization of PdCMs by illumination with blue light (450–490 nm). This allowed us to study their physiological properties in intact cardiac tissue (Wang et al., 2017). The original aim of generating such a model was to create a tool to study adrenergic cells and adrenergic-derived cells selectively. We subsequently identified a distinct subpopulation of Pnmt-derived cardiomyocytes in murine heart (Wang et al., 2017). The genotypes of offspring showed successful cell-type specific expression of Channelrhodopsin-2 (ChR2)-tdTomato under control of *Pnmt* promoter in Pnmt-Cre-ChR2 animals. Several types of ChR2/tdTomato fluorescence positive cells were identified based on their morphology: small triangular-shaped cells with positive Pnmt immunofluoresent staining that primarily appeared to be located in interstitial spaces. These cells are consistent with the ICA cells previously reported in the literature. A large number of elongated, rod-shaped ChR2/tdTomato positive cells were also found. Based on their myocyte appearance, and the expression of α-actinin (myocyte marker), we confirmed that they are cardiomyocytes, and termed them Pnmt -derived cardiomyocytes (PdCMs) (Wang et al., 2017).

UNIQUE DISTRIBUTION OF PNMT-DERIVED CARDIOMYOCYTES

PdCMs have a unique distribution to the left heart and cardiac conduction system (Ni et al., 2017; Wang et al., 2017). As shown in **Figure 1**, tdTomato fluorescence in coronal heart sections taken from Pnmt-Cre-ChR2 mice reveals a strong lateralization to the left side of the heart, dispersed throughout the left atrium and left ventricle. Concentrated ChR2-tdTomato fluorescence was also observed throughout the cardiac conduction system, including the sinoatrial node and atrioventricular node. Pnmt-Cre-ChR2 heart sections were stained with the myocyte marker α-actinin to demonstrate co-localization of α-actinin and tdTomato in the left ventricle, providing compelling evidence that many Pnmt-derived cells are cardiomyocytes. SAN and AVN sections were also stained for the pacemaker cell marker HCN4, and demonstrated co-localization with tdTomato. Interestingly, areas with high PdCMs density overlap with the area of rich sympathetic innervation (Kimura et al., 2012). It is not yet known whether this corresponding distribution suggests some kind of functional connection between Pnmt-derived cardiomyocytes with sympathetic nerve endings. Future investigation into this relationship may reveal important localized cardiac regulation mechanisms.

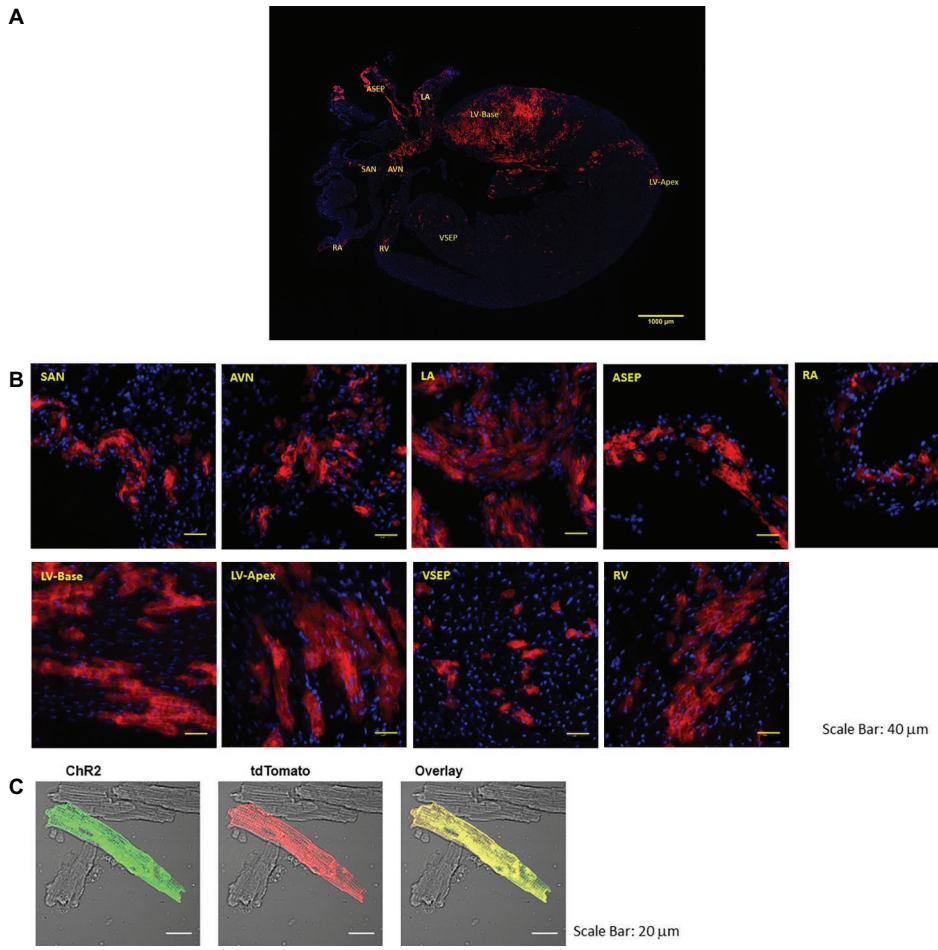

FIGURE 1 | Representative images of the coronal section and selected regions from the section of an adult ChR2/tdTomato mouse heart showing fluorescence and morphology of the ChR2/tdTomato positive cells. **(A)** A representative coronal section from an adult ChR2/tdTomato mouse heart; **(B)** inserts of zoom-in views showing tdTomato fluorescence in different regions of the heart; the labeling of the inserts indicates the corresponding locations as marked in **(A)**. SAN, sinoatrial node; AVN, atrioventricular node; LA, left atrium; RA, right atrium; LV, left ventricle; RV, right ventricle; ASEP, atrial septum; VSEP, ventricular septum. **(C)** Immunostaining of ChR2 with anti-ChR2 antibody; tdTomato fluorescence in isolated LV cardiomyocytes; overlay showing co-localization of ChR2 and tdTomato [Adapted with permission from Wang et al. (2017) and Ni et al. (2017)].

ELECTROPHYSIOLOGICAL PROPERTIES OF PNMT-DERIVED CARDIOMYOCYTES

The excitability and contractility of PdCMs has been studied using optogenetic models (Ni et al., 2017; Wang et al., 2017). Whole *ex vivo* Pnmt-Cre-ChR2 hearts were isolated and stimulated using 470-nm light pulses. We observed a clear electrical response correlated to the distribution of PdCMs. Targeted light pulses were shown to trigger excitation of the left atrium and left ventricle, but not of the right atrium and right ventricle. The light-based excitability of Pnmt-derived cardiomyocytes was also demonstrated using optical mapping of voltage and Ca^{2+} signals, in dissected atrial tissue or *ex vivo* hearts in Pnmt-Cre-ChR2 mice. This confirmed equivalent optogenetic triggering abilities of atrial and ventricular membrane voltage and intracellular Ca^{2+} signals (Ni et al., 2017; Wang et al., 2017). The contractile ability of PdCMs was also confirmed in individual isolated PdCMs (Ni et al., 2017; Wang et al., 2017). Direct optogenetic stimulation triggered contraction of PdCMs, but not of conventional myocytes isolated from Pnmt-Cre-ChR2 mouse heart, confirming intact excitation-contraction coupling in Pnmt-derived cardiomyocytes (Ni et al., 2017; Wang et al., 2017). This demonstrates the mechanical response triggered by light-sensitive channels (ChR2s) and illustrates the feasibility for direct optogenetic control in cardiomyocyte contraction at single cell level.

A POTENTIAL ROLE IN LOCALIZED ADRENERGIC SIGNALING

Although a subset of Pnmt-derived cardiomyocytes express Pnmt, they do not produce tyrosine hydroxylase or dopamine β-hydroxylase, and therefore cannot synthesize norepinephrine.

Most of the norepinephrine released from cardiac sympathetic nerve endings is reabsorbed into the nerve endings through the peripheral norepinephrine transporter (uptake-1 mechanism), and is recycled or metabolized in the cytoplasm of neurons (Ziegler et al., 2002). In addition to the neuronal uptake-1 mechanism, norepinephrine can also be taken up by nonneuronal tissues, including cardiomyocytes, *via* the uptake-2 mechanisms (Ziegler et al., 2002). The NA uptake-2 mechanism is facilitated by transporter protein 3 (EMT/OCT3) (Ziegler et al., 2002). As some Pnmt-derived cardiomyocytes express Pnmt, they may possess the ability to uptake norepinephrine through uptake-2 mechanism and subsequently convert it to epinephrine. Such potential role of Pnmt-derived cardiomyocytes needs to be further examined.

It is known that autonomic dysfunction including sympathetic hyperactivity often coincides with cardiac pathologies including heart failure, diabetic cardiomyopathy, myocardial ischemia, and infarction (Ma et al., 1997; Ishise et al., 1998; Motte et al., 2005). It is an important cause of ventricular arrhythmia, and is therefore a predictive index of morbidity and mortality (La Rovere et al., 1998; Nolan et al., 1998). Catecholamines and their oxidation products cause a direct toxic effect on the myocardium. Catecholamine-mediated myocardial stunning has been implicated in the pathogenesis of stress-induced cardiomyopathy in both animal models and human subjects. (Ueyama et al., 2002; Kassim et al., 2008; Gupta et al., 2018)

Biopsy of the myocardium in patients with pheochromocytoma or stress-induced cardiomyopathy shows similar histological findings. The clinical features in pheochromocytoma-related cardiomyopathy include hypertension, dilated or hypertrophic cardiomyopathy, and pulmonary edema due to cardiogenic and noncardiogenic factors, cardiac arrhythmias, and even cardiac arrest. Stress-related cardiomyopathy such as takotsubo cardiomyopathy occurs primarily in postmenopausal women. It has been suggested that lack of estrogen replacement in the postmenopausal state may predispose women to takotsubo cardiomyopathy (Kuo et al., 2010; Gupta et al., 2018).

OPEN QUESTIONS AND FUTURE PERSPECTIVES

How PNMT-Derived Cardiomyocytes Are Thought to Arise in Heart Development?

Figure 2 illustrates the schematic depiction of how PdCMs are thought to arise in heart development. By the blastocyst stage of embryonic development, pluripotent embryonic stem cells (ESCs) form and give rise to the ectoderm, mesoderm, and endoderm layers and cell types. A portion of mesoderm progenitors become committed to heart development (i.e., cardiac progenitor cells, CPCs – not shown), some of which become neuroendocrine progenitor cells (NEPCs) in the heart. A subset of these cells express Pnmt (Pnmt$^+$ cells) and become intrinsic cardiac adrenergic (ICA) cells (Ebert et al., 1996; Huang et al., 1996) that appear in the heart prior to cardiac neural crest cell (CNCC) invasion (Ebert and Thompson, 2001). Fate-mapping studies with Pnmt-Cre/LacZ and Pnmt-Cre/ChR2 have shown that some of these ICA cells appear to transdifferentiate further into PdCMs (Ebert et al., 2004; Osuala et al., 2011; Ni et al., 2017; Wang et al., 2017). Notably, most PdCMs studied to date do not appear to actively express Pnmt, though some appear to retain that capability or may transiently express markers for both ICA and myocyte phenotypes for some duration during the transdifferentiation process (Owji et al., 2013). There are a number of open questions regarding this model as illustrated by the question marks (?) in **Figure 2**. It is unclear, for example, if neural crest cells also contribute

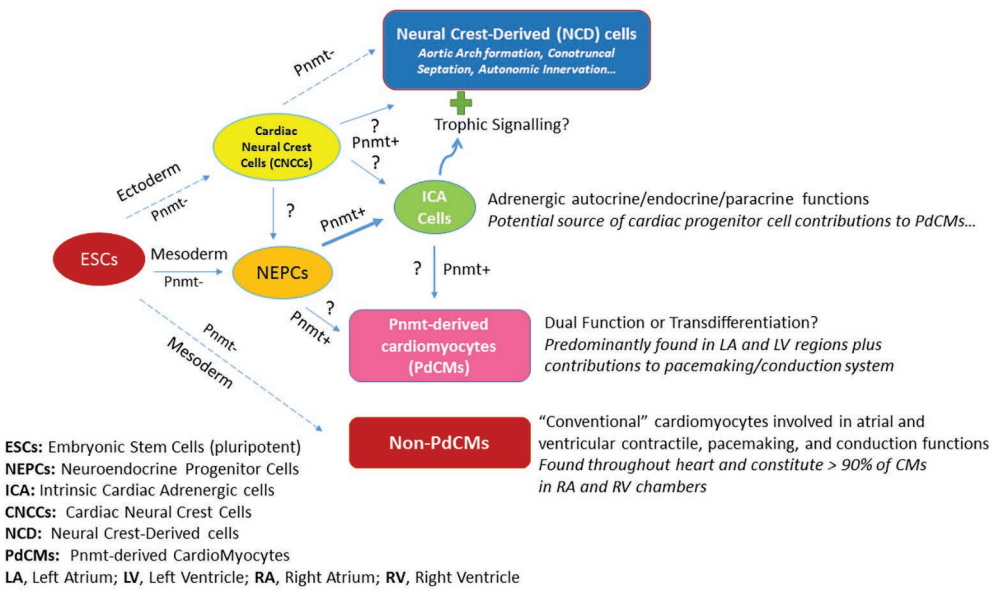

FIGURE 2 | Schematic depiction of how PdCMs are thought to arise in heart development.

to NEPCs and ICA cells in the heart. There are clearly Pnmt$^+$ NCD cells in the vicinity of the heart, but studies have yet to demonstrate any specific contributions made by NCD Pnmt$^+$ cells in heart development, though there is certainly evidence that ICA cells are located in the myocardial layers of the conotruncal regions, and it is well known that signals emanating from these regions are important for epithelial-mesenchymal transformations leading to septation. Further, there is strong evidence that the aortic arches are exquisitely sensitive to epinephrine during their formative period as topical administration of epinephrine leads to increases in aortic arch anomalies in the chick embryo model (Hodach et al., 1974, 1975). Given the spatiotemporal proximity of ICA cells during these formations, we speculate that they may exert trophic (paracrine) actions to influence the development of NCD cells/tissues including aortic arches, conotruncal septation, and/or autonomic innervation of the heart. While most cardiomyocytes in the heart are not derived from Pnmt$^+$ cells (non-PdCMs), there are surprisingly large proportions of the LV and LA as well as the pacemaking and conduction cardiomyocytes that are marked by Pnmt expression at some point in their history (PdCMs). The most likely source of these PdCMs is ICA cells, but we cannot yet rule out that there could be other progenitor cell types such as NEPCs, non-PdCMs, or other as yet unidentified cell types that may also contribute to their production. Once cells become PdCMs, most of them appear to lose the ability to express Pnmt and other neuroendocrine markers, though some may retain for a period of time and may thus serve "dual function" roles in that they have specialized cardiomyocyte phenotypes (e.g., atrial and ventricular contractile, pacemaking, conduction) in addition to NEPC or ICA-like phenotypes.

The Physiological Role of Phenylethanolamine-N-Methyl Transferase-Derived Cardiomyocytes

The physiological role of PdCMs requires further investigation. There are many unanswered questions, such as whether PdCMs have any adrenergic endocrine or paracrine role. It seems that they do not for the most part, though we do not have quantitative evidence for this. Some do indeed express Pnmt, but to be adrenergic, they would also need to express the three other enzymes in the pathway or at the very least be able to take up norepinephrine, which could then be converted to epinephrine by Pnmt. They would also have to possess secretory capability into adulthood as Huang et al. showed is present in early development (Huang et al., 1996). From our own studies, we have generally seen an inverse relationship between adrenergic endocrine and myocyte phenotypes, though some overlap has been observed. In other words, the question is whether PdCMs arise from ICA cells that gain a myocyte phenotype, do they transdifferentiate from ICA cells into myocytes, or some of both? Furthermore, if PdCMs are not adrenergic (i.e., arise from transdifferentiation), can they become adrenergic again (reverse transdifferentiate back to earlier phenotype)? If so, under what conditions might that occur? In conclusion, our understanding of biology and physiological function of PdCMs is limited, future efforts with a focus on the above challenging issues would greatly improve such understanding.

AUTHOR CONTRIBUTIONS

TS, XF, SE, and ML contributed to the draft-writing. WC, XT, XO, and DT contributed to the editing and proof-reading. SE and ML produced the Figures. ML is responsible for the correction, editing, and final approval.

FUNDING

This study was supported by grants from MRC (G10002647, G1002082 to ML); BHF (PG/14/80/31106, PG/16/67/32340, PG/12/21/29473, PG/11/59/29004 to ML; PG/17/55/33087); BHF CRE at Oxford (to ML) and by National Natural Science Foundation of China (grant No. 81700308 and No. 31871181).

REFERENCES

Ebert, S. N., Baden, J. M., Mathers, L. H., Siddall, B. J., and Wong, D. L. (1996). Expression of phenylethanolamine N-methyltransferase in the embryonic rat heart. *J. Mol. Cell. Cardiol.* 28, 1653–1658. doi: 10.1006/jmcc.1996.0155

Ebert, S. N., Rong, Q., Boe, S., Thompson, R. P., Grinberg, A., and Pfeifer, K. (2004). Targeted insertion of the cre-recombinase gene at the phenylethanolamine n-methyltransferase locus: a new model for studying the developmental distribution of adrenergic cells. *Dev. Dyn.* 231, 849–858. doi: 10.1002/dvdy.20188

Ebert, S. N., and Thompson, R. P. (2001). Embryonic epinephrine synthesis in the rat heart before innervation: association with pacemaking and conduction tissue development. *Circ. Res.* 88, 117–124. doi: 10.1161/01.RES.88.1.117

Gupta, S., Goyal, P., Idrees, S., Aggarwal, S., Bajaj, D., and Mattana, J. (2018). Association of endocrine conditions with takotsubo cardiomyopathy: a comprehensive review. *J. Am. Heart Assoc.* 7:e009003. doi: 10.1161/JAHA.118.009003

Hodach, R. J., Gilbert, E. F., and Fallon, J. F. (1974). Aortic arch anomalies associated with the administration of epinephrine in chick embryos. *Teratology* 9, 203–209. doi: 10.1002/tera.1420090211

Hodach, R. J., Hodach, A. E., Fallon, J. F., Folts, J. D., Bruyere, H. J., and Gilbert, E. F. (1975). The role of beta-adrenergic activity in the production of cardiac and aortic arch anomalies in chick embryos. *Teratology* 12, 33–45. doi: 10.1002/tera.1420120105

Huang, M.-H., Bahl, J. J., Wu, Y., Hu, F., Larson, D. F., Roeske, W. R., et al. (2005). Neuroendocrine properties of intrinsic cardiac adrenergic cells in fetal rat heart. *Am. J. Phys.* 288, H497–H503. doi: 10.1152/ajpheart.00591.2004

Huang, M. H., Friend, D. S., Sunday, M. E., Singh, K., Haley, K., Austen, K. F., et al. (1996). An intrinsic adrenergic system in mammalian heart. *J. Clin. Invest.* 98, 1298–1303. doi: 10.1172/JCI118916

Ignarro, L. J., and Shideman, F. E. (1968a). Appearance and concentrations of catecholamines and their biosynthesis in the embryonic and developing chick. *J. Pharmacol. Exp. Ther.* 159, 38–48.

Ignarro, L. J., and Shideman, F. E. (1968b). Norepinephrine and epinephrine in the embryo and embryonic heart of the chick: uptake and subcellular distribution. *J. Pharmacol. Exp. Ther.* 159, 49–58.

Ignarro, L. J., and Shideman, F. E. (1968c). The requirement of sympathetic innervation for the active transport of norepinephrine by the heart. *J. Pharmacol. Exp. Ther.* 159, 59–65.

Ishise, H., Asanoi, H., Ishizaka, S., Joho, S., Kameyama, T., Umeno, K., et al. (1998). Time course of sympathovagal imbalance and left ventricular dysfunction in conscious dogs with heart failure. *J. Appl. Physiol.* 84, 1234–1241. doi: 10.1152/jappl.1998.84.4.1234

Kassim, T., Clarke, D., Mai, V., Clyde, P., and Shakir, K. M. (2008). Catecholamine-induced cardiomyopathy. *Endocr. Pract.* 14, 1137–1149. doi: 10.4158/EP.14.9.1137

Kimura, K., Ieda, M., and Fukuda, K. (2012). Development, maturation, and transdifferentiation of cardiac sympathetic nerves. *Circ. Res.* 110, 325–336. doi: 10.1161/CIRCRESAHA.111.257253

Kuo, B. T., Choubey, R., and Novaro, G. M. (2010). Reduced estrogen in menopause may predispose women to takotsubo cardiomyopathy. *Gend. Med.* 7, 71–77. doi: 10.1016/j.genm.2010.01.006

La Rovere, M. T., Bigger, J. T. Jr., Marcus, F. I., Mortara, A., and Schwartz, P. J. (1998). Baroreflex sensitivity and heart-rate variability in prediction of total cardiac mortality after myocardial infarction. ATRAMI (autonomic tone and reflexes after myocardial infarction) investigators. *Lancet* 351, 478–484. doi: 10.1016/S0140-6736(97)11144-8

Ma, R., Zucker, I. H., and Wang, W. (1997). Central gain of the cardiac sympathetic afferent reflex in dogs with heart failure. *Am. J. Phys.* 273, H2664–H2671. doi: 10.1152/ajpheart.1997.273.6.H2664

Motte, S., Mathieu, M., Brimioulle, S., Pensis, A., Ray, L., Ketelslegers, J. M., et al. (2005). Respiratory-related heart rate variability in progressive experimental heart failure. *Am. J. Physiol. Heart Circ. Physiol.* 289, H1729–H1735. doi: 10.1152/ajpheart.01129.2004

Ni, H., Wang, Y., Crawford, W., Zhang, S., Cheng, L., Zhang, H., et al. (2017). Three-dimensional image reconstruction of distribution of Pnmt+ cell-derived cells in murine heart. *Sci. Data* 4:170134. doi: 10.1038/sdata.2017.134

Nolan, J., Batin, P. D., Andrews, R., Lindsay, S. J., Brooksby, P., Mullen, M., et al. (1998). Prospective study of heart rate variability and mortality in chronic heart failure: results of the United Kingdom heart failure evaluation and assessment of risk trial (UK-heart). *Circulation* 98, 1510–1516. doi: 10.1161/01.CIR.98.15.1510

Osuala, K., Telusma, K., Khan, S. M., Wu, S., Shah, M., Baker, C., et al. (2011). Distinctive left-sided distribution of adrenergic-derived cells in the adult mouse heart. *PLoS One* 6:e22811. doi: 10.1371/journal.pone.0022811

Owji, A., Varudkar, N., and Ebert, S. (2013). Therapeutic potential of Pnmt+ primer cells for neuro/myocardial regeneration. *Am. J. Stem Cells* 22, 137–154.

Ueyama, T., Kasamatsu, K., Hano, T., Yamamoto, K., Tsuruo, Y., and Nishio, I. (2002). Emotional stress induces transient left ventricular hypocontraction in the rat via activation of cardiac adrenoceptors a possible animal model of 'Tako-Tsubo' cardiomyopathy. *Circ. J.* 66, 712–713. doi: 10.1253/circj.66.712

Wang, Y., Lin, W. K., Crawford, W., Ni, H., Bolton, E. L., Khan, H., et al. (2017). Optogenetic control of heart rhythm by selective stimulation of cardiomyocytes derived from Pnmt+ cells in murine heart. *Sci. Rep.* 7:40687. doi: 10.1038/s41598-017-18302-0

Ziegler, M. G., Bao, X., Kennedy, B. P., Joyner, A., and Enns, R. (2002). Location, development, control, and function of extraadrenal phenylethanolamine N-methyltransferase. *Ann. N. Y. Acad. Sci.* 971, 76–82. doi: 10.1111/j.1749-6632.2002.tb04437.x

Conflict of Interest Statement: The authors declare that the research was conducted in the absence of any commercial or financial relationships that could be construed as a potential conflict of interest.

frontiers in Physiology

PROTOCOLS
published: 25 June 2019
doi: 10.3389/fphys.2019.00755

A Protocol for Transverse Cardiac Slicing and Optical Mapping in Murine Heart

S. He[1†], Q. Wen[2†], C. O'Shea[3†], R. Mu-u-min[4†], K. Kou[1], A. Grassam-Rowe[4], Y. Liu[5], Z. Fan[5], X. Tan[1], X. Ou[1‡], P. Camelliti[6‡], D. Pavlovic[3‡] and M. Lei[1,4‡]*

[1] Key Laboratory of Medical Electrophysiology of Ministry of Education and Medical Electrophysiological Key Laboratory of Sichuan Province, Institute of Cardiovascular Research, Southwest Medical University, Luzhou, China, [2] Institute of Cardiology, Union Hospital, Tongji Medical College, Huazhong University of Science and Technology, Wuhan, China, [3] Institute of Cardiovascular Sciences, University of Birmingham, Birmingham, United Kingdom, [4] Department of Pharmacology, University of Oxford, Oxford, United Kingdom, [5] Department of Cardiovascular Medicine, Southwest Medical University, Luzhou, China, [6] School of Biosciences and Medicine, University of Surrey, Guildford, United Kingdom

OPEN ACCESS

Edited by:
Bas J. Boukens, University of Amsterdam, Netherlands

Reviewed by:
Mathilde R. Rivaud, Netherlands Heart Institute, Netherlands
Franziska Schneider-Warme, Universitäts-Herzzentrum Freiburg-Bad Krozingen, Germany

***Correspondence:**
M. Lei
ming.lei@pharm.ox.ac.uk

[†]*Joint first authors*

[‡]*Joint senior authors*

Specialty section:
This article was submitted to Cardiac Electrophysiology, a section of the journal Frontiers in Physiology

Received: *08 December 2018*
Accepted: *31 May 2019*
Published: *25 June 2019*

Citation:
He S, Wen Q, O'Shea C, Mu-u-min R, Kou K, Grassam-Rowe A, Liu Y, Fan Z, Tan X, Ou X, Camelliti P, Pavlovic D and Lei M (2019) A Protocol for Transverse Cardiac Slicing and Optical Mapping in Murine Heart. Front. Physiol. 10:755. doi: 10.3389/fphys.2019.00755

Thin living tissue slices have recently emerged as a new tissue model for cardiac electrophysiological research. Slices can be produced from human cardiac tissue, in addition to small and large mammalian hearts, representing a powerful *in vitro* model system for preclinical and translational heart research. In the present protocol, we describe a detailed mouse heart transverse slicing and optical imaging methodology. The use of this technology for high-throughput optical imaging allows study of electrophysiology of murine hearts in an organotypic pseudo two-dimensional model. The slices are cut at right angles to the long axis of the heart, permitting robust interrogation of transmembrane potential (V_m) and calcium transients (CaT) throughout the entire heart with exceptional regional precision. This approach enables the use of a series of slices prepared from the ventricles to measure V_m and CaT with high temporal and spatial resolution, allowing (i) comparison of successive slices which form a stack representing the original geometry of the heart; (ii) profiling of transmural and regional gradients in V_m and CaT in the ventricle; (iii) characterization of transmural and regional profiles of action potential and CaT alternans under stress (e.g., high frequency pacing or β-adrenergic stimulation) or pathological conditions (e.g., hypertrophy). Thus, the protocol described here provides a powerful platform for innovative research on electrical and calcium handling heterogeneity within the heart. It can be also combined with optogenetic technology to carry out optical stimulation; aiding studies of cellular V_m and CaT in a cell type specific manner.

Keywords: optical mapping, transverse cardiac slice, membrane potentials, Ca^{2+} transients, murine heart

INTRODUCTION

Thin living tissue slices are a widely used experimental preparation for electrophysiological studies of the brain (Accardi et al., 2016). Slices have recently been adopted as a promising model for the investigations of cardiac electrophysiology in different species, for example: viral delivery, culturing, and mechanical stimulation (Halbach et al., 2006; Bussek et al., 2009; Camelliti et al., 2011;

Wang et al., 2015; Kang et al., 2016; Thomas et al., 2016; Randi et al., 2017; Watson et al., 2017, 2019; Wen et al., 2018). Importantly, cardiac slices exhibit similar electrophysiological characteristics to the intact heart and respond to the application of pharmacological compounds similarly to the whole heart (Bussek et al., 2009; Camelliti et al., 2011; Wen et al., 2018). They have advantages for investigating transmural and regional characteristics of a variety of physiological parameters of the heart, thus providing a promising experimental model for heart research.

Because of feasibility for genetic modification, the mouse has been widely used for exploring molecular, cellular and systemic mechanisms underlying inherited and acquired cardiac arrhythmic diseases (Nerbonne and Kass, 2005; Huang, 2017). Despite the popularity of mouse models in cardiac arrhythmic research, cardiac transmural heterogeneities of action potential and Ca^{2+} transient characteristics, which are vitally important for phenotypic and mechanistic research in cardiac disease conditions, have only been explored recently in the mouse heart (Wen et al., 2018). We reported a robust approach for transverse cardiac slicing and optical mapping of transmembrane potential (V_m) and intracellular Ca^{2+} transient (CaT) in murine hearts, providing unprecedented and potentially high-throughput characterization of action potentials (APs) and intracellular Ca^{2+} transients *everywhere* in the mouse ventricles (Wen et al., 2018). Such an approach can be potentially adapted for large mammalian hearts and human tissue, thus representing a powerful *in vitro* model system for translational cardiovascular research (Thomas et al., 2016; Randi et al., 2017; Watson et al., 2017, 2019). Using this technique, we demonstrated the feasibility of our new approach to cardiac slicing for systematic analysis of intrinsic transmural and regional gradients in V_m and CaT in murine ventricular tissue (Wen et al., 2018).

In the present protocol, we describe a detailed feasible transverse slicing method, cutting slices at right angles to the long axis of the heart and combined it with a high-throughput optical imaging technique as a new approach for studying cellular electrophysiology of murine heart in an organotypic pseudo two-dimensional ventricular tissue model. Our method enables the use of a series of slices prepared from the ventricles to simultaneously measure V_m and CaT with high temporal and spatial resolution allowing comparison of transmural and regional profiles of APs and CaTs. This technique can potentially be combined with other molecular techniques such as *in situ* immunostaining and virus transfection to gain insight into arrhythmia mechanisms in various heart disease conditions.

MATERIALS AND EQUIPMENT

Animals

Animals used were 10–12 weeks, 20–25 g, male C57BL mice or Pnmt-Cre/ Channelrhodopsin 2 (ChR2) mice as we previously reported (Wang et al., 2017). The Pnmt-Cre/ChR2 mouse line exhibits cell-type specific expression of ChR2 by crossing B6.Cg-*Gt (ROSA)26Sor*$^{tm27.1(CAG-COP4H134R/tdTomato)Hze}$/J strain (Stock No. 012567, Jackson Labs) with a Cre transgenic strain under the control of a *Pnmt* promoter (Wang et al., 2017). ChR2 was specifically introduced into murine cells expressing the *Phenylethanolamine n-methyltransferase* (*Pnmt*) gene, which encodes for the enzyme responsible for conversion of noradrenaline to adrenaline. The murine model led to the identification of a distinctive class of Pnmt-expressing neuroendocrine cells and their descendants (i.e., $Pnmt^+$ cell derived cardiomyocytes) within the heart (Wang et al., 2017).

All procedures including animal subjects have been approved by Institutional Animals Ethics Committees at Southwest Medical University, Luzhou, China or Department of Pharmacology at University of Oxford, United Kingdom and the national guidelines under which the institution operates. All mice used in this study were maintained in a pathogen−free facility at Southwest Medical University or University of Oxford. Mice were given *ad libitum* access to food and water. The authors confirm that they have taken all steps to minimize the animals' pain and suffering.

Chemicals and Reagents

The relevant information of the chemicals and reagents are described in **Table 1**.

Instruments and Equipment

- Dumont forceps (Medical Equipment Factory of Shanghai Medical Instruments Co., Ltd., Shanghai, China).
- Mayo scissors (Medical Equipment Factory of Shanghai Medical Instruments Co., Ltd., Shanghai, China).
- Kelly hemostatic forceps (Medical Equipment Factory of Shanghai Medical Instruments Co., Ltd., Shanghai, China).
- Iris forceps (Medical Equipment Factory of Shanghai Medical Instruments Co., Ltd., Shanghai, China).
- Syringe Filter, Aquo-system, 0.45 μm/13 mm (Sangon Biotech Shanghai, China, F513143-0001).
- Langendorff perfusion system.
- Perfusion pump (Longer Precision Pump Co., Ltd., Baoding, China, BT100-2J).
- Vibration slicer (Leica VT1000s, Nussloch, Germany).
- EMCCD camera (Evolve 512, Photometrics, Tucson, AZ, United States).
- MacroLED light source (Cairn Research, Faversham, United Kingdom).
- MyoPacer EP field stimulator (Ion Optix Co., Milton, MA, United States S006152).
- Electrical stimulation chamber (custom-made by the workshop of Department of Pharmacology, University of Oxford).
- Heater Controller (custom-made by the workshop of Department of Pharmacology, University of Oxford).

Solutions

- Krebs solution (containing in mM: NaCl 119, $NaHCO_3$ 25, NaH_2PO_4 1.0, KCl 4.7, $MgCl_2$ 1.05, $CaCl_2$ 1.35, and glucose 10; equilibrated with 95% O_2/5% CO_2, pH 7.4) at 37°C, pH = 7.35–7.4.
- HEPES buffered BDM solution (in mM: NaCl 140; KCl 4.7; glucose 10; HEPES 10; $MgCl_2$ 1.05; $CaCl_2$ 1.35; pH 7.4)

TABLE 1 | Reagents utilized.

Chemical and catalog references	Supplier
NaCl (SLBS2340V)	Sigma-Aldrich, St. Louis, MO, United States
$NaHCO_3$ (SLBX3605)	Sigma-Aldrich
NaH_2PO_4 (BCBW9042)	Sigma-Aldrich
KCl (SLBS5003)	Sigma-Aldrich
$MgCl_2$ (BCBS6841V)	Sigma-Aldrich
$CaCl_2$ (SLBK1794V)	Sigma-Aldrich
Glucose (SLBT4811V)	Sigma-Aldrich
HEPES (W1122DO10)	Sangon biological, Shanghai, China
2,3-butanedione monoxime (BDM) (29297)	Sigma-Aldrich
Blebbistatin (SLBV5564)	Tocris Bioscience, Minneapolis, MN, United States
Voltage-sensitive dye RH237 (1971387)	Thermo Fisher Scientific, Waltham, MA, United States
Calcium indicator Rhod-2AM (1890519)	Invitrogen, Carlsbad, CA, United States
Dimethyl sulfoxide (DMSO) (RNBT7442)	Sigma-Aldrich
Heparin Sodium (H51021209)	Chengdu Haitong Pharmaceutical Co., Ltd., Chengdu, China
Avertin (2,2,2-tribromoethanol)	Sigma-Aldrich Poole, Dorset, United Kingdom
Pluronic F127 (1899021)	Invitrogen, Carlsbad, CA, United States
Low-melt agarose (A600015.0005)	BBI Life Sciences, Shanghai, China

containing the excitation–contraction uncoupler 2,3-butanedione monoxime (BDM, 10 mM) and was stored at 4°C.
- Blebbistatin stock solution, 10 mM in DMSO.
- Voltage-sensitive dye RH237 stock solution, 1.25 mg/mL in DMSO.
- Calcium indicator Rhod-2AM stock solution, 1 mg/mL in DMSO.

Preparation of Experimental Setup(s)

- Prepare the Langendorff perfusion system. Turn on the perfusion system pump. Starting the peristaltic pump that is used for retrograde perfusion. Wash the perfusion system with 1 L deionized water with initial flow rate at 90 ml/min. Once all the deionized water has evacuated from the chamber, circulate the Krebs solution and pass it through a 0.45 μm filter. Keep Krebs solution at 37°C with a water jacket, circulated and oxygenated by bubbling O_2/CO_2 (95%/5%) gas into the solution. Adjust the flow rate to 4 ml/min.
- Prepare the optical mapping system (**Figure 1**), a custom-designed system equipped with an EMCCD camera. The excitation light for Ca^{2+} sensitive dye Rhod-2 and voltage sensitive dye RH237 is provided by four MacroLED lamps (525 nm, 1750 lumen, 7 mm^2 emitters, Cairn Research) with aspheric condensers driven using MacroLED control boxes and digitally modulated from Metamorph software. LEDs are directed onto the slices from the four corners of the bath, to produce an even, near-critical, illumination at approximately 30 mm, with equal distance from 4 corners. An ET525/50 sputter coated filter (Chroma Technology) is used to remove any out-of-band light for each LED.
  Samples are imaged using a custom MacroScope (Cairn Research) with an F/0.95, 25 mm C-mount camera lens, spaced to give a working distance of approximately 40 mm. The fluorescence emission light is split with a 635 nm longpass dichroic mirror and subsequently filtered (Vm: 662 nm LP, CaT: 585/40 nm) to separate the Ca^{2+} and voltage signals based on their wavelengths using the OptoSplit apparatus (Cairn Research). Once split, the Vm and CaT signals are imaged on to the camera such that they are reproduced side-by-side on the sensor and recorded simultaneously (Vm imaged on one side of the chip, CaT on the other).
- Prepare the vibratome. Install a new blade at the holder and fill the cooling chamber with crushed ice.

PROCEDURE

Figure 2 shows the major steps of the protocol.

Harvest, Cannulation, and Perfusion of Mouse Heart (30 min)

(1) Anesthetize the animal with 1.2% Avertin solution (0.5–0.8 ml I.P.) containing heparin (200 units I.P.), ensuring lack of pain reflex, prior to sacrifice (Complete in 10 min).
(2) Open the chest, quickly remove the heart and keep the heart in oxygenated (95% O_2, 5% CO_2), (37 ± 1°C) Krebs solution. Using a dissecting microscope, identify the aorta and make a clean cut across the ascending aorta below the right subclavian artery. Cannulate the aorta onto a custom-made cannula and tie with 4-0 black-braided silk suture around the cannula. After cannulation, retrogradely perfuse the heart and superfuse with constant-temperature (37 ± 1°C) Krebs solution. The retrograde perfusion rate was adjusted in the range of 3.5–4.0 mL/min (Complete this step in 3 min).
(3) Important! Insert a small silicon tube (0.7 mm diameter) into the left ventricular cavity through the left atrial

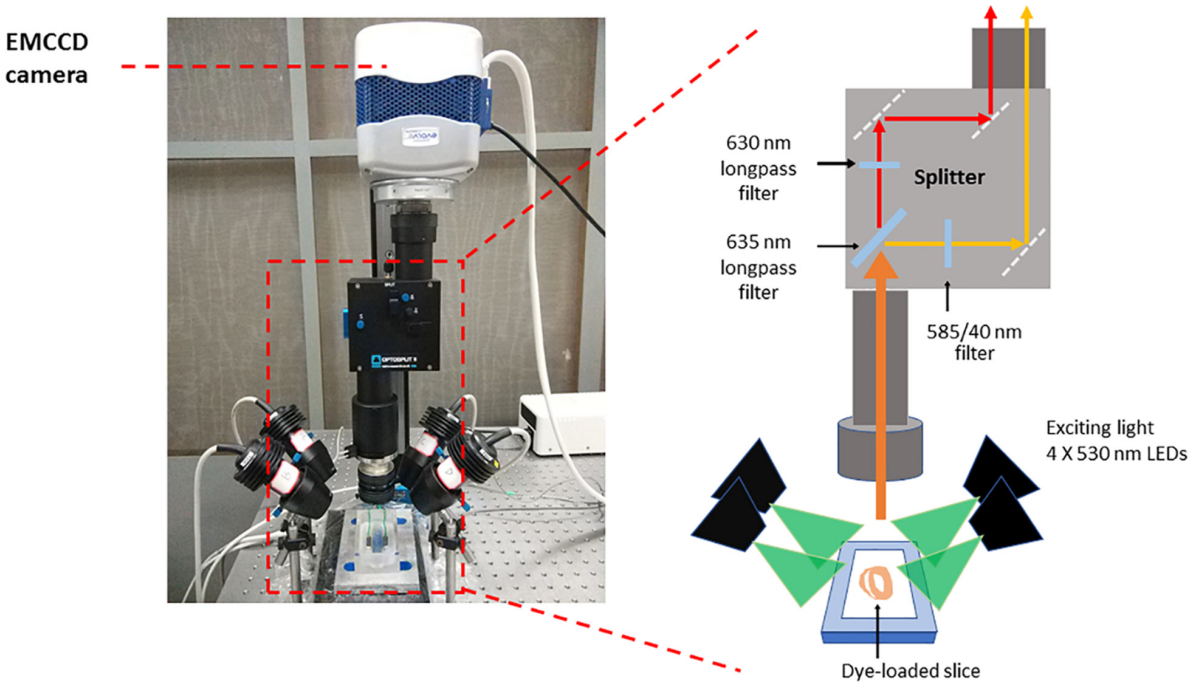

FIGURE 1 | Optical mapping set-up. The system consists of a camera (Photometrics Evolve Delta 512) running under Metamorph (Molecular Devices) in Light-speed mode, giving a high temporal resolution of sub-frames, up to 1000 frames/sec, and spatial resolution at the sample of 74 × 74 μm per pixel. The sample was imaged using a custom MacroScope (Cairn Research) with an F/0.95, 25 mm C-mount camera lens, spaced so as to give a working distance of approximately 40 mm. The excitation light was provided by a four light emitting diode MacroLED lamps (525 nm, 1750 lumen, 7 mm^2 emitters, Cairn Research) with aspheric condensers directed onto the slices from the four corners of the bath, so as to produce an even, near-critical, illumination at approximately 30 mm. The LEDs were driven using MacroLED control boxes and digitally modulated from Metamorph software with a National Instruments multifunction card. The LEDs were individually filtered using ET525/50 sputter coated filters (Chroma Technology) to remove any out-of-band light. The fluorescence emission light was split with a 610 nm long-pass dichroic mirror and corresponding emitters to separate the Ca^{2+} and voltage signals based on their wavelengths. The voltage-sensitive dye, RH237, emits signals which exhibit a peak at 670 nm, while Rhod-2 AM has a peak emission at approximately 600 nm and, once split by the dichroic mirror, these two signals are imaged on to the camera such that they are reproduced side-by-side on the sensor and recorded simultaneously. This dichroic and adjustable mirror unit, the OptoSplit, was provided by Cairn Research with filters from Chroma Technologies (United States). CaT fluorescence was collected at 585 ± 40 nm and Vm using a 662 nm long pass filter. Vm and CaT measurements were taken at maximal resolution (128 × 128 pixels; pixel area 74 × 74 μm) at a rate of 1000 frames/s.

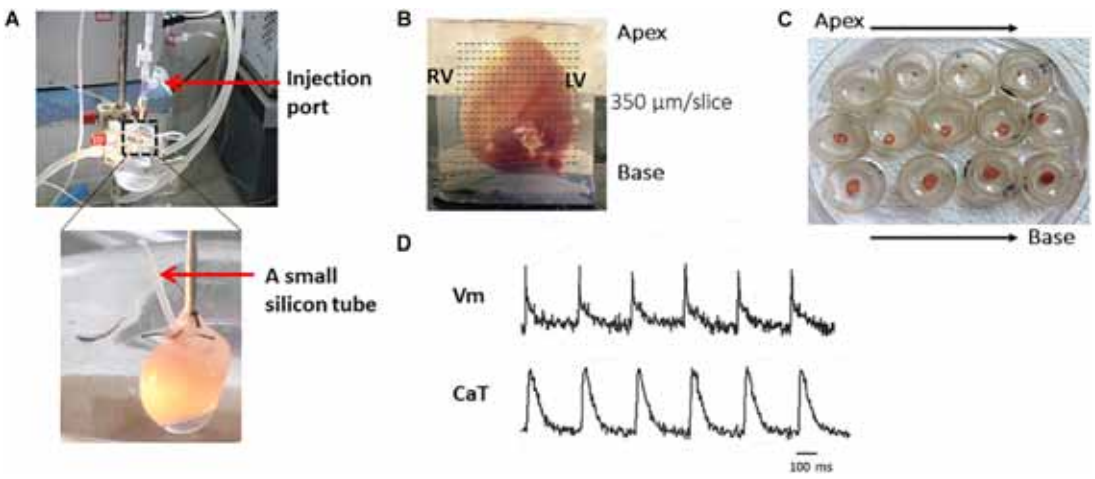

FIGURE 2 | The major steps of the protocol. Representative harvested mouse heart and transverse slices from apex to base. Briefly, after the Langendoff perfusion steps **(A)**, embed the heart in 4% low-melting agarose and cut with right angle to the long axis by Leica VT1000s vibratome **(B)**. Slices are transferred to petri dishes **(C)** and voltage and calcium transients recorded **(D)**.

appendage in order to prevent ventricular pressure increasing due to solution congestion and to prevent acidification of the perfusate trapped in the left ventricular cavity. This is especially important after the suppression of ventricular contractions with an excitation-contraction uncoupler.

After the dyes are loaded, the steps described in Sections "Chemicals and Reagents," "Instruments and equipment," and "Solutions" should be performed in the dark.

Load Calcium and Voltage Sensitive Dyes and Excitation-Contraction Uncoupler (50–60 min)

(1) Before dye loading, ensure the isolated heart is beating rhythmically without ischemia (10 min).
(2) Mix 50 μl calcium indicator Rhod-2 AM 1:1 with Pluronic F127 (20% solution in DMSO) and then dilute in 1 ml Krebs solution. Recirculate oxygenated (95% O_2, 5% CO_2) Krebs solution at constant-temperature (37 ± 1°C) and then inject Rhod-2 AM solution slowly over 7–10 min through the injection port near the cannula.
(3) Continue to recirculate Krebs solution after finishing injection (now, the perfusate contains Rhod-2 AM and Pluronic F127) (20 min).
(4) During this time, dilute 30 μl voltage-sensitive dye RH237 (1.25 mg/ml stock) in 1 ml Krebs solution.
(5) Switch to perfusion with oxygenated (95% O_2, 5% CO_2), constant-temperature (37 ± 1°C), Krebs solution and perfuse the heart for 2–3 min. Then inject RH237 solution slowly over 7–10 min through the injection port.
(6) After loading the voltage dye, recirculate oxygenated Krebs solution containing 10 μM blebbistatin [maintaining constant temperature at 37 ± 1°C] until the heart stops beating (10–15 min).
(7) Whilst waiting for the heart to stop beating, prepare equipment and solutions for ventricular slicer. A standard razor blade is cut into half and placed on the blade holder so that the blunt side of the blade was tight up against the holder. A circle of solidified agar is mounted on the ventricular slicer's plunger using superglue.

Ventricular Slicing, Harvest, and Recovery (60–70 min)

(1) Take the heart off the Langendorff setup.
(2) Carry out all dissections in ice cold HEPES buffered BDM solution. Remove atria and connective tissue from the ventricles to flatten the base.
(3) Mount base of the heart on solidified 4% agarose of slicer's plunger using surgical glue.
(4) Freshly prepare 4% low-melt agarose, cool on ice, and pour to cover the whole heart. Surround the plastic cap with the metal support.
(5) After the agarose is solidified, place the ventricular slicer plunger inside the metal merged into vibratome bath until it reaches stop point. Fill the ventricular slicer bath with ice-cold HEPES buffered BDM solution.
(6) Cut slices transversally at a thickness of 300–350 μm, with speed of 0.05 mm/s, amplitude of 1 mm and vibration frequency of 80 Hz (2 min per slice).
(7) On average 14 ventricular slices are harvested. Transfer each slice (other than the first which was usually discarded) to a petri dish containing ice-cold HEPES buffered BDM solution for 10 min. Pin the slices on small pieces of thin square shape Sylgard sheets (1 × 1 cm in diameter, 0.2 cm thickness), cover with mesh. Then transfer the slices to 1st, 2nd, and 3rd petri dishes filled with oxygenated blebbistatin Krebs solution (10 μM) at room temperature (RT) for 10 min in each dish.
(8) Repeat slicing procedure until the last slice is harvested.

Optical Mapping

(1) Place each slice in oxygenated blebbistatin Krebs solution (10 μM) in 37°C tissue bath for 2–3 min to equilibrate.
(2) Place the slice into a custom-made stimulation chamber filled with 37°C oxygenated blebbistatin Krebs solution (10 μM) between the two pacing electrodes. Use pin(s) and mesh to flatten the slice.
(3) Place the slices into the optical mapping setup (**Figure 2**, details in Materials and equipment). For field pacing, stimulate with square pulses of 2 ms duration, at voltages 1.5 times above threshold (minimum voltage required to pace tissue) with 1:1 coupling.
(4) For optical pacing, the tissues are paced through the activation of ChR2 light-sensitive channels. This is achieved by the delivery of 470 nm blue light pulses (2–10 ms pulse width) generated by OptoFlash (Cairn Research, Faversham, United Kingdom). Pulses are triggered by a 1401 digitiser and Spike 2 software (Cambridge Electronic Design). Approximate blue light intensity is measured with a 818-ST2 Wand Detector connected to a 843 R Power meter (both Newport Corporation, CA, United States) and we estimate an average irradiance in our experiments of 0.1–0.3 mW/mm^2 based on an approximate distance of 1–2 cm between Sylgard and liquid light guide (Oriel instruments Model No 77525).
(5) For AP and CaT alternans investigations, stimulate slices at frequencies of 2, 4, 8 and 16 Hz. Between pacing protocols, turn off the LED lights to minimize photobleaching (and other possible side effects, including phototoxicity). When testing, turn off the oxygenation to avoid motion artifacts.
(6) After experiment is finished, clean the perfusion system with deionized water.

Data Analysis

(1) Recorded image files are loaded into an optical mapping analysis software ElectroMap[1] (O'Shea et al., 2019). Pre-process images with application of 3 × 3 pixel Gaussian spatial filter and top-hat (kernel length = 100 ms) baseline correction.

[1]https://github.com/CXO531/ElectroMap

(2) Measure action potential duration (APD)/Calcium transient duration (CaTD) at desired repolarization/decay percentage at each pixel across the tissue, as measured from time of maximum upstroke velocity. Voltage-calcium latency can be measured as time difference between AP and CaT peak.
(3) For assessment of conduction velocity, render activation map by measuring activation time, for example by measuring depolarization midpoint or upstroke time (dV/dt max). Conduction velocity across the slice can then be quantified using multi-vector polynomial method with a local window size of 5 × 5 pixels (Bayly et al., 1998).

Exemplar Results

Figure 1 shows the optical mapping set-up. After the slices were prepared, slices were pre-incubated at room temperature in Krebs solution containing 10 μM blebbistatin for an optimal recovery time, prior to electrophysiological assessment using a custom-designed optical mapping system.

Figure 2 shows the major steps of the protocol. To achieve optimal dye loading, the voltage dye RH237 and/or Ca^{2+} dye Rhod-2 AM were loaded through the coronary circulation using the Langendorff perfusion system (**Figure 2A**). Prevention of blood clot formation was essential for optimal dye loading and was achieved by initial injection of heparin (200–300 units) before animal sacrifice. Ventricles were embedded in low-melting temperature agarose as illustrated in **Figure 2B** to provide structural support to the tissue during sectioning. Slices were cut at right angles to the long axis of the heart from the apex to the base, and thicknesses from 300–350 μm found to be the best thickness to achieve optimal recordings for both Vm and CaT (**Figure 2B**). **Figure 2C** shows viable slices obtained with the optimized protocol and representative V_m and CaT signals.

Figure 3A shows fluorescence images of voltage dye RH237 and Ca^{2+} dye Rhod-2 AM as imaged using the optical mapping setup. Using this protocol, and the optical imaging setup, we are able to dually measure parameters such as AP duration (**Figure 3B**) and CaT duration and (**Figure 3C**). The "rundown" of the Vm and CaT signals was monitored for up to 4 h, the average signal "rundown" being less than 25%. Our experiments usually finished within 3 h from the beginning of Langendorff perfusion of the heart.

Figure 4 shows an example of activation (**Figure 4A**) and APD75 (**Figure 4B**) maps reconstructed from electrical and light-paced APs in a ventricular slice from Pnmt-Cre/ChR2 mouse heart. Also shown are exemplar V_m signals from different regions of the ventricle.

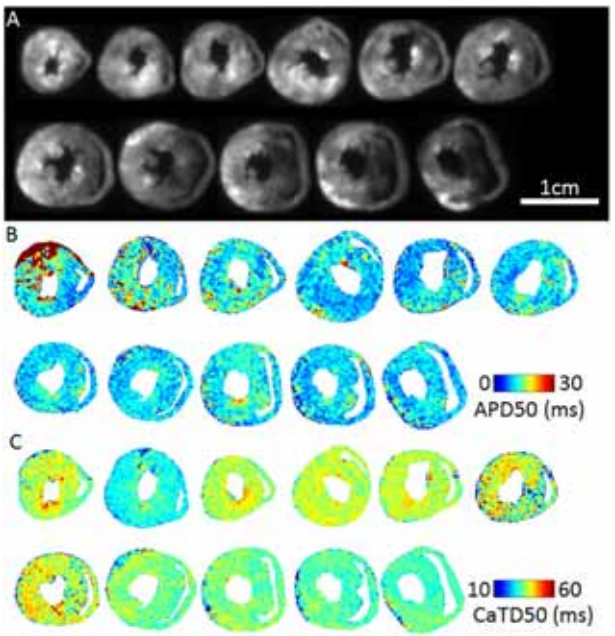

FIGURE 3 | Dual Vm and CaT imaging in murine transverse ventricular slices. **(A)** Fluorescence image (voltage-RH237) of transverse slices of murine ventricles from apex to base, dual loaded with both transmembrane voltage (RH237) and intracellular calcium dyes (Rhod-2 AM). **(B)** Representative maps of AP duration (APD50) at 2 Hz pacing frequency (500 ms pacing cycle length) recorded from apex to base ventricular slices. **(C)** Representative maps of Calcium transient duration (CaTD50) at 2 Hz pacing frequency recorded from apex to base ventricular slices.

DISCUSSION

The protocol described here allows high resolution mapping of V_m and CaT on thin transverse slices cut at right angles to the long axis of the heart, permitting robust interrogation of V_m and CaT throughout the entire heart with exceptional regional precision. Since the apico-basal location of each slice is known and every slice is fully transmural, such rich data allows for characterization of regional AP and CaT properties. This includes AP and CaT durations, alternans threshold, transmural activation and conduction velocities, and correlation of AP and CaT properties such as voltage-calcium coupling latency in each slice. The main processes of the protocol include: (i) Preparing solutions and experimental setup; (ii) Harvesting, cannulation and perfusion of the mouse heart by Langendorff perfusion; (iii) Loading calcium and voltage sensitive dyes and excitation-contraction uncoupler; (iv) Ventricular Slicing; (v) Optical mapping; (vi) Image processing and analysis. The protocol was further developed since it was first published (Wen et al., 2018) in two major aspects: (i) simultaneous dual dye images allowing correlation of AP and CaT properties in each slice; (ii) implementing improved image processing and analysis such as correlation of AP and CaT properties.

Applications

Our novel approach potentially provides not only a unique technique applicable to hearts of other species (such as widely used rat and rabbit), but also other tissues such as brain, adrenal medullary tissue, gut, etc. As we demonstrate here (**Figure 4**), such slice imaging technique can be also combined with optogenetic technology to carry out

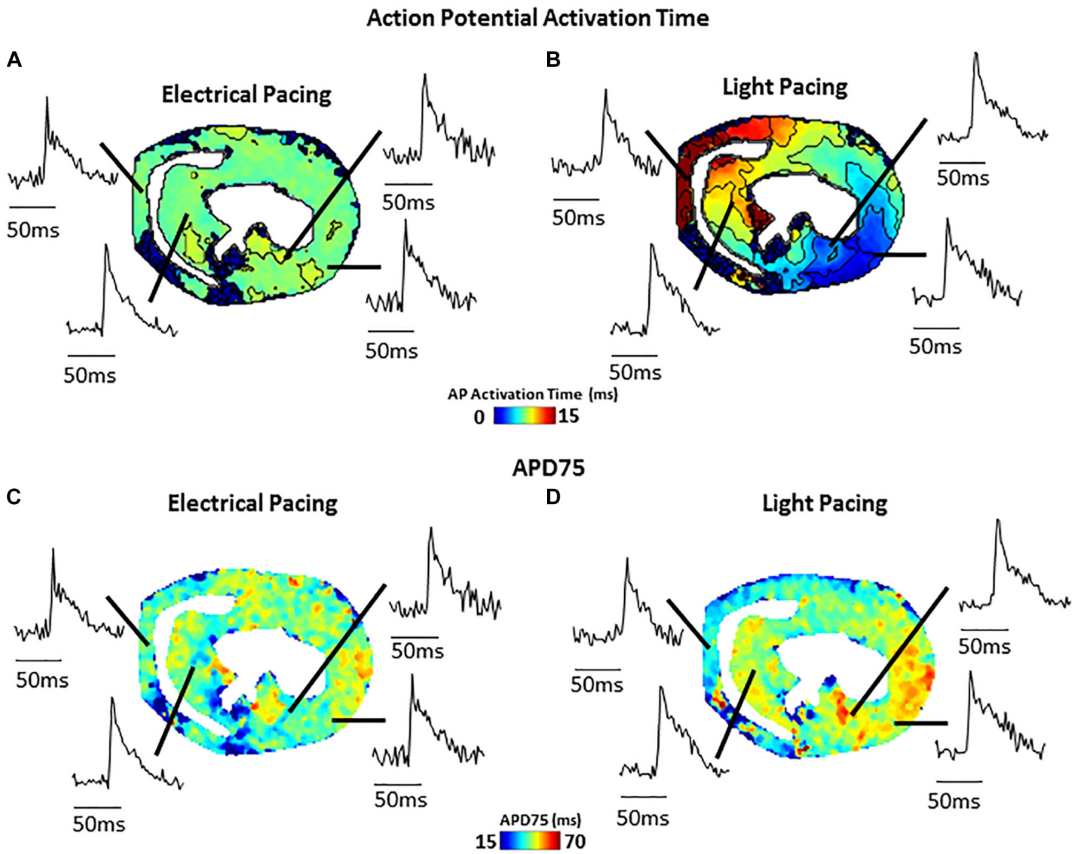

FIGURE 4 | Comparison of electrical (field stimulation) and light (470 nm pulses) pacing in murine transverse ventricular slices. **(A)** Activation map and example signals (transmembrane voltage, RH237) from slice paced using electrical field stimulation. **(B)** Activation map and example signals from the same slice paced using blue light stimulation of ChR2. **(C)** APD75 map from slice during electrical field stimulation. **(D)** APD75 map from slice during blue light stimulation.

optogenetic light stimulation of specific cells. Such an approach could be further extended by use of genetically encoded reporter proteins allowing cell-type specific study of V_m and Ca^{2+} signals, as well as cell-specific activation. We believe that the approach would be of considerable interest to researchers in manifold biomedical research fields and would serve as a useful platform for further innovative biomedical research.

Advantages

Firstly, a critical advantage of our cardiac slice model is the ability to provide access to any region of the ventricles, thus enabling exploration of regional and transmural differences. This is particularly important for the mouse heart, given that other *in vitro* tissue preparations, such as ventricular wedges, are not feasible for small hearts. Secondly, this technique may prove extremely valuable for characterizing regional arrhythmogenic changes in genetic murine models of cardiovascular disease (e.g., catecholaminergic polymorphic ventricular tachycardia, hypertrophic cardiomyopathy), as well as comprehensive regional characterization of remodeling in acquired pathologies (myocardial infarction, pressure-overload heart failure). Thirdly, depending on the optics, camera resolution, and slice size and position, it may be possible to image several or all slices from a single mouse heart simultaneously, giving a high throughput platform to electrophysiological investigations. Finally, it can also be combined with optogenetic technology to carry out optogenetic light stimulation – aiding studies requiring precise manipulation of cellular V_m and CaT.

Limitations and Adaptations

(i) Possibility of tissue injury increasing regional Vm and CaT differences. This can be overcome by optimized protocol with very slow cutting speed, embedding in supportive but oxygen permeable medium, and use of blebbistatin as uncoupler during slice preparation. (ii) Rundown of the V_m and CaT signals. The "rundown" of the V_m and CaT signals was also monitored for up to 4 h, the average signal "rundown" being less than 25%. Our experiments usually finished within 3 h. This can be overcome by efficient imaging processes, and the application of 0.5 mM Probenecid in the recovery and recording solutions to reduce the Ca^{2+} dye loss. (iii) The measurements of the parameters under electrical pacing condition was conducted by field stimulation (considering the fragile dedicated slice preparation), thus our approach may suffer from tissue activation occurring at the same

time point across the preparation. Whilst this is not what we observed regularly in our data, this approach may affect the conduction velocity (CV) measurement. A better approach with point stimulation or selective optical activation of a subset of cells (**Figure 4**) should be pursued.

ETHICS STATEMENT

Animals used were 10–12 weeks, 20–25 g, male B57BL mice. All procedures including animal subjects have been approved by the Institutional Animals Ethics Committees at the Southwest Medical University, Luzhou, China or the Department of Pharmacology at the University of Oxford and the national guidelines under which the institution operates. All mice used in this study were maintained in a pathogen−free facility at the Southwest Medical University or the University of Oxford. Mice were given *ad libitum* access to food and water. The authors confirm that they have taken all steps to minimize the animals' pain and suffering.

AUTHOR CONTRIBUTIONS

SH, QW, RM, XT, and XO carried out the experiments. CO'S and DP carried out the data process and data analysis. PC and ML designed the experiments. SH, QW, RM, XT, XO, and ML drafted the manuscript. PC, CO'S, and DP revised and edited the manuscript. All authors have made a substantial contribution to the manuscript.

FUNDING

This study was supported by the MRC (G10002647 and G1002082 to ML), the BHF (PG/14/80/31106, PG/16/67/32340, PG/12/21/29473, and PG/11/59/29004 to ML), (FS/17/33/32931 to PC and ML), and (PG/17/55/33087, RG/17/15/33106 to DP), the BHF CRE at Oxford (ML) grants, EPSRC (EP/L016346/1 to DP), the National Natural Science Foundation of China (Nos. 81700308 and 31871181) and the Royal Society (RSG\R1\180198 to PC).

REFERENCES

Accardi, M. V., Pugsley, M. K., Forster, R., Troncy, E., Huang, H., and Authier, S. (2016). The emerging role of in vitro electrophysiological methods in CNS safety pharmacology. *J. Pharmacol. Toxicol. Methods* 81, 47–59. doi: 10.1016/j.vascn.2016.03.008

Bayly, P. V., KenKnight, B. H., Rogers, J. M., Hillsley, R. E., Ideker, R. E., and Smith, W. M. (1998). Estimation of conduction velocity vector fields from epicardial mapping data. *IEEE Trans. Biomed. Eng.* 45, 563–571. doi: 10.1109/10.668746

Bussek, A., Wettwer, E., Christ, T., Lohmann, H., Camelliti, P., and Ravens, U. (2009). Tissue slices from adult mammalian hearts as a model for pharmacological drug testing. *Cell Physiol. Biochem.* 24, 527–536. doi: 10.1159/000257528

Camelliti, P., Al-Saud, S. A., Smolenski, R. T., Al-Ayoubi, S., Bussek, A., Wettwer, E., et al. (2011). Adult human heart slices are a multicellular system suitable for electrophysiological and pharmacological studies. *J. Mol. Cell Cardiol.* 51, 390–398. doi: 10.1016/j.yjmcc.2011.06.018

Halbach, M., Pillekamp, F., Brockmeier, K., Hescheler, J., Müller-Ehmsen, J., and Reppel, M. (2006). Ventricular slices of adult mouse hearts - a new multicellular in vitro model for electrophysiological studies. *Cell Physiol. Biochem.* 18, 1–8. doi: 10.1159/000095132

Huang, C. L. (2017). Murine electrophysiological models of cardiac arrhythmogenesis. *Physiol. Rev.* 97, 283–409. doi: 10.1152/physrev.00007.2016

Kang, C., Qiao, Y., Li, G., Baechle, K., Camelliti, P., Rentschler, S., et al. (2016). Human organotypic cultured cardiac slices: new platform for high throughput preclinical human trials. *Sci. Rep.* 6:28798. doi: 10.1038/srep28798

Nerbonne, J. M., and Kass, R. S. (2005). Molecular physiology of cardiac repolarization. *Physiol. Rev.* 85, 1205–1253. doi: 10.1152/physrev.00002.2005

O'Shea, C., Holmes, A. P., Yu, T. Y., Winter, J., Wells, S. P., Correia, J., et al. (2019). ElectroMap: high-throughput open-source software for analysis and mapping of cardiac electrophysiology. *Sci. Rep.* 9:1389–1389. doi: 10.1038/s41598-018-38263-2

Randi, A. M., Kane, C., Perbellini, F., Bardi, I., Gorelik, J., Sikkel, M. B., et al. (2017). Investigation of cardiac fibroblasts using myocardial slices. *Cardiovasc. Res.* 114, 77–89. doi: 10.1093/cvr/cvx152

Thomas, R. C., Singh, A., Cowley, P. M., Myagmar, B.-E., Montgomery, M. D., Swigart, P. M., et al. (2016). A myocardial slice culture model reveals alpha-1A-adrenergic receptor signaling in the human heart. *JACC Basic Trans. Sci.* 1, 155–167. doi: 10.1016/j.jacbts.2016.03.005

Wang, K., Lee, P., Mirams, G. R., Sarathchandra, P., Borg, T. K., Gavaghan, D. J., et al. (2015). Cardiac tissue slices: preparation, handling, and successful optical mapping. *Am. J. Physiol. Heart Circ. Physiol.* 308, H1112–H1125. doi: 10.1152/ajpheart.00556.2014

Wang, Y., Lin, W. K., Crawford, W., Ni, H., Bolton, E. L., Khan, H., et al. (2017). Optogenetic control of heart rhythm by selective stimulation of cardiomyocytes derived from Pnmt+ cells in murine heart. *Sci. Rep.* 7:40687. doi: 10.1038/srep40687

Watson, S. A., Scigliano, M., Bardi, I., Ascione, R., Terracciano, C. M., and Perbellini, F. (2017). Preparation of viable adult ventricular myocardial slices from large and small mammals. *Nat. Prot.* 12:2623. doi: 10.1038/nprot.2017.139

Watson, S. A., Terracciano, C. M., and Perbellini, F. (2019). Myocardial slices: an intermediate complexity platform for translational cardiovascular research. *Cardiovasc. Drugs Ther.* 33, 239-244. doi: 10.1007/s10557-019-06853-5

Wen, Q., Gandhi, K., Capel, R. A., Hao, G., O'Shea, C., Neagu, G., et al. (2018). Transverse cardiac slicing and optical imaging for analysis of transmural gradients in membrane potential and Ca2+ transients in murine heart. *J. Physiol.* 596, 3951–3965. doi: 10.1113/JP276239

Conflict of Interest Statement: The authors declare that the research was conducted in the absence of any commercial or financial relationships that could be construed as a potential conflict of interest.

frontiers in Physiology

ORIGINAL RESEARCH
published: 04 April 2019
doi: 10.3389/fphys.2019.00272

Optogenetic Monitoring of the Glutathione Redox State in Engineered Human Myocardium

Irina Trautsch[1,2†], Eriona Heta[1,2†], Poh Loong Soong[1,2], Elif Levent[1,2], Viacheslav O. Nikolaev[3,4], Ivan Bogeski[2,5], Dörthe M. Katschinski[2,5], Manuel Mayr[6] and Wolfram-Hubertus Zimmermann[1,2]*

[1] Institute of Pharmacology & Toxicology, University Medical Center Göttingen, Göttingen, Germany, [2] DZHK (German Center for Cardiovascular Research), Partner Site Göttingen, Göttingen, Germany, [3] Institute for Experimental Cardiovascular Research, University Medical Center Hamburg-Eppendorf, Hamburg, Germany, [4] DZHK (German Center for Cardiovascular Research), Partner Site Hamburg/Kiel/Lübeck, Hamburg, Germany, [5] Institute for Cardiovascular Physiology, University Medical Center Göttingen, Göttingen, Germany, [6] King's British Heart Foundation Centre, King's College London, London, United Kingdom

Redox signaling affects all aspects of cardiac function and homeostasis. With the development of genetically encoded fluorescent redox sensors, novel tools for the optogenetic investigation of redox signaling have emerged. Here, we sought to develop a human heart muscle model for in-tissue imaging of redox alterations. For this, we made use of (1) the genetically-encoded Grx1-roGFP2 sensor, which reports changes in cellular glutathione redox status (GSH/GSSG), (2) human embryonic stem cells (HES2), and (3) the engineered heart muscle (EHM) technology. We first generated HES2 lines expressing Grx1-roGFP2 in cytosol or mitochondria compartments by TALEN-guided genomic integration. Grx1-roGFP2 sensor localization and function was verified by fluorescence imaging. Grx1-roGFP2 HES2 were then subjected to directed differentiation to obtain high purity cardiomyocyte populations. Despite being able to report glutathione redox potential from cytosol and mitochondria, we observed dysfunctional sarcomerogenesis in Grx1-roGFP2 expressing cardiomyocytes. Conversely, lentiviral transduction of Grx1-roGFP2 in already differentiated HES2-cardiomyocytes and human foreskin fibroblast was possible, without compromising cell function as determined in EHM from defined Grx1-roGFP2-expressing cardiomyocyte and fibroblast populations. Finally, cell-type specific GSH/GSSG imaging was demonstrated in EHM. Collectively, our observations suggests a crucial role for redox signaling in cardiomyocyte differentiation and provide a solution as to how this apparent limitation can be overcome to enable cell-type specific GSH/GSSG imaging in a human heart muscle context.

Keywords: optogenetics, engineered human myocardium, redox-reporters, stem cells, cardiomyocytes, fibroblasts, roGFP, GSH

OPEN ACCESS

Edited by:
Christopher Huang, University of Cambridge, United Kingdom

Reviewed by:
Houzao Chen, Chinese Academy of Medical Sciences, China
Matthew W. Kay, George Washington University, United States

****Correspondence:***
Wolfram-Hubertus Zimmermann w.zimmermann@med.uni-goettingen.de

† These authors have contributed equally to this work

Specialty section:
This article was submitted to Cardiac Electrophysiology, a section of the journal Frontiers in Physiology

Received: *05 November 2018*
Accepted: *28 February 2019*
Published: *04 April 2019*

Citation:
Trautsch I, Heta E, Soong PL, Levent E, Nikolaev VO, Bogeski I, Katschinski DM, Mayr M and Zimmermann W-H (2019) Optogenetic Monitoring of the Glutathione Redox State in Engineered Human Myocardium. Front. Physiol. 10:272. doi: 10.3389/fphys.2019.00272

INTRODUCTION

Reactive oxygen species (ROS) can be damaging to cells if produced in excess, but also contribute to physiological signaling within and between cells (Sies et al., 2017). In cardiomyocytes, ROS are implicated in fundamental mechanisms of electromechanical coupling, such as the regulation of calcium release from the sarcoplasmic reticulum via mechanosensitive microtubule-dependent oxidation (termed X-ROS) of the ryanodine receptor (RyR2; Prosser et al., 2011) or

oxidation mediated homodimer formation of PKGIα, leading to phospholamban (PLN) phosphorylation and enhanced diastolic relaxation (Scotcher et al., 2016). Redox signals have also been shown to alter cardiac metabolism via O-GlcNAcylation of fatty acid transporters (Nabeebaccus et al., 2017). Many other mechanisms have been reported and are summarized in excellent reviews (Burgoyne et al., 2012; Shao et al., 2012; Santos et al., 2016).

Reactive oxygen species are produced by two major mechanisms: (1) as byproduct of the electron transport chain function in mitochondria (Bertero and Maack, 2018) and (2) via the catalytic activity of NADPH oxidases (NOXs; Zhang et al., 2013). The main NOX isoforms in cardiomyocytes are the highly regulated NOX2 and NOX4, which is thought to be constitutively active. Activity of NOX5 is postulated to contribute to redox signaling in cardiac fibroblasts (Zhang et al., 2013), demonstrating cell type specific ROS production in the heart and suggesting cell type specific ROS signaling. Given the short half-life and fast removal by antioxidant enzymes (Stone and Yang, 2006) it is likely that ROS signaling is strictly compartmentalized, as recently reported for X-ROS signaling (Prosser et al., 2011). The identification of the pathophysiological relevance of ROS production in cellular compartments should be facilitated by the use of cell-type and organelle restricted genetically engineered redox sensors (Morgan et al., 2011; Gibhardt et al., 2016). In contrast to classical dyes for ROS quantification - such as dichlorodihydrofluorescein diacetate (H2DCFDA), Amplex® Red or boronate based probes (Rezende et al., 2018) - transgenic sensors allow for stable, long-term measurements of ROS, such as H_2O_2 (Belousov et al., 2006; Gutscher et al., 2009; Morgan et al., 2016) and the redox potential of ROS scavengers, such as glutathione (Gutscher et al., 2008).

The widely used glutathione redox potential sensor Grx1-roGFP2 was developed by the fusion of redox sensitive roGFP2 with the human glutaredoxin-1 (Grx1) domain to improve the specificity of roGFP2 toward reporting the glutathione redox state (Gutscher et al., 2008). The sensor exhibits excitation maxima at 408 nm for oxidized Grx1-roGFP2 and 488 nm for reduced Grx1-roGFP2, with emission at 500–530 nm. Ratiometric imaging of the fluorescence emission at the indicated excitation wavelengths allows for the calculation of the ratio of reduced to oxidized glutathione (GSH/GSSG). As the reaction is fully reversible, dynamics of GSH/GSSG changes can be detected in living cells. From this data, the glutathione redox potential (E_{GSH}) can be calculated (Meyer and Dick, 2010). Furthermore, localization to cellular compartments can be achieved by fusing Grx1-roGFP2 to organelle targeting sequences, such as in the mitochondria targeted mito-Grx1-roGFP2 variant. Cardiomyocyte specific expression of cytosolic and mitochondrial Grx1-roGFP2 in a mouse model recently revealed that the E_{GSH} in the mitochondrial matrix is more reduced compared to the cytosolic E_{GSH} (Swain et al., 2016). A recent study employed fluorescent redox sensors in a model of sudden cardiac death in guinea pig, elucidating the effect of mitochondrial ROS production in chronic beta adrenergic stimulation (Dey et al., 2018), while others have used organelle targeted redox sensors to investigate the redox effect of insulin signaling in mice (Steinhorn et al., 2017). These studies and their findings demonstrate how redox sensors can add to our understanding in disease initiation and progression. However, they are limited by the use of animal models, with their model intrinsic differences in pathophysiology compared to the human.

Here we report the to our knowledge first application of Grx1-roGFP2 in human embryonic stem cell-derived cardiomyocytes as well as engineered human myocardium (EHM; Tiburcy et al., 2017) for in-tissue glutathione redox state imaging.

MATERIALS AND METHODS

Cloning of Redox Sensor Expression Constructs

Grx1-roGFP2 and mito-Grx1-roGFP2 coding sequences were amplified by PCR from pLPCX backbone vectors (kind gift by Tobias Dick, Heidelberg) with engineered SalI and PacI restriction sites. Sensor sequences were inserted into the multiple cloning site (MCS) of a modified pAAVS-CAG-MCS-EF1-puro vector. Similarly, the coding sequence for Grx1-roGFP2 was cloned into a lentiviral backbone vector (pGIPZ) under the control of the CMV promoter. Correct insert integration was verified by colony PCR, restriction digest, and sequencing.

TSA Cell Culture

TSA201 cells (human embryonic kidney cells [*aka* HEK293]; ECACC), used to validate transgene expression and localization, were grown in high glucose DMEM (Thermo Scientific) supplemented with 10% fetal calf serum (FCS). Cells were digested using 0.05% Trypsin-EDTA (Thermo Scientific), counted and seeded at 0.05×10^6 cells /cm^2. Transfection with 2 μg DNA per 6-well for redox sensor integration was carried out using PolyFect Transfection reagent (Qiagen). Cells were selected with 3 μg/ml puromycin.

Human Embryonic Stem Cell Culture (HES)

HES2 cells (ES International, Singapore) were cultured on irradiated feeders in Knock-out DMEM supplemented with 20% Knock-out Serum Replacement, 2 mmol/L glutamine, 1% non-essential amino acids (NEAA), 100 U/mL penicillin, and 100 μg/mL streptomycin (all Thermo Scientific) and further supplemented with 10 ng/mL FGF2 (PeproTech). For feeder-free culture and differentiation, cells were plated on 1:120 growth factor reduced Matrigel™ (Corning)-coated plates and grown in E8 medium (Stem Cell Technologies). Ethical approval for the use of HES was obtained from the Central Ethic Committee for Stem Cell Research (ZES; permit #12; reference number: 1710-79-1-4-16).

HES Electroporation

HES2 cells were dispersed into single cell suspensions by incubation with TrypLE (Thermo Scientific). Electroporation with the Neon transfection system (Thermo Scientific) was carried out according to manufacturer's protocol. Briefly, one

million HES2 were resuspended in 100 µl buffer R and mixed with 444 ng pAAVS1-[mito-]Grx1-roGFP2, 28 ng pTALEN-HA-R and 28 ng pTALEN-HA-L (AAVS1 TALE-Nuclease Kit, System Biosciences). Electroporation was performed with a single pulse at 1,200 V for 40 ms. Cells were then immediately transferred onto γ-irradiated feeder plates in HES medium with 5 µmol/L ROCK inhibitor Y27632 (Stemgent). After 4 days of recovery, cells were transferred onto Matrigel™ coated plates and cultured in E8 medium. Selection with 0.4 µg/mL puromycin was performed for 5 days. Single fluorescent colonies were transferred manually and expanded. Genotyping was performed to confirm transgene integration. We obtained one positive Grx1-roGFP2 clone and 14 clones positive for mito-Grx1-roGFP2 of which one clone was selected for use in all further experiments. Pluripotency was confirmed using flow cytometry detection for Oct4 (96 ± 1%, 96 ± 0.5%), Nanog (94 ± 3%, 93 ± 2%) and Tra1-60 (96 ± 1%, 97 ± 2% for the Grx1-roGFP2 and mito-Grx1-roGFP2 lines, respectively, n = 3 independent passage; **Supplementary Figure 1**). Transgene integration was analyzed using Universal Genome Walker kit (Clontech). We could not confirm targeted integration into the AAVS1 locus, but determined random integration into several loci, including chromosome 2, p21, promotor flank region (mito-Grx1-roGFP2) and chromosome 16, STXB1, intron 1 (Grx1-roGFP2).

Lentivirus Production and Transduction

TSA201 cells were transfected with the Grx1-roGFP2 encoding expression plasmid pGIPZ-CMV-Grx1-roGFP2, packaging plasmid psPAX2 (Addgene plasmid #12260) and envelope plasmid pMD2.G (Addgene plasmid #12259; both kindly provided by the Trono Lab, EPFL) using PolyFect (Qiagen). Culture supernatant containing viral particles was harvested after 72 h and filtered through 0.45 µm filter (Millex® Syringe filter units, Merck Millipore). Cardiomyocytes differentiated from HES2 (hCM) and human foreskin fibroblasts (hFF; SCRC 1041, ATCC) were transduced in the presence of polybrene (0.8 mg/mL, Sigma) and incubated for 72 h at 5% CO2 and 37°C before analysis of transduction efficiency.

Cardiac Differentiation and Cardiomyocyte Culture

HES2 cardiac differentiation was carried out as previously described (Tiburcy et al., 2017). HES-derived hCM were cultured on Matrigel™-coated plates in RPMI 1640 supplemented with GlutaMAX, 1 mmol/L sodium pyruvate, 100 U/ml penicillin, 100 µg/ml streptomycin (all Thermo Scientific), 200 µmol/L L-ascorbic acid-2-phosphate sesquimagnesium salt hydrate (Sigma-Aldrich) and 2% B27 supplement (Thermo Scientific).

Engineered Human Myocardium

Engineered human myocardium (EHM) was constructed as previously described (Tiburcy et al., 2017). Briefly, hCM and hFFs were mixed at a 70:30% ratio with pH-neutralized collagen type I and concentrated culture medium on ice (total cell number per EHM: 1.45×10^6). The reconstitution mix was cast into circular molds (450 µL / EHM). After 3 days in culture, consolidated EHM were transferred on stretch devices and cultured for 20 days in IMDM with 4% B27 minus Insulin, 1% non-essential amino acids, 100 U/ml penicillin, 100 µg/ml streptomycin (all Thermo Scientific), 100 ng/µl IGF-1, 10 ng/µl FGF-2, 5 ng/µl VEGF (all PeproTech); supplemented with 5 ng/µl TGF-beta (PeproTech) for the first 72 h of culture. After 21 days of culture, EHM were subjected to isometric force measurements as previously described (Tiburcy et al., 2017) and redox imaging.

Life Cell Imaging of Mitochondria

Cells were seeded onto glass bottom imaging dishes (Zell-Kontakt) using growth conditions stated above. Staining with TMRM was carried out according to manufacturer's recommendations. Briefly, cells were incubated for 30 min in a standard cell culture incubator with 50 nmol/L TMRM and 10 µg/mL Hoechst-3342 in normal growth medium followed by two washes with PBS (Thermo Scientific). Cells were then imaged in imaging buffer (in mmol/L: 114 NaCl, 5.4 KCl, 1 $MgCl_2$, 2 $CaCl_2$, 10 HEPES; pH 7.4) on an Olympus IX81 fluorescence microscope using Xcellence pro software.

GSH/GSSG Imaging

Transgenic cells were seeded on 25 mm diameter glass coverslips using growth conditions stated above. GSH/GSSG imaging was performed using a pH-buffered imaging solution (in mmol/L: 114 NaCl, 5.4 KCl, 1 $MgCl_2$, 2 $CaCl_2$ [1 $CaCl_2$ for hCM], 10 HEPES; pH 7.4) in a 37°C climate chamber on a Zeiss D1 Observer microscope using ZEN image processing software (Zeiss). Images were acquired sequentially at 400 nm and 505 nm excitation using a YFP filter at 40× magnification every 3 s. Hydrogen peroxide (H_2O_2, a strong oxidant) or Dithiothreitol (DTT, a cell permeable thiol reducing agent) were added after a stable baseline was reached at 30 s. Likewise, lentivirally transduced hCM and hFF were seeded on Matrigel™-coated 24-well imaging plates (ZellKontakt) and fluorescence emission at 510 nm (upon excitation at 405 and 488 nm) was captured with an Olympus IX83 fluorescence microscope equipped with a cellVivo (Pecon) 37°C climate chamber using Visiview Software. H_2O_2 or DTT were added after a stable baseline was reached in both cell types. Image analysis was carried out using Fiji-ImageJ with the BioVoxxel Toolbox, Python 3.6 and GraphPad prism 7. ROIs were drawn by hand based on bright field and GFP images to correspond to single cells, as well as a background ROI not containing any cell per slide. Fluorescence intensities for each ROI in each channel were extracted and corresponding background values subtracted. The ratio of the corrected intensity values was normalized to the average of the baseline. Calculation of E_{GSH} was performed as previously described (Meyer and Dick, 2010).

Mitochondrial Isolation and Western Blot

Mitochondria were isolated from cells as previously established (Acín-Pérez et al., 2008). Briefly, 30×10^6 cells were resuspended, washed with PBS, and the cell pellet was frozen at −80°C and thawed to disrupt the membranes. After thawing, cells were resuspended in 83 mmol/L sucrose, 10 mmol/L HEPES, pH 7.2 and homogenized by 30 strokes using pestle B in a

2 mL Dounce homogenizer. An equal volume of 250 mmol/L sucrose, 30 mmol/L HEPES, pH 7.4 containing complete mini protease inhibitor cocktail (Roche) was added, followed by centrifugation for 5 min at 1,000 g and 4°C to pellet nuclei and remaining intact cells. The supernatant was then subjected to another round of centrifugation for 15 min at 12,000 g and 4°C to pellet mitochondria. The cytosolic fraction in the supernatant was collected for later analysis and the mitochondrial pellet was resuspended in 320 mmol/L sucrose, 1 mmol/L EDTA, 10 mmol/L TRIS–HCl (pH 7.4) containing complete mini protease inhibitor cocktail. Protein concentration was determined by Bradford assay. 25 μg of protein per sample was loaded onto a denaturing SDS–PAGE and subjected to electrophoretic separation at 120 V for 1 h. Proteins were transferred by semi-dry blotting onto a PVDF membrane. Unspecific binding was blocked by incubation with TBS-T containing 5% whole milk powder for 1 h. Primary antibody incubation was carried out overnight at 4°C. After 1 h incubation with secondary antibody solution, membranes were imaged using the femtoLUCENT PLUS-HRP Kit (G-Biosciences) in a Qiagen ChemiDoc^{TM} imaging chamber. For detailed information on the antibodies and dilutions used refer to **Table 1**.

Flow Cytometry

To assess pluripotency of HES lines, formaldehyde fixed cell samples were stained with Oct4-Alexa-647 (1:50; BD Biosciences), Nanog-Alexa-547 (1:25; Miltenyi), or Tra1-60-Alexa-647 (1:50; BD Biosciences) for 45 min. All samples, including negative controls, were exposed to Hoechst-3342 for nuclei labeling (Thermo Scientific). For a quantitative analysis of transgenic cardiomyocytes, samples were stained with anti-human alpha-actinin mouse monoclonal antibody (1:4,000; Sigma) for 60 min followed by anti-mouse IgG Alexa-633 (1:1,000; Invitrogen) and Hoechst-3342 staining for 45 min. For each sample, a negative control was incubated only with secondary antibody and Hoechst-3342. To assess the transduction efficiency of cardiomyocytes and fibroblasts, transduced and non-transduced cells were stained with SYTOX Red Dead Cell Stain (Thermo Scientific) for 15 min at room temperature and live cells analyzed for GFP expression. All flow cytometry samples were analyzed using a LSRII cytometer (BD Bioscience) and flowing software v2. In fixed samples, gating for intact cells was performed based on FSC-A vs. SSC-A and the Hoechst-3342 signal was used for cell DNA content assessment and exclusion of doublets. Marker gating was performed based on non-stained controls, gating for GFP signal was based on non-GFP control cell lines.

TABLE 1 | Antibodies used for Western Blotting.

Antibody	Species	Supplier	Cat#	Dilution
eGFP Tag	rb	Thermo Fisher	CAB4211	1:1,000
Total OXPHOS rodent WB antibody cocktail	ms	Abcam	ab110413	1:250
GAPDH	ms	ZYTOMED Systems	RGM2-6C5	1:50,000
α-tubulin	ms	Sigma	T5168	1:2,000
Anti mouse HRP	goat	Dako	P0260	1:10,000
Anti rabbit HRP	goat	Dako	P0448	1:5,000

Statistics

All data are displayed as means ± standard error of the mean (SEM). Biological replicates (n) are indicated with each data set. Statistical tests were performed as indicated in the legends and the main body of the manuscript. A p-value < 0.05 was considered statistically significant. Statistical testing was performed using GraphPad Prism 7.

RESULTS

Compartment Specific Expression of GSH Redox Sensors

We first generated TSA cells stably expressing Grx1-roGFP2 and mito-Grx1-roGFP2 by co-transfection of linearized donor vectors encoding for the respective sensors and TALEN-expression vectors to verify compartment (cytosol vs. mitochondria)-specific sensor location. Sensor expressing cells were purified by selection with puromycin. Life imaging of TSA cells confirmed co-localization of GFP and the mitochondrial TMRM signals in mito-Grx1-roGFP2 cells, whereas Grx1-roGFP2 expressing cells showed a uniform cytosolic distribution of the GFP signal (**Figure 1A** – GFP panels). To further interrogate the cytosolic and mitochondrial localization of Grx1-roGFP2, we performed Western blots for GFP protein in cytosolic and mitochondrial protein fractions. For Grx1-roGFP2 cells, the GFP signal was detected primarily in the cytosolic fraction, whereas in mito-Grx1-roGFP2 enrichment of GFP in the mitochondrial fraction was observed (**Figure 1B**). Wild type control cells were negative for GFP.

Generation of Functional GSH Reporter HES Cell Lines

We next generated human embryonic stem cell lines (HES2 background) with stable expression of Grx1-roGFP2 and mito-Grx1-roGFP2 by TALEN-mediated integration. The two investigated clonal cell lines demonstrated a uniform GFP signal (>95%; **Figure 2A** and **Supplementary Figure 1A**) and expression of the canonical pluripotency markers Oct4, Nanog and Tra1-60 (**Supplementary Figure 1B**). Correct localization and expression of GSH sensors was confirmed by Western blot analysis (**Figure 2B**). Next, we performed live dual excitation, single emission microscopy to assess functionality of the expressed sensors. Grx1-roGFP2 emits light at 500–530 nm upon stimulation with either 405 nm or 488 nm wavelength. The intensity of emitted fluorescence of the Grx1-roGFP2 reporter changes with the cellular GSH/GSSG state in an inversely correlated manner (**Figure 2C**). Live cell ratiometric imaging allows for the quantification of the cellular GSH redox state in real time (**Figure 2D**). In both HES lines, Grx1-roGFP2-HES2 and mito-Grx1-roGFP2-HES2, the sensor reacted in a concentration

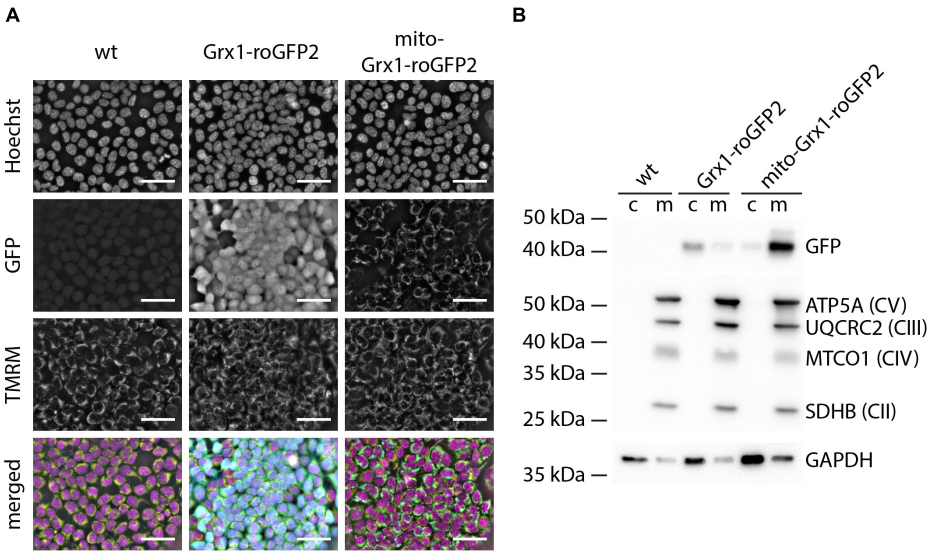

FIGURE 1 | TSA cells express Grx1-roGFP2 in a compartment specific manner. **(A)** Live cell imaging of roGFP-reporter (GFP), TMRM (mitochondria) and Hoechst (DNA) in TSA cells demonstrated the anticipated cytosolic and mitochondrial localization of Grx1-roGFP2 and mito-Grx1-roGFP2, respectively; note that the GFP signal in the Grx1-roGFP2 condition fills the whole cell, whereas the mito-Grx1-roGFP2 signal superimposes with the spatially confined perinuclear TMRM signal and presents as a distinct rim around the nucleus because of the high nucleus to cytosol ratio in TSA cells. Scale bars: 50 μm. **(B)** Representative Western blot analysis to confirm enrichment of the respective roGFP2 reporters in cytosolic (c) and mitochondria (m) compartments. The mitochondrial compartment is characterized by proteins of the electron transport chain complexes I - IV (SDHB: Succinate dehydrogenase complex iron sulfur subunit B, MTCO1: Cytochrome c oxidase I, UQCRC2: ubiquinol-cytochrome c reductase core protein II, ATP5A: ATP synthase subunit alpha).

dependent manner to oxidation by H_2O_2 with an increase in fluorescence ratio (R/R_0) under 405 nm excitation over 488 nm excitation (**Figures 2E,F**). Reduction upon stimulation with increasing concentrations of DTT led to a concentration dependent decrease of the fluorescence ratio (**Figures 2G**, **H**). The maximally observed R/R_0 upon oxidation with 300 μmol/L H_2O_2 was 1.9 ± 0.01 for Grx1-roGFP2-HES2 (n = 241 cells) and 1.8 ± 0.01 for mito-Grx1-roGFP2-HES2 (n = 182 cells). Upon reduction with 10 mmol/L DTT R/R_0 decreased to 0.7 ± 0.007 in Grx1-roGFP2-HES2 (n = 197 cells) and 0.6 ± 0.003 in mito-Grx1-roGFP2-HES2 (n = 193 cells).

GSH/GSSG Imaging in Grx1-roGFP2-HES2 Derived Cardiomyocytes

We next subjected Grx1-roGFP2-HES2 and mito-Grx1-roGFP2-HES2 to a well-defined and highly robust directed cardiac differentiation protocol (Tiburcy et al., 2017). Flow cytometry analyses confirmed a yield of 80–95% α-actinin$^+$ cardiomyocytes for both cell lines and no obvious differences to non-transgenic isogenic controls. Notably, all α-actinin$^+$ Grx1-roGFP2 and mito-Grx1-roGFP2 cardiomyocytes (hCM) were also GFP$^+$ by flow cytometry analysis (**Supplementary Figure 2**). Upon stimulation with 100 μmol/L H_2O_2 a maximal R/R_0 of 3.3 ± 0.01 was observed in Grx1-roGFP2-hCM (n = 176 cells); a maximal R/R_0 of 2.0 ± 0.1 was observed in mito-Grx1-roGFP2-hCM (n = 325 cells; **Figures 3A,B**). Maximal reduction upon 1 mmol/L DTT resulted in a R/R_0 decrease to 0.9 ± 0.002 for Grx1-roGFP2-hCM (n = 170 cells) and 0.6 ± 0.005 for mito-Grx1-roGFP2-hCM (n = 325 cells). These findings were however, compromised by limited spontaneous beating activity (observed only in a small subsets of cardiomyocytes in 2 of 12 differentiations) and an obviously impaired sarcomerogenesis in the Grx1-roGFP2- and mito-Grx1-roGFP2-hCMs (**Figure 3C**, hCM wild type shown for comparison). To scrutinize whether the unanticipated dysfunction was due to the constitutive overexpression of Grx1-roGFP2 in our transgenic lines, we performed lentiviral transduction of differentiated, beating HES-derived hCM. Given the observation of similar developmental toxicity of the cytosolic and mitochondrial Grx1-roGFP2 variants, the greater R/R_0 dynamic range in Grx1- versus mito-Grx1-roGFP2 cells, and our ultimate goal to establish proof-of-concept for in-tissue GSH/GSSG imaging, we decided to focus on the cytosolic Grx1-roGFP2 variant in the following experiments.

Lentiviral Sensor Expression Does Not Impair Cardiomyocyte Function

Because fibroblasts play an essential role in natural and engineered cardiomyogenesis (Ieda et al., 2009; Tiburcy et al., 2017), we decided to lentivirally transduce differentiated HES2-derived hCM and human foreskin fibroblasts (hFF; **Figure 4A**) for subsequent use in the construction of contractile engineered human myocardium (EHM; Tiburcy et al., 2017). Transduction efficiency was 47 ± 7% for Grx1-roGFP2-hCM (n = 7) and 72 ± 6% for Grx1-roGFP2-hFF (n = 8; **Figure 4B**). In contrast to the observation in the directed differentiation of Grx1-roGFP2-HES2, lentivirally transduced hCM remained contractile with no obvious differences compared to non-transduced hCM. To

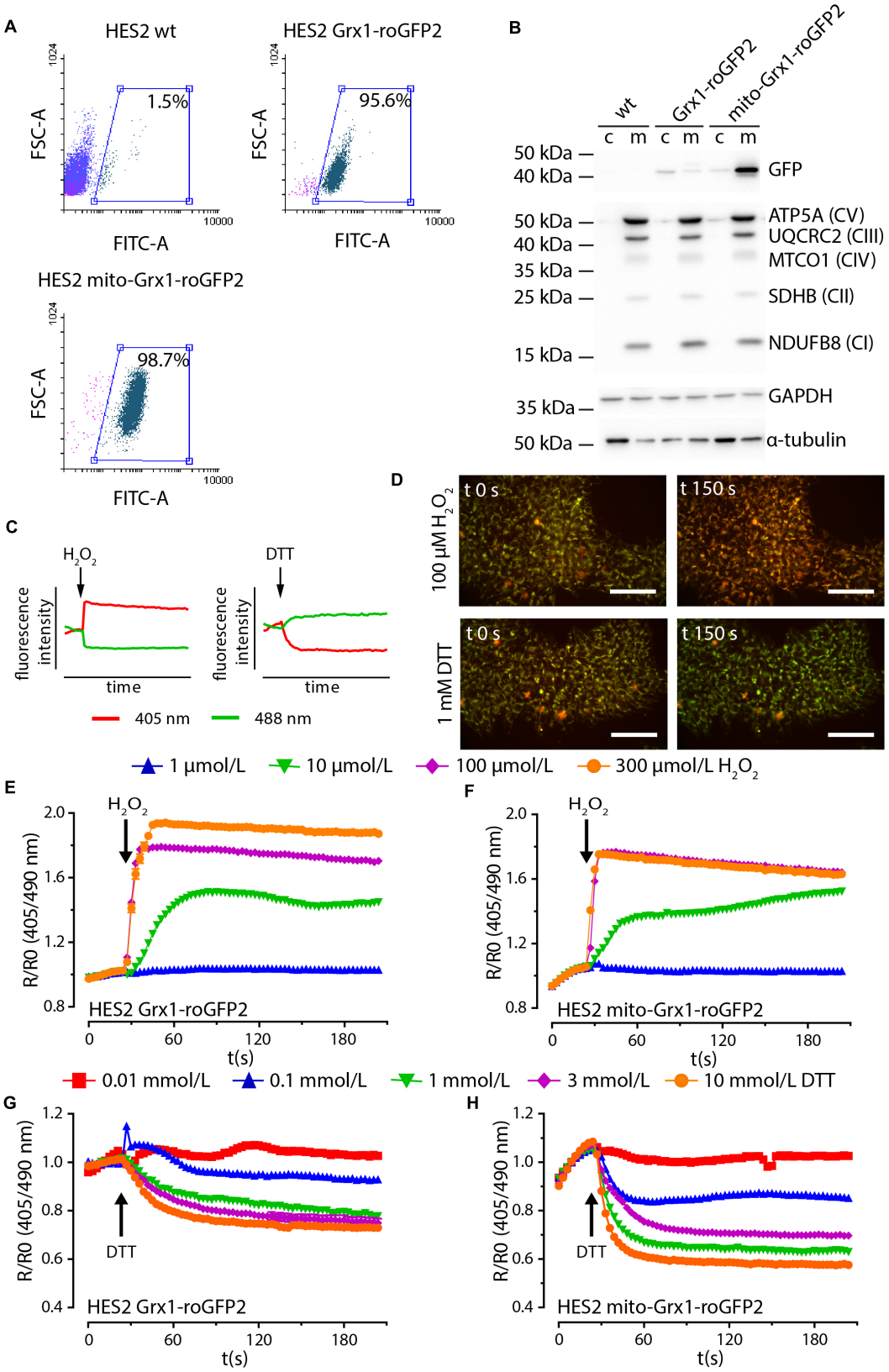

FIGURE 2 | Continued

FIGURE 2 | TALEN-modified HES2 express functional Grx1-roGFP2. **(A)** Flow cytometry analysis of GFP positive cells in genetically naïve (HES2 wt) and TALEN-modified Grx1-roGFP2 and mito-Grx1-roGFP2 HES2. **(B)** Representative Western blot analysis to confirm enrichment of the respective roGFP2 reporters in cytosolic (c) and mitochondria (m) compartments. The mitochondrial compartment is characterized by proteins of the electron transport chain complexes I - IV (NDUFB8: NADH: ubiquinone oxidoreductase subunit B8, SDHB: Succinate dehydrogenase complex iron sulfur subunit B, MTCO1: Cytochrome c oxidase I, UQCRC2: ubiquinol-cytochrome c reductase core protein II, ATP5A: ATP synthase subunit alpha). **(C)** Oxidation and reduction of roGFP2 results in an inversely correlated shift in fluorescence intensity under 408 and 488 nm excitation. **(D)** Fluorescence intensity shift in exemplary false colored images of HES2 mito-Grx1-roGFP2 cells at t = 0 s and t = 150 s upon oxidative (H_2O_2) and reductive (DTT) stimulation. Red: 400 nm excitation, green: 500 nm excitation, scale bars: 100 μm. **(E–H)** Change of roGFP2 fluorescence signal in HES2 Grx1-roGFP2 **(E,G)** and HES2 mito-Grx1-roGFP2 **(F,H)** as a function of time under oxidative (H_2O_2, E, F) and reductive (DTT, G, H) stimulation. H_2O_2 or DTT were added at 30 s. Grx1-roGFP2: n = 241 cells (300 μmol/L H_2O_2), n = 205 cells (100 μmol/L H_2O_2), n = 203 cells (10 μmol/L H_2O_2), n = 52 cells (1 μmol/L H_2O_2), n = 197 cells (10 mmol/L DTT), n = 264 cells (3 mmol/L DTT), n = 189 cells (1 mmol/L DTT), n = 58 cells (0.1 mmol/L DTT), n = 53 cells (0.01 mmol/L DTT); mito-Grx1-roGFP2: n = 182 cells (300 μmol/L H_2O_2), n = 301 cells (100 μmol/L H_2O_2), n = 305 cells (10 μmol/L H_2O_2), n = 57 cells (1 μmol/L H_2O_2), n = 193 cells (10 mmol/L DTT), n = 252 cells (3 mmol/L DTT), n = 274 cells (1 mmol/L DTT), n = 56 cells (0.1 mmol/L DTT), n = 57 cells (0.01 mmol/L DTT).

examine whether GSH/GSSG imaging is possible, we exposed lentivirally (lenti) transduced Grx1-roGFP2-hCM (**Figure 4C**) and Grx1-roGFP2-hFF (**Figure 4D**) to increasing concentrations of H_2O_2 (0.1–1,000 μmol/L) and DTT (0.01–1 mmol/L). Lenti-Grx1-roGFP2-hCM presented an all-or-nothing response at ≥ 10 μmol/L H_2O_2 with a maximal R/R_0 of 1.56 ± 0.04 at 100 μmol/L (n = 57; **Figure 4C**). In contrast, lenti-Grx1-roGFP2-hFF showed a concentration dependent increase of R/R_0 with maximal oxidation at 100 μmol/L H_2O_2 (1.78 ± 0.07, n = 41; **Figure 4D**). Maximal reduction was observed at 1 mmol/L DTT with a R/R_0 of 0.78 ± 0.01 (n = 58) and 0.36 ± 0.02 (n = 28) in lenti-Grx1-roGFP2-hCM (**Figure 4E**) and lenti-Grx1-roGFP2-hFF (**Figure 4F**), respectively. The estimated E_{GSH} was −289 ± 1 mV in Grx1-roGFP2-hCM and −269 ± 2 mV in Grx1-roGFP2-hFF ($p < 0.05$ by two-tailed, unpaired Student's t-test). As the reaction of hFF to oxidation or reduction appeared to be faster than in hCM, we quantified the time to half maximal ratio (t_{50}). In hCM, upon stimulation with 1,000 μmol/L H_2O_2, t_{50} was reached after 22 ± 2 ms (n = 39), while t_{50} in hFF was observed at 5 ± 0.3 ms (n = 41). Similarly, upon reduction with 1 mmol/L DTT, t_{50} was reached in 28 ± 1 ms in HFF (n = 28) and in 83 ± 3 ms in hCM (n = 58).

Redox Imaging in Engineered Human Myocardium

We finally tested whether lenti-Grx1-roGFP2-hCM and -hFF could be applied to perform cell-type specific in-tissue GSH/GSSG imaging in EHM. For this, we constructed EHM from defined mixtures of the Grx1-roGFP2-hCM (70%) and -hFF (30%) as recently described (**Figures 5A,B**; Tiburcy et al., 2017). To first test whether the Grx1-roGFP2 would disturb function, we performed force of contraction (FOC) analyses under isometric conditions and increasing calcium concentrations. These analyses confirmed that expression of the Grx1-roGFP2 reporter *per se* in differentiated hCM (**Figure 5C**) or hFF (**Figure 5D**) does not impair heart muscle function. We next tested whether cell type specific glutathione redox state can be imaged in EHM after exposure to maximally oxidizing concentrations of H_2O_2 (1 mmol/L) and maximally reducing concentrations of DTT (1 mmol/L). These experiments demonstrated a more pronounced fluorescence signal response to H_2O_2 and DTT in EHM comprised of lenti-Grx1-roGFP2-hCM and genetically naïve hFF (**Figure 5E**) compared to EHM comprised of genetically naïve hCM and lenti-Grx1-roGFP2-hFF (**Figure 5F**). This finding may be explained by the smaller cell body of hFF and the lower signal to noise (S/N) ratio in hFF-roGFP2 compared to the hCM-roGFP2. The E_{GSH} was −284 ± 4 mV for lenti-Grx-roGFP2-hCM containing EHM and −297 ± 34 mV for lenti-Grx-roGFP2-hFF containing EHM (n = 5 tissues/group).

DISCUSSION

Reactive oxygen species contribute to a variety of cardiac functions by their fundamental role in physiological signaling and pathological processes in the heart. The ROS production machinery and how ROS target individual proteins of the contractile machinery has been intensively investigated (Shao et al., 2012; Zhang et al., 2013; Bertero and Maack, 2018). However, knowledge on spatiotemporal activity of ROS in distinct cell species of the heart and their cellular compartments remains incomplete. Here we sought to develop a human heart muscle model for cell type-specific, in-tissue glutathione redox potential imaging via a recently developed protein sensor, namely Grx1-roGFP2 (Gutscher et al., 2008). We tested two different approaches for the generation of Grx1-roGFP2 expressing cardiomyocytes: (1) TALEN-mediated genome integration in human embryonic stem cells for subsequent cardiac differentiation and (2) lentiviral transduction of differentiated cardiomyocytes. Whilst TALEN-mediated integration of Grx1-roGFP2 for cytosolic and mitochondrial sensing of GSH/GSSG ratio was possible, we observed severely compromised sarcomerogenesis leading to contractile dysfunction in the two investigated Grx1-roGFP2 models. This may stem from the observed multiple random integrations, despite initially targeting the AAVS1 locus. However, the finding that sarcomerogenesis was similarly impaired in the Grx1- and mito-Grx1-roGFP2 lines, which exhibit different transgene integration sites, whilst lentiviral transduction of already differentiated cardiomyocytes was not toxic, argues for developmental toxicity of the roGFP2 reporter. One possible mechanism could be ROS buffering and thus impaired ROS signaling during early stages of cardiomyogenesis. Further investigations, including the screening for additional lines with random and AAVS1 targeted transgene integrations, will be required to clarify the underlying mechanism.

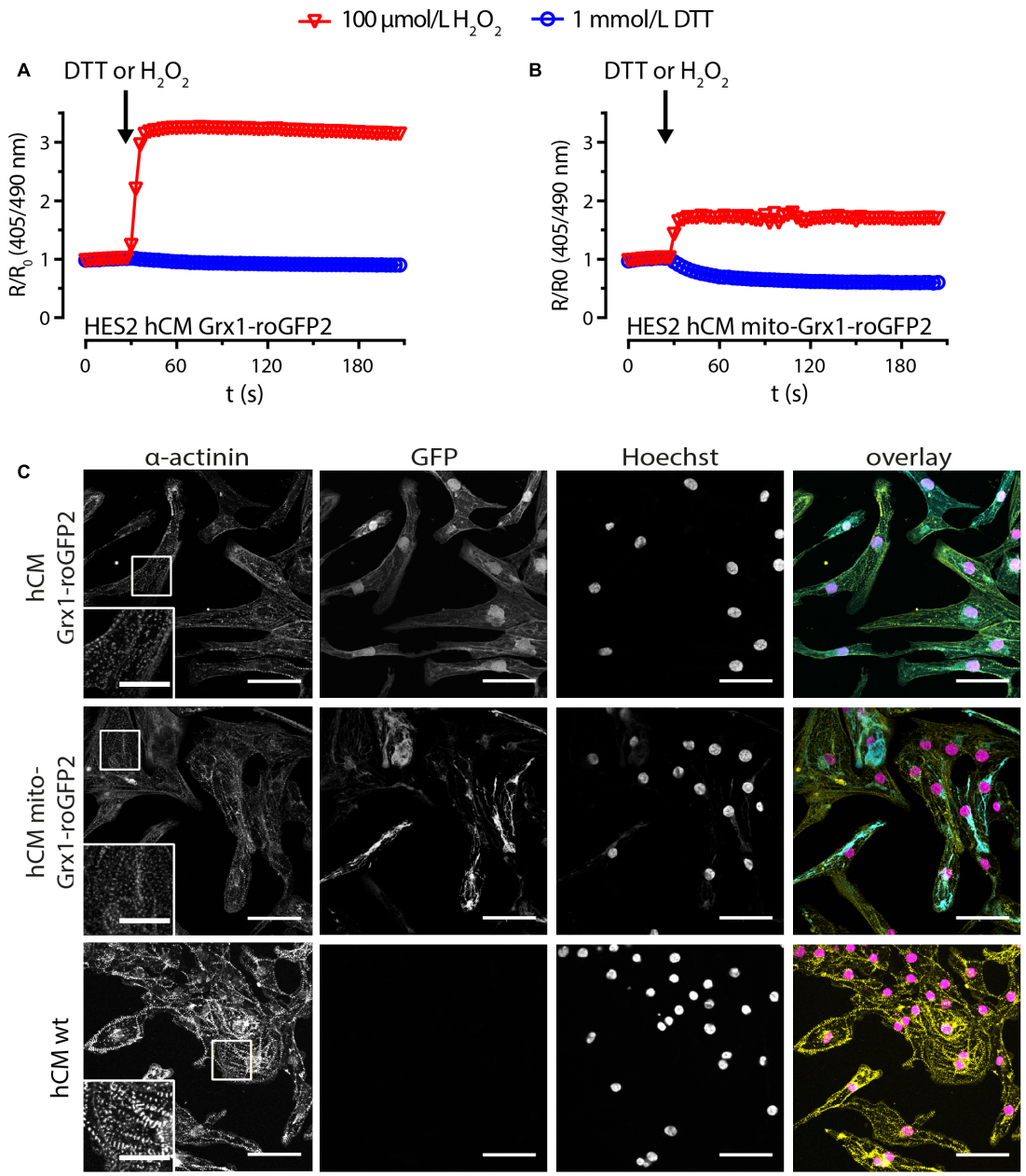

FIGURE 3 | HES-derived cardiomyocytes express functional roGFP2 sensors, but show an impaired sarcomere phenotype. Change of roGFP2 fluorescence signal in hCM from HES2 Grx1-roGFP2 **(A)** and HES2 mito-Grx1-roGFP2 **(B)** as a function of time under oxidative (H_2O_2) and reductive (DTT) stimulation. Grx1-roGFP2: n = 176 cells (100 µmol/L H_2O_2), n = 170 cells (1 mmol/L DTT), mito-Grx1-roGFP2: n = 325 cells (100 µmol/L H_2O_2), n = 325 cells (1 mmol/L DTT). **(C)** Immunofluorescence analysis after staining for α-actinin and DNA (Hoechst); GFP: roGFP2 reporter signal. Scale bars: 50 µm. Insets: magnifications of α-actinin labeled sarcomere structures, scale bars: 20 µm.

The finding of non-impaired cardiomyocyte function after lentiviral transduction is in line with the observation that transgenic mice with Grx1-roGFP2 expression under the control of the cardiomyocyte restricted MYH6-promotor do not show an obvious phenotype (Swain et al., 2016). With the transgenic expression of lenti-Grx1-roGFP2 in human cardiomyocytes and fibroblasts, it became feasible to construct engineered human myocardium (EHM) for in-tissue GSG/GSSG imaging. Importantly, the unimpaired contractile performance of EHM is a strong indicator for undisturbed sarcomerogenesis in EHM. This notion is supported by a number of studies showing the high sensitivity of the EHM model to pick up mechanisms underlying contractile dysfunction in patients with cardiomyopathy, such as in Duchenne Muscular Dystrophy (Long et al., 2018) and dilated cardiomyopathy (Streckfuss-Bömeke et al., 2017). The finding that Grx1-roGFP2 expressing fibroblasts in EHM do

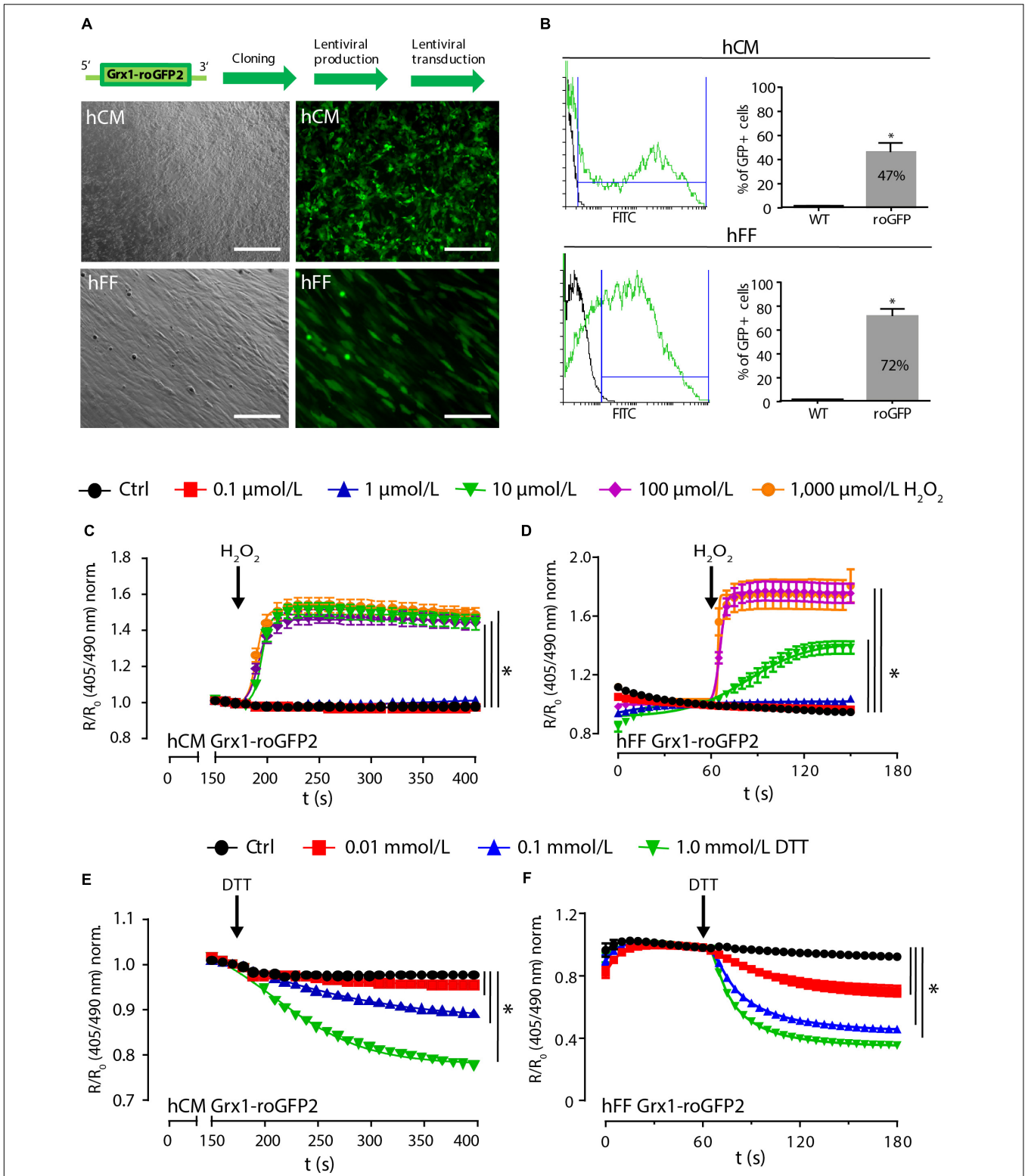

FIGURE 4 | Lentiviral expression of Grx1-roGFP2 reports redox changes in differentiated cardiomyocytes and fibroblasts. **(A)** Brightfield (left) and GFP fluorescence (right) images after lentiviral transduction of hCM and hFF; scale bars: 200 µm. **(B)** Flow cytometry analysis of transduction efficiency in hCM (47 ± 7%, $n = 7$) and hFF (72 ± 6%, $n = 8$); * $p < 0.05$, unpaired, two-tailed Student's t-test. Change of roGFP2 fluorescence signal in hCM **(C)** and hFF **(D)** as a function of time under oxidation by H_2O_2 at indicated concentrations ($n = 46$–71 [hCM]; $n = 19$–43 [hFF]). Change of roGFP2 fluorescence signal in hCM **(E)** and hFF **(F)** as a function of time under reduction by DTT at indicated concentrations ($n = 46$–85 [hCM]; $n = 21$–37 [hFF]).

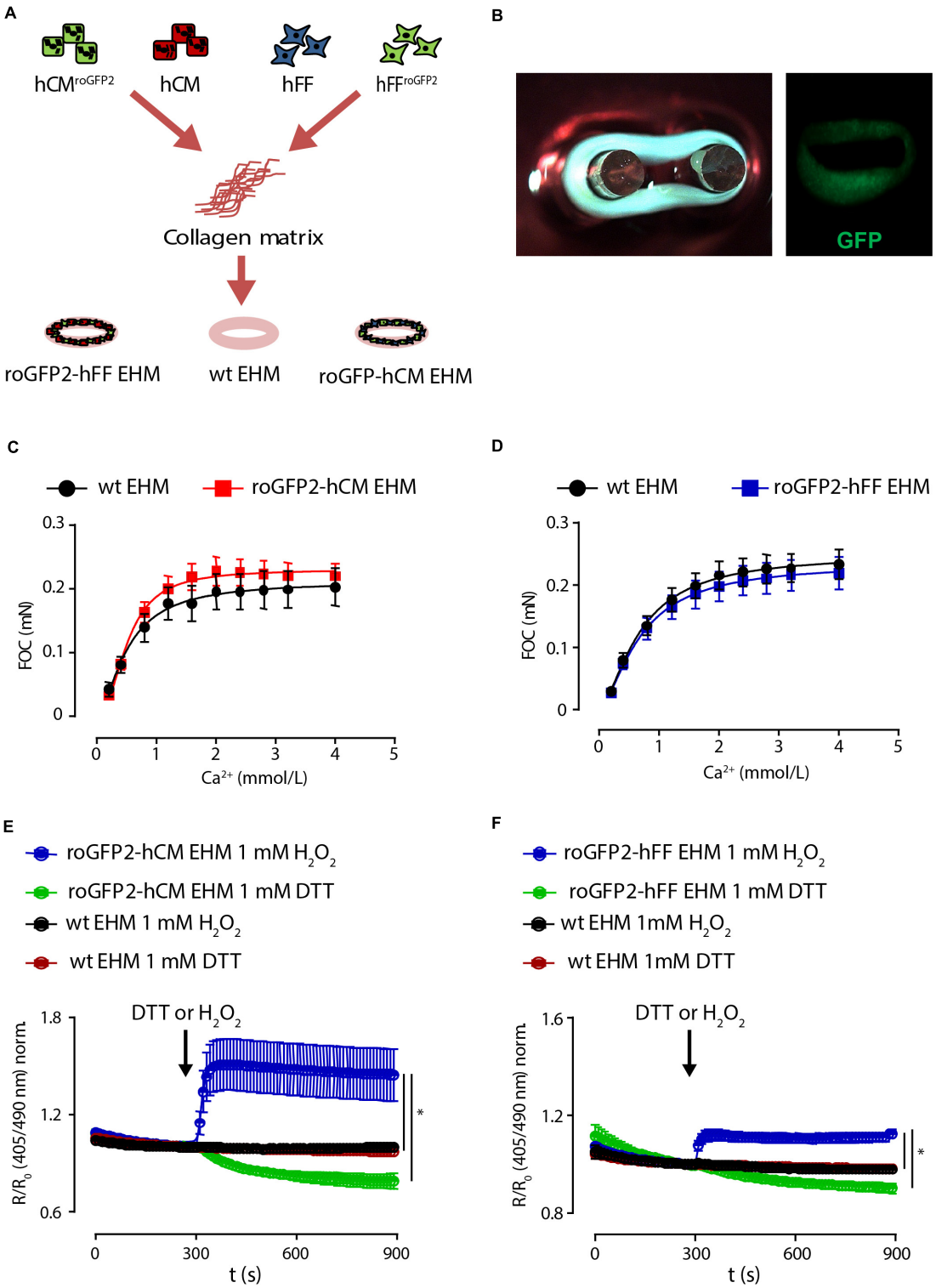

FIGURE 5 | Cell type specific imaging of Grx1-roGFP2 in EHM. **(A)** EHM were constructed from defined mixtures of genetically naïve and Grx1-roGFP2 expressing hCM or hFF in a collagen hydrogel to create tissue for cell type specific redox potential imaging. **(B)** Photograph and fluorescence image of EHM expressing Grx1-roGFP2 (GFP). Analysis of force of contraction (FOC) under isometric conditions and electrical field stimulation (1.5 Hz); maximal inotropic capacity was evaluated under increasing extracellular calcium concentrations: **(C)** EHM composed of Grx1-roGFP2 and genetically naïve (wt: wild type) hCM with genetically naïve hFF (n = 17/33); **(D)** EHM composed of Grx1-roGFP2 and genetically naïve (wt: wild type) hFF with genetically naïve hCM (n = 36/42). Change of roGFP2 fluorescence signal in EHM with Grx1-roGFP2 expressing hCM **(E)** and hFF **(F)** as a function of time under oxidation by H_2O_2 (1 mmol/L) and reduction by DTT (1 mmol/L).

not compromise its contractile function is another important observation, given the requirement for proper fibroblast function in *bona fide* and engineered cardiomyogenesis (Ieda et al., 2009; Tiburcy et al., 2017).

The differences in hCM-roGFP2 versus hFF-roGFP2 R/R_0 signal dynamic range in EHM (**Figures 5E,F**) may be explained by differences in cell composition (hCM > hFF) and cell volume (hCM > hFF) as well as differences in cell type-specific roGFP2 protein translation and redox state. Similarly, the smaller R/R_0 signal dynamic range of the hFF-roGFP2-EHM (**Figure 5F**) versus hFF-roGFP2-monolayer (**Figures 4D** and **F**) signal may stem from the smaller hFF cell body in EHM versus monolayer culture. The differences in hFF size are a reflection of differences in fibroblast biology in monolayer and EHM culture, with a dominant "stressed" myofibroblast phenotype in monolayer culture and a less "stressed" fibrocyte phenotype in EHM culture.

The determination of the maximal oxidative and reductive states in cells allows for the calculation of the glutathione redox potential (E_{GSH}; Meyer and Dick, 2010). Here, we identify apparent differences in E_{GSH} in cardiomyocytes and fibroblasts (-289 ± 1 mV vs. -269 ± 2 mV), supporting the notion that cell specific analyses will be key to understand the pathophysiological relevance of ROS. Interestingly, the cardiomyocyte and fibroblast E_{GSH} in EHM appeared to not differ, suggesting either a milieu effect or differences in E_{GSH} in the more matured cells in three-dimensional EHM versus monolayer cultures (Tiburcy et al., 2017).

By the use of the glutathione sensor (Grx1-roGFP2) we were naturally limited in our investigations to only one ROS-mechanism, namely glutathione oxidation/reduction. The use of additional ROS sensors as well as a combination of transgenic reporters and ROS-producing enzymes in a cell and compartment specific manner may be highly informative to decipher ROS signaling. In this context, we interpret our study as a first step toward this direction with proof-of-concept for the feasibility of in-human-heart-muscle GSH/GSSG imaging. Further studies will be required to make full use of the Grx1-roGFP2-reporter EHM model, which will include investigations of the consequences of specific pharmacological (e.g., simulated neurohumoral overstimulation), biophysical (e.g., controlled electromechanical stimulation), or disease (e.g., hypoxia or ischemia/reoxygenation) stimuli for the ROS-mediated control of heart muscle function.

DATA AVAILABILITY

All datasets generated for this study are included in the manuscript and/or the **Supplementary Files**.

AUTHOR CONTRIBUTIONS

IT, EH, PS, MM, and WHZ contributed to the conception and design of the study. IT, EH, and EL performed the experiments. VN, DMK, and IB supported the roGFP2 sensor imaging experiments. IT, EH, PS, and WHZ drafted the manuscript. All the authors contributed to manuscript revision, read, and approved the submitted version.

FUNDING

WHZ was supported by the DZHK (German Center for Cardiovascular Research) and the German Research Foundation (DFG: ZI 708/10-1, SFB 937 TP A18, SFB 1002 TP C04/S01, Fondation Leducq, and the MWK P2M program). WHZ, DMK, and IB were supported by DFG IRTG 1816. IB was supported by DFG SFB 1190.

ACKNOWLEDGMENTS

This work was part of the doctoral thesis of IT and EH within the GAUSS Molecular Medicine program and IRTG 1816 at the University Medical Center Göttingen.

SUPPLEMENTARY MATERIAL

The Supplementary Material for this article can be found online at: https://www.frontiersin.org/articles/10.3389/fphys.2019.00272/full#supplementary-material

REFERENCES

Acín-Pérez, R., Fernández-Silva, P., Peleato, M. L., Pérez-Martos, A., and Enriquez, J. A. (2008). Respiratory active mitochondrial supercomplexes. *Mol. Cell* 32, 529–539. doi: 10.1016/j.molcel.2008.10.021

Belousov, V. V., Fradkov, A. F., Lukyanov, K. A., Staroverov, D. B., Shakhbazov, K. S., Terskikh, A. V., et al. (2006). Genetically encoded fluorescent indicator for intracellular hydrogen peroxide. *Nat. Methods* 3, 281–286. doi: 10.1038/nmeth866

Bertero, E., and Maack, C. (2018). Calcium signaling and reactive oxygen species in mitochondria. *Circ. Res.* 122, 1460–1478. doi: 10.1161/CIRCRESAHA.118.310082

Burgoyne, J. R., Mongue-Din, H., Eaton, P., and Shah, A. M. (2012). Redox signaling in cardiac physiology and pathology. *Circ. Res.* 111, 1091–1106. doi: 10.1161/CIRCRESAHA.111.255216

Dey, S., DeMazumder, D., Sidor, A., Foster, D. B., and O'Rourke, B. (2018). Mitochondrial ROS drive sudden cardiac death and chronic proteome remodeling in heart failure. *Circ. Res.* 123, 356–371. doi: 10.1161/CIRCRESAHA.118.312708

Gibhardt, C. S., Zimmermann, K. M., Zhang, X., Belousov, V. V., and Bogeski, I. (2016). Imaging calcium and redox signals using genetically encoded fluorescent indicators. *Cell Calcium* 60, 55–64. doi: 10.1016/j.ceca.2016.04.008

Gutscher, M., Pauleau, A.-L., Marty, L., Brach, T., Wabnitz, G. H., Samstag, Y., et al. (2008). Real-time imaging of the intracellular glutathione redox potential. *Nat. Methods* 5, 553–559. doi: 10.1038/nmeth.1212

Gutscher, M., Sobotta, M. C., Wabnitz, G. H., Ballikaya, S., Meyer, A. J., Samstag, Y., et al. (2009). Proximity-based protein thiol oxidation by H2O2-scavenging peroxidases. *J. Biol. Chem.* 284, 31532–31540. doi: 10.1074/jbc.M109.059246

Ieda, M., Tsuchihashi, T., Ivey, K. N., Ross, R. S., Hong, T.-T., Shaw, R. M., et al. (2009). Cardiac fibroblasts regulate myocardial proliferation through beta1 integrin signaling. *Dev. Cell* 16, 233–244. doi: 10.1016/j.devcel.2008.12.007

Long, C., Li, H., Tiburcy, M., Rodriguez-Caycedo, C., Kyrychenko, V., Zhou, H., et al. (2018). Correction of diverse muscular dystrophy mutations in human engineered heart muscle by single-site genome editing. *Sci. Adv.* 4:eaa9004. doi: 10.1126/sciadv.aap9004

Meyer, A. J., and Dick, T. P. (2010). Fluorescent protein-based redox probes. *Antioxid. Redox Signal.* 13, 621–650. doi: 10.1089/ars.2009.2948

Morgan, B., Sobotta, M. C., and Dick, T. P. (2011). Measuring EGSH and H2O2 with roGFP2-based redox probes. *Free Radic. Biol. Med.* 51, 1943–1951. doi: 10.1016/j.freeradbiomed.2011.08.035

Morgan, B., Van Laer, K., Owusu, T. N. E., Ezeriņa, D., Pastor-Flores, D., Amponsah, P. S., et al. (2016). Real-time monitoring of basal H2O2 levels with peroxiredoxin-based probes. *Nat. Chem. Biol.* 12, 437–443. doi: 10.1038/nchembio.2067

Nabeebaccus, A. A., Zoccarato, A., Hafstad, A. D., Santos, C. X. C., Aasum, E., Brewer, A. C., et al. (2017). Nox4 reprograms cardiac substrate metabolism via protein O-GlcNAcylation to enhance stress adaptation. *JCI Insight* doi: 10.1172/jci.insight.96184 [Epub ahead of print].

Prosser, B. L., Ward, C. W., and Lederer, W. J. (2011). X-ROS signaling: rapid mechano-chemo transduction in heart. *Science* 333, 1440–1445. doi: 10.1126/science.1202768

Rezende, F., Brandes, R. P., and Schröder, K. (2018). Detection of hydrogen peroxide with fluorescent dyes. *Antioxid. Redox Signal.* 29, 585–602. doi: 10.1089/ars.2017.7401

Santos, C. X. C., Raza, S., and Shah, A. M. (2016). Redox signaling in the cardiomyocyte: from physiology to failure. *Int. J. Biochem. Cell Biol.* 74, 145–151. doi: 10.1016/j.biocel.2016.03.002

Scotcher, J., Prysyazhna, O., Boguslavskyi, A., Kistamas, K., Hadgraft, N., Martin, E. D., et al. (2016). Disulfide-activated protein kinase G Iα regulates cardiac diastolic relaxation and fine-tunes the frank–starling response. *Nat. Commun.* 7:13187. doi: 10.1038/ncomms13187

Shao, D., Oka, S., Brady, C. D., Haendeler, J., Eaton, P., and Sadoshima, J. (2012). Redox modification of cell signaling in the cardiovascular system. *J. Mol. Cell. Cardiol.* 52, 550–558. doi: 10.1016/j.yjmcc.2011.09.009

Sies, H., Berndt, C., and Jones, D. P. (2017). Oxidative stress. *Annu. Rev. Biochem.* 86, 715–748. doi: 10.1146/annurev-biochem-061516-045037

Steinhorn, B., Sartoretto, J. L., Sorrentino, A., Romero, N., Kalwa, H., Abel, E. D., et al. (2017). Insulin-dependent metabolic and inotropic responses in the heart are modulated by hydrogen peroxide from NADPH-oxidase isoforms NOX2 and NOX4. *Free Radic. Biol. Med.* 113, 16–25. doi: 10.1016/j.freeradbiomed.2017.09.006

Stone, J. R., and Yang, S. (2006). Hydrogen peroxide: a signaling messenger. *Antioxid. Redox Signal.* 8, 243–270. doi: 10.1089/ars.2006.8.243

Streckfuss-Bömeke, K., Tiburcy, M., Fomin, A., Luo, X., Li, W., Fischer, C., et al. (2017). Severe DCM phenotype of patient harboring RBM20 mutation S635A can be modeled by patient-specific induced pluripotent stem cell-derived cardiomyocytes. *J. Mol. Cell. Cardiol.* 113, 9–21. doi: 10.1016/j.yjmcc.2017.09.008

Swain, L., Kesemeyer, A., Meyer-Roxlau, S., Vettel, C., Zieseniss, A., Güntsch, A., et al. (2016). Redox imaging using cardiac myocyte specific transgenic biosensor mice. *Circ. Res.* 119, 1004–1016. doi: 10.1161/CIRCRESAHA.116.309551

Tiburcy, M., Hudson, J. E., Balfanz, P., Schlick, S., Meyer, T., Liao, M.-L. C., et al. (2017). Defined engineered human myocardium with advanced maturation for applications in heart failure modeling and repair. *Circulation* 135, 1832–1847. doi: 10.1161/CIRCULATIONAHA.116.024145

Zhang, M., Perino, A., Ghigo, A., Hirsch, E., and Shah, A. M. (2013). NADPH oxidases in heart failure: poachers or gamekeepers? *Antioxid. Redox Signal.* 18, 1024–1041. doi: 10.1089/ars.2012.4550

Conflict of Interest Statement: The authors declare that the research was conducted in the absence of any commercial or financial relationships that could be construed as a potential conflict of interest.

frontiers in Physiology

ORIGINAL RESEARCH
published: 05 March 2019
doi: 10.3389/fphys.2019.00168

Adeno-Associated Virus Mediated Gene Delivery: Implications for Scalable *in vitro* and *in vivo* Cardiac Optogenetic Models

*Christina M. Ambrosi[1,2], Gouri Sadananda[1], Julie L. Han[2] and Emilia Entcheva[1,2]**

[1] Department of Biomedical Engineering, Stony Brook University, Stony Brook, NY, United States, [2] Department of Biomedical Engineering, George Washington University, Washington, DC, United States

Adeno-associated viruses (AAVs) provide advantages in long-term, cardiac-specific gene expression. However, AAV serotype specificity data is lacking in experimental models relevant to cardiac electrophysiology and cardiac optogenetics. We aimed to identify the optimal AAV serotype (1, 6, or 9) in pursuit of scalable rodent and human models using genetic modifications in cardiac electrophysiology and optogenetics, in particular, as well as to elucidate the mechanism of virus uptake. *In vitro* syncytia of primary neonatal rat ventricular cardiomyocytes (NRVMs) and human induced pluripotent stem cell-derived cardiomyocytes (hiPSC-CMs) were infected with AAVs 1, 6, and 9 containing the transgene for eGFP or channelrhodopsin-2 (ChR2) fused to mCherry. *In vivo* adult rats were intravenously injected with AAV1 and 9 containing ChR2-mCherry. Transgene expression profiles of rat and human cells *in vitro* revealed that AAV1 and 6 significantly outperformed AAV9. In contrast, systemic delivery of AAV9 in adult rat hearts yielded significantly higher levels of ChR2-mCherry expression and optogenetic responsiveness. We tracked the mechanism of virus uptake to purported receptor-mediators for AAV1/6 (cell surface sialic acid) and AAV9 (37/67 kDa laminin receptor, LamR). *In vitro* desialylation of NRVMs and hiPSC-CMs with neuraminidase (NM) significantly decreased AAV1,6-mediated gene expression, but interestingly, desialylation of hiPSC-CMs increased AAV9-mediated expression. In fact, only very high viral doses of AAV9-ChR2-mCherry, combined with NM treatment, yielded consistent optogenetic responsiveness in hiPSC-CMs. Differences between the *in vitro* and *in vivo* performance of AAV9 could be correlated to robust LamR expression in the intact heart (neonatal rat hearts as well as adult human and rat hearts), but no expression *in vitro* in cultured cells (primary rat cells and hiPS-CMs). The dynamic nature of LamR expression and its dependence on environmental factors was further corroborated in intact adult human ventricular tissue. The combined transgene expression and cell surface receptor data may explain the preferential efficiency of AAV1/6 *in vitro* and AAV9 *in vivo* for cardiac delivery and mechanistic knowledge of their action can help guide cardiac optogenetic

OPEN ACCESS

Edited by:
Ming Lei,
University of Oxford, United Kingdom

Reviewed by:
Teun P. de Boer,
Utrecht University, Netherlands
Xiaoqiang Tang,
Sichuan University, China

***Correspondence:**
Emilia Entcheva
entcheva@gwu.edu

Specialty section:
This article was submitted to Cardiac Electrophysiology, a section of the journal Frontiers in Physiology

Received: *30 October 2018*
Accepted: *12 February 2019*
Published: *05 March 2019*

Citation:
Ambrosi CM, Sadananda G, Han JL and Entcheva E (2019) Adeno-Associated Virus Mediated Gene Delivery: Implications for Scalable in vitro and in vivo Cardiac Optogenetic Models. Front. Physiol. 10:168. doi: 10.3389/fphys.2019.00168

efforts. More broadly, these findings are relevant to future efforts in gene therapy for cardiac electrophysiology abnormalities *in vivo* as well as for genetic modifications of cardiomyocytes by viral means *in vitro* applications such as disease modeling or high-throughput drug testing.

Keywords: AAV, cardiac optogenetics, channelrhodopsin-2, LamR, sialic acid, iPS-CM, rat heart, gene therapy

INTRODUCTION

The use of adeno-associated viruses (AAVs) as transgene delivery vehicles in disease treatment requires comprehensive assessments of their performance and safety profiles. Advantages of AAVs include long-term expression, tissue tropism from 13 serotypes, and the ability to transduce both dividing and non-dividing cells (Aikawa et al., 2002; Muller et al., 2006; Williams et al., 2010; Srivastava, 2016). Recent clinical trials have explored the use of AAVs in the treatment of electromechanical consequences of heart failure, specifically in the upregulation of SERCA2a, a Ca^{2+} ATPase, known to be downregulated during the progression of the disease (CUPID; Jessup et al., 2011). Although a recent CUPID phase IIb trial concluded that the delivery of SERCA2a by AAV serotype 1 did not improve symptoms of heart failure in patients, no safety issues or adverse effects were observed (Greenberg et al., 2016). As of June 2017, there have been 183 clinical trials in humans using AAV[1].

Concurrent to the exploration of AAV use in clinical trials, optogenetics has been rapidly developing as a promising tool in cardiac electrophysiology research (reviewed in Entcheva, 2013; Ambrosi et al., 2014; Montgomery et al., 2016; Pianca et al., 2017). Optogenetics relies on the genetic modification of cells and tissues to induce the expression of light-sensitive opsins for precise bi-directional control of activity. The technique allows for functional manipulation of target cells/tissues with high specificity through genetic modification, in addition to the superior spatiotemporal resolution afforded by optical means (Ambrosi et al., 2014). Consequently, the field of optogenetics requires highly efficient transgene delivery vehicles for cardiac applications. Such virally mediated optogenetic manipulations are "scalable" as they permit the parallel investigation of many cells *in vitro* for high-throughput all-optical cardiac electrophysiology (Dempsey et al., 2016; Klimas et al., 2016) and allow cardiac applications *in vivo* across different animal species, beyond the usual mouse transgenic models.

In this study, we investigated the efficiency and mechanisms of infection of three select AAV serotypes (1, 6, and 9) with known affinity for cardiac tissue in pursuit of scalable *in vitro* and *in vivo* models for cardiac optogenetics. Our study was motivated by the inconsistency of available data and study design evaluating serotype specificity in various animal models (see **Supplementary Table S1** for a brief literature review). For instance, AAV9 has been shown to have highly efficient transgene delivery to the heart in the mouse and rat in a variety of studies (Inagaki et al., 2006; Pacak et al., 2006; Bish et al., 2008; Zincarelli et al., 2008); however, AAV1 and AAV6 are identified as superior for the heart in other studies (Kawamoto et al., 2005; Wang et al., 2005; Muller et al., 2006; Seiler et al., 2006; Palomeque et al., 2007; Zincarelli et al., 2008; Zhu et al., 2012; Kuken et al., 2015). In addition, developmental serotype specificity (i.e., preferential transgene expression in neonates versus adults) has also been suggested in studies involving dogs (Yue et al., 2008) and rhesus macaques (Pacak et al., 2006). A more recent work identified AAV6 as an efficient serotype for the infection of stem-cell derived cardiomyocytes (Rapti et al., 2015). Clinically and *in vivo*, AAV-mediated gene delivery is the approach of choice, including for expression of optogenetic tools. While a number of suitable options exist for gene delivery *in vitro* other than AAV-mediated gene transfer, there is often convenience in being able to utilize the same vectors for both studies *in vitro* and *in vivo*.

We used several experimental platforms relevant to the development of viral models for cardiac optogenetics. *In vitro* we assessed serotype performance in commonly used multicellular models of cardiac tissue – neonatal rat ventricular cardiomyocytes (NRVMs) and human induced pluripotent stem cell-derived cardiomyocytes (hiPSC-CM; Klimas et al., 2016). Adult rats were also systemically infected with AAVs as their larger size compared to mice allows for *in vivo* manipulations for cardiac research, including the insertion and implantation of fiber-based devices for long-term cardiac recording and stimulation (Klimas and Entcheva, 2014).

MATERIALS AND METHODS

Procedures involving animals were performed in accordance with institutional guidelines at both Stony Brook University (SBU) and George Washington (GW) University and conform to NIH guidelines for the care and use of laboratory animals. The reported experiments were prospectively approved by the GW Animal Care and Use Committee (IACUC) under numbers #A335 (for the neonatal rat culture) and #A339 (for the adult rat experiments).

Human heart tissue for protein analysis was procured through the Washington Regional Transplant Community (WRTC) program in Washington, DC, United States, and was provided to GW after de-identification by the procurement company.

Further details of the methods are provided in the **Supplementary Material**.

In vitro

Cardiomyocyte Preparation

Neonatal rat ventricular cardiomyocytes were isolated using a previously published technique (Jia et al., 2011; Ambrosi et al., 2015). In short, cardiomyocytes from the ventricles

[1]www.abedia.com/wiley

of 2–3 day old Sprague–Dawley rats were enzymatically isolated with trypsin (USB, Cleveland, OH, United States) and collagenase (Worthington Biochemical Corporation, Lakewood, NJ, United States) and the presence of fibroblasts was minimized by pre-plating.

Frozen hiPSC-CMs (iCell Cardiomyocytes^2; Cellular Dynamics, Madison, WI, United States) were thawed according to the manufacturer's instructions. Cells were plated on fibronectin-coated (50 μg/mL; Fisher Scientific) glass-bottomed 96-well plates at a density of 156,000 cells/cm^2.

Infection With AAV Serotypes and Ad-hChR2(H134R)-eYFP

Viral particles for pseudotyped AAV serotypes 1, 6, and 9 containing the transgene for eGFP were obtained from the University of Pennsylvania Vector Core (Philadelphia, PA, United States) or UPenn Core – AAV1/6/9.CB7.CI.eGFP.WPRE.rBG). The adenovirus (AdV) containing the transgene for channelrhodopsin2 fused to the reporter eYFP [Ad-CMV-hChR2(H134R)-eYFP] was prepared at the SBU Stem Cell Facility and characterized previously (Ambrosi and Entcheva, 2014).

Viral infection of NRVMs was completed in suspension immediately after cell isolation as described previously (Ambrosi and Entcheva, 2014). NRVMs were exposed to viral doses ranging in multiplicity of infection (MOI) from 100 to 2000 for AAV and 25 for AdV. Cells were plated on fibronectin-coated (50 μg/mL) glass-bottomed 96-well plates at a density of 400,000 cells/cm^2.

hiPSC-CMs were infected after 5 days of culture once confluent monolayers had formed. Cells were exposed to viral doses ranging in MOI from 100 to 100,000 for AAV and 250 for AdV for a total of 2 h at 37°C.

Desialylation Treatment

To investigate the role of cell surface N-linked sialic acid in AAV infection, NRVMs and hiPSC-CMs were pre-treated with neuraminidase (NM; Type III, from *Vibrio cholera*; 25, 250, and 500 mU/mL; Sigma-Aldrich, St. Louis, MO, United States) for 2 h at 37°C prior to exposure to AAV particles as described above. NM, a broad-spectrum sialidase, has been shown to significantly reduce cell surface sialic acid and directly impact infectivity by AAVs 1 and 6 in a variety of other non-cardiac cell types (Wu et al., 2006).

TGF-β1 Treatment

To investigate the role of the 37/67 kDa laminin cell surface receptor in AAV9 infection, hiPSC-CMs were treated with recombinant human transforming growth factor-β1 (10 ng/mL; EMD Millipore) for 24 h at 37°C prior to infection. An existing report has shown upregulated LamR protein expression in cardiomyocytes upon TGF-β1 treatment (Wenzel et al., 2010).

Localization and Quantification of AAV Infection by eGFP

Monolayers were fixed with 3.7% formaldehyde 5 days after AAV infection. Cells were stained with DAPI (Fisher Scientific) and imaged using either an Olympus Fluoview FV1000 confocal system (for NRVMs) or a Nikon Eclipse TE2000U fluorescent system (for hiPSC-CMs) to quantify transgene (eGFP) expression.

Immunohistochemistry

Monolayers were permeabilized with 0.2% Triton-X 100 (Fisher Scientific) and stained with antibodies either for sarcomeric α-actinin (Sigma–Aldrich, St. Louis, MO, United States) or the 37/67 kDa laminin receptor (LamR) (Abcam, Cambridge, MA, United States). Secondary antibodies were conjugated to either AlexaFluor 488 or AlexaFluor 647 (Invitrogen).

Western Blots of LamR

Protein was extracted from adult human hearts available through the transplant program (ventricular portion of a middle-aged male and a middle-aged female patient's hearts) and from human iPS-CMs (cultured for 7 days).

The antibody for the 37/67 kDa LamR receptor from Abcam was used in tandem with a fluorescent secondary antibody from Invitrogen to run the Western blots using protein collected from the cells and tissue samples. GAPDH antibody labeling (Abcam) was used as a normalization protein band, and ImageJ was used for quantification.

Optogenetic Control of the Engineered Cardiac Syncytium

Cell monolayers infected with Ad-CMV-hChR2(H134R)-eYFP (MOIs 25 and 250, respectively) or AAV9.CAG.hChR2(H134R)-mCherry.WPRE.SV40 (MOI 50,000–100,000 ± 500 mU/mL NM) were stained with the calcium- and voltage-sensitive dyes and optically mapped using our recently published all-optical, high-throughput system for dynamic cardiac electrophysiology, termed OptoDyCE (Klimas et al., 2016, 2018). The excitation filter for the actuating LED was 470/28 nm, the LED illumination for the voltage (di-4-ANBDQBS or Berst1) and calcium (Rhod-4AM) measurements was filtered as follows: 655/40 nm and 535/50, respectively. Fluorescence was collected by iXon Ultra 897 EMCCD; Andor, after passing through the emission filter 595/40 nm+700LP. Note that the UPenn Core considers the CAG and the CB7 promoters equivalent and uses them interchangeably; both are ubiquitous promoters, derivatives of CMV (Miyazaki et al., 1989).

In vivo

Systemic Infection With AAV Serotypes

Adult male Sprague–Dawley rats (n = 4, 7–8 weeks old) were systemically injected with 0.5×10^{12} pseudotyped viral particles of serotypes 1 and 9 obtained from the UPenn Core – AAV1/9.CAG.hChR2(H134R)-mCherry.WPRE.SV40. The weight of the rats at the time of injection was between 220 and 250 g, therefore, the viral delivery was about 2.14×10^{12} vp/kg.

Localization and Quantification of AAV Infection by mCherry

Rats were anesthetized with a ketamine (75–95 mg/kg)/xylazine (5 mg/kg) cocktail and maintained on 1.5% isoflurane while a variety of tissues (including the heart, brain, liver, and kidney)

were excised 4 weeks after viral injection. The tissues were fixed in 3.7% formaldehyde and imaged both macroscopically (IVIS Lumina Series III, PerkinElmer) and microscopically (Olympus Fluoview FV1000) for the presence of mCherry indicating successful transgene delivery.

Immunohistochemistry for LamR

Neonatal (2–3 days old, $n = 2$) and adult (11–12 weeks old, $n = 2$) rat hearts were fixed in 3.7% formaldehyde and embedded in paraffin. Tissue sections were stained with the polyclonal rabbit antibody for the 37/67 kDa LamR (Abcam, Cambridge, MA, United States) followed by a biotinylated anti-rabbit secondary antibody (Vector Laboratories, Burlingame, CA, United States). Breast carcinoma sections were used as a positive control.

Optogenetic Control of the Heart in the Open Chest

Functional assessment of transgene expression was tested by applying an epicardial S1 pacing protocol *in situ* in the open chest. Briefly, the rat was anesthetized with a ketamine (75–95 mg/kg)/xylazine (5 mg/kg) cocktail, intubated, and maintained on 1.5% isoflurane supplemented with oxygen throughout the procedure. The heart was exposed via a median sternotomy and optical stimulation was delivered with a fiber optics-coupled diode-pumped solid-state laser (470 nm; Shanghai Laser, Shanghai, China) directed on the left ventricular free wall. An ECG (Simple Scope, 2000; UFI, Morro Bay, CA, United States) was continuously recorded as the optical energy was increased in order to achieve 100% capture in the heart.

The heart, brain, liver, and kidney were excised from the animal and fixed in 3.7% formaldehyde. Fluorescent macroscopic and microscopic imaging for mCherry was then completed as described above.

Statistics

All data are shown as the mean ± standard error of the mean (SEM). Statistically significant differences were identified using ANOVA followed by Tukey–Kramer's test with a significance level of $p < 0.05$.

RESULTS

AAV6 Outperforms AAV1 and AAV9 *in vitro*

Recent applications of cardiac optogenetics *in vitro*, illustrating increased-throughput electrophysiology, require the use of viral vectors to deliver genetically encoded optical sensors or actuators (Leyton-Mange et al., 2014; Zhuge et al., 2014; Dempsey et al., 2016; Klimas et al., 2016). While typically AdV or lentiviral (LV) delivery has been employed in such applications, there is also interest in assessing the potential utilization of AAV vectors developed for *in vivo* applications as very few studies have been conducted in this area (Rapti et al., 2015). To systematically quantify serotype-specific and dose-dependent AAV infection, NRVMs and hiPSC-CMs were infected with AAVs 1, 6, and 9 containing the transgene for eGFP (**Figure 1**). Transgene expression was cardiomyocyte-specific, as eGFP was consistently co-localized in the same cells with positive immunostaining for α-actinin (**Figure 1A**). Although we employed strategies in the isolation of the NRVMs to reduce the presence of fibroblasts, a small number of fibroblasts are co-cultured with the cardiomyocytes, as can be seen in the non-eGFP/α-actinin-positive areas of **Figure 1A**. The hiPSC-CMs are, however, a purified population of cardiomyocytes and we have not observed any fibroblasts during culture.

AAV1- and AAV6-mediated eGFP expression was dose (MOI)-dependent in both NRVMs and hiPSC-CMs (**Figures 1B–E**). Quantification of the AAV-mediated dose-dependency of expression showed that infection by AAV6 resulted in significantly higher transgene expression at all MOIs for NRVMs and MOIs greater than 10,000 for hiPSC-CMs. Transgene expression due to AAV1 infection was also observed, but at significantly lower levels than AAV6-mediated expression. AAV9-mediated eGFP expression was not detected at these viral doses in either cell type (**Figure 1F**). It should also be noted that hiPSC-CMs require viral doses two orders of magnitude greater than NRVMs (MOI 10,000 versus 100) to show baseline eGFP expression.

Viral doses greater than those shown in **Figure 1** resulted in significant cell death within the monolayers. **Supplementary Figure S1** shows representative images of propidium iodide uptake (as a marker of dead cells) in NRVMs as a function of MOI. We quantified no significant differences in cell death across MOIs and serotypes; however, there is a trend toward increasing cell death with AAV1 infection at MOI 2000 (**Supplementary Figure S1D**).

AAV9 Outperforms AAV1 *in vivo*

A prior report on cardiac optogenetics, involving systemic delivery of AAV9 encoding for the channelrhodopsin-2 (ChR2) transgene, showed robust and long-lasting expression and functionality in mice (Vogt et al., 2015). However, except for a recent brief report (Nyns et al., 2016), to date this minimally invasive transduction approach has not been extended to larger animals, which may be more suitable for the study of cardiac arrhythmias due to size and ease of endoscopic access (Klimas and Entcheva, 2014). Here, systemic delivery of viral particles in the adult rat was employed through the lateral tail vein to assess the *in vivo* specificity of AAVs 1 and 9 (**Figure 2**). Unfortunately, the UPenn core does not offer AAV6 with ChR2, hence that serotype was not tested *in vivo* here. Four weeks after viral injection, excised hearts, brains, livers, and kidneys were assessed macroscopically for mCherry fluorescence (**Figure 2A**). AAV9-mediated infection resulted in global ventricular mCherry expression, while AAV1-mediated infection resulted in no cardiac transgene expression (with fluorescence comparable to sham viral injections) at a dose of 0.5×10^{12} viral particles per rat (equivalent to about 2.14×10^{12} vp/kg). Other excised organs (brain, liver, and kidney) showed little to no signs of AAV-mediated infection in all animals.

In rats infected with AAV9, mCherry expression in cardiomyocytes was robust and, not only expressed from apex to base as was observed with the macroscopic fluorescent imaging, but also expressed from the epicardium to the

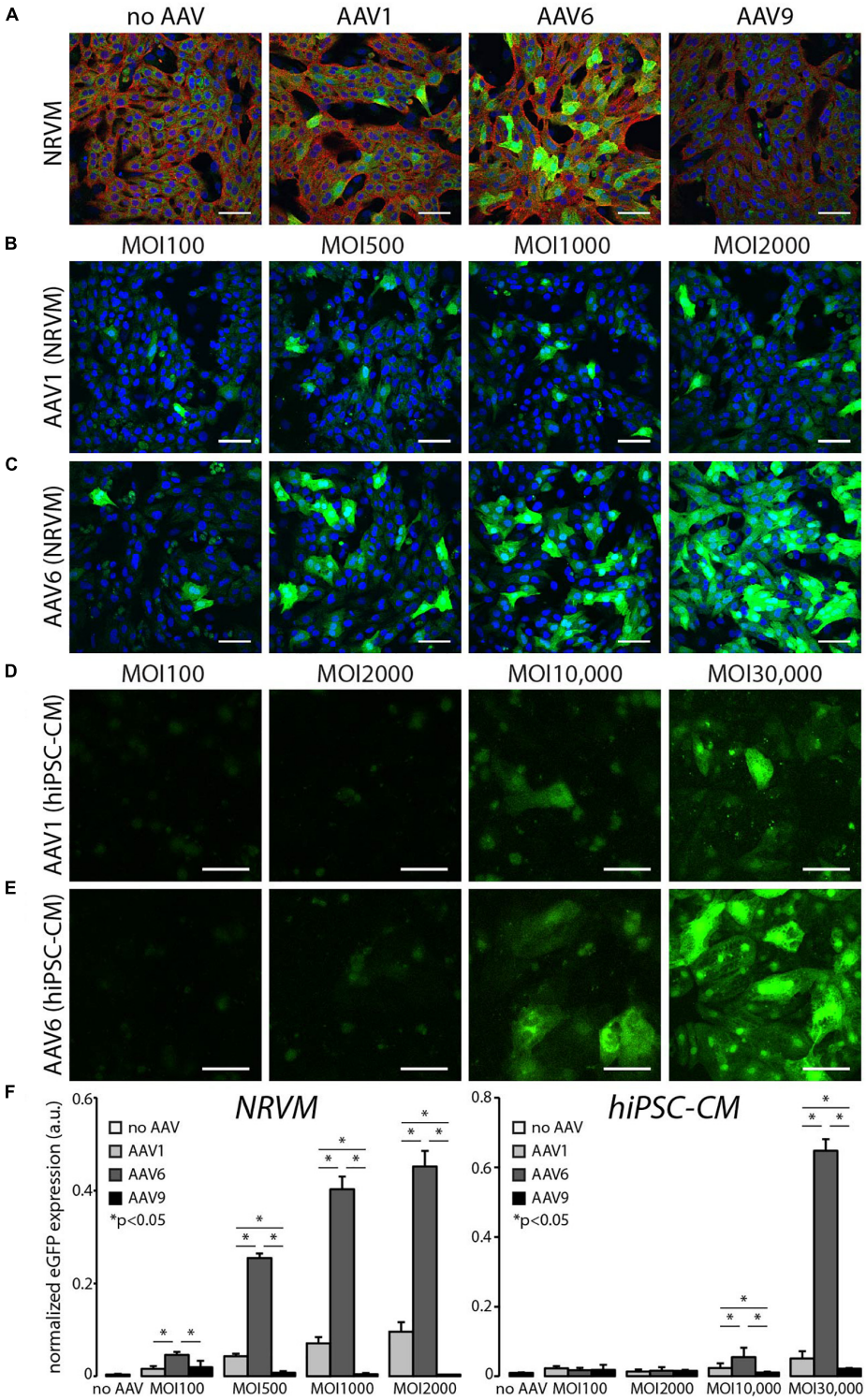

FIGURE 1 | *In vitro* AAV6-mediated transgene expression is superior to the use of AAV1 and AAV9 in rat and human cardiomyocytes. **(A)** Cardiomyocyte-specific eGFP expression in NRVMs and hiPSC-CMs using AAV1, 6, and 9. AAV9-mediated expression did not exhibit levels of fluorescence above that of autofluorescence in non-infected control cells. Cell nuclei were labeled with DAPI (blue, NRVMS only), AAV-infected cells expressed eGFP (green), and cardiomyocytes were labeled with α-actinin (red); MOI 1000. **(B,D)** AAV1-mediated and **(C,E)** AAV6-mediated eGFP expression at four viral doses 5 days post-infection. hiPSC-CMs required viral doses two orders of magnitude greater than NRVMs (MOI 10,000 versus MOI 100) to show threshold eGFP expression. All scale bars are 50 μm and color-enhanced images are shown. **(F)** Quantification of the dose-dependent increase in eGFP expression in NRVMs and hiPSC-CMs. AAV6-mediated eGFP expression was significantly higher than AAV1-mediated expression at all viral doses. Data are presented as mean ± SEM (n = 3–7 independent samples per group). *Significance level at $p < 0.05$.

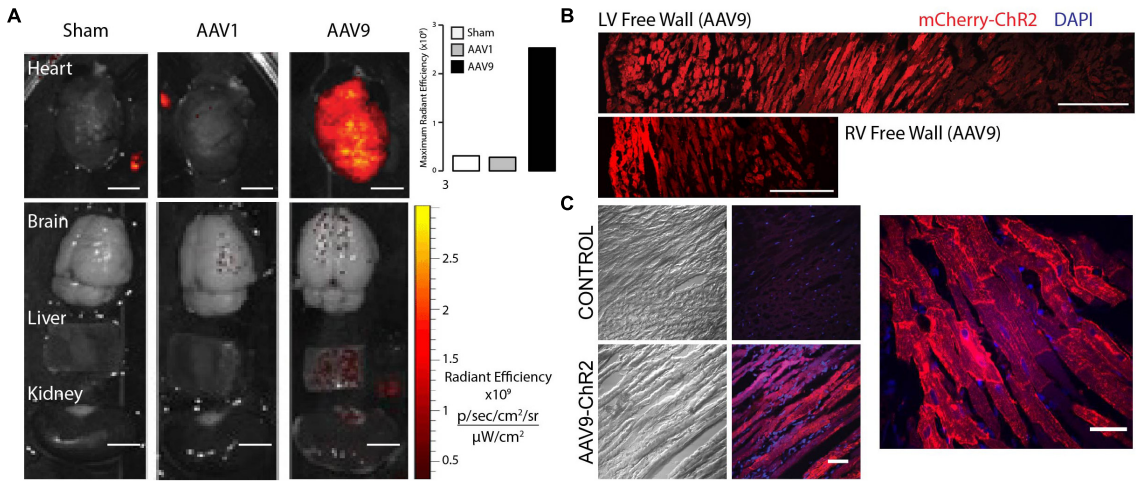

FIGURE 2 | *In vivo* AAV9-mediated mCherry expression in the adult rat heart provides robust, predominantly cardiomyocyte-specific transgene delivery. **(A)** Systemic delivery of 0.5×10^{12} viral particles resulted in robust cardiac-specific expression of mCherry in 4 weeks using AAV9, but not AAV1 as measured using radiant efficiency. Other major organs (including brain, liver, and kidney) showed little to no signs of AAV-mediated infection. Scale bars are 500 µm. **(B)** AAV9-mediated transgene delivery resulted in transmural ChR2-mCherry expression in both the LV and RV free walls. Scale bars are 250 µm. **(C)** High-resolution images (brightfield and fluorescence) show cardiomyocyte-specific ChR2-mCherry expression using AAV9-mediated delivery. Scale bars are 50 µm.

endocardium in both the left ventricular and right ventricular free walls (**Figure 2B**). Higher resolution microscopic imaging of AAV9-infected and sham hearts confirmed that observed fluorescence was not due to tissue auto-fluorescence and was localized to myocytes (**Figure 2C**).

AAV Serotype Infection Is Mediated by Different Receptors on the Cardiomyocyte Surface

Previous studies have shown that infection by different AAV serotypes is mediated by a variety of cell surface receptors (for review, see Vance et al., 2015). Specifically, cell surface N-linked sialic acid has been proposed as the primary receptor for AAV1 and AAV6 to infect and transduce cells (Wu et al., 2006). There are at least two mechanisms of AAV9-mediated cell infection/transduction involving two different receptors: terminal galactose on cell surface glycoproteins (Shen et al., 2011) (that can be made available for AAV9 entry upon desialylation) and the 37/67 kDa LamR (Akache et al., 2006). **Figure 3** provides a visual overview of the mechanisms of infectivity of cardiomyocytes we investigated in this study.

In order to probe the mechanisms of our differential observations of AAV serotype specificity *in vitro* (**Figure 1**) and *in vivo* (**Figure 2**), we explored the roles of both sialic acid and LamR in AAV-mediated transgene expression in cardiomyocytes. As indicated in **Figure 3A** by the arrow, we hypothesized that the removal of sialic acid by NM would block AAV1- and AAV6-mediated infection of cells. On the other hand, the same removal of sialic acid would also free up terminal galactose on the cell surface thus enhancing AAV9-mediated infection (**Figure 3B**, left panel). Similarly, AAV9 infection would be enhanced by the presence of LamR on the cell surface (**Figure 3B**, right panel).

In vitro Desialylation Modulates AAV-Mediated Gene Expression

Treatment of both NRVMs and hiPSC-CMs with NM, a broad spectrum sialidase, to remove cell surface sialic acid significantly reduced eGFP expression via AAV1 and AAV6 (**Figure 4**). In NRVMs, AAV1-mediated eGFP expression was completely abolished by 25 mU/mL NM, whereas AAV6-mediated expression was reduced to the point where only a few individual cells were eGFP-positive (**Figures 4A,B**). AAV9-mediated eGFP expression was unaffected in NRVMs as we did not observe the purported enhanced entry of AAV9 (**Figure 3B**) even at higher NM doses.

The same dose of NM in hiPSC-CMs never completely eliminated transgene expression, but AAV1 and AAV6-mediated infection was significantly reduced (**Figures 4C,D**), similar to the effect observed in NRVMs and in line with the predictions from **Figure 3A**. Interestingly, the application of NM to hiPSC-CMs in combination with AAV9 infection significantly increased transgene expression (**Figures 4C,D**). The additional application of 20× our standard NM dose (500 mU/mL), resulted in a further increase in AAV9-mediated gene expression, beyond that of AAV1-mediated expression without NM (**Figure 4D**), presumably by exposing terminal cell surface galactose for infection by AAV9, as illustrated in **Figure 3B**, and in contrast to our findings in NRVM.

Expression of the 37/67 kDa Laminin Receptor (LamR) in the Intact Heart: Adult and Neonatal Rat Hearts and Adult Human Hearts

The observed discrepancies in AAV serotype-mediated transgene expression *in vitro* (where AAV6 was most efficient) and *in vivo*

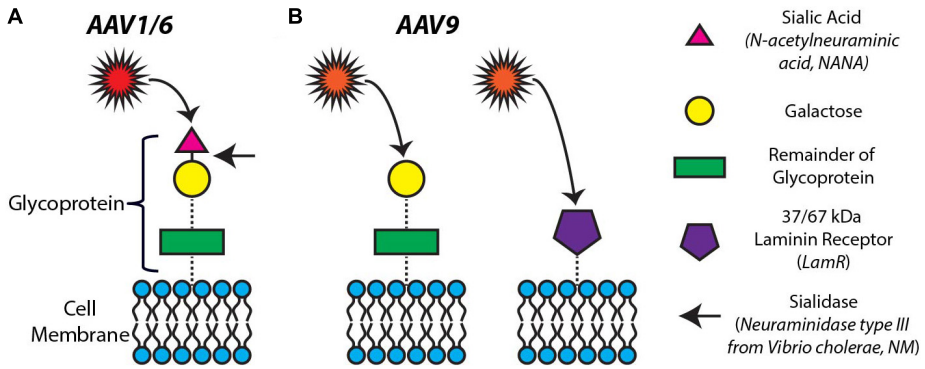

FIGURE 3 | Proposed mechanisms of infectivity for AAV1, 6, and 9. **(A)** Cell surface N-linked sialic acid has been proposed as the primary receptor for AAV1 and 6 to infect and transduce cells. The removal of sialic acid by neuraminidase (targeting the portion of the glycoprotein indicated by the arrow) is expected to block the AAV1,6-mediated transduction of cells. **(B)** AAV9-mediated cell infection/transduction has been attributed to two receptors: terminal galactose on cell surface glycoproteins (left panel) and the 37/67 kDa laminin receptor (LamR) (right panel).

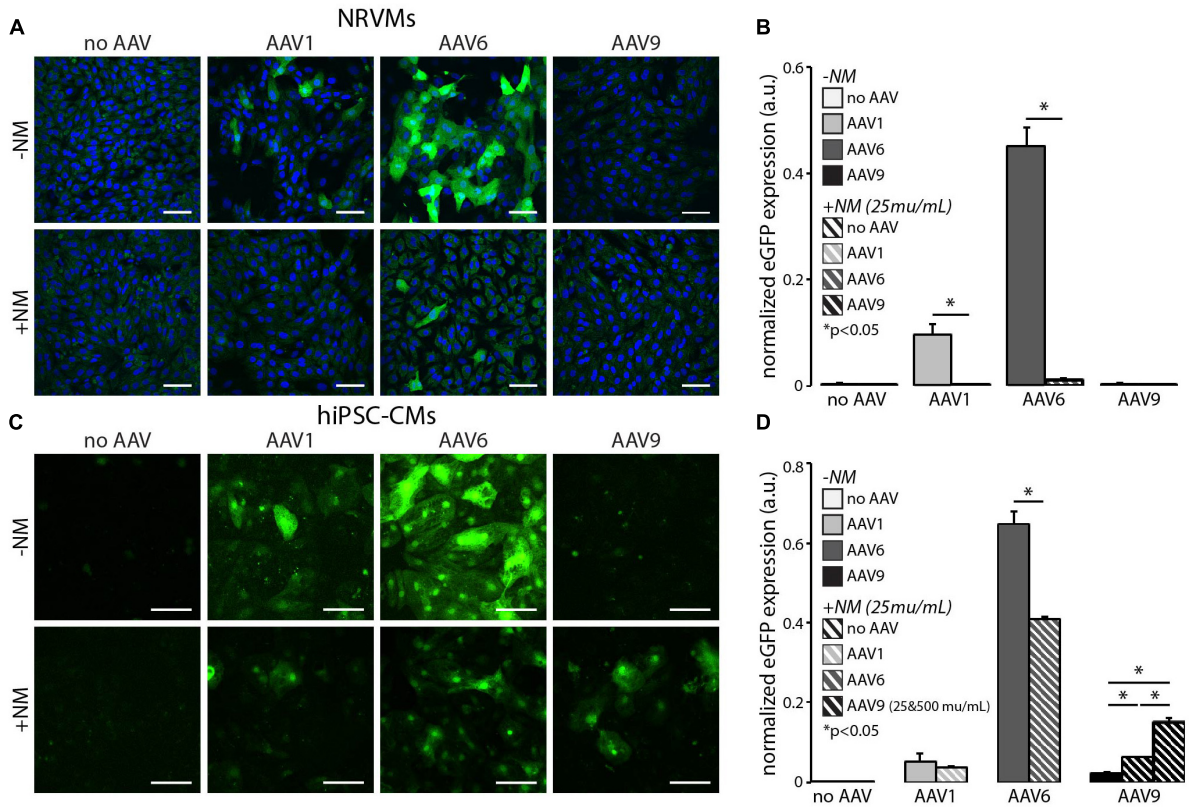

FIGURE 4 | *In vitro* desialylation modulates AAV-mediated eGFP expression in NRVMs and hiPSC-CMs. Cardiomyocyte-specific eGFP expression with (+NM, 25 mU/mL) and without (−NM) neuraminidase treatment prior to viral infection in **(A)** NRVMs at MOI 2000 and **(C)** hiPSC-CMs at MOI 30,000. Cell nuclei were labeled with DAPI (blue, NRVMs only) and AAV-infected cells expressed eGFP (green). All scale bars are 50 μm and color-enhanced images are shown. Quantification of eGFP expression with and without desialylation in all three serotypes in **(B)** NRVMs and **(D)** hiPSC-CMs. eGFP expression mediated by AAV1 and 6 significantly decreased in both cell types, whereas transgene expression mediated by AAV9 significantly increased in hiPS-CMs only. Application of a higher dose of NM (500 mU/mL) in hiPSC-CMs infected with AAV9 resulted in even greater eGFP expression. Data are presented as mean ± SEM (n = 3–7 independent samples per group). *Significance level at $p < 0.05$.

(where AAV9 was most efficient) were further elucidated by investigating the presence of LamR which is purported to be a cell surface receptor for AAV9, as previously discussed. Our data show that LamR is not present *in vitro* in monolayers of NRVMs, nor in hiPSC-CMs (**Figure 5A** and **Supplementary Figure S2A**), but appears to be globally present *in vivo* in both

the adult and neonatal rat heart (**Figure 5B** and **Supplementary Figure S3B**). Wild-type HeLa cells served as our *in vitro* positive control (**Figure 5A**) and tissue sections of breast carcinoma served as our *in vivo* positive control (**Figure 5B** and **Supplementary Figure S3A**). Experimental samples without the primary antibody showed that *in vivo* the secondary antibody did not yield any non-specific staining (**Figure 5C**).

These observations were extended to the adult human heart. Western blots of LamR protein in samples of fresh human hearts versus hiPS-CMs corroborated the difference in LamR expression between the intact heart and cardiomyocytes in culture (**Figure 6**).

Given our LamR expression data in NRVMs, hiPSC-CMs, rat and human hearts, it is important to note that the expression of LamR is dynamic and significantly affected by the tissue/culture environment. Specifically, we have observed the paucity of LamR expression in the *in vitro* environment with isolated cells (**Figure 5A** and **Supplementary Figure S2**) compared to its robust presence in intact tissues (**Figures 5B**, **6** and **Supplementary Figure S3**).

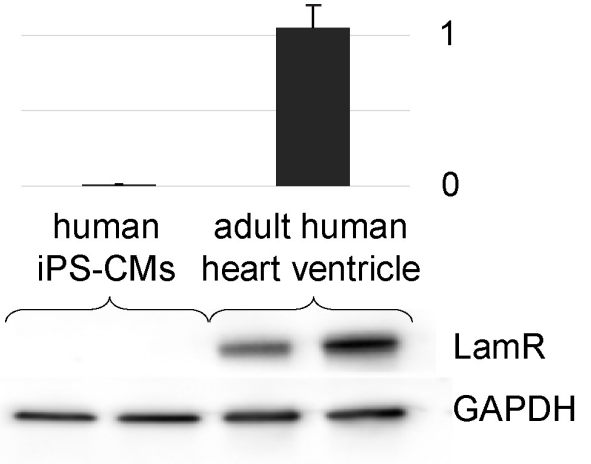

FIGURE 6 | The 37/67 kDa LamR is expressed in the intact human heart. Western blots of LamR protein in fresh samples from male and female human hearts and from cultured hiPS-CMs corroborate the difference in expression (lack of LamR in the cultured myocytes and abundance in the intact human heart). GAPDH was used as a loading control and for normalization purposes.

TGF-β1 Treatment Does Not Significantly Affect AAV9-Mediated Gene Expression

Since the presence of LamR was not detected *in vitro* in NRVMs and hiPSC-CMs, we followed up on an earlier report (Wenzel et al., 2010) and pre-treated the monolayers with TGF-β1 (10 ng/mL for 24 h) in an attempt to increase LamR expression and facilitate AAV infectivity. Our data, however, show that TGF-β1 application does not significantly increase the expression of LamR (**Supplementary Figures S2A,B**) and minimally increases AAV9-mediated eGFP expression (**Supplementary Figure S4**).

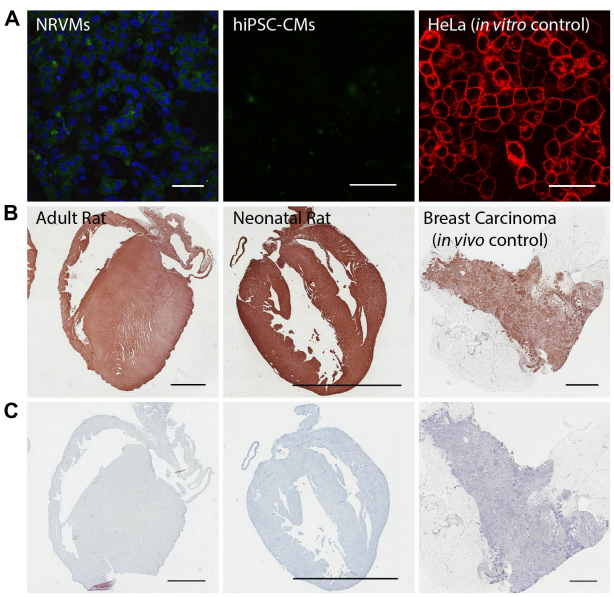

FIGURE 5 | The 37/67 kDa LamR is expressed in the rat heart, but not in cultured NRVMs and hiPSC-CMs. **(A)** Negative *in vitro* immunostains of NRVMs and hiPSC-CMs for LamR. Concurrent immunostaining of HeLa cells, serving as a positive *in vitro* control for LamR. Scale bars are 50 μm. **(B)** Positive immunostains of adult and neonatal rat hearts. Concurrent immunostaining of breast carcinoma tissue, serving as a positive *in vivo* control for LamR. **(C)** Negative controls of tissue (stained with no primary LamR antibody) showed no contribution to the positive stain by non-specific secondary antibody staining. Scale bars in **B**,**C** are 3 mm.

Viral Delivery of Optogenetic Tools

The growing use of optogenetics in cardiac applications motivated our search for optimized parameters for the optical control of the heart under various experimental conditions. One such application is the development of high-throughput all-optical electrophysiology for drug screening and cardiotoxicity testing (Dempsey et al., 2016; Klimas et al., 2016). The current study revealed that the environment (i.e., *in vitro* versus *in vivo*) is of great importance with regard to preferential serotype specificity. Cultured cardiomyocytes tend to lose cell surface receptors (LamR) critical to mediating *in vivo* AAV9 infection (**Figure 5**), although those receptors are present to some degree *in situ* in cultured explanted human cardiac tissue. Consequently, the specific environment may require different means for efficiently inscribing optical control.

AAV6-mediated transgene delivery resulted in acceptable expression levels, similar to those of our previous studies using AdV delivery (Ambrosi and Entcheva, 2014; Ambrosi et al., 2015; Klimas et al., 2016). However, the required dose (MOI) was orders of magnitude higher (**Supplementary Figure S5**), and the time required for transgene expression with AAV is not optimal for primary cells. Here AAV infection required 5 days for the cells to reach peak transgene expression, whereas

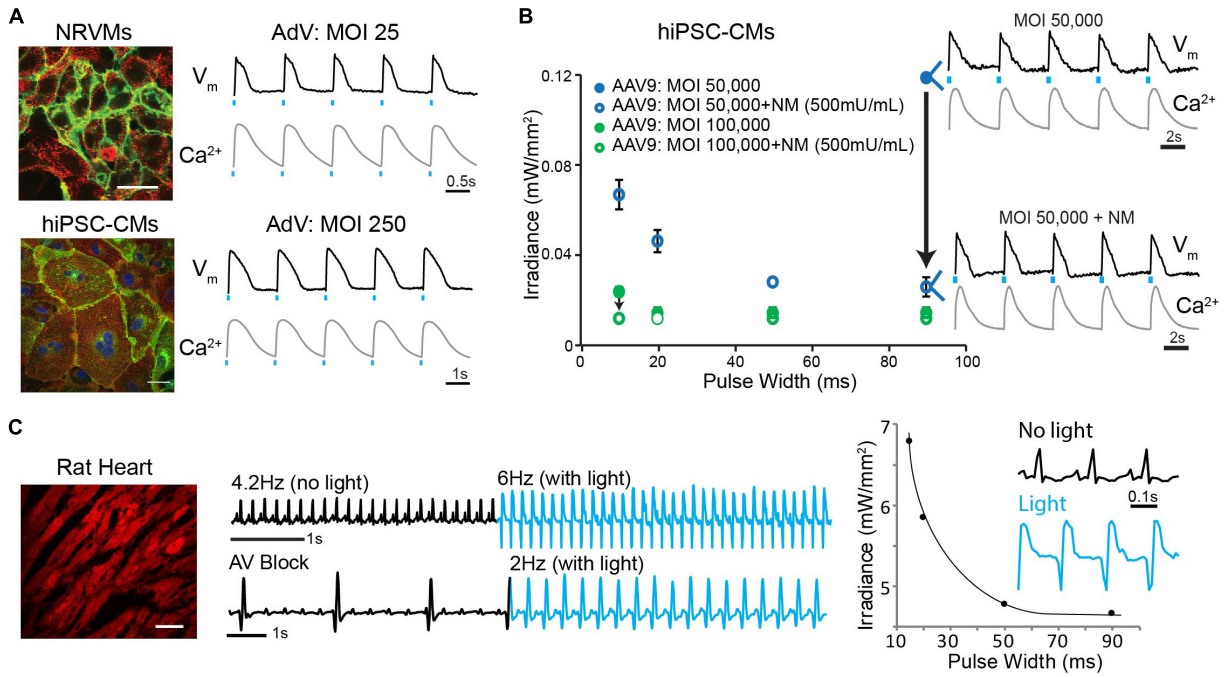

FIGURE 7 | Robust *in vitro* and *in vivo* optogenetic control of the heart. **(A)** Adenoviral (AdV)-mediated ChR2-eYFP expression and functional measurements in NRVMs (MOI 25) and hiPSC-CMs (MOI 250) 2 days post-infection. Functional measurements were acquired using voltage- (di-4-ANBDQBS) and calcium- (Rhod4) sensitive dyes and example traces with optical pacing are shown. Cell nuclei were labeled with DAPI (blue) and AdV-infected cells expressed eYFP (green). Alpha-actinin staining (red) showed the cardiospecificity of the ChR2-eYFP infection. **(B)** Strength-duration curves for AAV9-mediated ChR2 expression in hiPSC-CMs. Conditions for infection included MOIs of 50,000–100,000 and NM applications of 500 mU/mL. Black arrows show the effect of NM treatment on lowering irradiance (mW/mm^2) requirements; shown are voltage and calcium traces for the case of using MOI 50,000 without and with NM treatment. Data are presented as mean ± SEM (n = 3 per group). **(C)** AAV9-mediated ChR2-mCherry expression in the intact adult rat heart after 4 weeks results in optically sensitive myocardium *in situ* (left panel). A 0.8 mm diameter optical fiber was used to optically control electrical activity from the LV free wall as recorded using ECG (middle panel). Optical pacing resulted in an increased heart rate, as well as significant morphological changes in the QRS complex (right panel); the irradiance needed for this point stimulation was substantially higher than *in vitro*. Spatial scale bars are 50 μm in **B**,**C**. Temporal scale bars are as indicated.

in our previous studies >95% of NRVMs and hiPSC-CMs expressed ChR2 within 24–48 h using an AdV (**Figure 7A**; Ambrosi et al., 2015; Klimas et al., 2016). *In vitro* optical control was confirmed using all-optical electrophysiology (combining optical mapping by voltage- and calcium-sensitive dyes with simultaneous optogenetic stimulation; Klimas et al., 2016).

Although *in vitro* AAV9-mediated transgene delivery was deemed less optimal than AAV1,6-mediated delivery (**Figure 1**), successful expression of ChR2-mCherry using AAV9 was achieved under very specific conditions, as hypothesized and explored in this study (**Figure 7B**). A pre-treatment of hiPSC-CM monolayers with 500 mU/mL NM (20× the dose required to cause desialylation, **Figure 4**), followed by AAV9 infection at very high MOIs of 50,000–100,000 (5–10× the minimum dose for baseline transgene expression, **Figure 1**) resulted in optogenetic responsiveness. In all four cases (MOI 50,000 ± NM and MOI 100,000 ± NM), ChR2-mCherry was expressed resulting in an optically sensitive cardiac syncytium. However, at the lower concentration of MOI 50,000 only (no NM) and relevant low-light stimulation, only one out of three samples was optically excitable, and it only responded to long light pulses. As illustrated in **Figure 7B**, the strength-duration relationship showed the effect of NM treatment on improving optical responsiveness as compared to infection alone (black arrows). The strength-duration curve with NM treatment is similar to what we have reported previously with AdV in NRVM (for example, Yu et al., 2015). Despite successful transgene expression, infection at such high MOIs resulted in significant cell death (data not shown).

Extending this to the whole animal, here we show systemic delivery and successful expression of ChR2-mCherry in the adult rat heart 4 weeks after viral injection using AAV9 with a generic promoter (**Figure 7C**). Optical sensitivity was confirmed by rate and QRS morphology changes in the ECG, when using an optical fiber to deliver light to the left ventricle in the open chest of the anesthetized rat.

DISCUSSION

We investigated *in vitro* and *in vivo* AAV serotype specificity in rat and human models suitable as scalable experimental platforms for cardiac optogenetics. Different optimal serotypes were identified for *in vivo* and *in vitro* use. Namely, *in vitro* AAV6-mediated transgene expression was superior to AAV1,9-mediated delivery due to the presence of cell surface N-linked

sialic acid (**Figures 1**, **4**). The subsequent enzymatic removal of sialic acid significantly reduced or abolished AAV6- and AAV1-mediated gene delivery, independent of cell type. AAV1 and AAV6 are 99% homologous and belong to the same branch of the phylogenetic tree; the N-linked sialic acid receptor has been suggested as the primary receptor for both of these serotypes (as also corroborated by our data), yet it is recognized that the AAV viral entry is more complex (Vance et al., 2005). For example, the secondary receptor for AAV6 is reported to be the epidermal growth factor receptor (EGFR), while for AAV1 the secondary receptor remains unknown. These differences can explain the quantitatively different performance of the two serotypes in our cells despite qualitatively similar response.

AAV9, on the other hand, belongs to a separate branch on the phylogenetic tree and shares 82% homology with AAV1, 6 and with the most widely used in clinical trials AAV2(Vance et al., 2005). Interestingly, the same desialylation process that suppressed AAV6 and AAV1 entry enhanced AAV9-mediated expression but only in hiPSC-CMs (**Figure 4**). In contrast, *in vivo* serotype specificity in the adult rat favored delivery by AAV9, likely mediated by the presence of cell surface LamR (**Figures 2**, **5**). The latter appears ubiquitous in the intact heart but could not be found in cultured cardiomyocytes (absence confirmed in primary neonatal rat myocytes and in human iPS-CMs). An argument against cardiomyocyte maturity being the central driver for LamR expression or its loss is presented by the observation that the intact neonatal rat heart, with presumably less mature cells, has just as strong expression of LamR as the adult rat heart (**Figure 5B**). In this study, fibronectin-coated dishes were used only. The composition of the extracellular matrix may affect viral uptake – for example, for cancer cells expressing LamR (e.g., HeLa), addition of laminin decreased the expression of the receptor and the viral uptake (Akache et al., 2006). Other culture-related conditions, including proper mass transport, oxygenation, proper fuel/nutrients in the medium, may influence the LamR expression.

The emergence of human stem-cell derived cardiomyocytes and their combination with genetically encoded sensors and actuators (Leyton-Mange et al., 2014; Zhuge et al., 2014; Dempsey et al., 2016; Klimas et al., 2016) has prompted a closer look at the performance of various viral vectors, including AAVs (Rapti et al., 2015) due to the convenience of sharing the usage of such vectors for both *in vivo* and *in vitro* applications. The results presented here, showing preferential infectivity of cardiomyocytes *in vitro* (AAV6 > AAV1 >> AAV9), are consistent with a recent report in human stem-cell derived cardiomyocytes (Rapti et al., 2015). Interestingly, we find that the ease of viral infection in the *in vitro* environment seems to be dependent on two major factors: the viral vector itself (AAV, AdV, or lentivirus) and the state of differentiation of the target cell (**Supplementary Figure S5**). In our experience, primary cardiomyocytes are the easiest to infect (i.e., requiring the lowest viral doses for >80% cell transgene expression) using AdV (Ambrosi and Entcheva, 2014; Ambrosi et al., 2015) and AAV (explored in this study). iPSC-CMs require 10–100× increased viral doses compared to primary cardiomyocytes for the same efficiency of expression, and the presumably least differentiated cells, cardiac fibroblasts, require the highest viral doses (Yu and Entcheva, 2016), although we have not tested AAVs on the latter cell type (**Supplementary Figure S5**). Similar observations have been reported for pluripotent stem cells before and after differentiation into cardiomyocytes (Rapti et al., 2015). While AAV delivery appears sub-optimal for *in vitro* use (compared to LV or AdV application), our dissection of the mechanism of viral entry suggests some strategies to improve infectivity with select AAVs, e.g., desialylation enhances AAV9-mediated entry, while sialic acid on the cardiomyocyte surface promotes AAV6 entry.

Optogenetics in the intact organism requires the genetic modification of cells and tissues, and hence it necessitates the development of efficient, safe tools for gene therapy. Methods for non-viral transfer of genetic material, including electroporation, ballistic DNA transfer, and cationic lipid-based gene transfer, are known to be less efficient and the persistence of transgene expression is short-lived (Ramamoorth and Narvekar, 2015). Therefore, viral transfer of genetic material through the use of AdVs, lentiviruses, and AAVs is desirable. AAVs are preferred due to their comparatively low immunogenicity (Zaiss et al., 2002). *In vivo*, AAV-mediated transgene delivery has been used for cardiac optogenetics in rodent hearts (Nussinovitch and Gepstein, 2015; Vogt et al., 2015; Nyns et al., 2016). AAV9-mediated expression of ChR2 in the mouse heart yielded highly efficient and cardiac-specific transduction when applied by a minimally invasive systemic route (Vogt et al., 2015); a recent report used a similar delivery but with a very high dose of cardiac-specific viral vector in the rat (Nyns et al., 2016). Direct cardiac injections of AAV9 encoding for the ChR2 transgene also resulted in optical responsiveness of the rat heart (Nussinovitch and Gepstein, 2015). However, systemic delivery is preferred not only because of its minimally invasive nature (and hence, suitability for translation), but also because of better uniformity of expression (Prasad et al., 2011; Vogt et al., 2015).

The purpose of this study was to provide practical information to users of commercially available viral constructs as much as possible to ensure easy reproducibility. Here, we used only commercially available constructs for the tested AAV viruses, obtainable through the UPenn Core, and we stayed consistent when comparing the different serotypes. No commercial version was available for AAV6 with ChR2 through the UPenn Core; therefore, it was not included in the *in vivo* tests. For the AdV studies *in vitro*, we have developed viral vectors, and these are available to outside investigators upon request. Different promoters were used for different portions of this study, limited by the commercially available viral vectors. All serotypes of AAV (1,6,9) used either CAG or CB7 promoter, while the AdV constructs had the CMV promoter. CMV, CAG, and CB7 are all strong ubiquitous promoters that are commonly used. CAG/CB7 are considered identical and interchangeable by the UPenn Core and there is no literature to differentiate between the performance of the two. CAG/CB7 is a synthetic promoter, a derivative of CMV with added transcribed sequence from chicken beta-actin

gene and enhancer elements (Miyazaki et al., 1989). In most cases, CAG/CB7 is considered a stronger version of CMV.

The direct comparisons between AAV serotypes were done using identical promoters to avoid influence by this factor. For example, the revealed superior performance of AAV6 *in vitro* compared to AAV1 and 9 is not impacted by the promoter itself. Similarly, the superior performance of AAV9 over AAV1 for *in vivo* optogenetics is not influenced by the promoter itself, CAG/CB7. Considering the more potent CAG/CB7, compared to the CMV used with the AdV vectors *in vitro*, the dramatically better performance of AdV delivery over AAV serotypes *in vitro* also holds true.

AAV serotypes 1, 6, and 9 have shown different degrees of gene transfer to the heart (**Supplementary Table S1**). The specificity of cardiac transduction is dose-dependent. For example, AAV9 delivered systemically in mice at 10^{11} MOI is rather cardiac-specific without affecting other organs; however, at 10^{12} MOI, it also transduces liver, skeletal muscle, and pancreas (Inagaki et al., 2006). Scaling of viral dose from mice to rats by body weight ratio yields about 5–10 times higher amount of virus needed for cardiac-specific transduction. Indeed, 10^{12} MOI in rats showed heart-specific transduction with AAV9 (no expression in liver, kidney, brain, lung; Cataliotti et al., 2011). Our results are similar. In addition to the AAV tissue tropism, the use of cardiac-specific promoters, such as cardiac troponin T (cTnT), has been shown to further increase specificity; however, the level of expression derived from tissue-restricted promoters may not be as high as from ubiquitous viral promoters (Prasad et al., 2011).

Of critical importance in the use of AAV serotypes for optimized gene therapy applications is consideration of the mechanism of infectivity. In this study, we not only identified optimal serotypes for *in vitro* and *in vivo* use, but also explored the mechanism of infection and fundamental differences between experimental platforms. Specifically, our results are consistent with AAV9 infection being mediated by either terminal galactose (**Figure 4**, only in hiPS-CMs) or LamR (**Figure 5**). Identification of unique cell surface receptors in the heart and other organs will continue to drive the design of truly optimized AAV serotypes for cardiac electrophysiology applications, such as optogenetics, and beyond.

DATA AVAILABILITY

The raw data supporting the conclusions of this manuscript will be made available by the authors, without undue reservation, to any qualified researcher.

AUTHOR CONTRIBUTIONS

CA, GS, and JH performed the experiments, analyzed the data, and produced figures. CA conducted the rat experiments. GS and CA performed the *in vitro* experiments. JH analyzed protein expression. EE and CA conceived the study and oversaw the project. CA and GS produced an initial draft of the manuscript, which was edited by EE.

FUNDING

This work was supported by the National Institutes of Health (Grant Nos. R01HL111649, R01HL144157, and R21EB023106 to EE) and the National Science Foundation (Grant Nos. 1623068 and 1705645 to EE).

ACKNOWLEDGMENTS

We acknowledge the technical support provided by the Research Pathology Core Laboratories at both Stony Brook University and George Washington University and the assistance of veterinary personnel in the Division of Laboratory Animal Resources at Stony Brook University and the Animal Research Facility at George Washington University. We also acknowledge members of the Entcheva lab for help with some experiments, as well as the Efimov lab for procurement of human heart tissue for the Western blots.

SUPPLEMENTARY MATERIAL

The Supplementary Material for this article can be found online at: https://www.frontiersin.org/articles/10.3389/fphys.2019.00168/full#supplementary-material

REFERENCES

Aikawa, R., Huggins, G. S., and Snyder, R. O. (2002). Cardiomyocyte-specific gene expression following recombinant adeno-associated viral vector transduction. *J. Biol. Chem.* 277, 18979–18985. doi: 10.1074/jbc.M201257200

Akache, B., Grimm, D., Pandey, K., Yant, S. R., Xu, H., and Kay, M. A. (2006). The 37/67-kilodalton laminin receptor is a receptor for adeno-associated virus serotypes 8, 2, 3, and 9. *J. Virol.* 80, 9831–9836. doi: 10.1128/JVI.00878-06

Ambrosi, C. M., Boyle, P. M., Chen, K., Trayanova, N. A., and Entcheva, E. (2015). Optogenetics-enabled assessment of viral gene and cell therapy for restoration of cardiac excitability. *Sci. Rep.* 5:17350. doi: 10.1038/srep17350

Ambrosi, C. M., and Entcheva, E. (2014). Optogenetic control of cardiomyocytes via viral delivery. *Methods Mol. Biol.* 1181, 215–228. doi: 10.1007/978-1-4939-1047-2_19

Ambrosi, C. M., Klimas, A., Yu, J., and Entcheva, E. (2014). Cardiac applications of optogenetics. *Prog. Biophys. Mol. Biol.* 115, 294–304. doi: 10.1016/j.pbiomolbio.2014.07.001

Bish, L. T., Morine, K., Sleeper, M. M., Sanmiguel, J., Wu, D., Gao, G., et al. (2008). Adeno-associated virus (AAV) serotype 9 provides global cardiac gene transfer superior to AAV1, AAV6, AAV7, and AAV8 in the mouse and rat. *Hum. Gene Ther.* 19, 1359–1368. doi: 10.1089/hum.2008.123

Cataliotti, A., Tonne, J. M., Bellavia, D., Martin, F. L., Oehler, E. A., Harders, G. E., et al. (2011). Long-term cardiac pro-B-type natriuretic peptide gene delivery prevents the development of hypertensive heart disease in spontaneously hypertensive rats. *Circulation* 123, 1297–1305. doi: 10.1161/CIRCULATIONAHA.110.981720

Dempsey, G. T., Chaudhary, K. W., Atwater, N., Nguyen, C., Brown, B. S., McNeish, J. D., et al. (2016). Cardiotoxicity screening with simultaneous optogenetic

pacing, voltage imaging and calcium imaging. *J. Pharmacol. Toxicol. Methods* 81, 240–250. doi: 10.1016/j.vascn.2016.05.003

Entcheva, E. (2013). Cardiac optogenetics. *Am. J. Physiol. Heart Circ. Physiol.* 304, H1179–H1191. doi: 10.1152/ajpheart.00432.2012

Greenberg, B., Butler, J., Felker, G. M., Ponikowski, P., Voors, A. A., Desai, A. S., et al. (2016). Calcium upregulation by percutaneous administration of gene therapy in patients with cardiac disease (CUPID 2): a randomised, multinational, double-blind, placebo-controlled, phase 2b trial. *Lancet* 387, 1178–1186. doi: 10.1016/S0140-6736(16)00082-9

Inagaki, K., Fuess, S., Storm, T. A., Gibson, G. A., McTiernan, C. F., Kay, M. A., et al. (2006). Robust systemic transduction with AAV9 vectors in mice: efficient global cardiac gene transfer superior to that of AAV8. *Mol. Ther.* 14, 45–53. doi: 10.1016/j.ymthe.2006.03.014

Jessup, M., Greenberg, B., Mancini, D., Cappola, T., Pauly, D. F., Jaski, B., et al. (2011). Calcium upregulation by percutaneous administration of gene therapy in cardiac disease (CUPID): a phase 2 trial of intracoronary gene therapy of sarcoplasmic reticulum Ca2+-ATPase in patients with advanced heart failure. *Circulation* 124, 304–313. doi: 10.1161/CIRCULATIONAHA.111.022889

Jia, Z., Valiunas, V., Lu, Z., Bien, H., Liu, H., Wang, H. Z., et al. (2011). Stimulating cardiac muscle by light: cardiac optogenetics by cell delivery. *Circ. Arrhythm Electrophysiol.* 4, 753–760. doi: 10.1161/CIRCEP.111.964247

Kawamoto, S., Shi, Q., Nitta, Y., Miyazaki, J., and Allen, M. D. (2005). Widespread and early myocardial gene expression by adeno-associated virus vector type 6 with a beta-actin hybrid promoter. *Mol. Ther.* 11, 980–985. doi: 10.1016/j.ymthe.2005.02.009

Klimas, A., Ambrosi, C. M., Yu, J., Williams, J. C., Bien, H., and Entcheva, E. (2016). OptoDyCE as an automated system for high-throughput all-optical dynamic cardiac electrophysiology. *Nat. Commun.* 7:11542. doi: 10.1038/ncomms11542

Klimas, A., and Entcheva, E. (2014). Toward microendoscopy-inspired cardiac optogenetics *in vivo*: technical overview and perspective. *J. Biomed. Opt.* 19:80701. doi: 10.1117/1.JBO.19.8.080701

Klimas, A., Ortiz, G., Boggess, S., Miller, E. W., and Entcheva, E. (2018). Multimodal on-axis platform for all-optical electrophysiology with near-infrared probes in human stem-cell-derived cardiomyocytes. *bioRxiv* [Preprint]. doi: 10.1101/269258

Kuken, B. N., Aikemu, A. N., Xiang, S. Y., and Wulasihan, M. H. (2015). Effect of SERCA2a overexpression in the pericardium mediated by the AAV1 gene transfer on rapid atrial pacing in rabbits. *Genet. Mol. Res.* 14, 13625–13632. doi: 10.4238/2015.October.28.24

Leyton-Mange, J. S., Mills, R. W., Macri, V. S., Jang, M. Y., Butte, F. N., Ellinor, P. T., et al. (2014). Rapid cellular phenotyping of human pluripotent stem cell-derived cardiomyocytes using a genetically encoded fluorescent voltage sensor. *Stem Cell Rep.* 2, 163–170. doi: 10.1016/j.stemcr.2014.01.003

Miyazaki, J., Takaki, S., Araki, K., Tashiro, F., Tominaga, A., Takatsu, K., et al. (1989). Expression vector system based on the chicken beta-actin promoter directs efficient production of interleukin-5. *Gene* 79, 269–277. doi: 10.1016/0378-1119(89)90209-6

Montgomery, K. L., Iyer, S. M., Christensen, A. J., Deisseroth, K., and Delp, S. L. (2016). Beyond the brain: optogenetic control in the spinal cord and peripheral nervous system. *Sci. Transl. Med.* 8:337rv335. doi: 10.1126/scitranslmed.aad7577

Muller, O. J., Leuchs, B., Pleger, S. T., Grimm, D., Franz, W. M., Katus, H. A., et al. (2006). Improved cardiac gene transfer by transcriptional and transductional targeting of adeno-associated viral vectors. *Cardiovasc. Res.* 70, 70–78. doi: 10.1016/j.cardiores.2005.12.017

Nussinovitch, U., and Gepstein, L. (2015). Optogenetics for *in vivo* cardiac pacing and resynchronization therapies. *Nat. Biotechnol.* 33, 750–754. doi: 10.1038/nbt.3268

Nyns, E. C., Kip, A., Bart, C. I., Plomp, J. J., Zeppenfeld, K., Schalij, M. J., et al. (2016). Optogenetic termination of ventricular arrhythmias in the whole heart: towards biological cardiac rhythm management. *Eur. Heart J.* 38, 2132–2136. doi: 10.1093/eurheartj/ehw574

Pacak, C. A., Mah, C. S., Thattaliyath, B. D., Conlon, T. J., Lewis, M. A., Cloutier, D. E., et al. (2006). Recombinant adeno-associated virus serotype 9 leads to preferential cardiac transduction *in vivo*. *Circ. Res.* 99, e3–e9. doi: 10.1161/01.RES.0000237661.18885.f6

Palomeque, J., Chemaly, E. R., Colosi, P., Wellman, J. A., Zhou, S., Del Monte, F., et al. (2007). Efficiency of eight different AAV serotypes in transducing rat myocardium *in vivo*. *Gene Ther.* 14, 989–997. doi: 10.1038/sj.gt.3302895

Pianca, N., Zaglia, T., and Mongillo, M. (2017). Will cardiac optogenetics find the way through the obscure angles of heart physiology? *Biochem. Biophys. Res. Commun.* 482, 515–523. doi: 10.1016/j.bbrc.2016.11.104

Prasad, K. M., Xu, Y., Yang, Z., Acton, S. T., and French, B. A. (2011). Robust cardiomyocyte-specific gene expression following systemic injection of AAV: *in vivo* gene delivery follows a Poisson distribution. *Gene Ther.* 18, 43–52. doi: 10.1038/gt.2010.105

Ramamoorth, M., and Narvekar, A. (2015). Non viral vectors in gene therapy- an overview. *J. Clin. Diagn. Res.* 9, GE01–GE06. doi: 10.7860/JCDR/2015/10443.5394

Rapti, K., Stillitano, F., Karakikes, I., Nonnenmacher, M., Weber, T., Hulot, J. S., et al. (2015). Effectiveness of gene delivery systems for pluripotent and differentiated cells. *Mol. Ther. Methods Clin. Dev.* 2:14067. doi: 10.1038/mtm.2014.67

Seiler, M. P., Miller, A. D., Zabner, J., and Halbert, C. L. (2006). Adeno-associated virus types 5 and 6 use distinct receptors for cell entry. *Hum. Gene Ther.* 17, 10–19. doi: 10.1089/hum.2006.17.10

Shen, S., Bryant, K. D., Brown, S. M., Randell, S. H., and Asokan, A. (2011). Terminal N-linked galactose is the primary receptor for adeno-associated virus 9. *J. Biol. Chem.* 286, 13532–13540. doi: 10.1074/jbc.M110.210922

Srivastava, A. (2016). *In vivo* tissue-tropism of adeno-associated viral vectors. *Curr. Opin. Virol.* 21, 75–80. doi: 10.1016/j.coviro.2016.08.003

Vance, M. A., Mitchell, A., and Samulski, R. J. (2005). "AAV biology, infectivity and therapeutic use from bench to clinic," in *Gene Therapy - Principles and Challenges*, ed. D. Hashad (Rijeka: InTech).

Vance, M. A., Mitchell, A., and Samulski, R. J. (2015). "AAV biology, infectivity and therapeutic use from bench to clinic," in *Gene Therapy - Principles and Challenges*, ed. D. D. Hashad (Rijeka: InTech).

Vogt, C. C., Bruegmann, T., Malan, D., Ottersbach, A., Roell, W., Fleischmann, B. K., et al. (2015). Systemic gene transfer enables optogenetic pacing of mouse hearts. *Cardiovasc. Res.* 106, 338–343. doi: 10.1093/cvr/cvv004

Wang, Z., Zhu, T., Qiao, C., Zhou, L., Wang, B., Zhang, J., et al. (2005). Adeno-associated virus serotype 8 efficiently delivers genes to muscle and heart. *Nat. Biotechnol.* 23, 321–328. doi: 10.1038/nbt1073

Wenzel, S., Henning, K., Habbig, A., Forst, S., Schreckenberg, R., Heger, J., et al. (2010). TGF-beta1 improves cardiac performance via up-regulation of laminin receptor 37/67 in adult ventricular cardiomyocytes. *Basic Res. Cardiol.* 105, 621–629. doi: 10.1007/s00395-010-0108-1

Williams, P. D., Ranjzad, P., Kakar, S. J., and Kingston, P. A. (2010). Development of viral vectors for use in cardiovascular gene therapy. *Viruses* 2, 334–371. doi: 10.3390/v2020334

Wu, Z., Miller, E., Agbandje-McKenna, M., and Samulski, R. J. (2006). Alpha2,3 and alpha2,6 N-linked sialic acids facilitate efficient binding and transduction by adeno-associated virus types 1 and 6. *J. Virol.* 80, 9093–9103. doi: 10.1128/JVI.00895-06

Yu, J., Chen, K., Lucero, R. V., Ambrosi, C. M., and Entcheva, E. (2015). Cardiac optogenetics: enhancement by all-trans-retinal. *Sci. Rep.* 5:16542. doi: 10.1038/srep16542

Yu, J., and Entcheva, E. (2016). Inscribing optical excitability to non-excitable cardiac cells: viral delivery of optogenetic tools in primary cardiac fibroblasts. *Methods Mol. Biol.* 1408, 303–317. doi: 10.1007/978-1-4939-3512-3_21

Yue, Y., Ghosh, A., Long, C., Bostick, B., Smith, B. F., Kornegay, J. N., et al. (2008). A single intravenous injection of adeno-associated virus serotype-9 leads to whole body skeletal muscle transduction in dogs. *Mol. Ther.* 16, 1944–1952. doi: 10.1038/mt.2008.207

Zaiss, A. K., Liu, Q., Bowen, G. P., Wong, N. C., Bartlett, J. S., and Muruve, D. A. (2002). Differential activation of innate immune responses by adenovirus and adeno-associated virus vectors. *J. Virol.* 76, 4580–4590. doi: 10.1128/JVI.76.9.4580-4590.2002

Zhu, X., McTiernan, C. F., Rajagopalan, N., Shah, H., Fischer, D., Toyoda, Y., et al. (2012). Immunosuppression decreases inflammation and increases AAV6-hSERCA2a-mediated SERCA2a expression. *Hum. Gene. Ther.* 23, 722–732. doi: 10.1089/hum.2011.108

Zhuge, Y., Patlolla, B., Ramakrishnan, C., Beygui, R. E., Zarins, C. K., Deisseroth, K., et al. (2014). Human pluripotent stem cell tools for cardiac optogenetics. *Conf. Proc. IEEE Eng. Med. Biol. Soc.* 2014, 6171–6174. doi: 10.1109/EMBC.2014.6945038

Zincarelli, C., Soltys, S., Rengo, G., and Rabinowitz, J. E. (2008). Analysis of AAV serotypes 1-9 mediated gene expression and tropism in mice after systemic injection. *Mol. Ther.* 16, 1073–1080. doi: 10.1038/mt.2008.76

Conflict of Interest Statement: The authors declare that the research was conducted in the absence of any commercial or financial relationships that could be construed as a potential conflict of interest.

frontiers in Physiology

REVIEW
published: 07 March 2019
doi: 10.3389/fphys.2019.00182

Cardiac Optogenetics and Optical Mapping – Overcoming Spectral Congestion in All-Optical Cardiac Electrophysiology

Christopher O'Shea[1,2,3], Andrew P. Holmes[1,4], James Winter[1], Joao Correia[5], Xianhong Ou[6], Ruirui Dong[6], Shicheng He[6], Paulus Kirchhof[1,7], Larissa Fabritz[1,7], Kashif Rajpoot[2†] and Davor Pavlovic[1*†]*

[1] Institute of Cardiovascular Sciences, University of Birmingham, Birmingham, United Kingdom, [2] School of Computer Science, University of Birmingham, Birmingham, United Kingdom, [3] EPSRC Centre for Doctoral Training in Physical Sciences for Health, School of Chemistry, University of Birmingham, Birmingham, United Kingdom, [4] Institute of Clinical Sciences, University of Birmingham, Birmingham, United Kingdom, [5] Institute of Microbiology and Infection, School of Biosciences, University of Birmingham, Birmingham, United Kingdom, [6] Key Laboratory of Medical Electrophysiology of Ministry of Education, Collaborative Innovation Center for Prevention and Treatment of Cardiovascular Disease/Institute of Cardiovascular Research, Southwest Medical University, Luzhou, China, [7] Department of Cardiology, UHB NHS Trust, Birmingham, United Kingdom

Optogenetic control of the heart is an emergent technology that offers unparalleled spatio-temporal control of cardiac dynamics via light-sensitive ion pumps and channels (opsins). This fast-evolving technique holds broad scope in both clinical and basic research setting. Combination of optogenetics with optical mapping of voltage or calcium fluorescent probes facilitates 'all-optical' electrophysiology, allowing precise optogenetic actuation of cardiac tissue with high spatio-temporal resolution imaging of action potential and calcium transient morphology and conduction patterns. In this review, we provide a synopsis of optogenetics and discuss in detail its use and compatibility with optical interrogation of cardiac electrophysiology. We briefly discuss the benefits of all-optical cardiac control and electrophysiological interrogation compared to traditional techniques, and describe mechanisms, unique features and limitations of optically induced cardiac control. In particular, we focus on state-of-the-art setup design, challenges in light delivery and filtering, and compatibility of opsins with fluorescent reporters used in optical mapping. The interaction of cardiac tissue with light, and physical and computational approaches to overcome the 'spectral congestion' that arises from the combination of optogenetics and optical mapping are discussed. Finally, we summarize recent preclinical work applications of combined cardiac optogenetics and optical mapping approach.

Keywords: optogenetic, optical mapping, fluorescence, cardiac, action potential, calcium, conduction (action potential), arrhythmias

OPEN ACCESS

Edited by:
Christopher Huang, University of Cambridge, United Kingdom

Reviewed by:
Gil Bub, McGill University, Canada
Arkady M. Pertsov, Upstate Medical University, United States
Crystal M. Ripplinger, University of California, Davis, United States

****Correspondence:***
Kashif Rajpoot
k.m.rajpoot@bham.ac.uk
Davor Pavlovic
d.pavlovic@bham.ac.uk

† These authors share senior authorship

Specialty section:
This article was submitted to Cardiac Electrophysiology, a section of the journal Frontiers in Physiology

Received: *14 October 2018*
Accepted: *14 February 2019*
Published: *07 March 2019*

Citation:
O'Shea C, Holmes AP, Winter J, Correia J, Ou X, Dong R, He S, Kirchhof P, Fabritz L, Rajpoot K and Pavlovic D (2019) Cardiac Optogenetics and Optical Mapping – Overcoming Spectral Congestion in All-Optical Cardiac Electrophysiology. Front. Physiol. 10:182. doi: 10.3389/fphys.2019.00182

INTRODUCTION

Over the past 30 years high resolution camera technologies and development of several potentiometric and intracellular calcium sensors has led to optical mapping becoming a valuable tool in cardiac research (Salama et al., 1987; Boukens and Efimov, 2014). Electrical conduction, action potential and calcium transient morphology can be directly measured, quantified, and tracked across multicellular cardiac preparations in high spatio-temporal resolution, unparalleled by traditional electrode techniques (Herron et al., 2012; Yu et al., 2014). Optical mapping has hence played a pivotal role in cardiac research, providing several insights into physiology and pathophysiology of the heart (Jalife, 2003; Myles et al., 2012; Syeda et al., 2016; Winter et al., 2018).

Conversely, optogenetics shifts light to an actuator role to control and tune EP behavior through genetically introducing photosensitive ion channels and pumps (opsins), able to depolarize and hyperpolarize excitable cells. This emergent technology, with its foundations in neuroscience, is now increasingly exploited by heart researchers. Optogenetic pacing of cardiac preparations has now been reported in several experimental models (Park et al., 2014; Vogt et al., 2015; Zhu et al., 2016; Nyns et al., 2017). Beyond rhythm control, optogenetics has been used to terminate arrhythmias in both *ex vivo* and *in vivo* rodent hearts (Bruegmann et al., 2016, 2018; Nyns et al., 2017), suppress and manipulate rotors in cardiomyocyte monolayers (Feola et al., 2017; Watanabe et al., 2017) and elucidate the function of both cardiomyocyte (Wang et al., 2017) and non-cardiomyocyte (Hulsmans et al., 2017) cellular subpopulations in the heart. Hence, optogenetics presents a pivotal emergent technology for basic research, while some of its unique features make it a potentially transformative clinical tool for both pacing and arrhythmia termination.

Combination of optogenetics with optical imaging of cellular monolayers and whole hearts allows 'all-optical' cardiac EP investigation (**Figure 1**); an approach that has seen growing application in cardiac research (Entcheva, 2013; Nussinovitch and Gepstein, 2015b; Entcheva and Bub, 2016). Owing to contactless operation and high spatio-temporal resolution, all-optical systems are uniquely capable of high throughput control and study of complex phenomena that can arise in excitable media. High spatio-temporal understanding of cardiac behavior in response to optical actuation, aside from providing an invaluable research tool, is also vital if optogenetics is to transition to clinical utility.

The requirement and employment of all-optical approach has been expansively presented in recent reviews (Entcheva and Bub, 2016; Crocini et al., 2017). In the present article, we discuss the basic tools of optogenetics (opsins), and optical mapping (voltage and calcium sensors). We focus on their dual use in all-optical setups, including their mechanisms of action, delivery to cardiac tissue, spectral compatibility and highlight technical considerations and advances that have made all-optical systems practical. Additionally, benefits of all-optical cardiac control and EP interrogation when compared to traditional contact techniques are discussed, and we highlight recent applications of combined cardiac optogenetics and optical mapping approaches.

TOOLS OF OPTOGENETICS – OPSINS

The development of optogenetics as a valuable research tool stems from the discovery and cloning of microbial opsins that behave as light-gated ionic channels in the early to mid-2000s – Channelrhodopsins (Nagel et al., 2003, 2005; Boyden et al., 2005). In particular Channelrhodopsin2 (ChR2), and variants thereof, is by far the most utilized opsin in optogenetics. On excitation by blue light (∼470 nm) of threshold irradiance, ChR2 opens as its covalently bound photosensitive chromophore, all-trans retinal, isomerizes (Nagel et al., 2003). The opening of the channel allows ions, including Na^+, to cross the cellular membrane, as occurs in phase 0 of the action potential, initiating depolarization. Hence, cells expressing ChR2 can be effectively stimulated with blue light, initiating and/or prolonging the action potential (**Figure 2A**). As well as being light sensitive, ChR2 also acts in a voltage dependent manner, with decreasing conductance at more positive membrane potentials and a reversal potential near 0mV (Lin, 2010; Park et al., 2014).

Enhancement of the native properties of ChR2 is vital for the future use of optogenetics in cardiac tissue, due to relatively small currents generated by wild type ChR2 (steady state current ∼0.25 nA) and large absorption and scattering of visible light by biological chromophores. This limits optical penetration depth, preventing transmural opsin activation from deep tissue. Deep activation would be advantageous for synchronous cardiac activation and has been demonstrated as an important factor in successful re-entry termination (Karathanos et al., 2016; Watanabe et al., 2017). One possible method to realize deep tissue activation is red-shifting of the excitation window toward the 'biological window' of 650–1350 nm, where the extinction coefficient of biological tissue is greatly reduced (Smith et al., 2009). Light in this wavelength range can penetrate a few centimeters into the cardiac tissue and thus more light can reach and activate deep tissue opsins. Furthermore, decreasing the threshold irradiance required for photocurrent activation and/or increasing channel conductance or opening times, can aid deep tissue activation and reduce energy requirements in optogenetic applications.

Hence, since its isolation and cloning, ChR2 has undergone several alterations including variants with enhanced conductance [ChR2-H134R (Nagel et al., 2005), ChR2-T159C (Berndt et al., 2011), ChR2-XXL (Dawydow et al., 2014)], Ca^{2+} permeability [CatCh (Kleinlogel et al., 2011)] and red shifted spectral properties [ReaChR (Lin et al., 2013)]. Additionally, channelrhodopsins separate from ChR2 have been cloned from distinct algae species and subsequently optimized [CheRiff (Hochbaum et al., 2014)], while chimeras of ChR1 and ChR2 have also demonstrated enhanced photocurrents [ChIEF (Lin et al., 2009)]. These developments have led to a plethora of available depolarizing opsins with diverse spectral and kinetic properties (Schneider et al., 2015). Equally, it has been shown how exogenously supplemented all-trans retinal can significantly increase light sensitivity of ChR2, although concentration dependent cytotoxic effects were also observed (Yu et al., 2015).

An important factor in enhancing the photocurrent of native Channelrhodopsins is the effects mutagenesis can have on the

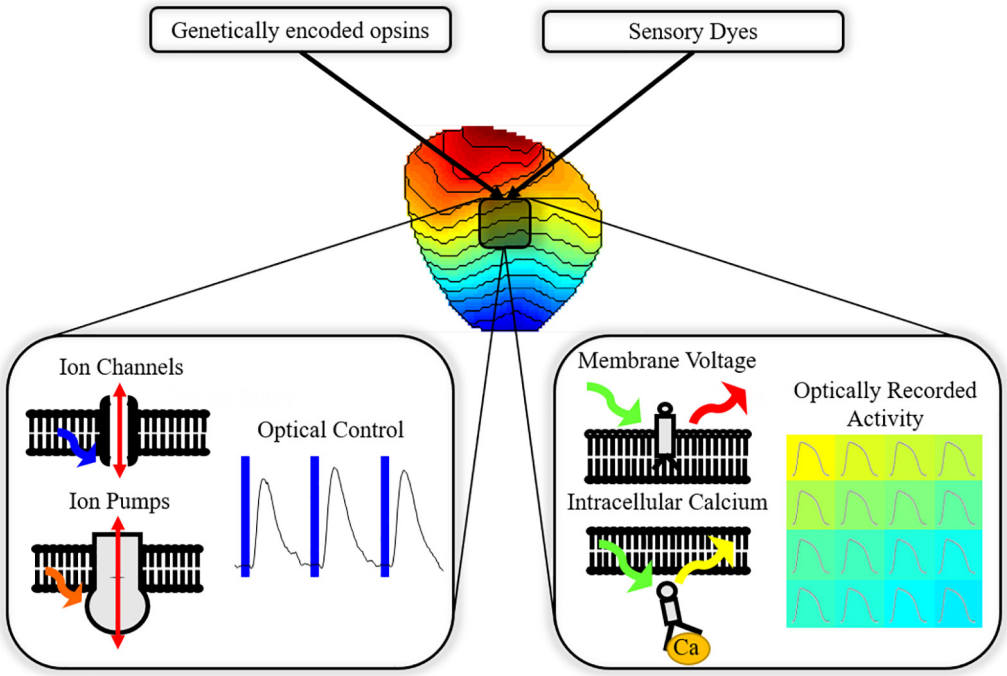

FIGURE 1 | All-optical electrophysiology. Cardiac preparations treated with opsins and sensors allow simultaneous optically driven control of the heart (pacing or modulation of the action potential) and optical recording of action potential or calcium handling across the myocardium.

photocycle kinetics. By prolonging channel opening times after the cessation of light activation, light sensitivity can be improved by a short pulse leading to a long-lasting photocurrent, e.g., ChR2-D156A which exhibits a dark off time of > 150 s (Bamann et al., 2010). However, significant slowing of the channel kinetics is detrimental to dynamic initiation and control of membrane perturbation. Therefore, the channelrhodopsins that have found most use in all optical setups (ChR2-H134R, CatCh, ReaChR, and CheRiff) are those whose enhanced photocurrents have been achieved with only moderate prolongation compared to wild type ChR2, which exhibits on and off time constants of ∼0.2 and ∼10 ms respectively (Nagel et al., 2003).

Aside from depolarizing Channelrhodopsins, hyperpolarizing opsin pumps include halorhodopsin Cl^- pumps (e.g., eNpHR3.0) and bacteriorhodopsin proton pumps (e.g., Arch and ArchT) (Kandori, 2015). Hyperpolarizing opsins allow selective suppression and shortening of action potentials (**Figure 2B**), and have been utilized for applications such as suppressing *in vivo* cardiac motion for high resolution imaging in zebrafish (Mickoleit et al., 2014). Thanks to distinct absorption characteristics in comparison with ChR2, a cardiac preparation expressing both depolarizing and hyperpolarizing opsins can be selectively stimulated and silenced simply by tuning illumination wavelength, thereby allowing comprehensive control of the action potential. While opsins can be expressed independently, gene-fusion enables formation of protein complexes such as ChR2-ArchT, allowing co-localization and bi-directional control of membrane voltage with one protein complex (Nussinovitch et al., 2014; Streit and Kleinlogel, 2018).

Hyperpolarizing pumps suffer from restricted photocurrent as one ion is transported per absorbed photon (Berndt et al., 2011). Anion channelrhodopsins (ACRs), with the potential for enhanced conductance driven instead by electrochemical gradients, were first realized by mutation of channelrhodopsins to infer Cl^- conductance, although with some remaining cationic conductance and slowing of the channel kinetics (Berndt et al., 2014; Wietek et al., 2014). Subsequently, naturally occurring ACRs with reduced cationic conductance have been discovered and cloned (Govorunova et al., 2015). Preliminary studies indicate that reduced light intensities are required to optically induce hyper- and repolarizing currents in cardiomyocytes using these novel ACRs, compared to pumps (Govorunova et al., 2016). Greater structural and functional understanding of both natural (Kim et al., 2018) and designed (Kato et al., 2018) ACRs promises further optimization of inhibitory channels.

Prolonged use and activation of inhibitory pumps or channels based on conductance of H^+ or Cl^- can detrimentally alter intracellular ionic concentrations (Alfonsa et al., 2015; Bernal Sierra et al., 2018). One promising avenue to potentially circumvent this limitation is the development of tools which more closely mimic the resting and repolarization mechanisms of excitable cells via light activated K^+ conductance. Several approaches have now been tested, including recently published PAC-K constructs which combine a cAMP-gated K^+ channel with photo-activated nucleotidyl cyclase, allowing optical silencing of cardiomyocyte (and neuron) activity (Bernal Sierra et al., 2018). These constructs, however, do not currently allow for fast responsive control of membrane potential, eliciting

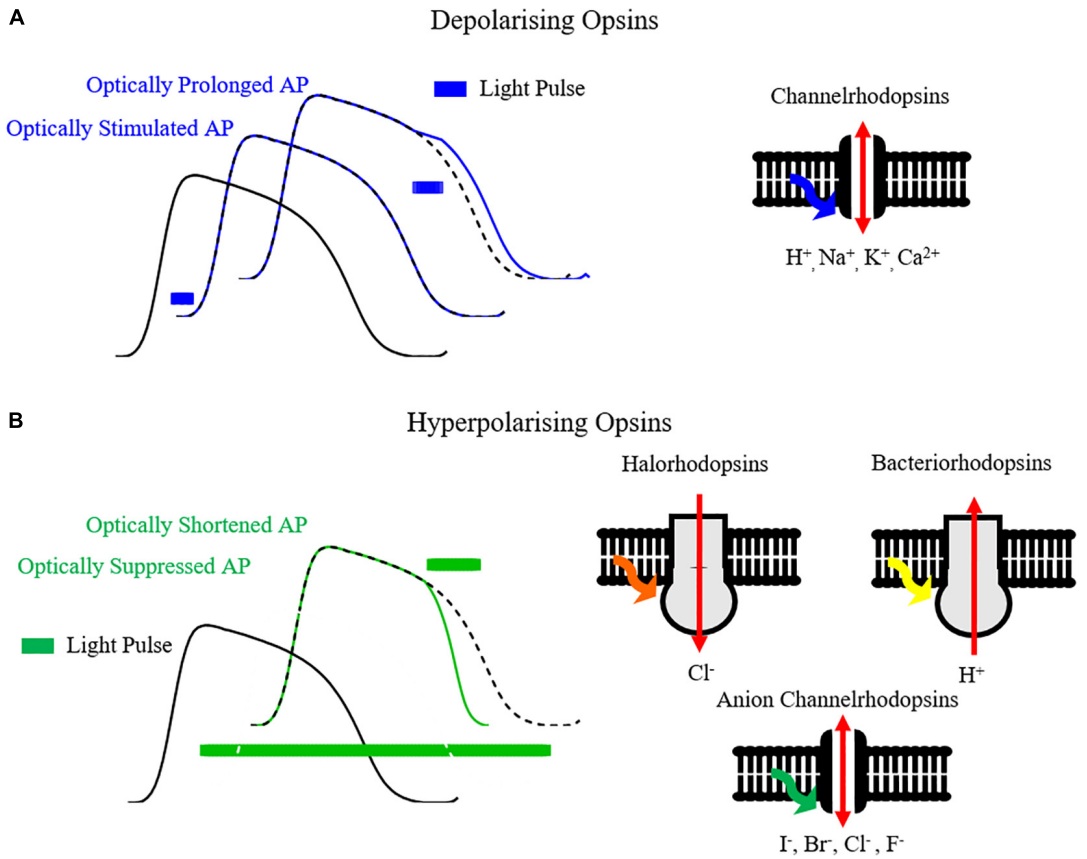

FIGURE 2 | Optogenetic control of the cardiac action potential. **(A)** Opsins such as channelrhodopsins, by conducting cations such as H^+, Na^+, K^+, Ca^{2+} on light activation, can depolarize the cell membrane and hence initiate or prolong the cardiac action potential. **(B)** Hyperpolarizing opsins such as Halorhodopsins (Cl^- pumps), Bacteriorhodopsins (H^+ pumps) and Anion Channelrhodopsins (I^-, Br^-, Cl^-, F^- channels) can shorten or completely suppress the action potential.

hyperpolarization lasting minimally for 100 ms, preventing dynamic control during the action potential.

Delivery of Opsins in Cardiac Tissue

Optogenetic control requires reliable, rapidly responsive, and reversible generation of depolarizing and hyperpolarizing currents by the expression of the light gated ionic transport proteins. The first barrier to achieving cardiac optogenetic perturbation therefore is effective delivery and expression of desired opsins in cardiac preparations. Pioneering cardiac optogenetic studies in 2010 transgenically expressed ChR2 in zebrafish (Arrenberg et al., 2010) and mouse (Bruegmann et al., 2010). ChR2 expressing mouse lines remain prevalent (Quiñonez Uribe et al., 2018) and interventions such as Cre recombinase allow powerful research strategies (Wang et al., 2017).

However, requirement for transgenic expression of opsins is costly, time-consuming and limits clinical application of optogenetics (Knollmann, 2010). Therefore, other techniques have been explored exploiting tandem-cell-unit (Jia et al., 2011) and viral (Abilez et al., 2011; Vogt et al., 2015) delivery of ChR2 and other opsins. Tandem-cell-unit delivery centers on the concept where previously non-excitable cells, transfected to express ChR2, are grafted into cardiomyocyte preparations. The cells couple to the cardiomyocytes via gap junctional proteins and act as 'sparks,' initiating depolarization of coupled cardiomyocytes on light stimulation (Jia et al., 2011).

In viral delivery, opsin genes are encoded in lentiviruses, adenoviruses, or adeno-associated viruses (AAV). Viral methods allow for tissue or cell selectivity, depending on the promoter used, and can be directly injected to realize light excitability. Importantly for future clinical utility of optogenetics, there is increasing evidence that AAVs can be safely and efficaciously used in the heart (Bera and Sen, 2017) and systemic viral delivery can be used to promote cardiac specific ChR2 expression *in vivo* (Ambrosi et al., 2019). In wild type mice for example, AAV injection has shown to result in stable and long lasting ventricular (Vogt et al., 2015; Bruegmann et al., 2016) and atrial (Bruegmann et al., 2018) expression of ChR2. However, transfection rates and consequently optical sensitivity remain variable between treated hearts, and there is some evidence of chamber discrepancies with atrial transfection rates lower than ventricular (Vogt et al., 2015; Bruegmann et al., 2016, 2018). Hence, extensive effort is ongoing to realize the most effective method to introduce optical excitability to cardiac tissue (Ambrosi et al., 2015).

Reports that high-level expression of lentiviral-delivered ChR2 in NRVMs is associated with cytotoxicity also need to be carefully

considered if translational potential of this technology is to be fully realized. The mechanisms underpinning cytotoxicity are unclear, with Ca^{2+} overload and membrane damage being implicated (Li et al., 2017). Further work on mechanistic insight into cytotoxicity is required to ensure safe use of ChR2 and other opsins in cardiac optogenetics.

OPTICAL VOLTAGE AND CALCIUM SENSORS

Synthetic Sensors

A range of sensors are utilized in optical mapping to image transmembrane voltage, as well fluctuations in cytosolic and sarcoplasmic reticulum Ca^{2+} concentrations (Broyles et al., 2018). Synthetic sensors are small molecules that are most commonly introduced to *ex vivo* hearts via Langendorff perfusion, or via superfusion to both *in vitro* and *ex vivo* preparations.

The most popular voltage sensors are 'fast' synthetic styryl sensors, such as di-4-ANEPPS and rh-237, which embed within the plasma membrane, **Figure 1**. As the transmembrane voltage changes, for example during the cardiac action potential, these sensors exhibit fast responding (femto- to picosecond) spectrally shifted fluorescent output due to shifts in charge state and hence dipole energy levels (electrochromism) (Loew et al., 1978; Miller, 2016). Longpass filtering the emitted fluorescence beyond the emission spectra maximum therefore allows recording of optical signals exhibiting fluorescence intensity proportional to cellular membrane voltage changes, i.e., optical action potentials (OAP) (Herron et al., 2012).

On the other hand, intracellular Ca^{2+} sensors such as rhod-2AM are designed to internalize within the cell, **Figure 1**. They are commonly esterified to neutralize the charge, aiding intracellular uptake. The ester is then enzymatically cleaved once in the cell, leaving behind a Ca^{2+} chelator and a fluorophore. As Ca^{2+} is chelated, fluorescence output increases, and subsequently decreases upon dissociation, reporting the changing $[Ca^{2+}]$ in the intracellular space where the sensor localizes, either in the cytosol or sarcoplasmic reticulum (Jaimes et al., 2016).

Genetically Encoded Sensors

Alternatively to small molecule synthetic sensors, voltage and calcium responsive protein sensors can be genetically encoded to achieve cell specific indicator expression (Liao et al., 2015; Quinn et al., 2016). These are collectively termed genetically encoded voltages/calcium indicators (GEVIs/GECIs), constructed by the fusion of voltage/Ca^{2+} sensitive and fluorescent proteins (Scanziani and Häusser, 2009). Genetic indicators can be used to independently measure voltage or Ca^{2+}, but can also be fused to create dual voltage-calcium constructs such as CaViar (Hou et al., 2014) which combines QuasAr2 (GEVI) with GCaMP6f (GECI). Furthermore, co-expressed indicator and actuator pairs offer a unique ability to provide all-genetic, all-optical electrophysiological study (Chang et al., 2017). The "Optopatch" platform for example combines genetic indicators with CheRiff and has been utilized both in establishing all-optical mouse lines and as a high throughput cardiotoxicity screening platform for all-optical pacing with simultaneous voltage and intracellular calcium measurement (Hochbaum et al., 2014; Dempsey et al., 2016; Björk et al., 2017).

Synthetic vs. Genetically Encoded Sensors

Genetic indicators rely on conformational changes to directly alter their fluorescence response or via eliciting processes such as Forster resonance energy transfer (FRET). Consequently, compared to the 'fast' small-molecule sensors, an important limiting factor of current genetically encoded indicators is their response times which are typically in the order of milliseconds (Kaestner et al., 2015). This can prove problematic when measuring the sub millisecond phenomena involved in cardiac depolarization, repolarization and calcium handling (Koopman et al., 2017). Indeed, OAPs recorded by genetic indicators exhibit a significantly altered morphology compared to simultaneously measured OAPs using syntenic sensors (Shinnawi et al., 2015). Coupled to this, the relatively straightforward application to *ex vivo* and *in vitro* preparations makes synthetic sensors more commonly utilized in optical mapping studies (Herron et al., 2012), and to date the pioneering all-optical setups (**Table 1**).

Synthetic sensors will non-specifically stain all the cell subpopulations in cardiac preparations. In contrast, genetic sensors can be successfully utilized *in vivo* and *in vitro* to cell specifically stain cardiomyocytes (or other cell types) (Hou et al., 2014; Dempsey et al., 2016). They hence allow long-term, cell specific, imaging of electrical and calcium activity, currently not possible with synthetic sensors. Furthermore, synthetic sensors suffer from internalization, phototoxicity and cytotoxicity making them only suitable for short-term imaging of cardiac preparations (Kaestner et al., 2015). The extent to which synthetic sensors exhibit toxicity is dependent on study specific parameters including experimental model, sensors concentration and illumination protocols. For example, di-4-ANBDQBS has been shown to exhibit little phototoxicity even at high illumination intensities (Kanaporis, 2012). In this case, the sensor was loaded into guinea pig ventricular preparations and illumination time was restricted to 1 min. In other studies, continuous illumination of di-4-ANBDQBS for 10 min showed significant phototoxic effects compared to a genetic sensor in both human induced pluripotent stem cell cardiomyocyte monolayers (Shaheen et al., 2018), and single cells (Streit and Kleinlogel, 2018). Thus, both of these studies suggest that despite their slower response kinetics, GEVIS and GECIs are valuable tools not only for *in vivo* study but also in situations where phototoxic effects are prominent, such as cellular monolayers and single cells (Fast and Kléber, 1994; Broyles et al., 2018; Streit and Kleinlogel, 2018).

DESIGNING AN ALL-OPTICAL SETUP

The development of a successful all-optical system relies on a number of key features, unique when compared to single purpose, single cell, optical mapping or optogenetic setups.

TABLE 1 | Opsin and sensor combinations used in all-optical setups, with opsin excitation, sensor excitation, and sensor emission spectral characteristics from a specific study.

Opsin	Opsin Excitation λ (nm)	Sensor	Type	Excitation source	Sensor Excitation λ (nm)	Sensor Emission λ (nm)	Reference	Other studies using specified Opsin/Sensor combination
		Voltage Sensors						
ChR2 variants: ChR2-H134R, CatCh, CheRiff (Depolarizing)	470	di-4-ANBDQBS	Synthetic	LED	660 (655/40)	LP700	Klimas et al., 2016	Nussinovitch and Gepstein, 2015a; Yu et al., 2015; Feola et al., 2017; Majumder et al., 2018
		di-4-ANBDQPQ	Synthetic	LED	625 (640/40)	774/140	Crocini et al., 2016	Scardigli et al., 2018; Streit and Kleinlogel, 2018; Quiñonez Uribe et al., 2018
		PGH1	Synthetic	LED	655(690/60)	LP760	Park et al., 2014	
		rh-237	Synthetic	Hg/Xe arc lamp	(560/55)	LP650	Li et al., 2017	Wang et al., 2017
		rh-421	Synthetic	Halogen lamp	(565/24)	630/69	Streit and Kleinlogel, 2018	
		rh-1691	Synthetic	—	—	—	Zaglia et al., 2015	
		BeRST1	Synthetic	LED	635(630/30)	LP665	Streit and Kleinlogel, 2018	
		di-4-ANEPPS	Synthetic	Halogen lamp	(525/50)	LP600	Watanabe et al., 2017	Bingen et al., 2014
		QuasAr 1	GEVI	Laser	593.5	LP665	Streit and Kleinlogel, 2018	
		QuasAr 2	GEVI	Laser	640	660-760	Dempsey et al., 2016	Björk et al., 2017
		Arch(D95N)	GEVI	Laser	647		Björk et al., 2017	
		Calcium Sensors						
		rhod-2AM	Synthetic	LED	530(535/50)	570-625	Klimas et al., 2016	Jia et al., 2011
		rhod-4AM	Synthetic	LED	530	LP565	Wang et al., 2017	
		GCaMP5f	GECI	Laser	488		Björk et al., 2017	
		GCaMP6f	GECI	Laser	488		Dempsey et al., 2016	
		Voltage Sensors						
ArchT (Hyperpolarizing)	566	QuasAr 1	GEVI	Laser	593.5	LP665	Streit and Kleinlogel, 2018	
		Voltage Sensors						
eNpHR3.0 (Hyperpolarizing)	590	PGH1	Synthetic	LED	655(690/60)	LP760	Park et al., 2014	

Opsin excitation wavelengths specified in the table are actual excitation wavelengths used in referenced studies. Sensor excitation wavelengths are shown as light source maxima with filtering shown in brackets. Bandpass filters shown as CWL/FWHM. LP, longpass.

Light must be delivered to both the opsins and the voltage or calcium sensors, demanding distinct illumination characteristics. The possibility of illumination crossover necessitates careful consideration of sensors, actuators and filtering requirements. **Table 1** summaries opsin-sensors combinations that allow stimulation of optical actuation, control and imaging in pivotal all-optical studies.

Opsin and Sensor Compatibility

For an all-optical system, the compatibility of opsins with voltage and Ca^{2+} sensors is paramount, as spectral overlap will result in unwanted crosstalk and perturbation of the cellular membrane. For example, the absorption spectra of the most commonly used synthetic voltage sensor di-4-ANEPPS (excitation peak = 475nm) overlaps with that of ChR2, **Figure 3**. Therefore, excitation of di-4-ANEPPS to optically measure voltage can also excite ChR2, perturbing the membrane potential (Park et al., 2014). With this spectral congestion in mind, it is not surprising that the pioneering all-optical setups imaging Ca^{2+} routinely used rhod-4AM (Jia et al., 2011), which exhibit less spectral overlap with ChR2.

The use of opsins or sensors with red-shifted absorption profiles is the most common solution to spectral congestion. In general, it is easier for an all-optical system to utilize a red-shifted sensor, as the further red-shift of fluorescence emission can then be simply long-pass or band-pass filtered before imaging. Pittsburgh I (PGH1) is a potentiometric sensor whose absorption and emission spectra are far red shifted in comparison to di-4-ANEPPS, with an excitation and emission peak of 608 and 880 nm respectively (in EtOH) (Salama et al., 2005). It was hence the first sensor used in an all-optical manner with concurrent opsin excitation and voltage mapping (Park et al., 2014). By allowing opsin excitation with simultaneous voltage mapping, this system demonstrated how optogenetics can be used to not only pace cardiac tissue but crucially also prolong the action potential by ChR2 excitation during repolarization, a potential therapeutic approach (Karathanos et al., 2014), or silence activity by eNpHR3.0 driven hyperpolarization (Park et al., 2014).

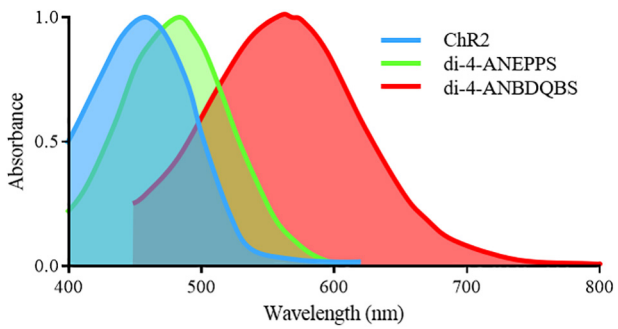

FIGURE 3 | Excitation spectra of the depolarizing opsin ChR2-H134 and voltage sensitive sensors di-4-ANEPPS and di-4-ANBDQBS. Significant overlap exists between the excitation spectra of ChR2 and di-4-ANEPPS, preventing imaging of di-4-ANEPPS without perturbing the membrane potential of ChR2 expressing cells. However, the red-shifted spectra of di-4-ANBDQBS does allow for excitation without simultaneous activation of ChR2.

Alongside PGH1, there are red-shifted variants of di-4-ANEPPS. They include di-4-ANBDQPQ and di-4-ANBDQBS, which share the same basic structure as di-4-ANEPPS but with a distinct chromophore and longer linker sizes. The result is red-shifted absorption and emission spectra, both effectively excited between 500 and 700 nm (**Figure 3**) and imaged from 700 to 900 nm (Matiukas et al., 2007). They are hence spectrally distinct from ChR2. Additionally, 'blue-shifted' opsins are being developed (Lam et al., 2017) which may help avoid spectral overlap, however, their use may be limited by tissue damage and penetration depth.

PGH1, di-4-ANBDQPQ, di-4-ANBDQBS and rh-1691 have all been successfully used in all-optical setups due to their favorable spectral properties. **Table 1** lists potentiometric and calcium sensors used concurrently with optogenetic control and gives examples of illumination and filter setups (discussed in more detail later) that have been employed to minimize actuator-sensor crosstalk. Despite spectral overlap, sensors such as di-4-ANEPPS and GCaMP based calcium indicators have also been used in all-optical setups. However, dual-excitation, and fluorescence baseline shifts on pulse excitation, result in the requirement for spatial separation between excitation and emission areas, or need for extensive pre- and post-acquisition filtering (Dempsey et al., 2016; Li et al., 2017; Wang et al., 2017).

Illumination Sources

For optical mapping, sensor excitation is most commonly achieved using LEDs which benefit from narrow wavelength spectra, long operational lifetimes and low heat emission (Beacher, 2008), though Tungsten-Halogen lamps, Mercury/Xeon arc lamps and lasers are also used. Illumination source is chosen based on a number of characteristics, including wavelength and power. However, illumination of the sample in terms of spatial and temporal homogeneity is of paramount importance for successful optical mapping. In contrast, optical actuation in optogenetics routinely requires impulse-like signals (temporal inhomogeneity) delivered to a specific area of the sample (spatial inhomogeneity). Additionality, a number of studies have demonstrated the importance of patterned light delivery to drive conduction dynamics and realize effective arrhythmia termination (Burton et al., 2015; Crocini et al., 2016; Feola et al., 2017). Therefore liquid crystal (Schmieder et al., 2017) and digital micromirror device (DMD) spatial light modulation coupled to an illumination source such as an LED, able to uniquely deliver synchronous patterned illumination, have been extensively used in cardiac optogenetics from its infancy (Arrenberg et al., 2010). DMDs utilize several hundred thousand or millions of hinged micrometer sized mirrors to deliver illumination patterns with high spatial resolution, an ability that has been key to several optogenetic based discoveries (Scardigli et al., 2018).

Furthermore, fiber-optic coupled LED (Prando et al., 2018) and laser-based approaches have been utilized. This has partially been driven by the potential to incorporate illuminating fibers in clinically used tools for precise spatial illumination *in vivo*

(Klimas and Entcheva, 2014). Devices incorporating micro LED illumination with photodetectors have also been developed (Xu et al., 2014), and further optimization of such unique light delivery strategies is crucial if latent clinical benefits of optogenetics are to be realized.

Optical Filtering

The use of compatible opsins and sensors to avoid spectral overlap has already been discussed. However, optical filtering is still crucial in effective excitation and imaging of samples, especially when considering the multiple light paths necessary in the majority of all-optical setups. Single wavelength filters utilized in all-optical setups can be broadly characterized as (i) Bandpass filters (ii) Long- or shortpass filters, and (iii) Dichroic mirrors/beam splitters (**Figure 4**). An idealized single wavelength bandpass filter (**Figure 4A**) absorbs wavelengths outside a defined window, characterized by a central wavelength (CWL) and full width half maximum (FWHM). A common use of bandpass filters in all optical setups is excitation filtering, where illumination light is filtered before reaching a sample to narrow spectral bandwidth with a relatively small FWHM filter. This helps avoid interference with other sensors or actuators (Jaimes et al., 2016). For example, an effective excitation filter for red shifted voltage sensor di-4-ANBDQPQ may be a 640/40 nm (CWL/FWHM) bandpass filter (Scardigli et al., 2018), placed between the illumination source and sample.

Longpass filters (**Figure 4B**) will absorb light with a wavelength below the CWL but will transmit light above this threshold (with the opposite holding for a shortpass filter with the same CWL). They therefore do not have an associated FWHM and are most used as emission filters, absorbing excitation light wavelengths while conserving the red-shifted fluorescence emission (Park et al., 2014). In conjunction with removing excitation light, longpass filtering is also necessary to effectively measure voltage dependent signals that arise from spectral shift, e.g., the electrochromic based indicators previously discussed, as the fluorescence must be imaged away from the emission maxima. Bandpass filters with red-shifted CWL compared to excitation wavelengths (and emission maxima if required) can also be used for emission filtering, i.e., between the sample and imaging device. For an effective emission bandpass filter, however, a large FWHM is often desirable to maximize the photon count at the imaging device, assuming absorbance of excitation light is maintained (Scardigli et al., 2018). **Table 1** summaries excitation and emission filtering setups that have been implemented in all-optical setups encompassing both voltage and calcium indicators.

Bandpass and longpass filters interact with light by either absorbing or transmitting depending on wavelength. Dichroic mirrors (or beam splitters), however, reflect certain wavelengths of light. An idealized longpass dichroic mirror for example (**Figure 4C**) transmits light with wavelength above the CWL and reflects (often at an angle of incidence of 45^o) wavelengths below this cut off. Therefore, aside from basic filtering that is also possible to achieve with longpass and bandpass filters, dichroic mirrors can be used for important functions such as directing light paths (Scardigli et al., 2018) and splitting emission in dual sensor setups to either separate cameras or sections of a single imaging chip (Dempsey et al., 2016; Wang et al., 2017). The filters outlined in **Figure 4** are known as single wavelength or single band filters, with one characterizing CWL. In contrast, multiband filters are characterized by multiple transmission wavelength regions. They have hence found particular utility in dual optical mapping setups to simultaneously filter voltage and calcium emission signals (Wang et al., 2015).

Removing Spectral Deconvolution Requirement

Problems with spectral overlap can be circumvented by utilizing optical imaging techniques that are not reliant on fluorescent sensors, i.e., do not require illumination. On initiation of the action potential, excitable cells exhibit changing light

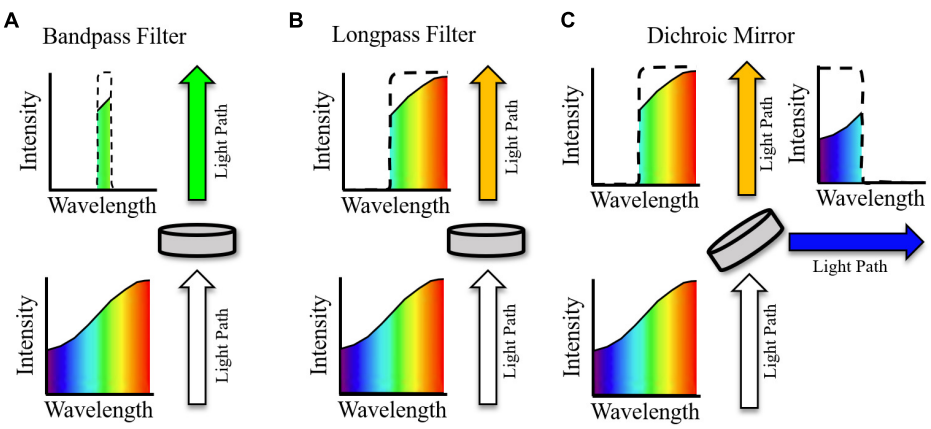

FIGURE 4 | Example effect of idealized optical filters on 'white' light. Arrows indicate path of light with indicated spectra pre and post filtering. **(A)** Bandpass filter. All wavelengths of light, other than those within the transmission window are absorbed. **(B)** Longpass filter. Light with wavelengths above the central wavelength (CWL) are transmitted, and all other wavelengths are absorbed. **(C)** Dichroic mirror. As with the longpass filter, light with wavelengths above the CWL are transmitted. Light with wavelengths below the CWL is reflected at an angle of incidence, commonly 45°.

scattering properties, changing contrast (Cohen et al., 1972). However, with well-thought out setup design such as contrast enhancing off-axis illumination, the optical changes of the cell have shown to be a useful (although limited) substitute to direct sensor imaging of transmembrane voltage (Burton et al., 2015). Although parameters such as action potential morphology cannot be accurately recovered, sensor free imaging allows non-invasive tracking of excitation waves through cellular monolayers, and simple integration with optogenetic actuators (Burton et al., 2015). More recently, there has been development of bioluminescent, rather than fluorescent GEVIs such as the FRET based LOTUS-V (Inagaki et al., 2017). As bioluminescent output is stimulated chemically by treatment with a substrate such as Furimazine rather than optically, no illumination is required. This avoids the need for spectral separation between any excitation light and actuators present and facilitates long-term voltage imaging. When expressed in human induced pluripotent stem cell cardiomyocytes, LOTUS-V has been shown to deliver comparable, action potential signals to the synthetic sensor di-8-ANEPPS, although values such as action potential duration were prolonged due to the slower response kinetics (milliseconds) of the FRET response compared to the 'fast' synthetic sensors (Inagaki et al., 2017). The use of bioluminescent sensors in all-optical setups may therefore provide an attractive alternative to fluorescent GEVIs.

Additionally, novel non-genetic techniques for optical cardiac excitation based on graphene substrates (Savchenko et al., 2018), x-ray and ultrasound activated nanoparticles (Berry et al., 2015), or infrared induced temperature gradients (McPheeters et al., 2017) can act as a solution to spectral overlap and to realize deep tissue activation. These optical pacing strategies, however, do not share some of the unique advantages that genetically induced optical de- and hyperpolarization allows, most prominently precise control over wave dynamics or cell-specific activation.

Imaging

As with many other areas of the life sciences, cardiac optical mapping has benefitted from continued advancement of camera technology. Photodiode arrays (PDAs) were utilized in the early optical mapping experiments that moved beyond single photomultiplier tubes (Salama et al., 1987). PDAs benefit from a large dynamic range (as the PDA is made up of large individual diodes) and enhanced sampling rates. Low fractional changes in sensor fluorescence and the sub millisecond dynamics of cardiac electrical activity make these invaluable features for successful optical mapping (Efimov and Salama, 2012).

However, due to the physical arrangement of individual diodes, the maximal spatial resolution of a PDA is more limited compared to charge-coupled device (CCD) and complementary metal oxide semiconductor (CMOS) cameras. In modern setups therefore, CCD and CMOS cameras dominate (Gloschat et al., 2018; Wen et al., 2018). Developments such as electron-multiplication in CCD cameras, and 2nd generation back illuminated 'scientific' CMOS cameras have helped improve dynamic ranges and noise levels of these cameras, while enhanced compatibility with standard computer interfaces such as USB-3 help alleviate previously prohibitive costs (Boukens and Efimov, 2014). Crucially, these cameras offer much higher spatial resolutions than possible with PDAs, capable of capturing > 10,000 pixel images at kHz sampling rates (Yu et al., 2017). The choice of imaging device for an all-optical setup does not differ considerably from a traditional optical mapping setup, and PDAs, CCD cameras and CMOS cameras have all been successfully utilized. Another important consideration is quantum efficiency of imaging devices in the far-red to near infrared wavelengths, if using red-shifted sensors.

Dual Voltage–Calcium All Optical Setups

Optical mapping of preparations dual loaded with both voltage and calcium sensors offers unique insights into the interplay between the cardiac action potential and Ca^{2+} handling (Myles et al., 2012). Achieving dual voltage-calcium optical mapping requires careful consideration of sensors spectra and filtering requirements. Addition of optical actuation, with its unique spectral, spatial, and temporal illumination requirements, further complicates the setup. Therefore to date, optical setups utilizing both voltage and calcium sensors have been shown to image the two indicators separately or sequentially (Klimas et al., 2016). In all-optical setups with simultaneous voltage-calcium imaging and optical pacing, spatial separation was necessary between pacing site and imaged area (Dempsey et al., 2016).

Computational Post-processing

In lieu of physical methods, computational methods can be used to overcome the spectral congestion that arises from optogenetic manipulation of optically mapped samples. However, it is important to note that these do not overcome undesired modulation of the membrane potential. A simple example is automatic identification and removal of optical pacing peaks by the application of several filters (Feola et al., 2017) or image frame removal (O'Shea et al., 2019). This is an effective strategy providing filtering/frame removal does not alter the fluorescence signal properties at pertinent times, and so ideally requires either temporal or spatial separation between pulsing peaks and fluorescence output.

Light pulses, however, can be more prohibitive to optical mapping analysis if pulses are applied during relevant phases of the cardiac cycle. For example, when pulses of light are delivered during the plateau and repolarization of the action potential, despite optical filtering attempts to avoid crosstalk, blue and green pulses can cause baseline shift in OAPs. As demonstrated by Park et al. (2014), to compensate for this, 'gap compensation' modeling procedures can be implemented. Briefly, this involves construction of a perturbation model of the optical emission ($F_{bluepulse}$) like shown in Equation 1

$$F_{bluepulse} = F_{fit} + A.\left[e^{-\frac{\left(t-t_{pulse}\right)}{\tau_{slow}}} - e^{-\frac{\left(t-t_{pulse}\right)}{\tau_{fast}}}\right]^2 \quad (1)$$

where F_{fit} is the model of a control action potential without blue light illumination, A is a constant, t is time, t_{pulse} is start time of the light pulse, and τ_{slow} and τ_{fast} are decay constants. The repolarization phase of the perturbed OAP

therefore is modeled by least square fitting a bi-exponential decay from the start of the blue light pulse allowing recovery of the OAP during optogenetically induced action potential prolongation (Park et al., 2014).

CONTACTLESS ACTUATION AND ELECTROPHYSIOLOGY

Both in basic research and clinically, electrode-based techniques for pacing and stimulation require direct or close contact to cardiac tissue. Although extensively exploited and effective, these actuation methods are not without limitation. The direct contact between electrodes and tissue can promote electrochemical reactions and reactive oxygen species formation. Conversely in some situations, for example in cardioversion strategies (Nyns et al., 2017) or in cardiomyocyte monolayers to improve signal quality (Lapp et al., 2017), simultaneous activation of the large areas is desired rather than at a single site. If the activation region needs to be changed then electrodes must be physically moved, limiting spatial flexibility and throughput. From a clinical perspective, implantable pacemaker and defibrillation devices are highly energy consuming, tissue damaging, prone to post-implantation complications and can cause psychological distress and reduced quality of life (Bruegmann et al., 2016; Israelsson et al., 2018).

Optogenetic pacing therefore is one of a few biological strategies being explored as a replacement for traditional pacemaker devices (Rosen et al., 2011) but undoubtably its most immediate beneficial quality is the ability realize unique basic research possibilities. Optogenetic opsins can be delivered to specific cell types (Hulsmans et al., 2017; Wang et al., 2017), providing novel research strategies, and promoting precise, repeatable and coordinated activation patterns. Conversely, by changing illumination conditions or the spatial arrangement of opsins expression, simultaneous excitation/suppression of large areas can be achieved. This can be applied in cellular monolayers, where concurrent activation can enhance signal quality, or in cardioversion strategies to terminate arrhythmias (Bruegmann et al., 2018). Contactless actuation avoids tissue damage due to the lack of tissue-electrode interface and can be realized in high-throughput applications such as multi-well cellular assays, discussed in more detail later (Klimas et al., 2016).

Optical mapping offers several clear advantages compared to electrode recording techniques. The spatial resolution achievable with optical mapping systems greatly outperforms multi-electrode array mapping systems. Furthermore, optical imaging can allow detailed, direct and multi-parameter investigation of voltage and calcium dynamics, whereas electrode techniques often make indirect measurements such as field potentials, where signals can be corrupted by noise and can alter significantly over time due to changes in electrode positioning or the maintenance of contact. Therefore, despite some notable disadvantages of optical study including requirement of contraction uncouplers and inability to perform *in vivo* experiments (Boukens and Efimov, 2014), optical mapping techniques have seen growing use, even prior to transformative capabilities of optical stimulation was made available. The recent combination of actuation and measurement in all-optical setups has therefore, in a relatively short timeframe, delivered remarkable insights into optogenetic pacing (Nussinovitch and Gepstein, 2015a), cell targeting (Wang et al., 2017) and arrhythmia termination (Feola et al., 2017); advancing basic understand and enhancing the prospect of future clinically relevant optical therapies.

EFFECTS OF LIGHT PACING ON ACTION POTENTIAL MORPHOLOGY AND PROPAGATION

For further implementation of optogenetic technologies, detailed understanding of whether optogenetic actuation affects cardiac electrical signal morphology is required. All-optical systems are uniquely advantageous for such investigations, as they are able to report key EP signal parameters for comparison against established techniques, while also providing high spatio-temporal recording of cardiac activation (Entcheva and Bub, 2016).

Recent work using human stem cell-derived cardiomyocytes expressing commercial optogenetic constructs OptoPatch and CaViar have demonstrated that optogenetic modulation does not significantly alter single cell electrophysiological properties (Björk et al., 2017). Furthermore, optogenetic manipulation of neonatal rat ventricular myocyte monolayers expressing ChR2 indicate unaltered conduction velocity, action potential duration and upstroke velocity compared to control cells, using either optogenetic or electrical actuation (Li et al., 2017). Computational insights have for the most part agreed with experimental findings by showing similar action potential morphologies and cell type dependent variability (Williams and Entcheva, 2015). Nevertheless, fundamental differences in electrical and optogenetic stimulation exist. Electrical current injection is traditionally achieved with a rectangular pulse delivered at short pulse widths of 2–10 ms (Myles et al., 2012; Holmes et al., 2016). ChR2 photocurrent exhibits slower onset kinetics, meaning longer pulse timescales can be required to reach excitation threshold (Williams and Entcheva, 2015). The effects of these stimulation differences on *in vitro* and *in vivo* cardiac electrophysiology require further examination.

APPLICATIONS OF ALL OPTICAL CARDIAC ELECTROPHYSIOLOGY

All-optical systems, in their relatively short period of existence, have expanded our understanding of cardiac pathophysiology thanks to their high spatio-temporal resolution and unique ability for targeted tissue excitation. Indeed, by optically mapping voltage in transgenic mice expressing ChR2, threshold excitation and vulnerable areas for proarrhythmic focal ectopic activity has been determined (Zaglia et al., 2015). All-optical setups have allowed demonstration and potential for utility of ChR2 mediated resynchronization

(Nussinovitch and Gepstein, 2015a) and have crucially informed the production of local rather than global areas of conduction block using patterned illumination. The patterned illumination shows similar success in arrhythmia termination but at lower energy costs than global activation (Crocini et al., 2016; Feola et al., 2017). However, whether optogenetic approaches confer energy reduction benefits, over established and effective electrode technologies requires detailed assessment in future studies.

Previously, optical mapping of arrhythmia dynamics in whole hearts has allowed mechanistically driven choice of patterned illumination in an 'open-loop' fashion - information based on previous recordings being used to dictate illumination patterns. Although this proved similarly effective as global illumination, there is reliance on consentient arrhythmia dynamics between hearts (Crocini et al., 2016). However, recent advancements including utilization of DMD illumination technology and high-speed data recording have demonstrated the potential of 'closed-loop' all-optical EP. Here, conduction disorders such as atrioventricular block can be detected by optical mapping and corrected by optical stimulation of ChR2 in real time. Real-time intervention can also conversely be used to setup and then study conduction abnormalities such as re-entry. These abilities make 'closed-loop' systems potentially vital going forward, allowing all-optical research in experimental models that is tunable in a manner hitherto only afforded by computational modeling, and at much reduced timescales (Scardigli et al., 2018). Similarly, all-optical control and output has shown the feasibility of engineering bioelectric tissues capable of complex information processing and in which all constituent parts are fully characterized (McNamara et al., 2016).

A major avenue for use of all-optical setups is the delivery of high-throughput platforms for cardiotoxicity screenings of candidate drug compounds (Klimas et al., 2016; Streit and Kleinlogel, 2018). These platforms are crucial in the context of the comprehensive *in vitro* pro-arrhythmia assay (CiPA) initiative – the recognition that cardiotoxicity screening should not focus solely on hERG channel interactions and must use experimental as well as computational methods (Fermini et al., 2016). All-optical methods are distinctly suited to the changing requirements of cardiotoxicity drug screening. As highlighted, the lack of requirement for direct contact makes optical actuation and optical recording much easier to scale to high-throughput parallelized applications, crucial for screening multiple drugs. As the reported voltage signals result from the sum of all ionic currents, significant alterations in any channel or pump function (not just hERG/I_{Kr}) in response to a drug will be evident, while Ca^{2+} handling abnormalities can also be screened with the use of appropriate sensors (Dempsey et al., 2016; Klimas et al., 2016). If specific channels warrant further investigation, all-optical methods can still be utilized by expression of channels in cells otherwise void of the ionic channels of interest (Streit and Kleinlogel, 2018), and the scalability of optical methods means analysis of other models apart from cell cultures may be achievable in the near future.

CONCLUSION AND FUTURE DIRECTIONS

Optogenetics is a technique that has developed into an immensely useful tool in basic cardiac research with clear, though as of yet unrealized, clinical potential (Entcheva, 2013). Fusion of optogenetics with optical mapping has been made possible by the substantial technical considerations and advances summarized in this review. All-optical electrophysiology, and indeed the field of cardiac optogenetics in general, however, remains a relatively new technique with several opportunities to further advance our understanding of electrical function in the heart.

Recent demonstration of 'closed-loop' all-optical investigation opens up a plethora of exciting opportunities for application of this exciting technology to key research questions, relevant in health and disease. 'Closed-loop' all-optical investigation studies could deliver faster, more physiologically relevant tools than even the most sophisticated computational cardiac models.

In contrast to cardiac research, optogenetics is widespread in neuroscience (Adamantidis, 2015). Effects on heart function and coupling of neurons and cardiac cells are often measured outcomes of neuromodulation. However, cardiac effects of optical neuromodulation are potentially limited to simply beating rate measurements (Nussinovitch and Gepstein, 2015b) or monitored using traditional techniques, with only isolated examples of optical mapping neuronal-cardiac effects (Dong et al., 2016). The combination of optical neuromodulation with all-optical cardiac electrophysiology could deliver unique insights into control of the heart by the nervous system (Wengrowski et al., 2015).

For optogenetic-based therapy to ever be realized in clinical practice, several technological and biological advances need to be implemented. These include novel methods for light and gene delivery to *in vivo* cardiac tissue, wireless control of implantable devices (Gagnon et al., 2017), and advanced materials uniquely designed for use in bio-integrated electronic circuits (Fang et al., 2016). However, regardless of future clinical utility, implementation of optogenetics in all-optical imaging systems has already proved a unique and transformative tool for cardiac research and will continue to be used in the study of the physiology and pathophysiology of the heart.

AUTHOR CONTRIBUTIONS

CO prepared the primary manuscript. AH, JW, JC, PK, LF, KR, and DP critically revised the manuscript. XO, RD, and SH provided intellectual content and technical insights. CO, JW, and DP produced the figures.

FUNDING

This work was funded by the EPSRC studentship (Sci-Phy-4-Health Centre for Doctoral Training L016346) to DP, KR, and LF, Wellcome Trust Seed Award Grant (109604/Z/15/Z) to DP, British Heart Foundation Grants

(PG/17/55/33087 and RG/17/15/33106) to DP, European Union [Grant Agreement No. 633196 (CATCH ME) to PK and LF], British Heart Foundation (FS/13/43/30324 to PK and LF; PG/17/30/32961 to PK and AH), and Leducq Foundation to PK. JW is supported by the British Heart Foundation (FS/16/35/31952).

REFERENCES

Abilez, O. J., Wong, J., Prakash, R., Deisseroth, K., Zarins, C. K., and Kuhl, E. (2011). Multiscale computational models for optogenetic control of cardiac function. *Biophys. J.* 101, 1326–1334. doi: 10.1016/j.bpj.2011.08.004

Adamantidis, A. (2015). Optogenetics: 10 years after ChR2 in neurons—views from the community. *Nat. Neurosci.* 18, 1213–1225. doi: 10.1038/nn.4091

Alfonsa, H., Merricks, E. M., Codadu, N. K., Cunningham, M. O., Deisseroth, K., Racca, C., et al. (2015). The contribution of raised intraneuronal chloride to epileptic network activity. *J. Neurosci.* 35, 7715–7726. doi: 10.1523/JNEUROSCI.4105-14.2015

Ambrosi, C. M., Boyle, P. M., Chen, K., Trayanova, N. A., and Entcheva, E. (2015). Optogenetics-enabled assessment of viral gene and cell therapy for restoration of cardiac excitability. *Sci. Rep.* 5:17350. doi: 10.1038/srep17350

Ambrosi, C. M., Sadananda, G., Klimas, A., and Entcheva, E. (2019). Adeno-associated virus mediated gene delivery: implications for scalable in vitro and in vivo cardiac optogenetic models. (in press). doi: 10.3389/fphys.2019.00168

Arrenberg, A. B., Stainier, D. Y. R., Baier, H., and Huisken, J. (2010). Optogenetic control of cardiac function. *Science* 330, 971–974. doi: 10.1126/science.1195929

Bamann, C., Gueta, R., Kleinlogel, S., Nagel, G., and Bamberg, E. (2010). Structural guidance of the photocycle of channelrhodopsin-2 by an interhelical hydrogen bond. *Biochemistry* 49, 267–278. doi: 10.1021/bi901634p

Beacher, J. (2008). LEDs for fluorescence microscopy. *Biophotonics Int.* 5324, 208–215. doi: 10.1117/12.525932

Bera, A., and Sen, D. (2017). Promise of adeno-associated virus as a gene therapy vector for cardiovascular diseases. *Heart Fail. Rev.* 22, 795–823. doi: 10.1007/s10741-017-9622-7

Bernal Sierra, Y. A., Rost, B. R., Pohfahl, M., Fernandes, A. M., Kopton, R. A., Moser, S., et al. (2018). Potassium channel-based optogenetic silencing. *Nat. Commun.* 9:4611. doi: 10.1038/s41467-018-07038-8

Berndt, A., Lee, S. Y., Ramakrishnan, C., and Deisseroth, K. (2014). Structure-guided transformation of channelrhodopsin into a light-activated chloride channel. *Science* 344, 420–424. doi: 10.5061/dryad.9r0p6

Berndt, A., Schoenenberger, P., Mattis, J., Tye, K. M., Deisseroth, K., Hegemann, P., et al. (2011). High-efficiency channelrhodopsins for fast neuronal stimulation at low light levels. *Proc. Natl. Acad. Sci. U.S.A.* 108, 7595–7600. doi: 10.1073/pnas.1017210108

Berry, R., Getzin, M., Gjesteby, L., and Wang, G. (2015). X-optogenetics and U-optogenetics: feasibility and possibilities. *Photonics* 2, 23–39. doi: 10.3390/photonics2010023

Bingen, B. O., Engels, M. C., Schalij, M. J., Jangsangthong, W., Neshati, Z., Feola, I., et al. (2014). Light-induced termination of spiral wave arrhythmias by optogenetic engineering of atrial cardiomyocytes. *Cardiovasc. Res.* 104, 194–205. doi: 10.1093/cvr/cvu179

Björk, S., Ojala, E. A., Nordström, T., Ahola, A., Liljeström, M., Hyttinen, J., et al. (2017). Evaluation of optogenetic electrophysiology tools in human stem cell-derived cardiomyocytes. *Front. Physiol.* 8:884. doi: 10.3389/fphys.2017.00884

Boukens, B. J., and Efimov, I. R. (2014). A century of optocardiography. *IEEE Rev. Biomed. Eng.* 7, 115–125. doi: 10.1109/RBME.2013.2286296

Boyden, E. S., Zhang, F., Bamberg, E., Nagel, G., and Deisseroth, K. (2005). Millisecond-timescale, genetically targeted optical control of neural activity. *Nat. Neurosci.* 8, 1263–1268. doi: 10.1038/nn1525

Broyles, C., Robinson, P., and Daniels, M. (2018). Fluorescent, bioluminescent, and optogenetic approaches to study excitable physiology in the single cardiomyocyte. *Cells* 7:E51. doi: 10.3390/cells7060051

Bruegmann, T., Beiert, T., Vogt, C. C., Schrickel, J. W., and Sasse, P. (2018). Optogenetic termination of atrial fibrillation in mice. *Cardiovasc. Res.* 114, 713–723. doi: 10.1093/cvr/cvx250

Bruegmann, T., Boyle, P. M., Vogt, C. C., Karathanos, T. V., Arevalo, H. J., Fleischmann, B. K., et al. (2016). Optogenetic defibrillation terminates ventricular arrhythmia in mouse hearts and human simulations. *J. Clin. Invest.* 126, 3894–3904. doi: 10.1172/JCI88950

Bruegmann, T., Malan, D., Hesse, M., Beiert, T., Fuegemann, C. J., Fleischmann, B. K., et al. (2010). Optogenetic control of heart muscle in vitro and in vivo. *Nat. Methods* 7, 897–900. doi: 10.1038/nmeth.1512

Burton, R. A. B., Klimas, A., Ambrosi, C. M., Tomek, J., Corbett, A., Entcheva, E., et al. (2015). Optical control of excitation waves in cardiac tissue. *Nat. Photonics* 9, 813–816. doi: 10.1038/nphoton.2015.196

Chang, Y. F., Broyles, C. N., Brook, F. A., Davies, M. J., Turtle, C. W., Nagai, T., et al. (2017). Non-invasive phenotyping and drug testing in single cardiomyocytes or beta-cells by calcium imaging and optogenetics. *PLoS One* 12:e0174181. doi: 10.1371/journal.pone.0174181

Cohen, L. B., Keynes, R. D., and Landowne, D. (1972). Changes in axon light scattering that accompany the action potential: current-dependent components. *J. Physiol.* 224, 727–752. doi: 10.1113/jphysiol.1972.sp009920

Crocini, C., Ferrantini, C., Coppini, R., Scardigli, M., Yan, P., Loew, L. M., et al. (2016). Optogenetics design of mechanistically-based stimulation patterns for cardiac defibrillation. *Sci. Rep.* 6:35628. doi: 10.1038/srep35628

Crocini, C., Ferrantini, C., Pavone, F. S., and Sacconi, L. (2017). Optogenetics gets to the heart: a guiding light beyond defibrillation. *Prog. Biophys. Mol. Biol.* 130, 132–139. doi: 10.1016/j.pbiomolbio.2017.05.002

Dawydow, A., Gueta, R., Ljaschenko, D., Ullrich, S., Hermann, M., Ehmann, N., et al. (2014). Channelrhodopsin-2-XXL, a powerful optogenetic tool for low-light applications. *Proc. Natl. Acad. Sci. U.S.A.* 111, 13972–13977. doi: 10.1073/pnas.1408269111

Dempsey, G. T., Chaudhary, K. W., Atwater, N., Nguyen, C., Brown, B. S., McNeish, J. D., et al. (2016). Cardiotoxicity screening with simultaneous optogenetic pacing, voltage imaging and calcium imaging. *J. Pharmacol. Toxicol. Methods* 81, 240–250. doi: 10.1016/j.vascn.2016.05.003

Dong, X., Tung, L., Huganir, R., Dong, X., Lee, G., and Lee, G. (2016). Functional coupling with cardiac muscle promotes maturation of hPSC-derived sympathetic neurons. *Cell Stem Cell* 19, 95–106. doi: 10.1016/j.stem.2016.05.002

Efimov, I. R., and Salama, G. (2012). The future of optical mapping is bright RE?: review on?: " Optical imaging of voltage and calcium in cardiac cells and tissues" by Herron, Lee, and Jalife. *Circ. Res.* 10, e70–e71. doi: 10.1161/CIRCRESAHA.112.270033

Entcheva, E. (2013). Cardiac optogenetics. *AJP Heart Circ. Physiol.* 304, H1179–H1191. doi: 10.1152/ajpheart.00432.2012

Entcheva, E., and Bub, G. (2016). All-optical control of cardiac excitation: combined high-resolution optogenetic actuation and optical mapping. *J. Physiol.* 9, 2503–2510. doi: 10.1113/JP271559

Fang, H., Zhao, J., Yu, K. J., Song, E., Farimani, A. B., Chiang, C.-H., et al. (2016). Ultrathin, transferred layers of thermally grown silicon dioxide as biofluid barriers for biointegrated flexible electronic systems. *Proc. Natl. Acad. Sci. U.S.A.* 113, 11682–11687. doi: 10.1073/pnas.1605269113

Fast, V. G., and Kléber, A. G. (1994). Anisotropic conduction in monolayers of neonatal rat heart cells cultured on collagen substrate. *Circ. Res.* 75, 591–595. doi: 10.1161/01.RES.75.3.591

Feola, I., Volkers, L., Majumder, R., Teplenin, A., Schalij, M. J., Panfilov, A. V., et al. (2017). Localized optogenetic targeting of rotors in atrial cardiomyocyte monolayers. *Circ. Arrhythm. Electrophysiol.* 10:e005591. doi: 10.1161/CIRCEP.117.005591

Fermini, B., Hancox, J. C., Abi-Gerges, N., Bridgland-Taylor, M., Chaudhary, K. W., Colatsky, T., et al. (2016). A new perspective in the field of cardiac safety testing through the comprehensive in vitro proarrhythmia assay paradigm. *J. Biomol. Screen.* 21, 1–11. doi: 10.1177/1087057115594589

Gagnon, L. L., Gagnon-Turcotte, G., Popek, A., Chatelier, A., Chahine, M., and Gosselin, B. (2017). "A wireless system for combined heart optogenetics and electrocardiography recording," in *Proceedings of the IEEE International Symposium on Circuits and Systems (ISCAS)*, (Piscataway, NJ: IEEE), 1–4. doi: 10.1109/ISCAS.2017.8050365

Gloschat, C., Aras, K., Gupta, S., Faye, N. R., Zhang, H., Syunyaev, R. A., et al. (2018). RHYTHM: an open source imaging toolkit for cardiac panoramic optical mapping. *Sci. Rep.* 8:2921. doi: 10.1038/s41598-018-21333-w

Govorunova, E. G., Cunha, S. R., Sineshchekov, O. A., and Spudich, J. L. (2016). Anion channelrhodopsins for inhibitory cardiac optogenetics. *Sci. Rep.* 6:33530. doi: 10.1038/srep33530

Govorunova, E. G., Sineshchekov, O. A., Janz, R., Liu, X., and Spudich, J. L. (2015). Natural light-gated anion channels: a family of microbial rhodopsins for advanced optogenetics. *Science* 349, 647–650. doi: 10.1126/science.aaa7484

Herron, T. J., Lee, P., and Jalife, J. (2012). Optical imaging of voltage and calcium in cardiac cells & tissues. *Circ. Res.* 110, 609–623. doi: 10.1161/CIRCRESAHA.111.247494

Hochbaum, D. R., Zhao, Y., Farhi, S. L., Klapoetke, N., Werley, C. A., Kapoor, V., et al. (2014). All-optical electrophysiology in mammalian neurons using engineered microbial rhodopsins. *Nat. Methods* 11, 825–833. doi: 10.1038/NMETH.3000

Holmes, A. P., Yu, T. Y., Tull, S., Syeda, F., Kuhlmann, S. M., O'Brien, S.-M., et al. (2016). A regional reduction in Ito and IKACh in the Murine posterior left atrial myocardium is associated with action potential prolongation and increased Ectopic activity. *PLoS One* 11:e0154077. doi: 10.1371/journal.pone.0154077

Hou, J. H., Kralj, J. M., Douglass, A. D., Engert, F., and Cohen, A. E. (2014). Simultaneous mapping of membrane voltage and calcium in zebrafish heart *in vivo* reveals chamber-specific developmental transitions in ionic currents. *Front. Physiol.* 5:344. doi: 10.3389/fphys.2014.00344

Hulsmans, M., Clauss, S., Xiao, L., Aguirre, A. D., King, K. R., Hanley, A., et al. (2017). Macrophages facilitate electrical conduction in the heart. *Cell* 169, 510–522.e20. doi: 10.1016/j.cell.2017.03.050

Inagaki, S., Tsutsui, H., Suzuki, K., Agetsuma, M., Arai, Y., Jinno, Y., et al. (2017). Genetically encoded bioluminescent voltage indicator for multi-purpose use in wide range of bioimaging. *Sci. Rep.* 7:42398. doi: 10.1038/srep42398

Israelsson, J., Thylén, I., Strömberg, A., Bremer, A., and Årestedt, K. (2018). Factors associated with health-related quality of life among cardiac arrest survivors treated with an implantable cardioverter-defibrillator. *Resuscitation* 132, 78–84. doi: 10.1016/j.resuscitation.2018.09.002

Jaimes, R., Walton, R. D., Pasdois, P., Bernus, O., Efimov, I. R., and Kay, M. W. (2016). A technical review of optical mapping of intracellular calcium within myocardial tissue. *Am. J. Physiol. Heart Circ. Physiol.* 310, H1388–H1401. doi: 10.1152/ajpheart.00665.2015

Jalife, J. (2003). Rotors and spiral waves in atrial fibrillation. *J. Cardiovasc. Electrophysiol.* 14, 776–780. doi: 10.1046/j.1540-8167.2003.03136.x

Jia, Z., Valiunas, V., Lu, Z., Bien, H., Liu, H., Wang, H. Z., et al. (2011). Stimulating cardiac muscle by light cardiac optogenetics by cell delivery. *Circ. Arrhythmia Electrophysiol.* 4, 753–760. doi: 10.1161/CIRCEP.111.964247

Kaestner, L., Tian, Q., Kaiser, E., Xian, W., Müller, A., Oberhofer, M., et al. (2015). Genetically encoded voltage indicators in circulation research. *Int. J. Mol. Sci.* 16, 21626–21642. doi: 10.3390/ijms160921626

Kanaporis, G. (2012). Optical mapping at increased illumination intensities. *J. Biomed. Opt.* 17:096007. doi: 10.1117/1.JBO.17.9.096007

Kandori, H. (2015). Ion-pumping microbial rhodopsins. *Front. Mol. Biosci.* 2:52. doi: 10.3389/fmolb.2015.00052

Karathanos, T. V., Bayer, J. D., Wang, D., Boyle, P. M., and Trayanova, N. A. (2016). Opsin spectral sensitivity determines the effectiveness of optogenetic termination of ventricular fibrillation in the human heart: a simulation study. *J. Physiol.* 594, 6879–6891. doi: 10.1113/JP271739

Karathanos, T. V., Boyle, P. M., and Trayanova, N. A. (2014). Optogenetics-enabled dynamic modulation of action potential duration in atrial tissue: feasibility of a novel therapeutic approach. *Europace* 16, iv69–iv76. doi: 10.1093/europace/euu250

Kato, H. E., Kim, Y. S., Paggi, J. M., Evans, K. E., Allen, W. E., Richardson, C., et al. (2018). Structural mechanisms of selectivity and gating in anion channelrhodopsins. *Nature* 561, 349–354. doi: 10.1038/s41586-018-0504-5

Kim, Y. S., Kato, H. E., Yamashita, K., Ito, S., Inoue, K., Ramakrishnan, C., et al. (2018). Crystal structure of the natural anion-conducting channelrhodopsin GtACR1. *Nature* 561, 343–348. doi: 10.1038/s41586-018-0511-6

Kleinlogel, S., Feldbauer, K., Dempski, R. E., Fotis, H., Wood, P. G., Bamann, C., et al. (2011). Ultra light-sensitive and fast neuronal activation with the Ca2+-permeable channelrhodopsin CatCh. *Nat. Neurosci.* 14, 513–518. doi: 10.1038/nn.2776

Klimas, A., Ambrosi, C. M., Yu, J., Williams, J. C., Bien, H., and Entcheva, E. (2016). OptoDyCE as an automated system for high-throughput all-optical dynamic cardiac electrophysiology. *Nat. Commun.* 7:11542. doi: 10.1038/ncomms11542

Klimas, A., and Entcheva, E. (2014). Toward microendoscopy-inspired cardiac optogenetics *in vivo*?: technical overview and perspective. *J. Biomed. Opt.* 19:080701. doi: 10.1117/1.JBO.19.8.080701

Knollmann, B. C. (2010). Pacing lightly: optogenetics gets to the heart. *Nat. Methods* 7, 889–891. doi: 10.1038/nmeth1110-889

Koopman, C. D., Zimmermann, W. H., Knöpfel, T., and de Boer, T. P. (2017). Cardiac optogenetics: using light to monitor cardiac physiology. *Basic Res. Cardiol.* 112:56. doi: 10.1007/s00395-017-0645-y

Lam, P. Y., Mendu, S. K., Mills, R. W., Zheng, B., Padilla, H., Milan, D. J., et al. (2017). A high-conductance chemo-optogenetic system based on the vertebrate channel Trpa1b. *Sci. Rep.* 7:11839. doi: 10.1038/s41598-017-11791-z

Lapp, H., Bruegmann, T., Malan, D., Friedrichs, S., Kilgus, C., Heidsieck, A., et al. (2017). Frequency-dependent drug screening using optogenetic stimulation of human iPSC-derived cardiomyocytes. *Sci. Rep.* 7:9629. doi: 10.1038/s41598-017-09760-7

Li, Q., Ni, R. R., Hong, H., Goh, K. Y., Rossi, M., Fast, V. G., et al. (2017). Electrophysiological properties and viability of neonatal rat ventricular myocyte cultures with inducible ChR2 expression. *Sci. Rep.* 7:1531. doi: 10.1038/s41598-017-01723-2

Liao, M. L. C., De Boer, T. P., Mutoh, H., Raad, N., Richter, C., Wagner, E., et al. (2015). sensing cardiac electrical activity with a cardiac myocyte-targeted optogenetic voltage indicator. *Circ. Res.* 117, 401–412. doi: 10.1161/CIRCRESAHA.117.306143

Lin, J. Y. (2010). A user's guide to channelrhodopsin variants: features, limitations and future developments. *Exp. Physiol.* 96, 19–25. doi: 10.1113/expphysiol.2009.051961

Lin, J. Y., Knutsen, P. M., Muller, A., Kleinfeld, D., and Tsien, R. Y. (2013). ReaChR: a red-shifted variant of channelrhodopsin enables deep transcranial optogenetic excitation. *Nat. Neurosci.* 16, 1499–1508. doi: 10.1038/nn.3502

Lin, J. Y., Lin, M. Z., Steinbach, P., and Tsien, R. Y. (2009). Characterization of engineered channelrhodopsin variants with improved properties and kinetics. *Biophys. J.* 96, 1803–1814. doi: 10.1016/j.bpj.2008.11.034

Loew, L. M., Bonneville, G. W., and Surow, J. (1978). Charge shift optical probes of membrane potential. *Biochemistry* 17, 4065–4071. doi: 10.1021/bi00612a030

Majumder, R., Feola, I., Teplenin, A. S., Antoine, A. F., Vries, D., Pan, A. V., et al. (2018). Optogenetics enables real-time spatiotemporal control over spiral wave dynamics in an excitable cardiac system. *eLife* 7:e41076. doi: 10.7554/eLife.41076

Matiukas, A., Mitrea, B. G., Qin, M., Pertsov, A. M., Shvedko, A. G., Warren, M. D., et al. (2007). Near infrared voltage sensitive fluorescent dyes optimized for optical mapping in blood-perfused myocardium. *Heart Rhythm.* 4, 1441–1451. doi: 10.1037/a0018493.Understanding

McNamara, H. M., Zhang, H., Werley, C. A., and Cohen, A. E. (2016). Optically controlled oscillators in an engineered bioelectric tissue. *Phys. Rev. X* 6:031001. doi: 10.1103/PhysRevX.6.031001

McPheeters, M. T., Wang, Y. T., Werdich, A. A., Jenkins, M. W., and Laurita, K. R. (2017). An infrared optical pacing system for screening cardiac electrophysiology in human cardiomyocytes. *PLoS One* 12:e0183761. doi: 10.1371/journal.pone.0183761

Mickoleit, M., Schmid, B., Weber, M., Fahrbach, F. O., Hombach, S., Reischauer, S., et al. (2014). High-resolution reconstruction of the beating zebrafish heart. *Nat. Methods* 11, 919–922. doi: 10.1038/nmeth.3037

Miller, E. W. (2016). Small molecule fluorescent voltage indicators for studying membrane potential. *Curr. Opin. Chem. Biol.* 33, 74–80. doi: 10.1016/j.cbpa.2016.06.003

Myles, R. C., Wang, L., Kang, C., Bers, D. M., and Ripplinger, C. M. (2012). Local β-adrenergic stimulation overcomes source-sink mismatch to generate focal arrhythmia. *Circ. Res.* 110, 1454–1464. doi: 10.1161/CIRCRESAHA.111.262345

Nagel, G., Brauner, M., Liewald, J. F., Adeishvili, N., Bamberg, E., and Gottschalk, A. (2005). Light activation of channelrhodopsin-2 in excitable cells of caenorhabditis elegans triggers rapid behavioral responses. *Curr. Biol.* 15, 2279–2284. doi: 10.1016/j.cub.2005.11.032

Nagel, G., Szellas, T., Huhn, W., Kateriya, S., Adeishvili, N., Berthold, P., et al. (2003). Channelrhodopsin-2, a directly light-gated cation-selective membrane channel. *Proc. Natl. Acad. Sci. U.S.A.* 100, 13940–13945. doi: 10.1073/pnas.1936192100

Nussinovitch, U., and Gepstein, L. (2015a). Optogenetics for in vivo cardiac pacing and resynchronization therapies. *Nat. Biotechnol.* 33, 750–754. doi: 10.1038/nbt.3268

Nussinovitch, U., and Gepstein, L. (2015b). Optogenetics for suppression of cardiac electrical activity in human and rat cardiomyocyte cultures. *Neurophotonics* 2:031204. doi: 10.1117/1.NPh.2.3.031204

Nussinovitch, U., Shinnawi, R., and Gepstein, L. (2014). Modulation of cardiac tissue electrophysiological properties with light-sensitive proteins. *Cardiovasc. Res.* 102, 176–187. doi: 10.1093/cvr/cvu037

Nyns, E. C. A., Kip, A., Bart, C. I., Plomp, J. J., Zeppenfeld, K., Schalij, M. J., et al. (2017). Optogenetic termination of ventricular arrhythmias in the whole heart: towards biological cardiac rhythm management. *Eur. Heart J.* 38, 2132–2136. doi: 10.1093/eurheartj/ehw574

O'Shea, C., Holmes, A. P., Yu, T. Y., Winter, J., Wells, S. P., Correia, J., et al. (2019). ElectroMap: High-throughput open-source software for analysis and mapping of cardiac electrophysiology. *Sci. Rep.* 9:1389. doi: 10.1038/s41598-018-38263-2

Park, S. A., Lee, S.-R., Tung, L., and Yue, D. T. (2014). Optical mapping of optogenetically shaped cardiac action potentials. *Sci. Rep.* 4:6125. doi: 10.1038/srep06125

Prando, V., Da Broi, F., Franzoso, M., Plazzo, A. P., Pianca, N., Francolini, M., et al. (2018). Dynamics of neuroeffector coupling at cardiac sympathetic synapses. *J. Physiol.* 11, 2055–2075. doi: 10.1113/JP275693

Quinn, T. A., Camelliti, P., Rog-Zielinska, E. A., Siedlecka, U., Poggioli, T., O'Toole, E. T., et al. (2016). Electrotonic coupling of excitable and nonexcitable cells in the heart revealed by optogenetics. *Proc. Natl. Acad. Sci. U.S.A.* 113, 14852–14857. doi: 10.1073/pnas.1611184114

Quiñonez Uribe, R. A., Luther, S., Diaz-maue, L., and Richter, C. (2018). Energy-reduced arrhythmia termination using global photostimulation in optogenetic murine hearts. *Front. Physiol.* 9:1651. doi: 10.3389/fphys.2018.01651

Rosen, M. R., Robinson, R. B., Brink, P. R., and Cohen, I. S. (2011). The road to biological pacing. *Nat. Rev. Cardiol.* 8, 656–666. doi: 10.1038/nrcardio.2011.120

Salama, G., Choi, B. R., Azour, G., Lavasani, M., Tumbev, V., Salzberg, B. M., et al. (2005). Properties of new, long-wavelength, voltage-sensitive dyes in the heart. *J. Membr. Biol.* 208, 125–140. doi: 10.1007/s00232-005-0826-8

Salama, G., Lombardi, R., and Elson, J. (1987). Maps of optical action potentials and NADH fluorescence in intact working hearts. *Am. J. Physiol. Circ. Physiol.* 252, H384–H394. doi: 10.1152/ajpheart.1987.252.2.H384

Savchenko, A., Cherkas, V., Liu, C., Braun, G. B., Kleschevnikov, A., Miller, Y. I., et al. (2018). Graphene biointerfaces for optical stimulation of cells. *Sci. Adv.* 4:eaat0351. doi: 10.1126/sciadv.aat0351

Scanziani, M., and Häusser, M. (2009). Electrophysiology in the age of light. *Nature* 461, 930–939. doi: 10.1038/nature08540

Scardigli, M., Müllenbroich, C., Margoni, E., Cannazzaro, S., Crocini, C., Ferrantini, C., et al. (2018). Real-time optical manipulation of cardiac conduction in intact hearts. *J. Physiol.* 596, 3841–3858. doi: 10.1113/JP276283

Schmieder, F., Büttner, L., Czarske, J., Torres, M. L., Heisterkamp, A., Klapper, et al. (2017). "Holographically generated structured illumination for cell stimulation in optogenetics," in *Proceedings of the International Society for Optical Engineering* (Amsterdam: Elsevier).

Schneider, F., Grimm, C., and Hegemann, P. (2015). Biophysics of channelrhodopsin. *Annu. Rev. Biophys.* 44, 167–186. doi: 10.1146/annurev-biophys-060414-034014

Shaheen, N., Shiti, A., Huber, I., Shinnawi, R., Arbel, G., Gepstein, A., et al. (2018). Human Induced pluripotent stem cell-derived cardiac cell sheets expressing genetically encoded voltage indicator for pharmacological and arrhythmia studies. *Stem Cell Reports* 10, 1879–1894. doi: 10.1016/j.stemcr.2018.04.006

Shinnawi, R., Huber, I., Maizels, L., Shaheen, N., Gepstein, A., Arbel, G., et al. (2015). Monitoring human-induced pluripotent stem cell-derived cardiomyocytes with genetically encoded calcium and voltage fluorescent reporters. *Stem Cell Reports* 5, 582–596. doi: 10.1016/j.stemcr.2015.08.009

Smith, A. M., Mancini, M. C., and Nie, S. (2009). Bioimaging: second window for in vivo imaging. *Nat. Nanotechnol.* 4, 710–711. doi: 10.1038/nnano.2009.326

Streit, J., and Kleinlogel, S. (2018). Dynamic all-optical drug screening on cardiac voltage-gated ion channels. *Sci. Rep.* 8:1153. doi: 10.1038/s41598-018-19412-z

Syeda, F., Holmes, A. P., Yu, T. Y., Tull, S., Kuhlmann, S. M., Pavlovic, D., et al. (2016). PITX2 modulates atrial membrane potential and the antiarrhythmic effects of sodium-channel blockers. *J. Am. Coll. Cardiol.* 68, 1881–1894. doi: 10.1016/j.jacc.2016.07.766

Vogt, C. C., Bruegmann, T., Malan, D., Ottersbach, A., Roell, W., Fleischmann, B. K., et al. (2015). Systemic gene transfer enables optogenetic pacing of mouse hearts. *Cardiovasc. Res.* 106, 338–343. doi: 10.1093/cvr/cvv004

Wang, K., Lee, P., Mirams, G. R., Sarathchandra, P., Borg, T. K., Gavaghan, D. J., et al. (2015). Cardiac tissue slices: preparation, handling, and successful optical mapping. *Am. J. Physiol. Heart Circ. Physiol.* 308, H1112–H1125. doi: 10.1152/ajpheart.00556.2014

Wang, Y., Lin, W. K., Crawford, W., Ni, H., Bolton, E. L., Khan, H., et al. (2017). Optogenetic control of heart rhythm by selective stimulation of cardiomyocytes derived from Pnmt + cells in Murine heart. *Sci. Rep.* 7:40687. doi: 10.1038/srep40687

Watanabe, M., Feola, I., Majumder, R., Jangsangthong, W., Teplenin, A. S., Ypey, D. L., et al. (2017). Optogenetic manipulation of anatomical re-entry by light-guided generation of a reversible local conduction block. *Cardiovasc. Res.* 113, 354–366. doi: 10.1093/cvr/cvx003

Wen, Q., Gandhi, K., Capel, R. A., Hao, G., O'Shea, C., Neagu, G., et al. (2018). Transverse cardiac slicing and optical imaging for analysis of transmural gradients in membrane potential and Ca2+ transients in murine heart. *J. Physiol.* 596, 3951–3965. doi: 10.1113/JP276239

Wengrowski, A. M., Wang, X., Tapa, S., Posnack, N. G., Mendelowitz, D., and Kay, M. W. (2015). Optogenetic release of norepinephrine from cardiac sympathetic neurons alters mechanical and electrical function. *Cardiovasc. Res.* 105, 143–150. doi: 10.1093/cvr/cvu258

Wietek, J., Wiegert, J. S., Adeishvili, N., Schneider, F., Watanabe, H., Tsunoda, S. P., et al. (2014). Conversion of channelrhodopsin into a light-gated chloride channel. *Science* 344, 409–412. doi: 10.1126/science.1249375

Williams, J. C., and Entcheva, E. (2015). Optogenetic versus electrical stimulation of human cardiomyocytes: modeling insights. *Biophys. J.* 108, 1934–1945. doi: 10.1016/j.bpj.2015.03.032

Winter, J., Bishop, M., Wilder, C., O'Shea, C., Pavlovic, D., and Shattock, M. J. (2018). Sympathetic nervous regulation of cardiac alternans in the intact heart. *Front. Physiol.* 9:16. doi: 10.3389/fphys.2018.00016

Xu, L., Gutbrod, S. R., Bonifas, A. P., Su, Y., Sulkin, M. S., Lu, N., et al. (2014). 3D multifunctional integumentary membranes for spatiotemporal cardiac measurements and stimulation across the entire epicardium. *Nat. Commun.* 5:3329. doi: 10.1038/ncomms4329

Yu, J., Chen, K., Lucero, R. V., Ambrosi, C. M., and Entcheva, E. (2015). Cardiac optogenetics: enhancement by all-trans-retinal. *Sci. Rep.* 5:16542. doi: 10.1038/srep16542

Yu, T. Y., Dehghani, H., Brain, K. L., Syeda, F., Holmes, A. P., Kirchhof, P., et al. (2017). Optical mapping design for murine atrial electrophysiology. *Comput. Methods Biomech. Biomed. Eng. Imaging Vis.* 5, 368–378. doi: 10.1080/21681163.2015.1081079

Yu, T. Y., Syeda, F., Holmes, A. P., Osborne, B., Dehghani, H., Brain, K. L., et al. (2014). An automated system using spatial oversampling for optical mapping in murine atria. Development and validation with monophasic and transmembrane action potentials. *Prog. Biophys. Mol. Biol.* 115, 340–348. doi: 10.1016/j.pbiomolbio.2014.07.012

Zaglia, T., Pianca, N., Borile, G., Da Broi, F., Richter, C., Campione, M., et al. (2015). Optogenetic determination of the myocardial requirements for extrasystoles by cell type-specific targeting of ChannelRhodopsin-2. *Proc. Natl. Acad. Sci. U.S.A.* 112, E4495–E4504. doi: 10.1073/pnas.1509380112

Zhu, Y. C., Uradu, H., Majeed, Z. R., and Cooper, R. L. (2016). Optogenetic stimulation of Drosophila heart rate at different temperatures and Ca2+ concentrations. *Physiol. Rep.* 4:e12695. doi: 10.14814/phy2.12695

Conflict of Interest Statement: The authors declare that the research was conducted in the absence of any commercial or financial relationships that could be construed as a potential conflict of interest.

frontiers in Physiology

ORIGINAL RESEARCH
published: 28 January 2019
doi: 10.3389/fphys.2019.00016

Sudden Heart Rate Reduction Upon Optogenetic Release of Acetylcholine From Cardiac Parasympathetic Neurons in Perfused Hearts

*Angel Moreno[1†], Kendal Endicott[2†], Matthew Skancke[2†], Mary Kate Dwyer[1], Jaclyn Brennan[1], Igor R. Efimov[1], Gregory Trachiotis[2], David Mendelowitz[3] and Matthew W. Kay[1]**

[1] Department of Biomedical Engineering, The George Washington University, Washington, DC, United States, [2] Division of Cardiothoracic Surgery, Veterans Affairs Medical Center, Washington, DC, United States, [3] Department of Pharmacology and Physiology, The George Washington University, Washington, DC, United States

OPEN ACCESS

Edited by:
Christopher Huang,
University of Cambridge,
United Kingdom

Reviewed by:
Elena Tolkacheva,
University of Minnesota Twin Cities,
United States
Alexey V. Glukhov,
University of Wisconsin System,
United States

***Correspondence:**
Matthew W. Kay
phymwk@gwu.edu

[†] These authors have contributed equally to this work

Specialty section:
This article was submitted to Cardiac Electrophysiology, a section of the journal Frontiers in Physiology

Received: 30 September 2018
Accepted: 10 January 2019
Published: 28 January 2019

Citation:
Moreno A, Endicott K, Skancke M, Dwyer MK, Brennan J, Efimov IR, Trachiotis G, Mendelowitz D and Kay MW (2019) Sudden Heart Rate Reduction Upon Optogenetic Release of Acetylcholine From Cardiac Parasympathetic Neurons in Perfused Hearts. Front. Physiol. 10:16. doi: 10.3389/fphys.2019.00016

The balance of sympathetic and parasympathetic tone provides exquisite control of heart rate and contractility and has also been shown to modulate coronary flow and inflammation. Understanding how autonomic balance is altered by cardiac disease is an active area of research, and developing new ways to control this balance provides insights into disease therapies. However, achieving acute neuron-specific stimulation of autonomic neurons can be difficult in experiments that measure the acute effects of nerve stimulation on the heart. Conventional electrical and pharmacological approaches can be spatially and temporally non-selective. Cell-specific expression of light-activated channels (channelrhodopsin, ChR2) is a powerful approach that enables control of the timing and distribution of cellular stimulation using light. We present such an optogenetic approach where parasympathetic cardiac neurons are selectively photoactivated at high temporal precision to initiate cholinergic-mediated slowing of heart rate. Mice were crossbred to express ChR2 in peripheral cholinergic neurons using Cre-Lox recombination driven by a choline acetyltransferase (ChAT) promoter. Hearts from adult mice were excised, perfused, and the epicardium was illuminated (peak 460–465 nm) to photoactivate ChR2. In one set of studies, hearts were illuminated using a large-field LED light source. In other studies, a micro LED was placed on the right atrium to selectively illuminate the junction of the superior vena cava (SVC) and right atrium. The ECG was acquired before, during, and after tissue illumination to measure changes in heart rate. Upon illumination, hearts exhibited sudden and dramatic reductions in heart rate with restoration of normal heart rate after cessation of illumination. Delays in atrioventricular conduction were also observed. Heart rate reductions at the highest irradiance levels were similar to heart rate reductions caused by application of bethanechol (10 μM) or acetylcholine (800 μM). Atropine (50 nM) completely blocked the effect of ChR2 photoactivation, confirming cholinergic mediation. Optogenetic activation of intrinsic parasympathetic neurons reduced heart rate in an immediate, dose-dependent

fashion, resembling the slowing of sinus rate in response to acetylcholine. Our results demonstrate a new approach for controlling parasympathetic modulation of cardiac function by selectively activating the endogenous release of acetylcholine from intrinsic cardiac cholinergic neurons.

Key Message: Optogenetic photoactivation of intrinsic cardiac neurons provides immediate, tissue-specific stimulation with minimal cross-reactivity. Our results demonstrate that selective expression of channelrhodopsin within cardiac cholinergic neurons enables photoactivated release of acetylcholine, thereby instantaneously slowing sinus rate and altering atrioventricular conduction. This provides for in-depth examination of the endogenous interplay between cardiac autonomic neurons and the functional outcomes of downstream post-synaptic receptor activation.

Keywords: neurocardiac, cardiac optogenetics, autonomic nerve activation, cardiac parasympathetic tone, excised perfused hearts

INTRODUCTION

The balance of sympathetic and parasympathetic tone provides exquisite control of heart rate and contractility and has also been shown to modulate coronary flow (Reid et al., 1985; Kovach et al., 1995) and inflammation after myocardial injury (Calvillo et al., 2011; Garrott et al., 2017). Understanding how autonomic balance is altered by cardiac disease is an active area of research, and developing new ways to control this balance provides insights into disease therapies. In the laboratory, autonomic tone has been modulated by pharmacological activation of cardiomyocyte membrane receptors and by electrical stimulation of sympathetic ganglia or the vagus nerve. These methods are effective and initiate profound changes in heart rate (Ng et al., 2001; DeWitt et al., 2016). However, measuring changes in cardiac function that result from the release of neurotransmitter from a specific population of cardiac neurons (anatomic-functional probing) can be challenging because of the difficulty in achieving neuron-specific stimulation.

Optogenetics enables spatially and temporally specific stimulation of distinct cell types using light (Entcheva, 2013). Photostimulation of neurons expressing the light-gated cation channel channelrhodopsin (ChR2) initiates the immediate release of endogenous neurotransmitters (Deisseroth et al., 2006). Previous studies in brain slices having cholinergic neurons that express ChR2 demonstrated temporal control in the photoactivated release of acetylcholine (ACh) (Nagode et al., 2011; Ren et al., 2011; Hedrick et al., 2016). For the heart, cell-specific expression of ChR2 eliminates the need for complex anatomic dissections for electrical stimulation or the administration of circulating agonists that ubiquitously activate membrane receptors. With optogenetics, either branch of the cardiac autonomic nervous system could be selectively stimulated, with relative ease, in a temporally and regionally specific manner. For example, photoactivation of sympathetic neurons within the myocardium of perfused hearts was accomplished by illuminating the epicardium with blue light (Wengrowski et al., 2015). In those studies, the expression of ChR2 was targeted to catecholaminergic neurons using a Cre-Lox approach where the expression of Cre recombinase was promoted by tyrosine hydroxylase (TH), an enzyme involved in the production of norepinephrine.

The goal of the present studies was to demonstrate optogenetic photoactivation of intrinsic cardiac parasympathetic neurons and to measure the resulting changes in cardiac electrical activity. Our hypothesis was that hearts having ChR2 selectively expressed within cells that contain choline acetyltransferase (ChAT) could be photoactivated to induce changes in cardiac function consistent with muscarinic (M2) receptor activation. This is because ACh is produced by ChAT through the combination of acetyl-CoA with a free choline (Wessler et al., 1999) and is stored in synaptic vesicles within axon varicosities. Upon axonal depolarization, and the resulting increase in cytosolic calcium concentration, the vesicles dock with the membrane to release ACh, which binds to cardiomyocyte M2 receptors. This activates inhibitory G proteins (Irisawa et al., 1993) to modulate cardiomyocyte membrane currents that hyperpolarize the cell, slow spontaneous membrane depolarization of the sinoatrial node (SAN), and increase atrioventricular (AV) conduction time (Imaizumi et al., 1990). ACh also activates G protein-gated inwardly rectifying K^+ channels (GIRK, also known as I_{KACh}), which are thought to be a pivotal contributor to parasympathetic regulation of heart rate (Lee et al., 2018).

Previous studies have shown that electrical stimulation of the right and left vagus nerves induce immediate reductions in sinus rate and increases AV conduction time (Levy and Zieske, 1969; Ng et al., 2001). This is consistent with the release of ACh from parasympathetic cholinergic varicosities within those nodal regions (Imaizumi et al., 1990; Roy et al., 2014). Furthermore, local electrical stimulation of specific cardiac vagal ganglia in the fat pads, or their selective ablation, has revealed that the SAN and the AV node are innervated by distinct cholinergic axons (Randall et al., 1986; Sampaio et al., 2003). In rats, stimulation of the ganglion at the junction of the right SVC and right atrium slowed heart rate with little effect on AV conduction while stimulation of the ganglion at the junction of the inferior

pulmonary veins and left atrium slowed AV conduction without eliciting bradycardia (Sampaio et al., 2003). That study is an elegant example of anatomic-functional probing of the intrinsic cardiac nervous system to reveal new insights that could not be obtained by either administering exogenous neurotransmitters or by direct stimulation of the vagus nerve.

The studies presented here demonstrate an optogenetic approach for anatomic-functional probing of the parasympathetic nervous system that can be used with conventional excised perfused heart preparations. This is a corollary approach to our previous work detailing photoactivation of sympathetic axons (Wengrowski et al., 2015). Our results also demonstrate that cholinergic neurons remain active and viable following the severance of pre-ganglionic axons and, importantly, that the parasympathetic pathway, from post-ganglionic neuron stimulation to M2 receptor activation, can be successfully controlled using light in excised perfused hearts.

MATERIALS AND METHODS

Mice With Parasympathetic Neurons That Express ChR2

Approval for all animal protocols was obtained from the George Washington University's Animal Care and Use Committee and followed the National Institute of Health's Guide for the Case and Use of Laboratory Animals. Transgenic mice were crossbred to express ChR2 in cardiac parasympathetic neurons using Cre-Lox recombination and a ChAT promoter. One parent (Jackson Labs stock #006410) had homozygous expression of a ChAT promoter to direct the expression of Cre recombinase (Rossi et al., 2011) while the other parent (Jackson Labs stock #012569) had homozygous ChR2&EYFP fusion protein expression dependent upon Cre expression (Madisen et al., 2012). The enhanced yellow fluorescent protein (EYFP) enabled ChR2 expression to be visualized without fluorescent antibody staining. Genotyping of tail snips (Transnetyx) confirmed the genotype of the offspring (ChAT-Cre-ChR2&EYFP).

Whole-Mount Preparations and Confocal Microscopy

Multiphoton confocal imaging of excised right atria confirmed that ChR2&EYFP expression was localized to cells containing ChAT. In those studies, mice were anesthetized, cervically dislocated, the heart was rapidly excised, the aorta was cannulated, and the heart was flushed with phosphate buffered saline (PBS) containing heparin. Using a dissecting scope, the base of the heart, including the atria, was separated from the ventricles along the atrial-ventricular ridge and attached to a thin piece of polydimethylsiloxane (PDMS, Sylgard 184) (Rysevaite et al., 2011). The sample was then fixed with 4% paraformaldehyde in PBS for 2 h. The heart was then thoroughly washed with PBS (3 × 2 min, 2 × 15 min, 1 min × 30 min) and blocked for 2 h with 2% bovine serum albumin (BSA) (Sigma-Aldrich), 1% Triton X-100 (Sigma-Aldrich) in PBS. Next, the sample was placed in goat anti-ChAT primary antibody (EMD Millipore AB144P; 1:100 with 2% BSA) overnight at 4°C, with agitation. The sample was washed to remove all of the unbound primary antibody (3 min × 2 min, 2 min × 15 min, 1 h × 1 h, 1x overnight). Following this, the sample was incubated with an Alexa Fluor 647 conjugated donkey anti-goat secondary antibody (Jackson Immunoresearch 705-605-147; 1:300 with 2% BSA) overnight at 4°C, while shaking. The heart was then washed in PBS (3 min × 2 min, 2 min × 15 min, 1 h × 1 h, 1x overnight) and imaged using a Leica TCS SP8 MP multiphoton confocal microscope with a dry 10X lens. The sample was illuminated with light at 514 and 651 nm to visualize EYFP and the Alexa Fluor antibody, respectively.

To further examine the expression of ChR2&EYFP in cardiac neurons, hearts were excised from ChAT-Cre-ChR2&EYFP mice (n = 4) and the right atria (RA) were removed and placed in PBS at room temperature. Submerged atria were then positioned on the stage of the Leica multiphoton confocal microscope and imaged using a water emersion lens (25 μm× 1.0 μm critical aperture). Samples were illuminated at 514 nm to excite EYFP. Z stack images were acquired from the atriocaval junction (AC), at the intersection of the RA and the superior vena cava (SVC), to visualize EYFP fluorescence in three dimensions.

Excised Perfused Heart Preparations

Mice were anesthetized with ∼4% isoflurane. After confirming a surgical plane of anesthesia, hearts were rapidly excised, and the aorta was cannulated. Hearts were then retrogradely perfused via Langendorff at constant pressure between 60 and 80 mmHg using a modified Krebs–Henseleit solution (118 mM NaCl, 4.7 mM KCl, 1.25 mM $CaCl_2$, 0.57 mM $MgSO_4$, 25 mM $NaHCO_3$, 1.17 mM KH_2PO_4, 6 mM glucose). Perfusate was buffered to a pH between 7.35 and 7.45, warmed to 37°C, and oxygenated with 95% O_2/5% CO_2. Before beginning each protocol, perfused hearts were allowed to stabilize at normal sinus rhythm for at least 5 min. Hearts were then positioned with the RA/SVC junction face up (posterior side) for photoactivation. **Table 1** lists the number of animals used in each perfused heart study.

ECG Measurements

Three needle electrodes were positioned in an Einthoven configuration around hearts to record the bath-conducted ECG (**Figure 1A**). The signal was amplified and filtered (2122i Bioamplifier, UFI) and acquired using a PowerLab unit (PowerLab 8/35, AD Instruments). The ECG and heart rate (RR interval) were monitored in real time (LabChart, AD Instruments). The time of the P-wave and PQ intervals were measured before, during, and after specific illumination protocols.

Photoactivation Using a Spotlight LED

Light from a high-power blue LED spotlight (**Figure 1**, 460 nm peak wavelength, Mightex Systems) was directed onto the right atrium and pulsed for 20 s (5 ms pulse width at 5 Hz). The current powering this spotlight could be varied to provide

TABLE 1 | Number of animals used in each set of experiments.

Study	*n*
Spotlight LED (all intensities)	**10**
Bethanechol	4
Atropine	3
Micro LED	**10**
Atropine	6
Optical mapping	3
Photoactivation with intact Fat pad	**3**
Green light stimulation verification	3
Photoactivation desensitization	**3**
WT photoactivation test	**5**
Bethanechol	5
WT ACh	**9**

With the exception of wild-type mice, all animals expressed ChR2&EYFP in ChAT neurons, as verified by functional responses and/or whole-mount confocal fluorescence imaging.

a range of optical irradiances, enabling the measurement of "dose-response" changes in heart rate (HR). Irradiances between 0.68 and 1.81 mW/mm^2 (**Figure 1C**) were studied. This range was selected using results of previous studies (Wengrowski et al., 2015). After each illumination, light was withdrawn for 20 s and the heart was allowed to stabilize before applying the next illumination. The bath-conducted ECG was continuously recorded throughout each photoactivation protocol.

Photoactivation Using a Micro LED

Small solid-state LEDs (**Figure 1**) were used to focus excitation light within specific regions of the heart while also demonstrating that small LEDs could be effective in activating cardiac neurons that express ChR2. We chose surface-mount LEDs (Dialight 598 series, Vf 3.2V), with a peak wavelength at 465 nm and maximum irradiance of 2.4 mW/mm^2 (**Figures 1B,C**), to illuminate the RA/SVC junction (**Figure 1A**). Given the small size (1.6 mm × 0.8 mm × 0.7 mm) of these LEDs, significant illumination of adjacent areas of the heart was avoided, thereby eliciting only the response from targeted locations. To avoid electrical short circuits at the interface of the LED due to interaction with the surrounding electrolyte solution, the LEDs were encapsulated with PDMS (Sylgard 184). Due to the high resistivity of PDMS (2.9 × 10^{14} Ω.cm), this provided suitable thermal and electrical insulation. A thin layer of PDMS (15 μm)

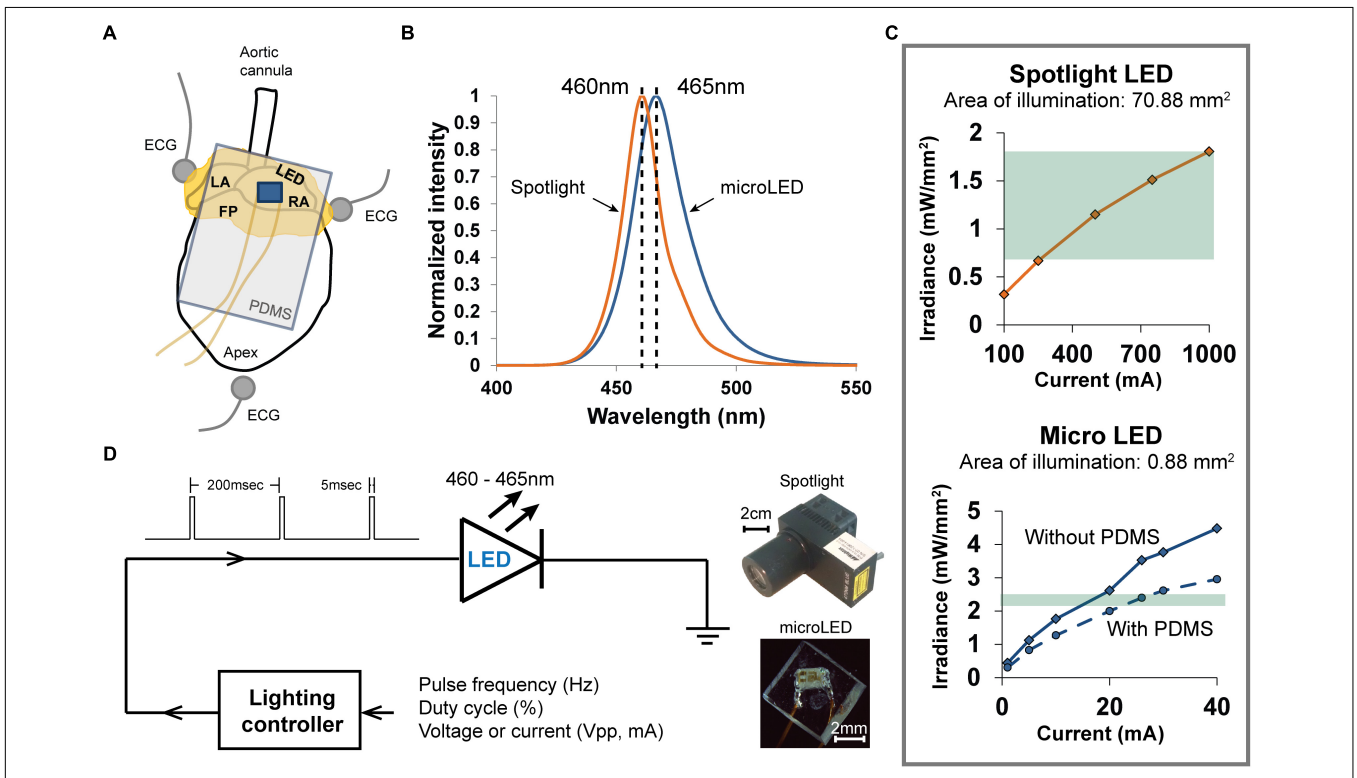

FIGURE 1 | Methods used to photoactivate ChR2 expressed within the cholinergic neurons of excised perfused mouse hearts. **(A)** Arrangement of the heart (fat pads shown in yellow) during an experiment when photoactivating ChR2 using a PDMS-encapsulated micro LED, which is shown lying on top of the RA. Three electrodes recorded the bath-conducted ECG. **(B)** The spectral distribution of light from the spotlight LED was centered at 460 nm. The spectral distribution of light from the micro LED was slightly wider and centered at 465 nm. **(C)** The relationship between emitted light (irradiance) and LED source current for the two illumination devices used in the experiments. High source currents (250–1000 mA) were required to generate sufficient irradiance (0.7–1.8 mW/mm^2) to activate ChR2 with the spotlight LED (top). The micro LED (bottom) provided ample irradiance (2.4 mW/mm^2) to activate ChR2 at low source currents (18–22 mA). The range of irradiance used in the experiments is denoted by the green regions. **(D)** Scheme for controlling the delivery of light from either light source. A lighting controller was programmed to deliver current to each LED as a pulse train at a specific frequency and duty cycle. The relative sizes of each LED source are shown on the right.

was first applied to the front of the LED, where the light is emitted, to minimize light attenuation. A second thicker layer of PDMS was then applied to the rest of the LED chip (**Figure 1D**). Current was delivered to micro LED devices in a manner similar to that used for spotlight illumination.

Administration of Muscarinic Agonists and Antagonists

The muscarinic agonists bethanechol (carbamyl-β-methylcholine chloride, Sigma) (10 μM) and ACh (acetylcholine chloride, Sigma) (800 μM) were administered to the perfusate as positive controls to measure the effects of ubiquitous activation of muscarinic receptors. This allowed the effects of photoactivation of cholinergic neurons to be compared to that of muscarinic activation by circulating agonists. To demonstrate cholinergic specificity of photoactivation, atropine (atropine sulfate, Sigma) (50 nM), a muscarinic antagonist, was administered to the perfusate. Cessation of changes due to photoactivation were then measured using the spotlight and micro LED at irradiances of 1.81 and 2.4 mW/mm^2, respectively; which provided the largest drop in HR without atropine.

Optical Mapping Experiments

To study sinus-mediated beats and atrio-ventricular conduction time, optical mapping of a voltage sensitive dye (di-4-ANEPPS) was performed before and after photoactivation using the micro LED. The dye (30 μL of 2.5 mM stock diluted in 1 mL of perfusate) was injected into the aorta. Upon verification of sufficient staining, blebbistatin (circulating concentration of 5 μM) was titrated into the perfusate to mechanically arrest hearts to prevent motion contamination of the optical signals. A high-power green LED light source with peak wavelength of 520 nm (UHP-Mic-LED-520, Prizmatix) illuminated the epicardial surface to energize the dye. Emitted light was long pass filtered (680 nm) and imaged with a MiCAM Ultima-L CMOS camera (SciMedia, Costa Mesa, CA, United States) with high spatial (100 × 100 pixels, 230 ± 20 μm per pixel) and temporal (1,000–3,000 frames/sec) resolution. The resulting optical action potential (OAP) datasets were stored for subsequent analysis.

Data Analysis and Statistics

Data are presented as mean ± standard error of the mean. Statistical analyses were performed using analysis of variance, paired *t*-test and Bonferroni *post hoc* testing using SPSS v24 with $p < 0.05$ indicating significance. Optical mapping datasets were pre-processed using custom MATLAB algorithms to increase contrast, normalize signals, and identify times of OAP depolarization.

RESULTS

Tissue Whole-Mount Fluorescence Microscopy

Neurons within right atria that expressed ChAT were labeled via immunohistochemistry with Alexa Fluor 647 to provide visual confirmation that ChAT and ChR2&EYFP expression were localized within the same axons (**Figure 2A**). Fluorescence overlap confirmed selective expression of ChR2&EYFP within cholinergic neurons. Right atrial nerve bundles that expressed ChR2&EYFP were also imaged at high resolution within the region of the atriocaval (AC) junction (**Figure 2B**). An extensive intertwining network of nerve fibers was observed, indicating robust expression of ChR2&EYFP in this animal model. Nerve bundles contained axons with diameters between 3 and 5.4 μm.

Heart Rate Reduction After Photoactivation

Following cannulation, perfused hearts (n = 10) stabilized at 320 ± 17 bpm. Immediately prior to illumination, average baseline HRs for each irradiance were 317 ± 18 bpm for 0.68 mW/mm^2, 321 ± 16 bpm for 1.15 mW/mm^2, and 319 ± 17 bpm for 1.81 mW/mm^2 (Mean ± SE). During illumination, HR demonstrated an immediate, dose-dependent reduction. Typical ECG signals before and during illumination are shown in **Figure 3A**. Average HRs during each irradiance level were (**Figure 3B**): 240 ± 22 bpm for 0.68 mW/mm^2, 208 ± 15 bpm for 1.15 mW/mm^2, and 175 ± 14 bpm for 1.81 mW/mm^2. Upon cessation of 20 s of illumination, average HRs returned to baseline after 5–10 s (315 ± 20, 318 ± 16, and 326 ± 19 bpm for 0.68, 1.15, and 1.81 mW/mm^2, respectively) regardless of the irradiance. Long-term photoactivation studies were performed where hearts (n = 3) were continuously illuminated for specific time intervals (5, 10, 30, and 60 min). Drops in HR were maintained for at least 30 min and returned to baseline after cessation of illumination (**Figure 3C**, top). During 60 min of continuous illumination, desensitization was observed after 35 min where HR started to rise and at 10 min after illumination HR remained low (**Figure 3C**, bottom).

As expected, wild-type animals with no ChR2 expression (n = 5) demonstrated no response to LED illumination, regardless of the irradiance (**Figure 3A**). This confirmed that changes in HR were not caused by the direct effects of illumination, such as heating. In fact, changes in epicardial temperature during illumination were <0.03°C.

In a subset of studies (n = 5), spotlight illumination of the RA near the AV node slowed HR and also induced AV block (**Figure 3A**). This occurred in both a 2:1 and 3:1 ratio for atrial to ventricular conduction, respectively. A prolonged PQ interval was observed during photoactivation that induced AV block (56.6 ± 3.6 vs. 59.7 ± 3.8 ms, p = 0.004) but no difference in the duration of atrial depolarization (P-wave duration, 12.7 ± 1.3 vs. 13 ± 1.3 ms, p = 0.356) was evident. At cessation of illumination, AV block was relieved, and hearts immediately returned to normal sinus rhythm.

Immediate HR reductions (n = 10 hearts) were also observed using the micro LED (2.4 mW/mm^2) (**Figure 3**). HR was 323 ± 17 bpm immediately prior to illumination with the micro LED. During illumination, average HR dropped to 184 ± 17 (**Figure 3B**). Average HR after cessation of illumination was 322 ± 17 bpm. AV block was not observed when the micro LED was directed toward the SA node (**Figure 3A**). In the

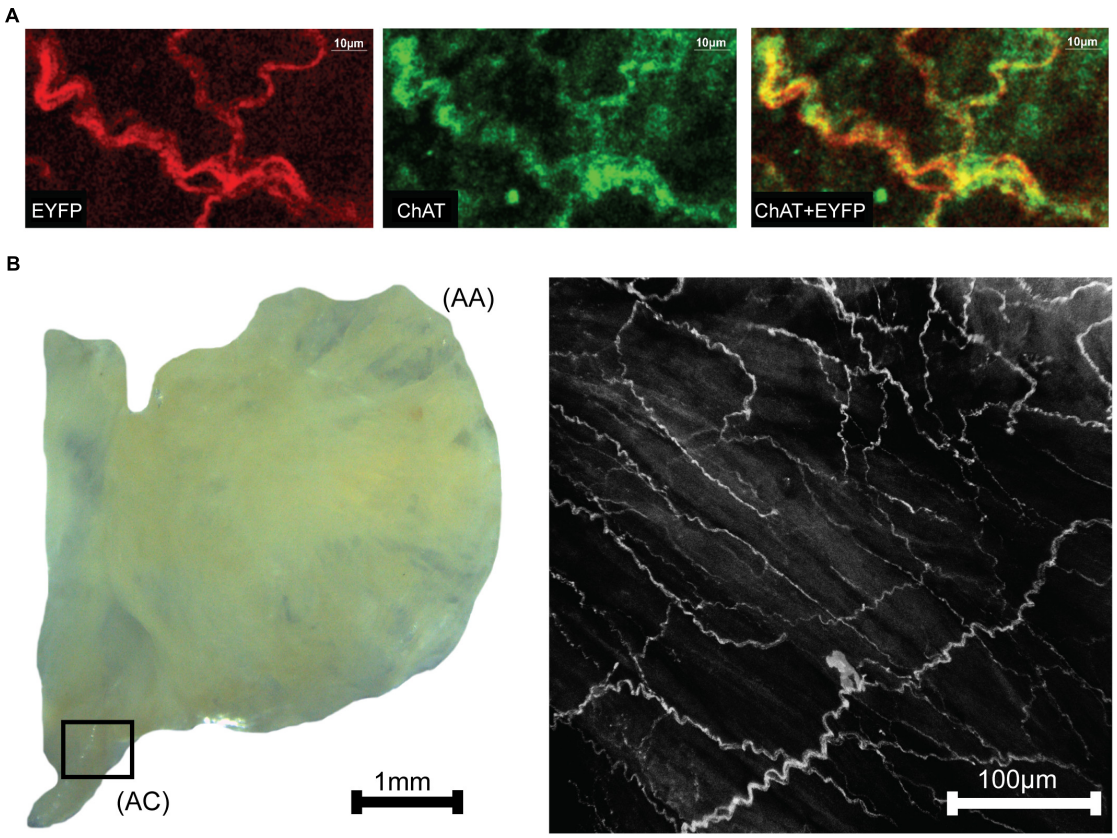

FIGURE 2 | Images showing colocalization of ChAT with ChR2&EYFP within the nerve bundles of the right atrium. **(A)** The fluorescence of EYFP (left: 514 nm excitation) and Alexa Fluor (middle: 651 nm excitation) were imaged within the RA. Fluorescence overlap (right) confirmed selective expression of ChR2&EYFP within cholinergic neurons. **(B)** Bright field image (left) of a typical excised right atrium used for multiphoton fluorescence microscopy of neurons expressing ChR2&EYFP. AC, atriocaval junction; AA, atrial appendage. Extensive intertwining networks of nerve fibers expressing ChR2&EYFP are shown on the right for a region of the AC junction, denoted as the box shown in the bright field image.

absence of AV block, no differences in atrial depolarization (P-wave) duration and PQ interval were observed before or during illumination (16 ± 2.4 vs. 17 ± 2.3 ms, $p = 0.117$ and 54 ± 4.5 vs. 53 ± 3.9 ms, $p = 0.298$, respectively). In a separate group ($n = 3$ hearts), the epicardial fat pads were carefully preserved during heart excision and cannulation. The average results of photoactivation in that subset of hearts was the same as that of all other hearts.

Bonferroni *post hoc* testing of each irradiance indicated that all levels had statistically significant HR reductions (**Figure 3B**) compared to baseline HR before photoactivation (**Table 2**). Furthermore, irradiances of 1.15 (35%, $p < 0.001$), 1.81 (45%, $p < 0.001$), and 2.4 mW/mm^2 (43%, $p < 0.001$) all had a larger impact on HR compared to 0.68 mW/mm^2 (24%, $p < 0.001$). There was no statistically significant intergroup difference in HR reductions between irradiances of 1.15, 1.81, and 2.4 mW/mm^2.

Effects of Muscarinic Agonists and an Antagonist

Bethanechol (10 μM) produced a long-term transient reduction in HR from 302 ± 27 to 130 ± 10 bpm (**Figure 3B**) ($n = 9$ hearts). Unpaired *t*-tests revealed no significant difference in HR reduction following bethanechol administration ($p = 0.09$) between hearts of either wild-type mice or ChAT-Cre-ChR2&EYFP mice. Bethanechol prolonged PQ interval (51 ± 4 vs. 57 ± 5 ms, $p < 0.001$) but did not modify the P-wave duration (12.1 ± 1.1 vs. 12.5 ± 1.5 ms, $p = 0.576$). ACh (800 μM) was administered to the hearts of wild-type mice ($n = 9$), resulting in a long-term transient HR reduction from 337 ± 25 to 182 ± 19 bpm (**Figure 3B**), significant AV delays (40.4 ± 1.6 vs. 45.3 ± 2.8 ms, $p < 0.001$), and preservation of P-wave duration (13.1 ± 0.7 vs. 12.8 ± 0.9 ms, $p = 0.32$). The observation that ACh did not alter the time of atrial depolarization is consistent with previous findings that ACh did not alter conduction velocity in canine right atria (Schuessler et al., 1990).

Atropine (50 nM) was administered to the hearts of ChAT-Cre-ChR2&EYFP mice ($n = 9$) and completely blocked the effects of photoactivation (330 ± 23 before illumination vs. 332 ± 24 bpm after illumination) (**Figure 3B**). No AV delay or atrial depolarization differences were observed before photoactivation with atropine or during photoactivation with atropine (54.8 ± 2.6 vs. 51.6 ± 3.3 ms,

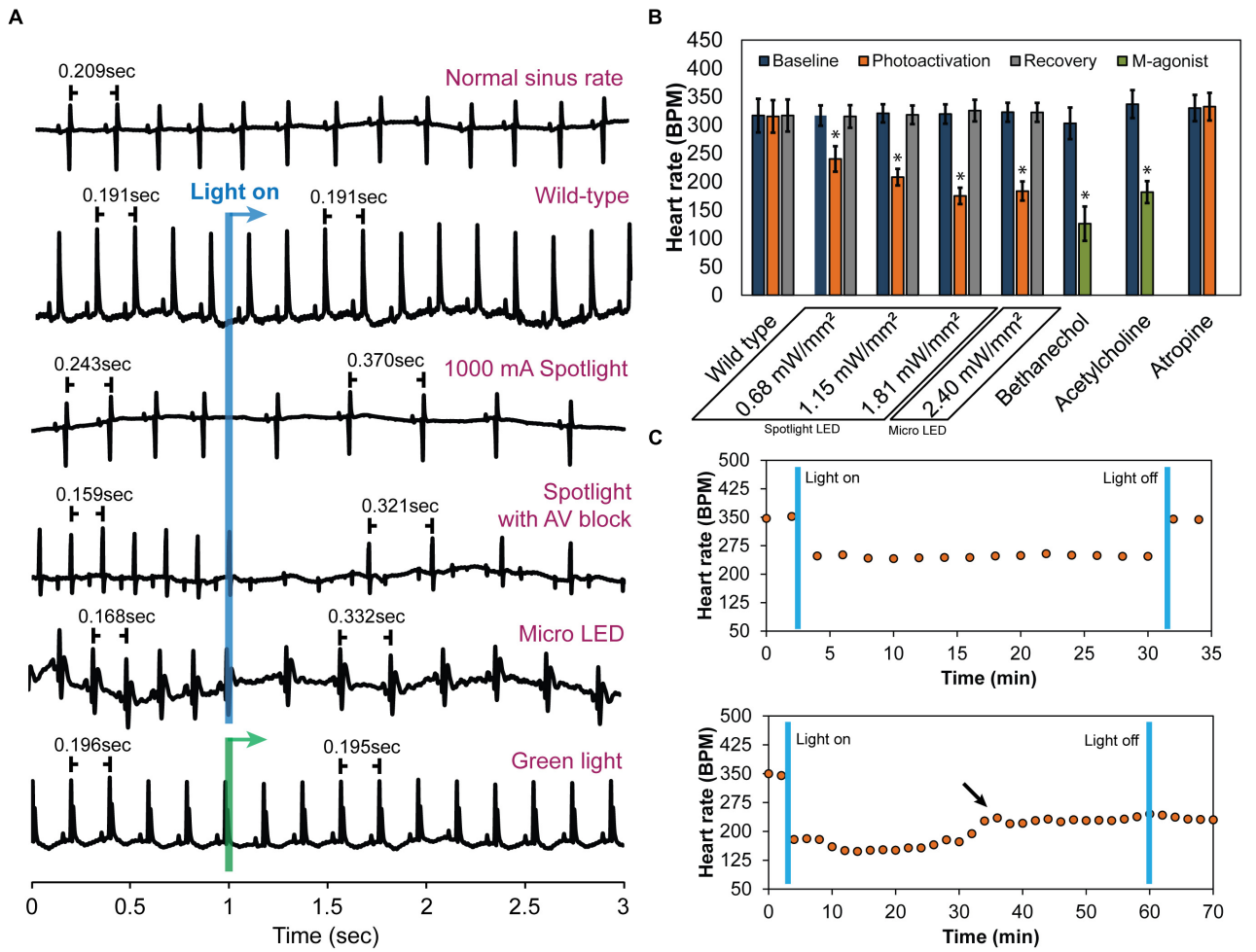

FIGURE 3 | The effect of cholinergic neuron photoactivation on sinus rate and AV conduction in perfused hearts from ChAT-Cre-ChR2&EYFP mice. **(A)** Six representative ECG signals demonstrate the effect of cholinergic neuron photoactivation on R-R interval and AV conduction. From top to bottom: (1) Typical baseline ECG before photoactivation. (2) Typical ECG at the onset of illuminating wild-type mouse hearts with the spotlight LED. No change in the ECG was observed. (3) Typical ECG at the onset of photoactivation using the spotlight LED at the highest source current. RR interval increased immediately. (4) Representative ECG showing AV block when illuminating the RA and AV node with the spotlight LED at the highest source current. Second-degree AV block was observed. (5) Typical ECG at the onset of photoactivation using the micro LED placed on top of the RA. RR interval increased immediately. (6) Representative ECG showing no change in HR at the onset of green light (peak 520 nm) illumination of the RA of ChAT-Cre-ChR2&EYFP mouse hearts. **(B)** Average HR changes (n = 10 hearts) at baseline, during photoactivation of the RA at four different irradiances (with either the spotlight or micro LED), and after cessation of illumination. Average HR changes are also shown for wild-type mice with no ChR2 expression (n = 5 hearts) and for the muscarinic agonists bethanechol (10 μM, n = 9 hearts) and acetylcholine (800 μM, n = 9 hearts). The muscarinic antagonist atropine (50 nM, n = 9 hearts) completely blocked changes in HR during photoactivation by the spotlight (1.81 mW/mm^2) and the micro LED (2.4 mW/mm^2). **(C)** Robustness and stability tests were performed to assess the effect of prolonged photoactivation (n = 3 hearts). **Top:** change in HR during 30 min of photoactivation. HR returned to baseline upon cessation of illumination. **Bottom:** change in HR during 60 min of photoactivation. The arrow indicates that the potency of photoactivation was reduced after 35–40 min of illumination. HR did not return to baseline until 20 min after cessation of illumination (data not shown).

p = 0.055 and 12.8 ± 0.9 vs. 11.9 ± 0.8 ms, p = 0.134, respectively).

Optical Mapping

Hearts were optically mapped (n = 3) before and after photoactivation to study sinus-mediated beats and to measure the delay between the early site of atrial depolarization and the early site of LV depolarization (**Figure 4**). The earliest site of activation that was mapped within the atria and LV was used to compute this AV delay. Micro LED illumination lengthened AV delay by 6 ms but did not appear to alter the site of early LV depolarization. Bethanechol lengthened AV delay by 8 ms but did not appear to alter the site of early LV depolarization. Although there is minor spectral overlap in the light from the green 520 nm spotlight used for optical mapping and the absorption spectrum of ChR2 (Nagel et al., 2003), there was no measurable response that resulted from the green light. This was verified during control studies (n = 3) where no change in HR was observed for the hearts of ChAT-Cre-ChR2&EYFP mice when the 520 nm spotlight used for optical mapping was used to illuminate the RA at the same

TABLE 2 | Percent HR reductions following cholinergic neuron photoactivation at each irradiance were analyzed using Bonferroni *post hoc* comparisons.

LED source	Irradiance (mW/mm^2)	HR reduction relative to pre-photoactivation	HR reduction relative to 0.68 mW/mm^2	HR reduction relative to 1.15 mW/mm^2	HR reduction relative to 1.81 mW/mm^2
Spotlight	0.68	24%, <0.001			
Spotlight	1.15	35%, <0.001	11%, 0.352		
Spotlight	1.81	45%, <0.001	21%, 0.003	11%, 0.422	
Micro LED	2.4	43%, <0.001	19%, 0.008	8%, 0.873	−2%, 1.000

The third column shows the average percentage that HR was reduced during photoactivation relative to pre-photoactivation. P values for corresponding percent reductions are also shown. Columns 4–6 compare HR reductions during photoactivation at each irradiance. Note the statistically significant difference in reduction for all irradiance levels compared to pre-photoactivation but no statistically significant difference between HR reductions at irradiance levels of 1.15, 1.81, and 2.4 mW/mm^2.

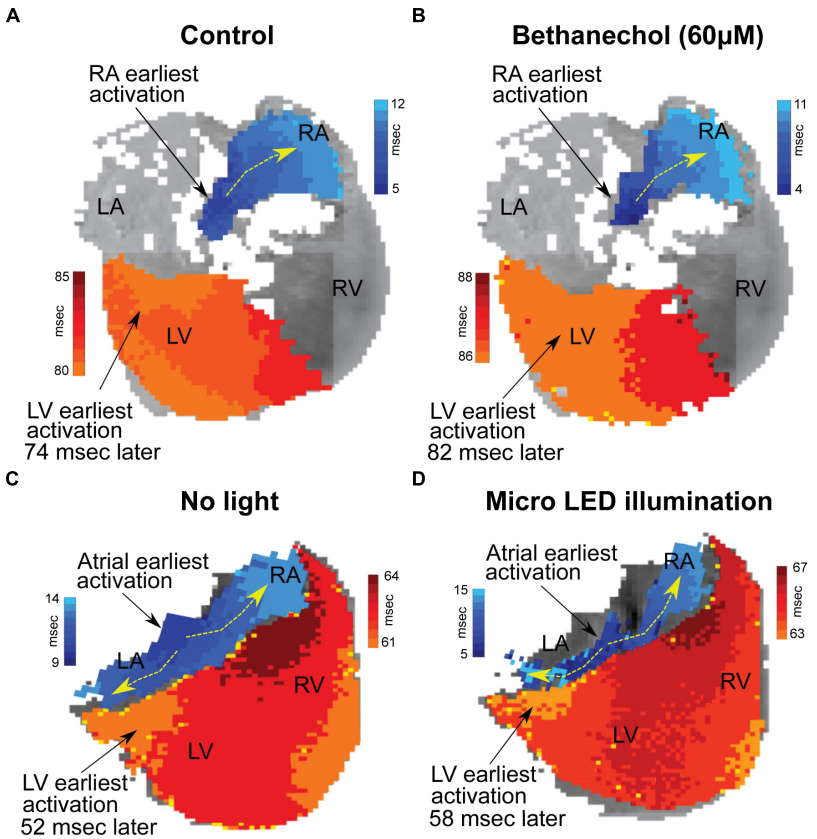

FIGURE 4 | Changes in conduction time between the atria and the ventricles induced by either bethanechol or photoactivation. Hearts (n = 3) were optically mapped to observe action potential propagation and to measure delays in conduction time between the atria and the ventricles, which was computed as the time difference between the earliest site of activation in the left ventricle (LV) and the earliest site of activation within the right atrium (RA). The PDMS-encapsulated micro LED was positioned on the base of the heart and directed toward the AC junction. **(A)** RA and LV early sites of activation mapped before administering bethanechol (60 μM). **(B)** Bethanechol lengthened AV delay by 8 ms but did not appear to alter the site of early LV depolarization. **(C)** RA and LV early sites of activation mapped before photoactivation. **(D)** Photoactivation using micro LED illumination lengthened AV delay by 6 ms but did not appear to alter the site of early LV depolarization.

duty cycle and frequency as that used for the 460 nm spotlight and the micro LED (**Figure 3A**).

DISCUSSION

Insights into cardiac autonomic neuroanatomy have been provided by early reports from Randall et al. (1986) and subsequently improved in studies by Sampaio et al. (2003) and Rysevaite et al. (2011). These groups successfully localized cardiac vagal ganglia and traced the parasympathetic neurons synapsing within the SA and AV nodes (Sampaio et al., 2003; Pauza et al., 2013). Observations from those studies indicate that the SA node is innervated by parasympathetic fibers originating from ganglia on both sides of the heart, but with a higher concentration of axons originating from right sided ganglia. Our work presents a novel approach to optogenetically drive endogenous parasympathetic release of

ACh from those neurons to elicit downstream changes in cardiac function through the preservation of post-ganglionic parasympathetic neurons in excised hearts, either with or without intact fat pads. The specificity of cholinergic neuron photoactivation was confirmed with muscarinic receptor agonists and antagonists and verified with optical mapping demonstrating a lengthening of conduction time between the atria and ventricles. Photoactivation maintained low heart rates during short stimulation periods and for up to 30 min of continuous illumination; however, gradual decline of parasympathetic response during stimulation was observed after approximately 35 min. This was possibly a result of desensitization of the post-synaptic muscarinic receptors, progressive decrease in the release of ACh, or a fading of effector response (Martin et al., 1982; Yamasaki et al., 1993).

The irradiance-dependent response that we observed supports and extends previous results of reduced heart rates following electrical stimulation of the vagus nerve in animal models (Degeest et al., 1965; Levy and Zieske, 1969; Choate and Feldman, 2003; Brack et al., 2004). Heart rate reductions during cholinergic neuron photoactivation were consistent with graded reductions in heart rate with increased strength of electrical stimulation of the vagus nerve (Ng et al., 2001). Furthermore, our findings are consistent with the chronotropic cholinergic response observed during exogenous administration of ACh (Takahashi et al., 2003). ACh has been shown to induce a dose-dependent reduction of sinus rate of approximately 25–67% (Glukhov et al., 2010; Lang et al., 2011) in isolated mouse hearts, similar to our results of 46% maximal reduction. However, AV delay was considerably longer during such ubiquitous muscarinic activation (>24% (Lang et al., 2011)) compared to our approach, where we observed only up to 12% increase in AV conduction delay in some hearts. Our finding of no detectable change in P-wave duration during photoactivation is also consistent with previous reports that found no change in right atrial conduction velocity during ACh perfusion (Schuessler et al., 1990).

Photoactivation using the micro LED, which provided the highest irradiance in our studies, produced a response similar to ubiquitous pharmacologic activation of muscarinic receptors, as observed with bethanechol. In addition to the effects of increased irradiance, the micro LED was more localized to the right atrial epicardium, having a high concentration of parasympathetic innervation, particularly at the RA/SVC junction (Ripplinger et al., 2016). Light from the micro LED could be oriented to selectively illuminate areas of the atria, such as the SA node, resulting in heart rate reductions without significant increases in AV delay, similar to the results of previous studies (Randall et al., 1986; Sampaio et al., 2003). On the other hand, non-selective illumination of the atria, that included the SA and AV nodes, by the spotlight LED resulted in a reduction of heart rate that was accompanied by an AV conduction delay.

Irradiances for optogenetic activation of cardiac tissues typically range from 0.5 to 10 mW/mm^2, depending upon the cell type (Bruegmann et al., 2010; Entcheva, 2013; Ambrosi et al., 2015; Nyns et al., 2016). This range is consistent with the results of our LED spotlight and micro LED illumination. In future studies, the use of LED spotlight illumination could be helpful to confirm ChR2&EYFP expression, to generate quick HR responses. The micro LED lends itself to detailed study of the neuroanatomy of vagal inputs due to its more localized illumination. In addition, future devices for animals might soon be available to implant such micro LEDs into transgenic mice for *in vivo* optogenetic activation of specific nerve populations (Kim et al., 2010; Xu et al., 2014).

Limitations

Our studies sought to examine intrinsic parasympathetic pathways and downstream responses in mouse hearts using an optogenetic approach to selective cholinergic neuron activation. We did not address specific cellular mechanisms at the post-synaptic level that control downstream signaling. Our studies focused on illumination of the RA/SVC junction – the presumed location of the sinoatrial node and did not focus in detail on the differences in the effect of left versus right sided parasympathetic stimulation. While directed at this general area, the focus of our spotlight LED was inexact. We believe this to be responsible for the variation in response demonstrated by the various irradiances studied using the spotlight LED and also for the induction of AV block, which could be a consequence of asynchronous or hyperparasympathetic stimulation, especially around the AV node (Ardell and Randall, 1986; Schiereck et al., 2000). Using a more targeted illumination approach, in future studies we plan to further elucidate the exact neuronal pathways responsible for parasympathetic responses. *In vivo* studies may also be valuable to understand the whole-animal response to light activation of cardiac parasympathetic pathways.

CONCLUSION

Cardiac autonomic tone is a prevailing modulator of cardiac output and understanding the mechanisms of its control has taken center stage as the aging population suffers from degenerative cardiac disease. Existing electrical and pharmacological approaches to autonomic modulation, while effective in activating sympathetic and parasympathetic pathways, are non-selective proximal modulators. Optogenetic actuation of cardiac neurons provides a targeted, binary input with minimal cross-reactivity on distal cardiac tissue and is a powerful approach for in-depth examination of the endogenous interplay between the sympathetic and parasympathetic arms of the cardiac autonomic system.

We crossbred mice to express ChR2 in peripheral cholinergic neurons using Cre-Lox recombination driven by a ChAT promoter. Upon illumination, excised perfused hearts from these animals exhibited sudden and dramatic reductions in heart rate with restoration of the previous heart rate after cessation of illumination. Such photoactivation of intrinsic cholinergic neurons reduced heart rate in an immediate, dose-dependent fashion, resembling the slowing of sinus rate in response to ACh. Our results demonstrate a new approach for controlling cardiac parasympathetic activity by selectively activating the endogenous

release of ACh from intrinsic cardiac cholinergic neurons. This approach also enables spatiotemporal anatomic-functional probing of the intrinsic cardiac nervous system to reveal new insights that could be difficult to obtain using conventional approaches.

AUTHOR CONTRIBUTIONS

AM, KE, and MS provided equal first-author contributions, designed and conducted the experiments, analyzed the data, and wrote the manuscript. AM and MS generated the final figures. MD, KE, and AM conducted the confocal imaging. MD conducted immunohistochemistry and edited the manuscript. JB and KE conducted the optical mapping experiments. IE and GT provided overall intellectual input and edited the manuscript. MK and DM conceived the experiments, analyzed the data, provided overall intellectual input, and edited the manuscript.

FUNDING

This work was supported by grants from the National Institutes of Health [R01-HL095828 (MK), R01-HL133862 (DM), R01-HL115415 (IE)], research fellowships from the Veterans Affairs Medical Center (KE and MS), a Leducq Foundation grant RHYTHM (JB and IE), and a Don J. Levy and Elma Levy fellowship (AM).

ACKNOWLEDGMENTS

The microscopy expertise of Anastas Popratiloff, MD., Ph.D. and the facilities GWU SEH Microscopy Core Facility are gratefully acknowledged. Matthew Stoyek, Ph.D. is gratefully acknowledged for guidance in antibody staining of ChAT. Matthew Colonnese, Ph.D. and Marnie Phillips, Ph.D. are gratefully acknowledged for providing mice used in early experiments. We also thank Emilia Entcheva, Ph.D. for many insightful discussions regarding photoactivation of channelrhodopsin within cardiac tissues.

REFERENCES

Ambrosi, C. M., Boyle, P. M., Chen, K., Trayanova, N. A., and Entcheva, E. (2015). Optogenetics-enabled assessment of viral gene and cell therapy for restoration of cardiac excitability. *Sci. Rep.* 5:17350. doi: 10.1038/srep17350

Ardell, J. L., and Randall, W. C. (1986). Selective vagal innervation of sinoatrial and atrioventricular nodes in canine heart. *Am. J. Physiol.* 251, H764–H773. doi: 10.1152/ajpheart.1986.251.4.H764

Brack, K. E., Coote, J. H., and Ng, G. A. (2004). Interaction between direct sympathetic and vagus nerve stimulation on heart rate in the isolated rabbit heart. *Exp. Physiol.* 89, 128–139. doi: 10.1113/expphysiol.2003.002654

Bruegmann, T., Malan, D., Hesse, M., Beiert, T., Fuegemann, C. J., Fleischmann, B. K., et al. (2010). Optogenetic control of heart muscle in vitro and in vivo. *Nat. Methods* 7, 897–900. doi: 10.1038/nmeth.1512

Calvillo, L., Vanoli, E., Andreoli, E., Besana, A., Omodeo, E., Gnecchi, M., et al. (2011). Vagal stimulation, through its nicotinic action, limits infarct size and the inflammatory response to myocardial ischemia and reperfusion. *J. Cardiovasc. Pharmacol.* 58, 500–507. doi: 10.1097/FJC.0b013e31822b7204

Choate, J. K., and Feldman, R. (2003). Neuronal control of heart rate in isolated mouse atria. *Am. J. Physiol. Heart Circ. Physiol.* 285, H1340–H1346. doi: 10.1152/ajpheart.01119.2002

Degeest, H., Levy, M. N., Zieske, H., and Lipman, R. I. (1965). Depression of ventricular contractility by stimulation of the vagus nerves. *Circ. Res.* 17, 222–235. doi: 10.1161/01.RES.17.3.222

Deisseroth, K., Feng, G., Majewska, A. K., Miesenbock, G., Ting, A., and Schnitzer, M. J. (2006). Next-generation optical technologies for illuminating genetically targeted brain circuits. *J. Neurosci.* 26, 10380–10386. doi: 10.1523/JNEUROSCI.3863-06.2006

DeWitt, E. S., Black, K. J., Thiagarajan, R. R., DiNardo, J. A., Colan, S. D., McGowan, F. X., et al. (2016). Effects of commonly used inotropes on myocardial function and oxygen consumption under constant ventricular loading conditions. *J. Appl. Physiol.* 121, 7–14. doi: 10.1152/japplphysiol.00058.2016

Entcheva, E. (2013). Cardiac optogenetics. *Am. J. Physiol. Heart Circ. Physiol.* 304, H1179–H1191. doi: 10.1152/ajpheart.00432.2012

Garrott, K., Dyavanapalli, J., Cauley, E., Dwyer, M. K., Kuzmiak-Glancy, S., Wang, X., et al. (2017). Chronic activation of hypothalamic oxytocin neurons improves cardiac function during left ventricular hypertrophy-induced heart failure. *Cardiovasc. Res.* 18, 32–39. doi: 10.1093/cvr/cvx084

Glukhov, A. V., Fedorov, V. V., Anderson, M. E., Mohler, P. J., and Efimov, I. R. (2010). Functional anatomy of the murine sinus node: high-resolution optical mapping of ankyrin-B heterozygous mice. *Am. J. Physiol. Heart. Circ. Physiol.* 299, H482–H491. doi: 10.1152/ajpheart.00756.2009

Hedrick, T., Danskin, B., Larsen, R. S., Ollerenshaw, D., Groblewski, P., Valley, M., et al. (2016). Characterization of channelrhodopsin and archaerhodopsin in cholinergic neurons of Cre-lox transgenic mice. *PLoS One* 11:e0156596. doi: 10.1371/journal.pone.0156596

Imaizumi, S., Mazgalev, T., Dreifus, L. S., Michelson, E. L., Miyagawa, A., Bharati, S., et al. (1990). Morphological and electrophysiological correlates of atrioventricular nodal response to increased vagal activity. *Circulation* 82, 951–964. doi: 10.1161/01.CIR.82.3.951

Irisawa, H., Brown, H. F., and Giles, W. (1993). Cardiac pacemaking in the sinoatrial node. *Physiol. Rev.* 73, 197–227. doi: 10.1152/physrev.1993.73.1.197

Kim, R.-H., Kim, D.-H., Xiao, J., Kim, B. H., Park, S.-I., Panilaitis, B., et al. (2010). Waterproof AlInGaP optoelectronics on stretchable substrates with applications in biomedicine and robotics. *Nat. Mater.* 9, 929–937. doi: 10.1038/nmat2879

Kovach, J. A., Gottdiener, J. S., and Verrier, R. L. (1995). Vagal modulation of epicardial coronary artery size in dogs. a two-dimensional intravascular ultrasound study. *Circulation* 92, 2291–2298. doi: 10.1161/01.CIR.92.8.2291

Lang, D., Glukhov, A. V., Efimova, T., and Efimov, I. R. (2011). Role of Pyk2 in cardiac arrhythmogenesis. *Am. J. Physiol. Heart Circ. Physiol.* 301, H975–H983. doi: 10.1152/ajpheart.00241.2011

Lee, S. W., Anderson, A., Guzman, P. A., Nakano, A., Tolkacheva, E. G., and Wickman, K. (2018). Atrial GIRK channels mediate the effects of vagus nerve stimulation on heart rate dynamics and arrhythmogenesis. *Front. Physiol.* 9:943. doi: 10.3389/fphys.2018.00943

Levy, M. N., and Zieske, H. (1969). Autonomic control of cardiac pacemaker activity and atrioventricular transmission. *J. Appl. Physiol.* 27, 465–470. doi: 10.1152/jappl.1969.27.4.465

Madisen, L., Mao, T., Kock, H., Zhuo, J., Berenyi, A., Fujisawa, S., et al. (2012). A toolbox of cre-dependent optogenetic transgenic mice for light-induced activation and silencing. *Nat. Neurosci.* 15, 793–802. doi: 10.1038/nn.3078

Martin, P., Levy, M. N., and Matsuda, Y. (1982). Fade of cardiac responses during tonic vagal stimulation. *Am. J. Physiol.* 243, H219–H225. doi: 10.1152/ajpheart.1982.243.2.H219

Nagel, G., Szellas, T., Huhn, W., Kateriya, S., Adeishvili, N., Berthold, P., et al. (2003). Channelrhodopsin-2, a directly light-gated cation-selective membrane channel. *Proc. Natl. Acad. Sci. U.S.A.* 100, 13940–13945. doi: 10.1073/pnas.1936192100

Nagode, D. A., Tang, A. H., Karson, M. A., Klugmann, M., and Alger, B. E. (2011). Optogenetic release of ach induces rhythmic bursts of perisomatic

ipscs in hippocampus. *PLoS One* 6:e27691. doi: 10.1371/journal.pone.0027691

Ng, G. A., Brack, K. E., and Coote, J. H. (2001). Effects of direct sympathetic and vagus nerve stimulation on the physiology of the whole heart–a novel model of isolated langendorff perfused rabbit heart with intact dual autonomic innervation. *Exp. Physiol.* 86, 319–329. doi: 10.1113/eph8602146

Nyns, E. C. A., Kip, A., Bart, C. I., Plomp, J. J., Zeppenfeld, K., Schalij, M. J., et al. (2016). Optogenetic termination of ventricular arrhythmias in the whole heart: towards biological cardiac rhythm management. *Eur. Heart J.* 38, 2132–2136. doi: 10.1093/eurheartj/ehw574

Pauza, D. H., Saburkina, I., Rysevaite, K., Inokaitis, H., Jokubauskas, M., Jalife, J., et al. (2013). Neuroanatomy of the murine cardiac conduction system. a combined stereomicroscopic and fluorescence immunohistochemical study. *Auton. Neurosci.* 176, 32–47. doi: 10.1016/j.autneu.2013.01.006

Randall, W. C., Milosavljevic, M., Wurster, R. D., Geis, G. S., and Ardell, J. L. (1986). Selective vagal innervation of the heart. *Ann. Clin. Lab. Sci.* 16, 198–208.

Reid, J. V, Ito, B. R., Huang, A. H., Buffington, C. W., and Feigl, E. O. (1985). Parasympathetic control of transmural coronary blood flow in dogs. *Am. J. Physiol.* 249, H337–H343. doi: 10.1152/ajpheart.1985.249.2.H337

Ren, J., Qin, C., Hu, F., Tan, J., Qiu, L., Zhao, S., et al. (2011). Habenula " cholinergic" neurons corelease glutamate and acetylcholine and activate postsynaptic neurons via distinct transmission modes. *Neuron* 69, 445–452. doi: 10.1016/j.neuron.2010.12.038

Ripplinger, C. M., Noujaim, S. F., and Linz, D. (2016). The nervous heart. *Prog. Biophys. Mol. Biol.* 120, 199–209. doi: 10.1016/j.pbiomolbio.2015.12.015

Rossi, J., Balthasar, N., Olson, D., Scott, M., Berglund, E., Lee, C. E., et al. (2011). Melanocortin-4 receptors expressed by cholinergic neurons regulate energy balance and glucose homeostasis. *Cell Metab.* 13, 195–204. doi: 10.1016/j.cmet.2011.01.010

Roy, A., Guatimosim, S., Prado, V. F., Gros, R., and Prado, M. A. (2014). Cholinergic activity as a new target in diseases of the heart. *Mol. Med.* 20, 527–537. doi: 10.2119/molmed.2014.00125

Rysevaite, K., Saburkina, I., Pauziene, N., Vaitkevicius, R., Noujaim, S. F., Jalife, J., et al. (2011). Immunohistochemical characterization of the intrinsic cardiac neural plexus in whole-mount mouse heart preparations. *Heart Rhythm* 8, 731–738. doi: 10.1016/j.hrthm.2011.01.013

Yamasaki, S., Stolfi, A., Liu, W., and Pickoff, A. S. (1993). Time-dependent changes in the chronotropic response to vagal stimulation in the newborn canine. *Pediatr. Res.* 34, 139–143. doi: 10.1203/00006450-199308000-00006

Sampaio, K. N., Mauad, H., Spyer, K. M., and Ford, T. W. (2003). Differential chronotropic and dromotropic responses to focal stimulation of cardiac vagal ganglia in the rat. *Exp. Physiol.* 88, 315–327. doi: 10.1113/eph8802525

Schiereck, P., Sanna, N., and Mosterd, W. L. (2000). AV blocking due to asynchronous vagal stimulation in rats. *Am. J. Physiol. Heart Circ. Physiol.* 278, H67–H73. doi: 10.1152/ajpheart.2000.278.1.H67

Schuessler, R. B., Bromberg, B. I., and Boineau, J. P. (1990). Effect of neurotransmitters on the activation sequence of the isolated atrium. *Am. J. Physiol.* 258, H1632–H1641. doi: 10.1152/ajpheart.1990.258.6.H1632

Takahashi, H., Maehara, K., Onuki, N., Saito, T., and Maruyama, Y. (2003). Decreased contractility of the left ventricle is induced by the neurotransmitter acetylcholine, but not by vagal stimulation in rats. *Jpn. Heart J.* 44, 257–270. doi: 10.1536/jhj.44.257

Wengrowski, A. M., Wang, X., Tapa, S., Posnack, N. G., Mendelowitz, D., and Kay, M. W. (2015). Optogenetic release of norepinephrine from cardiac sympathetic neurons alters mechanical and electrical function. *Cardiovasc. Res.* 105, 143–150. doi: 10.1093/cvr/cvu258

Wessler, I., Kirkpatrick, C. J., and Racké, K. (1999). The cholinergic "pitfall": Acetylcholine, a universal cell molecule in biological systems, including humans. *Clin. Exp. Pharmacol. Physiol.* 26, 198–205. doi: 10.1046/j.1440-1681.1999.03016.x

Xu, L., Gutbrod, S. R., Bonifas, A. P., Su, Y., Sulkin, M. S., Lu, N., et al. (2014). 3D multifunctional integumentary membranes for spatiotemporal cardiac measurements and stimulation across the entire epicardium. *Nat. Commun.* 5:3329. doi: 10.1038/ncomms4329

Conflict of Interest Statement: The authors declare that the research was conducted in the absence of any commercial or financial relationships that could be construed as a potential conflict of interest.

frontiers in Physiology

ORIGINAL RESEARCH
published: 17 December 2018
doi: 10.3389/fphys.2018.01806

Cardiac Electrophysiological Effects of Light-Activated Chloride Channels

Ramona A. Kopton[1,2,3], *Jonathan S. Baillie*[4], *Sara A. Rafferty*[4], *Robin Moss*[1,2], *Callum M. Zgierski-Johnston*[1,2], *Sergey V. Prykhozhij*[5], *Matthew R. Stoyek*[4], *Frank M. Smith*[6], *Peter Kohl*[1,2], *T. Alexander Quinn*[4,7] *and Franziska Schneider-Warme*[1,2]*

[1] Institute for Experimental Cardiovascular Medicine, University Heart Centre Freiburg–Bad Krozingen, Medical Center—University of Freiburg, Freiburg, Germany, [2] Faculty of Medicine, University of Freiburg, Freiburg, Germany, [3] Faculty of Biology, University of Freiburg, Freiburg, Germany, [4] Department of Physiology and Biophysics, Dalhousie University, Halifax, NS, Canada, [5] Department of Pediatrics, Dalhousie University, Halifax, NS, Canada, [6] Department of Medical Neuroscience, Dalhousie University, Halifax, NS, Canada, [7] School of Biomedical Engineering, Dalhousie University, Halifax, NS, Canada

During the last decade, optogenetics has emerged as a paradigm-shifting technique to monitor and steer the behavior of specific cell types in excitable tissues, including the heart. Activation of cation-conducting channelrhodopsins (ChR) leads to membrane depolarization, allowing one to effectively trigger action potentials (AP) in cardiomyocytes. In contrast, the quest for optogenetic tools for hyperpolarization-induced inhibition of AP generation has remained challenging. The green-light activated ChR from *Guillardia theta* (GtACR1) mediates Cl^--driven photocurrents that have been shown to silence AP generation in different types of neurons. It has been suggested, therefore, to be a suitable tool for inhibition of cardiomyocyte activity. Using single-cell electrophysiological recordings and contraction tracking, as well as intracellular microelectrode recordings and *in vivo* optical recordings of whole hearts, we find that GtACR1 activation by prolonged illumination arrests cardiac cells in a depolarized state, thus inhibiting re-excitation. In line with this, GtACR1 activation by transient light pulses elicits AP in rabbit isolated cardiomyocytes and in spontaneously beating intact hearts of zebrafish. Our results show that GtACR1 inhibition of AP generation is caused by cell depolarization. While this does not address the need for optogenetic silencing through physiological means (i.e., hyperpolarization), GtACR1 is a potentially attractive tool for activating cardiomyocytes by transient light-induced depolarization.

Keywords: heart, optogenetics, action potential, GtACR1, natural anion channelrhodopsin, zebrafish

OPEN ACCESS

Edited by:
Ming Lei,
University of Oxford, United Kingdom

Reviewed by:
Christopher Huang,
University of Cambridge, United Kingdom
Claudia Richter,
Max-Planck-Institut für Dynamik und Selbstorganisation, Germany

***Correspondence:**
Franziska Schneider-Warme
franziska.schneider@universitaets-herzzentrum.de

Specialty section:
This article was submitted to Cardiac Electrophysiology, a section of the journal Frontiers in Physiology

Received: *30 September 2018*
Accepted: *30 November 2018*
Published: *17 December 2018*

Citation:
Kopton RA, Baillie JS, Rafferty SA, Moss R, Zgierski-Johnston CM, Prykhozhij SV, Stoyek MR, Smith FM, Kohl P, Quinn TA and Schneider-Warme F (2018) Cardiac Electrophysiological Effects of Light-Activated Chloride Channels. Front. Physiol. 9:1806. doi: 10.3389/fphys.2018.01806

INTRODUCTION

Understanding multicellular electrophysiological interactions in intact biological tissue requires potent tools to measure and alter electrical behavior of interrogated cell populations in a controlled manner. In optogenetics, this can be implemented by cell-specific expression of fluorescent reporter proteins that are sensitive to changes in membrane voltage or cellular ion concentrations (pH, Ca^{2+}), and by optogenetic actuators (mainly retinal-binding microbial opsins) that act as light-activated ion conductors in the targeted cells (Deisseroth et al., 2006; Miesenböck, 2009). Cation non-selective channelrhodopsins such as ChR2 mediate light-gated currents that depolarize excitable cells, including neurons and cardiomyocytes, beyond the threshold for action potential

(AP) generation, thereby allowing optical pacing (Boyden et al., 2005; Bruegmann et al., 2010). Conversely, prokaryotic proton (e.g., ArchT), chloride (e.g., N_pHR), and sodium (e.g., KR2) pumps can mediate outward photocurrents that drive membrane hyperpolarization (Han and Boyden, 2007; Zhang et al., 2007; Han et al., 2011; Inoue et al., 2013; Grimm et al., 2018). These light-driven ion pumps have been used to silence neuronal activity *in vitro* and *in vivo* (Zhang et al., 2007; Gradinaru et al., 2008; Arrenberg et al., 2009; Han et al., 2011; Kato et al., 2015; Grimm et al., 2018) and to slow down heart rate or to block conduction by selectively illuminating either pacemaker or atrioventricular canal tissue in the developing zebrafish heart (Arrenberg et al., 2010). A major limitation of hyperpolarizing ion pumps is their capacity to maximally transport one ion per absorbed photon, requiring high membrane expression levels of the pump in combination with high-intensity sustained illumination to effectively inhibit AP generation (Gradinaru et al., 2010; Zhang et al., 2011; Mattis et al., 2012). Moreover, by actively transporting ions against electrochemical gradients, prolonged pump activation alters cellular energy balance and trans-membrane ion distribution, with potentially unintended side-effects on other facets of cellular behavior (Raimondo et al., 2012; Alfonsa et al., 2015; Mahn et al., 2016).

The optogenetic toolbox has recently been extended by anion-selective channelrhodopsins (ACR). First variants (ChloC, iC1C2) were engineered by targeted mutagenesis of cation channelrhodopsins and showed a residual proton conductance (Berndt et al., 2014; Wietek et al., 2014), which was largely eliminated in subsequent optimized variants (iChloC, iC++) (Wiegert et al., 2015; Berndt et al., 2016). Engineered ACR have been complemented by naturally occurring ACR, first identified in the cryptophyte species *Guillardia theta* (GtACR1 and GtACR2) (Govorunova et al., 2015a), and more than 20 related proteins have been reported so far (Govorunova et al., 2015b, 2017; Wietek et al., 2016). Upon expression in animal cells, GtACR1 and GtACR2 support large Cl^--mediated currents with high operational light sensitivity (Govorunova et al., 2015a). GtACR1 and GtACR2 have been used in a number of studies to inhibit neuronal firing by "shunting" the membrane potential toward the reversal potential (E_{rev}) for Cl^- (Malyshev et al., 2017; Mauss et al., 2017; Mohamed et al., 2017; Forli et al., 2018). First cardiac use of ACR was performed by Govorunova et al. comparing photocurrents of GtACR1 and the proton pump Arch3 in neonatal rat ventricular cardiomyocytes. GtACR1 required light intensities that were four orders of magnitude lower than those needed for Arch3 to activate photocurrents of comparable amplitudes. Using extracellular potential recordings, the authors observed that GtACR1-driven Cl^- currents reversibly inhibit spontaneous AP in cultured neonatal cardiomyocytes at light levels at which inhibition by Arch3 was inefficient (Govorunova et al., 2016).

In the current study, we characterize the electrophysiological and optical activation properties of GtACR1 in HEK 293T cells and primary cultured ventricular cardiomyocytes from rabbits. We assess the mechanism by which activation of GtACR1 may arrest cardiac AP and cellular contractions in rabbit isolated cardiomyocytes and in zebrafish hearts, both *ex* and *in vivo*. We show that GtACR1 enables large Cl^- currents that can be titrated by changing light intensity and/or light pulse duration. Using patch-clamp recordings, we observe depolarizing photocurrents at negative membrane potentials for all tested Cl^- concentrations. Using intracellular microelectrode recordings in zebrafish hearts, we confirm GtACR1-mediated depolarization of resting cells *in situ*. Thus, light-induced inhibition of cardiomyocyte excitability upon sustained GtACR1 activation is based on membrane depolarization. Short light pulses, in contrast, allow one to optically pace isolated cells and whole hearts, and to trigger cardiac contractions.

We conclude that ACR mediate depolarizing photocurrents in resting cardiomyocytes, which can be used for both activation and inhibition of cardiac activity. The observed inhibition is not based on reaching a physiological resting (re-/hyperpolarized) state. A suitable optogenetic tool to silence cardiomyocyte activation by clamping the membrane potential to diastolic resting potential levels by opening a K^+ conductance has recently been reported (Bernal Sierra et al., 2018), but further effort will need to be applied to accelerating the system's on- and off-kinetics. A rapid K^+-based silencing tool would be useful to temporarily block cardiac conduction in defined cell populations with the aim of investigating the basic mechanisms underlying atrial and ventricular arrhythmogenesis and cardioversion. In the future, this could facilitate the development of optimized strategies for arrhythmia termination, potentially by optogenetic approaches.

RESULTS

Ion Selectivity of GtACR1

We performed whole-cell patch-clamp recordings in transiently transfected HEK 293T cells to characterize in detail the GtACR1-mediated photocurrents and their ion dependency. Upon green-light application, GtACR1 activation results in large photocurrents whose direction and amplitude depends on the Cl^- concentration gradient (**Figures 1A–C**). E_{rev} for GtACR1-mediated currents are -15.0 ± 0.3, -1.7 ± 0.2, and $+35.6 \pm 1.1$ mV for extracellular Cl^- concentrations ($[Cl^-]_{ex}$) of 151.4, 71.4, and 11.4 mM, respectively, (with an intracellular Cl^- concentration $[Cl^-]_{in}$ of 54.0 mM) (**Figure 1G**). The experimentally observed reversal potentials deviate from calculated reversal potentials for a pure chloride channel at 25 °C in a non-linear manner (theoretical reversal potentials according to the Nernst equation are −26.5, −7.2, and +40.0 mV, respectively). Decreasing Cl^- levels of the internal (pipette) solution shifts reversal potentials to more negative values (-32.1 ± 1.0 and -45.8 ± 2.8 mV at 15 and 4 mM $[Cl^-]_{in}$, respectively; **Supplementary Figure 1A**), again with major deviations from theoretically predicted potentials for a pure Cl^- conductance (−59.4 and −93.4 mV, respectively). For all Cl^- concentration gradients tested, we observe inward currents (in line with a net outward movement of anions) at negative membrane potentials. To test for a potential additional cation conductance that would explain differences between theoretical and experimentally observed reversal potentials, we also varied external pH, K^+ and Na^+ concentrations. Photocurrent amplitudes and reversal

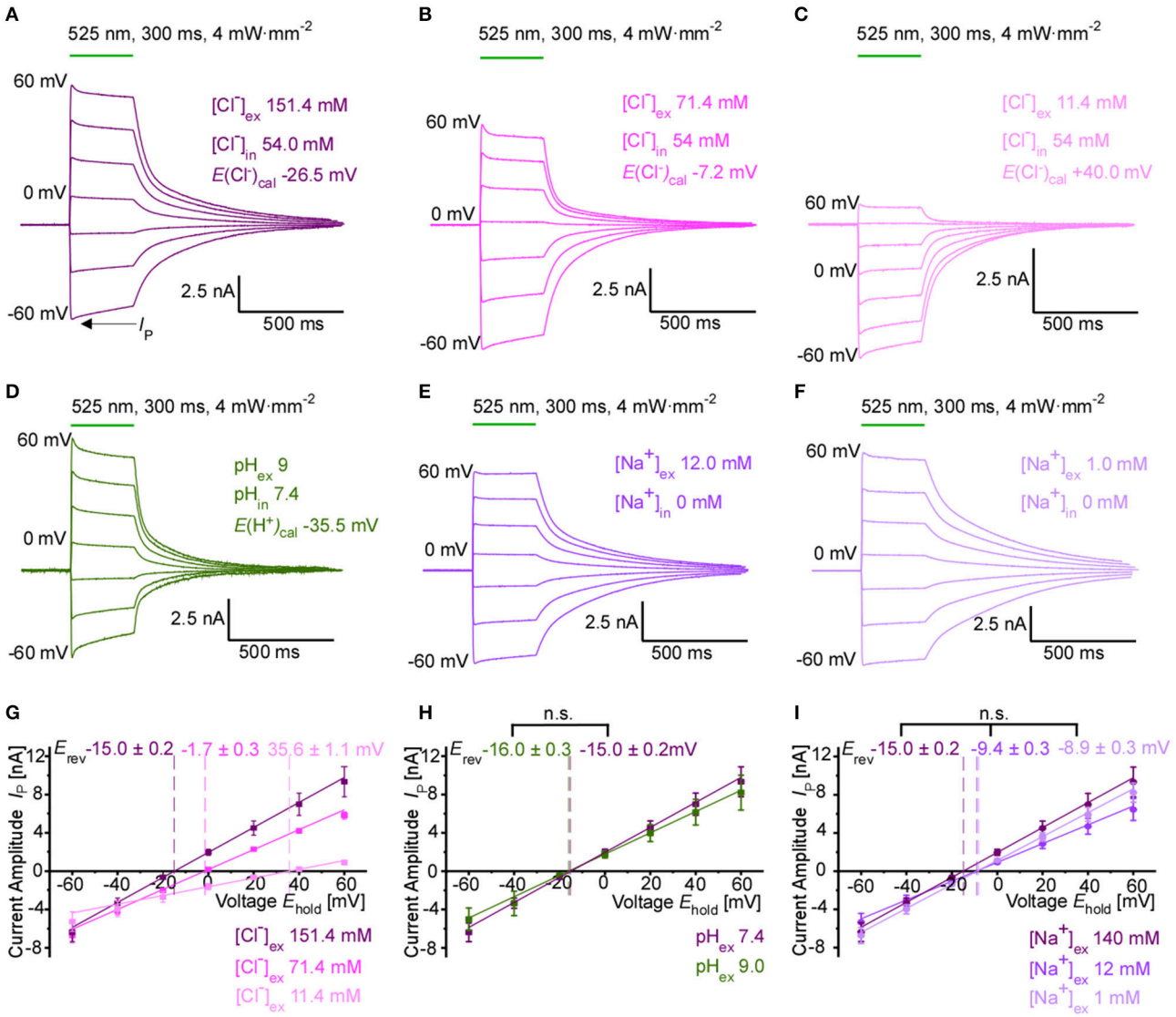

FIGURE 1 | Ion selectivity of GtACR1-driven photocurrents in HEK 293T cells. **(A–F)** Representative whole-cell currents at holding membrane potentials from −60 mV to +60 mV (step size 20 mV). Peak current I_P is indicated. The calculated reversal potential $E_{rev,cal}$ is stated at 25°C. Standard pipette solution contained 54 mM Cl^- and 0 mM Na^+. External bath solution contained **(A)** standard high, **(B)** moderately reduced and **(C)** strongly reduced Cl^- concentration. (**D**) Photocurrent using an alkaline external solution (pH 9.0), Cl^- concentrations as in **(A)**. **(E,F)** Photocurrent at moderately reduced **(E)** and strongly reduced Na^+ concentration **(F)**, Cl^- concentrations as in **(A)**. **(G)** *IE* relationship recorded at different external Cl^- concentrations (n = 8–12). Mean reversal potentials (E_{rev}) ± SE are marked in the respective color. **(H)** *IE* relationship recorded at pH 7.4 and pH 9.0 (n = 8–12, Mann-Whitney $p > 0.05$). **(I)** *IE* relationship recorded at various Na^+ concentrations (n = 10–12, Mann-Whitney $p > 0.05$).

potentials are not altered when reducing external proton concentration to pH 9.0 (**Figures 1D,H**) or varying external K^+ concentration (**Supplementary Figure 1B**). Decreasing the extracellular Na^+ concentration shifts the observed whole-cell current reversal potential to slightly more positive values (−9.4 ± 0.3 and −8.9 ± 0.3 mV at 12 and 1 mM $[Na^+]_{ex}$, respectively; $[Cl^-]_{in}$ of 54.0 mM), while average current amplitudes at negative membrane potentials appear unaffected (**Figures 1E,F,I**). Similar changes in reversal potential by variation of the internal Cl^- concentration, and the absence of a sensitivity to pH were confirmed in cardiomyocytes expressing GtACR1 (**Supplementary Figures 1C,D**).

Photoactivation of GtACR1 in Cardiomyocytes

Using adenoviral transduction, GtACR1-eGFP was expressed in cultured primary ventricular cardiomyocytes from rabbit hearts (**Figure 2A** insert). We performed whole-cell patch clamp recordings to test the functionality of the Cl^- channel in cardiomyocytes. At a holding potential of −60 mV, green light pulses elicit large inward currents that can be graded by applied light intensity and/or pulse duration (**Figures 2A–G**). Half-maximal peak amplitudes are reached at 3.08 and 0.93 $mW{\cdot}mm^{-2}$ for short light pulses of 1 and 10 ms, respectively. Using longer light pulses (≥100 ms) half-maximal amplitudes

TABLE 1 | Bi-exponential current decay after light activation of GtACR1 in ventricular cardiomyocytes.

Time constants at −60 mV	Low light intensity (0.1 mW·mm^{-2})		High intensity (4 mW·mm^{-2})	
	τ_{off1} (ms)	τ_{off2} (ms)	τ_{off1} (ms)	τ_{off2} (ms)
Short light pulses (10 ms)	32 ± 2	125 ± 19	46 ± 3	224 ± 18
Prolonged light pulses (300 ms)	36 ± 1	172 ± 14	48 ± 4 23 ± 3	271 ± 23 246 ± 15

Black values were obtained at −60 mV (n = 8); gray values reflect current decline at +20 mV (n = 20).

are observed at approximately 0.58 mW·mm^{-2}. Channel closure follows a bi-exponential decline after illumination terminates (see **Table 1** for τ values for selected exposure times and light intensities). When activated by longer light exposure, a proportion of channels inactivates (or transitions to an open state of lower conductance) resulting in stationary currents of reduced amplitude (**Figure 2D**). Repetitive channel activation results in transient channel inactivation reflected by reduction of the peak current (I_p) by 4%, which recovers to initial values with $\tau_{recovery}$ = (2.2 ± 0.2) s (**Figures 2H,I**). Our data provides evidence that GtACR1 is functional in cardiomyocytes without addition of external retinal and that current characteristics can be titrated using light pulses of different intensity and duration.

AP Inhibition Using Prolonged GtACR1 Activation *in vitro*

Based on previous reports using GtACR1 for neuronal and cardiac silencing, we assessed the utility of using GtACR1 to inhibit electrically evoked AP in ventricular cardiomyocytes. In current-clamp recordings, AP are triggered by 10-ms current ramps at 0.25 Hz. Prolonged green light application (64 s at 4 mW·mm^{-2}) results in membrane depolarization (to −21.0 ± 1.7 mV), thereby preventing further AP generation (**Figure 3A**). Light-induced inhibition is reversible, and AP before and after optical silencing show comparable durations at 90% repolarization (APD_{90}; **Figures 3B–D**). Using an illumination protocol with varying pulse duration and light intensity for repeated depolarization of cardiomyocytes, we found that the average membrane potential during repeated light exposure increases to more positive values over time (starting membrane potential: −59.6 mV, end membrane potential: −57.4 mV). This may be due to changes in intracellular ion concentrations (**Figure 3E**, for exemplary current traces see **Supplementary Figure 2**). In contrast, green light application does not affect resting membrane potential and APD_{90} in non-transduced control cells (**Supplementary Figures 1G,H**). Light-induced silencing of cardiomyocytes was also assessed in intact cells by measuring sarcomere length changes during electrical field stimulation. Similar to electrophysiological recordings, sustained light inhibits cardiomyocyte activity (**Figure 3F**). Upon onset of sustained illumination, we observed a short and low-amplitude contraction. While resting sarcomere length is slightly reduced in GtACR1-expressing cells compared to non-transduced control cells, no differences were observed in fractional sarcomere shortening or contraction kinetics before and after light-induced silencing compared to control cells (**Figures 3G,H**, **Supplementary Figures 1I–N**).

GtACR1-Mediated Optical Pacing *in vitro*

Since GtACR1 activation leads to cardiomyocyte membrane depolarization at negative membrane potentials, we tested whether GtACR1-expressing cardiomyocytes can be optically paced. Short low-intensity light pulses (10 ms, 0.1 mW·mm^{-2}) are sufficient to reliably trigger AP in cultured GtACR1-positive cells (**Figures 4D,E**), but not in wild-type controls. When compared to electrically induced AP (**Figures 4A–G**), optically stimulated AP show prolonged late repolarization, reflected by a significantly longer APD_{90}, while APD at 20% repolarization (APD_{20}) is not different between optical (OP) and electrical (EP) pacing. Also, optically triggered AP show a slower onset and a late depolarized phase, as seen in the voltage difference plot between optically and electrically stimulated AP shown in **Figure 4F**. Diastolic membrane potential was slightly increased (more positive) with EP compared to OP (**Supplementary Figure 1E**). Resting membrane potential and APD_{90} with OP are not altered when light intensity is increased from threshold to 2× threshold (**Figure 4H**, **Supplementary Figure 1F**). Finally, in experiments tracking sarcomere length changes in intact cells, we observe successful OP, leading to cardiomyocyte contractions similar to electrically triggered beats (**Figures 4I,J**).

Effects of Prolonged GtACR1 Activation in Intact Zebrafish Hearts

Zebrafish served as a model system to study effects of GtACR1 activation in native myocardium (Rafferty and Quinn, 2018; Ravens, 2018). GtACR1-eGFP was expressed specifically in cardiac myocytes in the hearts of zebrafish using Tol2 transposon transgenesis by microinjection of a cmlc2:GtACR1-eGFP plasmid at the one-cell stage. Fish with successful gene insertion, indicated by cardiac eGFP expression, were raised to 3 months. Hearts were isolated and intracellular microelectrode recordings of ventricular myocyte membrane potential were performed.

GtACR1-eGFP expression in the ventricle was largely epicardial and heterogeneous at the cellular level (**Supplementary Figure 3**), with regions of high eGFP expression next to eGFP-free areas at the whole-heart level (**Figures 5**, **6**). Light for activation of GtACR1 was focused on regions of high or no eGFP expression (spot size of 0.16 mm^2). When sustained light (5 mW·mm^{-2}) is applied to regions of high eGFP expression, there is an immediate depolarization of resting membrane potential (E_R) and a decrease in the maximum rate of membrane potential change (dE/dt_{max}) during the AP upstroke, as well as in AP amplitude (AP_{Amp}), APD_{50} and APD_{90} (**Figure 5**, n = 34 cells, N = 7 zebrafish). Additionally, in regions of high eGFP-expression in some hearts (N = 3/7), sustained light locally inhibits AP generation by depolarization of membrane potential (**Figure 6**). Ventricular contractions could also be inhibited *in vivo* by exposing the entire ventricle (spot

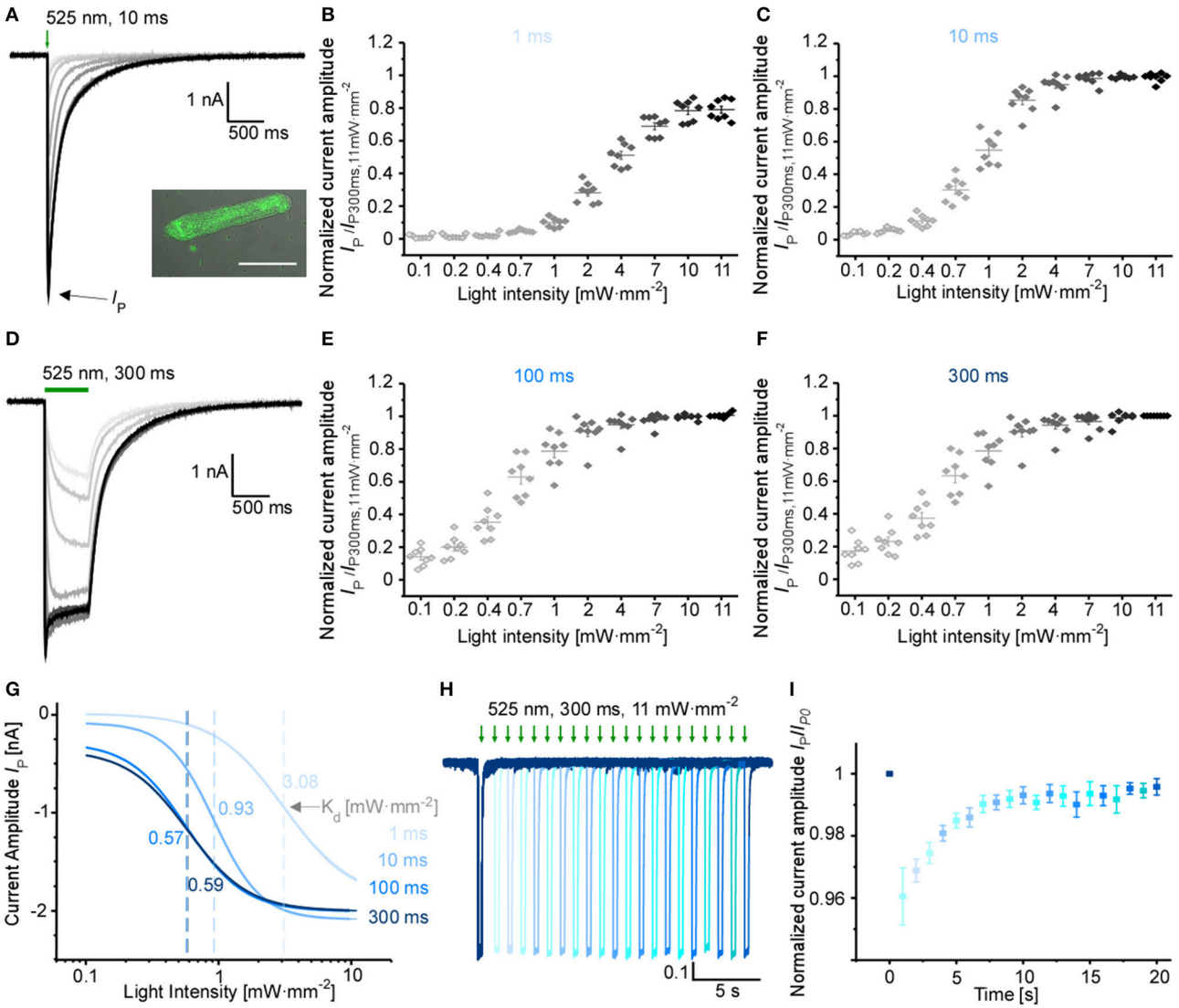

FIGURE 2 | Characterization of GtACR1 currents in rabbit isolated cardiomyocytes. **(A)** Representative voltage-clamp recordings at −60 mV using light pulses of 10 ms. The insert shows a fluorescence image of GtACR1-eGFP expressed in cultured cardiomyocytes. Scale bar 50 μm. **(B,C,E,F)** Light titration at various light intensities using light pulses of **(B)** 1 ms, **(C)** 10 ms, **(E)** 100 ms, **(F)** 300 ms ($n = 8$, $N = 2$). Please note non-linear scaling of x-axis. **(D)** Representative voltage-clamp-recordings at −60 mV using light pulses of 300 ms. **(G)** Mean peak current I_P was fitted by the Hill equation. Dissociation constant K_d [mW·mm^{-2}] was calculated for each light duration ($K_{d,1ms} = 3.08 \pm 0.17$, $K_{d,10ms} = 0.93 \pm 0.03$, $K_{d,\ 100ms} = 0.57 \pm 0.04$, $K_{d,300ms} = 0.59 \pm 0.04$). **(H)** Representative voltage-clamp recording at −60 mV. Each trace was normalized to the first peak. Dark interval of Δ1 s between light pulses in each dual-stimulation experiment. **(I)** Recovery of normalized peak current ($n = 7$, $N = 2$) during repeat optical stimulation, measured at maximum light intensity of 11 mW·mm^{-2} and light pulse duration of 300 ms.

size of 0.05 mm^2) of intact eGFP-positive zebrafish larvae (21 days post fertilization, $N = 3$) to sustained light (1.7 mW·mm^{-2}; **Supplementary Movie 1**).

Optical Pacing of Zebrafish Hearts

When pulsed light (10 ms, 2× sinus heart rate) of supra-threshold intensity (1.2 ± 0.2 mW·mm^{-2}; determined in each heart by increasing light intensity until AP stimulation occurred) is applied to regions of high eGFP expression, AP are elicited, resulting in OP of the heart (**Figure 5**). Comparison of AP, stimulated by OP and EP at the same rate, shows no difference in AP characteristics (**Supplementary Figure 4**). As with sustained light, pulsed light also had an effect *in vivo* in intact eGFP-positive zebrafish larvae, eliciting ventricular contractions resulting from OP. In contrast to GtACR1-expressing regions, neither sustained nor pulsed light application to eGFP-negative myocardial tissue in the same animals, or to ventricular myocardium from wild-type zebrafish ($N = 3$), induces any changes in membrane potential.

DISCUSSION

Tools to modulate cardiac electrophysiology in a spatio-temporally defined, cell-specific manner hold a key to improving

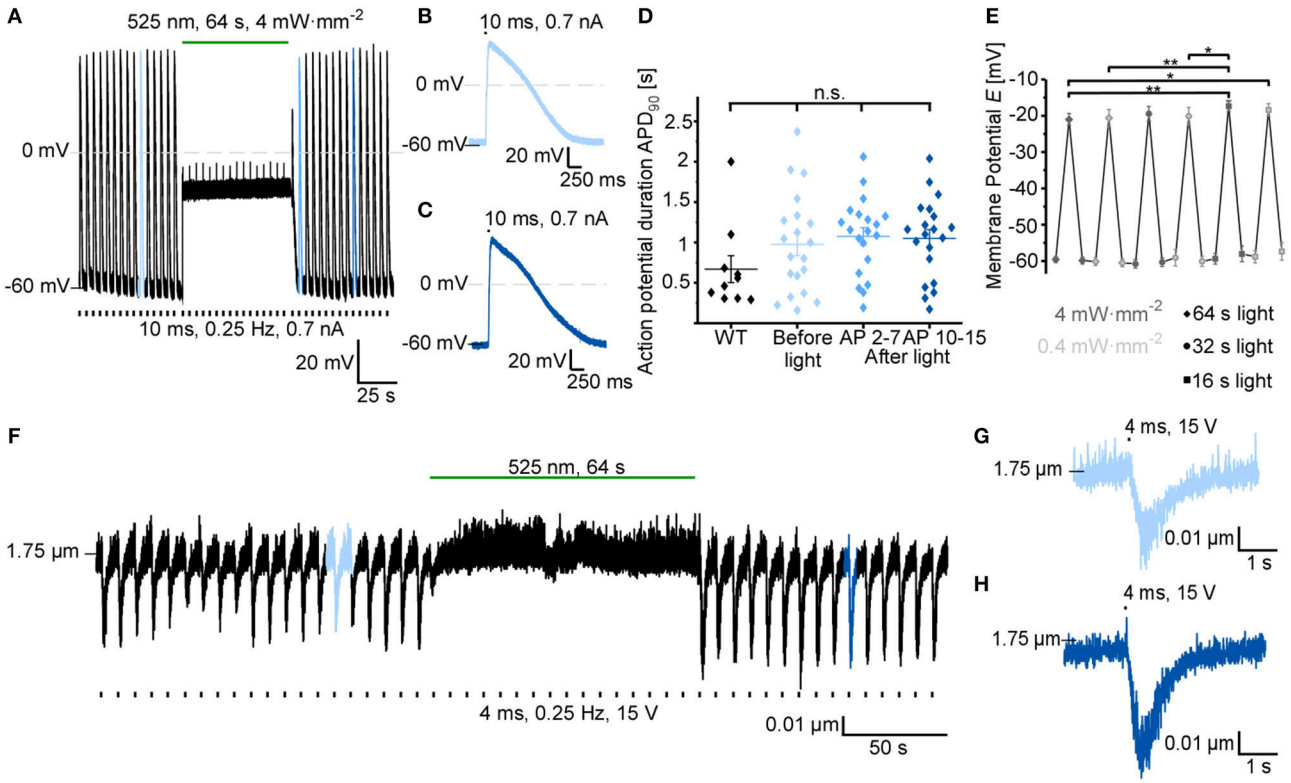

FIGURE 3 | GtACR1 inhibits electrically paced cardiomyocytes by depolarization. **(A)** Representative trace of cardiomyocyte membrane potential during electrical pacing (EP) at 0.25 Hz (current injections of 0.7 nA for 10 ms). A sustained 64 s light pulse inhibits AP generation by depolarizing the cell to about −20 mV. **(B)** 10th AP before light application. **(C)** 10th AP after end of light exposure. **(D)** Comparison of APD_{90} before light (AP 2-7) and at two different time points after light exposure (average APD_{90} of AP 2-7 and AP 10-15) to APD_{90} in non-transduced WT cells (WT $n = 10$, $N = 1$; GtACR1 transduced cells $n = 23$, $N = 2$). Wilcoxon test (WT vs. before light): $p > 0.05$. ANOVA one-way repeated Dunnett test (before vs. after light): $p > 0.05$. **(E)** Membrane potential E was recorded before, during and after light pulses of various durations (64 s, 32 s, 16 s) and light intensities (4 mW·mm^{-2}, 0.4 mW·mm^{-2}; $n = 11$, $N = 2$). Results of ANOVA one-way repeated Tukey are indicated in graph (*$p \leq 0.05$, **$p \leq 0.01$). **(F)** Representative sarcomere length recording. The cell was electrically paced at 0.25 Hz by field-stimulation (15 V) and sarcomere length shortening was inhibited by light for 64 s. **(G)** 6th contraction before light application. **(H)** 10th contraction after light application.

our understanding of electrophysiological signaling in health and disease. ChR2 can be used for optical pacing, and for inhibition of AP generation—albeit by non-physiological sustained depolarization of the resting membrane potential. Prolonged membrane depolarization will lead to ion concentration imbalances, which could be particularly problematic in diseased tissue (Schneider-Warme and Ravens, 2018). ACR have been used to inhibit AP generation in neuronal cell populations and neonatal rat ventricular cardiomyocytes (Govorunova et al., 2016; Malyshev et al., 2017; Mauss et al., 2017; Mohamed et al., 2017; Forli et al., 2018). Here, we investigate their use in rabbit cardiomyocytes, and in intact zebrafish hearts.

We show that green-light activation of GtACR1 triggers depolarizing photocurrents in resting cardiomyocytes. GtACR1 currents are based on Cl^- conductance, with only minor current contributions by cations, such as Na^+, K^+, or H^+. Accordingly, cardiomyocyte inhibition by sustained illumination is based on polarizing cells toward the reversal potential for Cl^-. In line with an estimated reversal potential between −40 and −33 mV in cardiac myocytes (Clemo et al., 1999; Baumgarten et al., 2005), GtACR1-mediated myocyte inhibition relies on membrane depolarization, thus preventing myocyte repolarization. While keeping cardiomyocytes at a depolarized potential can block re-excitation and conduction, sustained depolarization will result in Ca^{2+} and Na^+ overload *via* activation of additional ion fluxes, e.g., through L- and T-type Ca^{2+} or background Na^+ channels. This would be detrimental in cases where cells are already overloaded with Ca^{2+} or Na^+, e.g., when using GtACR1 for inhibition of cardiomyocyte activity to terminate arrhythmias in pathologically remodeled myocardium (note: thus far, all experiments studying depolarization-based optogenetic inhibition have used "healthy" cardiomyocytes as a model system).

In contrast to cardiomyocytes, the reversal potential for Cl^- is closer to the resting membrane potential in the somatodendritic compartment of neurons, in which ACR have a hyper- or re-polarizing effect. Thus, ACR activation mimics neuronal inhibition by postsynaptic $GABA_A$ receptors (Wiegert et al., 2017). It would be wrong, though, to assume that ACR necessarily hyperpolarize all resting cells—as shown here. There

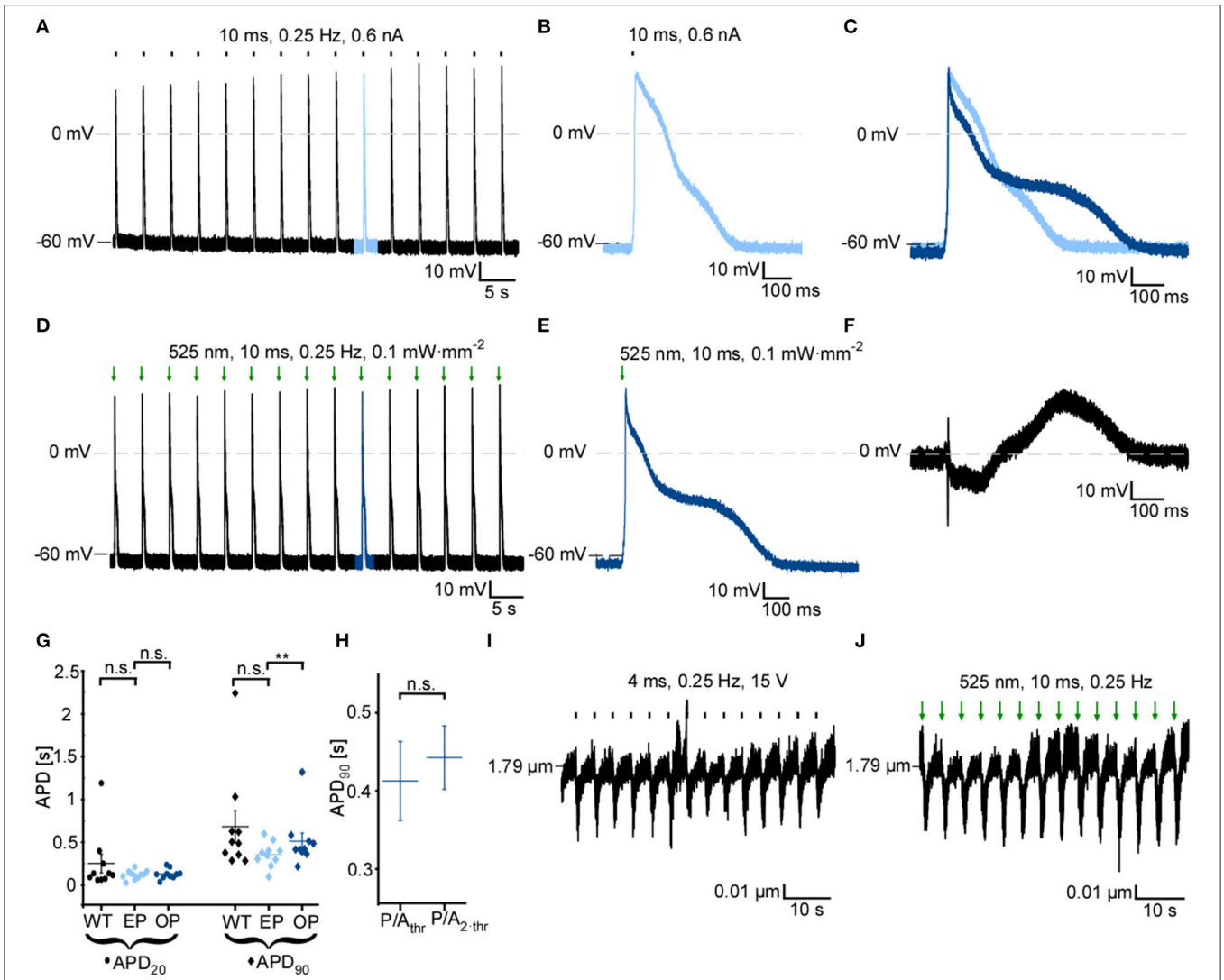

FIGURE 4 | GtACR1 activation by short light pulses enables optical pacing of cardiomyocytes. **(A)** Representative current-clamp recording at 0 pA during electrical pacing (EP) at 0.25 Hz using a current ramp of 0.6 nA, 10 ms. **(B)** 10th AP of electrically paced cardiomyocyte. **(C)** Overlay of the 10th AP of electrically (light blue) and optically (dark blue) paced cardiomyocyte. AP were aligned by dE/dt_{max}. **(D)** Representative current-clamp recording at 0 pA during optical pacing (OP) at 0.25 Hz by light pulses of 525 nm, 10 ms, 0.1 mW·mm^{-2}. **(E)** 10th AP of optically paced cardiomyocyte. **(F)** Difference of membrane potential during AP [shown in **(C)**] between OP and EP (E_{OP}-E_{EP}). **(G)** Comparison of AP duration of GtACR1-expressing cardiomyocytes during OP and EP to electrical stimulation of non-transduced WT cells ($n = 10$, $N = 2$). Mean APD_{20} and APD_{90} of the 10th to 15th AP are compared. Wilcoxon test (EP vs. OP): APD_{20} $p > 0.05$, APD_{90} $p < 0.01$, Mann-Whitney test (WT vs. EP): APD_{20} $p > 0.05$, APD_{90} $p > 0.05$. **(H)** APD_{90} of optically paced cardiomyocytes at threshold illumination (light power per area; P/A_{thr}) and two-times threshold light intensity ($P/A_{2\cdot thr}$). Wilcoxon test: $p > 0.05$ ($n = 6$, $N = 1$). **(I)** Sarcomere length recording of representative cell. Cardiomyocyte was electrically paced by field stimulation at 15 V, 0.25 Hz. **(J)** Sarcomere length recording of representative cell. OP by light pulses of 10 ms, 0.25 Hz. Statistical tests: n.s. $p > 0.5$, $^{**}p \leq 0.01$.

are neuronal compartments with elevated intracellular chloride concentrations, including presynaptic terminals and axons, where ACR activation can lead to depolarizing photocurrents. In fact, several studies have reported ACR-triggered presynaptic vesicle release and antidromic spikes (Mahn et al., 2016; Malyshev et al., 2017). To overcome these excitatory effects, soma-targeted ACR have been constructed by addition of the soma-targeting motifs of the K^+ channel $K_v2.1$ and telencephalin (Mahn et al., 2018; Messier et al., 2018). While optical inhibition with soma-targeted ACR can be effective in neurons, ACR-based cardiomyocyte inhibition is based on non-physiological sustained depolarization, as shown here both for isolated cells and myocytes within intact myocardium. A light-gated K^+ conductance could serve as a potent alternative for optical inhibition of excitatory cells (Bernal Sierra et al., 2018), as the resting potential of excitable cells is close to the K^+ reversal potential, thereby limiting secondary ion fluxes.

Based on depolarizing photocurrents, GtACR1 enables OP of cardiomyocytes *in vitro* and in zebrafish ventricles both *ex* and *in vivo*. In isolated myocytes, optically stimulated AP show

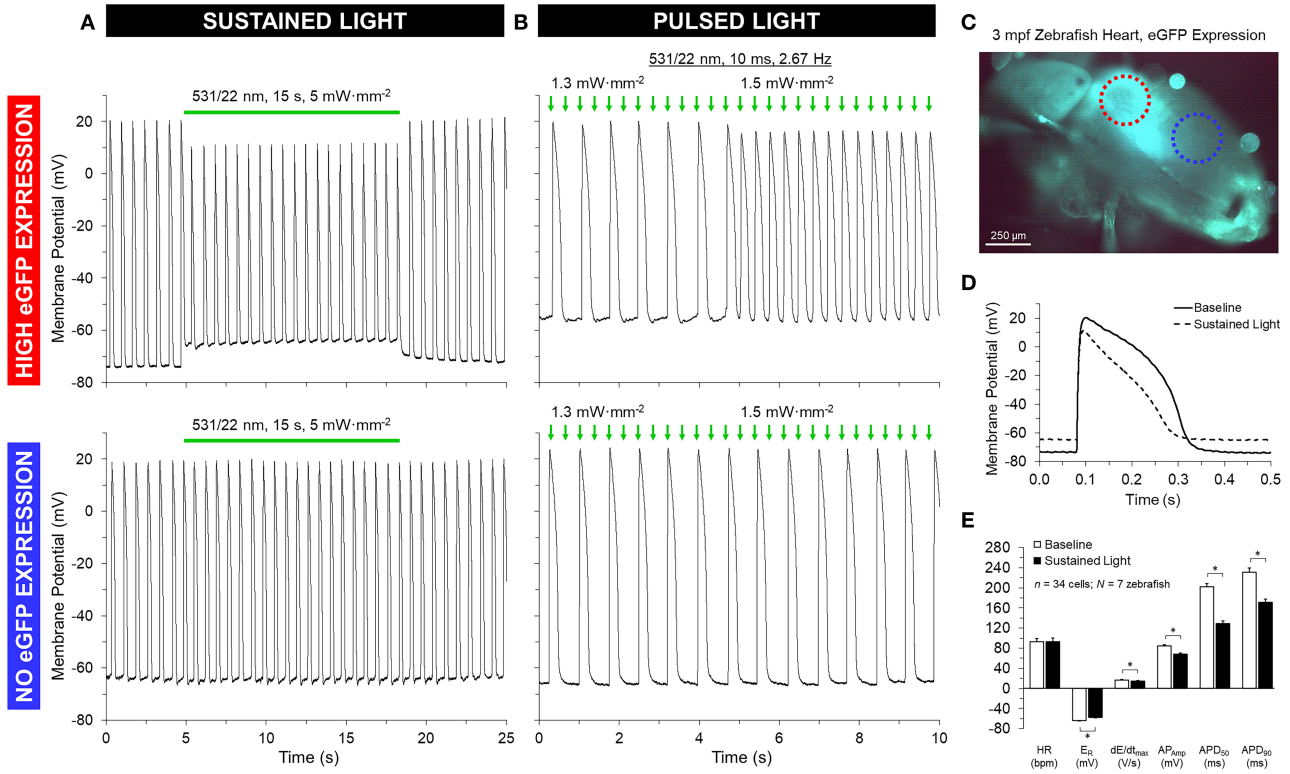

FIGURE 5 | GtACR1 activation depolarizes ventricular myocyte membrane potential in isolated zebrafish hearts. Regions of high or no eGFP expression on the ventricle of 3-months post fertilization (mpf) zebrafish isolated hearts were illuminated by a 0.16 mm^2 spot of 531/22 nm light sustained for 15 s or pulsed for 10 ms at a rate 2–3× sinus heart rate. **(A,D–E)** In the case of sustained light, in regions displaying eGFP expression (red circle in **C**) there was an immediate increase in resting membrane potential (E_R) and a decrease in the maximum rate of membrane depolarization (dE/dt_{max}), AP amplitude (AP_{Amp}), and APD at 50% and 90% repolarization (APD_{50} and APD_{90}). **(B)** In the case of pulsed light, the heart could be stimulated when light intensity was increased to supra-threshold values. **(A,B)** In both cases, there was no effect seen in regions displaying no eGFP expression (blue circle in **C**). *indicates $p < 0.0001$ by two-tailed paired Student's *t*-test.

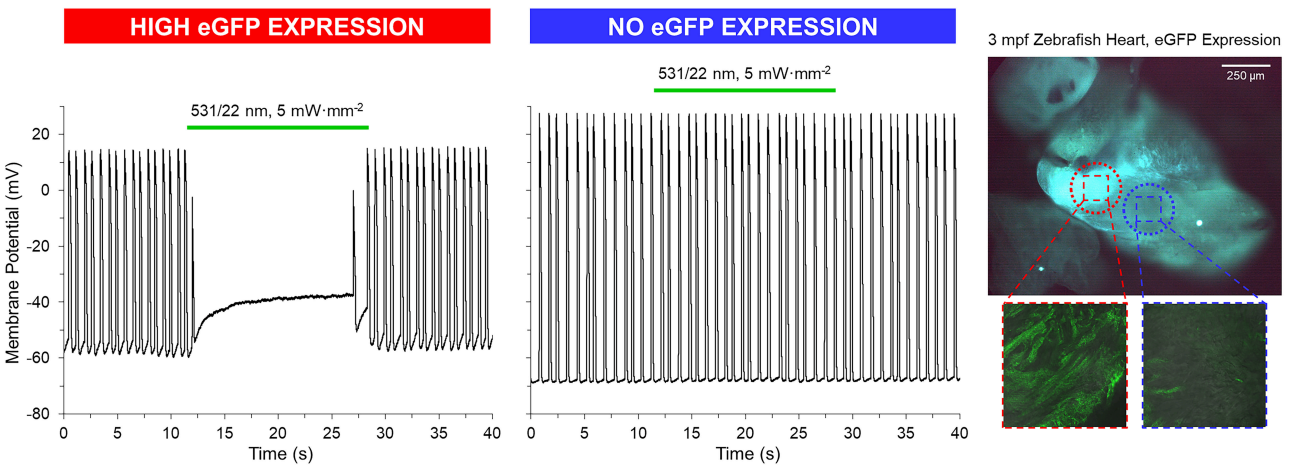

FIGURE 6 | GtACR1 activation can inhibit ventricular myocyte action potentials in isolated zebrafish hearts. In a subset of 3-months post fertilization (mpf) isolated zebrafish hearts ($n = 3/7$), a 0.16 mm^2 spot of 531/22 nm light applied to some eGFP expressing regions locally inhibited AP by depolarization of membrane potential, while there was no effect in regions with no eGFP expression (confirmed by live confocal microscopy).

delayed late repolarization, compared to electrically triggered AP. This can be explained by (i) the slow component of GtACR1 closing kinetics, resulting in residual photocurrents even after 200 ms (**Table 1**) and (ii) secondary activation of intrinsic Ca^{2+} channels (e.g., L-type Ca^{2+} channel) and/or the Na^{+}/Ca^{2+} exchanger in forward mode. Regarding photocurrent decline after illumination, one should take into account that channel closure is usually decelerated at more depolarized membrane voltages in channelrhodopsins, and only few variants (ChR2 T159C E123T; Chronos) display more or less voltage-insensitive closing kinetics (Schneider et al., 2015). In line with our data (**Table 1**), GtACR1 has been reported to show biphasic channel closure, with the fast component accelerating at depolarized potentials, whereas the slow component is similar at both positive and negative membrane voltages (Sineshchekov et al., 2015). To prevent prolongation of optical triggered AP, one could use an ACR with faster closing kinetics, such as the GtACR1-C237A mutant (Kim et al., 2018), PsACR1 (Govorunova et al., 2015b; Wietek et al., 2016) or ZipACR (Govorunova et al., 2017). In ventricular cells of intact zebrafish hearts, optically evoked AP display comparable amplitude and kinetics to same-frequency electrically stimulated AP. This difference between isolated and *in situ* myocytes may reflect effects of electrotonic coupling between GtACR1-expressing and non-expressing cells in the zebrafish heart. Indeed, confocal microscopy revealed heterogeneous GtACR1 expression at the cellular level, even in high eGFP-expression regions of zebrafish hearts, with direct proximity of expressing and non-expressing cells. Electrotonic effects may also explain the less pronounced GtACR1-mediated membrane depolarization observed in isolated zebrafish hearts, compared to rabbit isolated myocytes. Future studies with an established transgenic zebrafish line in which GtACR1-eGFP is expressed in myocytes homogeneously across the heart (generated by in-crossing the micro-injected fish used for testing in this study) will allow this hypothesis to be tested.

While ACR do not allow hyperpolarization of cardiomyocytes, they may be used to mimic Cl^{-} currents in cardiac cells. Both inward and outward chloride currents are present during the cardiac AP cycle and at least six families of Cl^{-} channels are functionally expressed in cardiomyocytes. Cl^{-} channels have been found to play a role in cardiac arrhythmogenesis, myocardial hypertrophy and heart failure, as well as in cardioprotection against ischemia reperfusion (Duan, 2013). ACR may be used to investigate the underlying roles of Cl^{-} channels in these disease settings, with light not only allowing for precise spatiotemporal control of ACR activity, but also enabling titration of current amplitudes by variation of light intensity and/or duration. Cell-type specific gene targeting may further enable investigating effects of Cl^{-} conductance on cells other than cardiomyocytes, and might be useful for studying heterocellular interactions between cardiomyocytes and non-myocytes (Johnston et al., 2017). Recent studies expressing optogenetic probes specifically in either cardiac macrophages of healthy mouse hearts, or in non-myocytes of ventricular scar-border zone tissue, showed functional electronic coupling of the targeted cell types to adjacent cardiomyocytes (Quinn et al., 2016; Hulsmans et al., 2017). The relevance of such coupling, however, both in normal homeostasis and in the context of cardiac tissue remodeling, remains to be determined. Optogenetic perturbation of electronically coupled non-myocytes might be a useful approach here, for example to modulate cardiac electrophysiological properties such as conduction velocity without interfering with cardiomyocyte function (as pioneered by Hulsmans et al., 2017).

Using GtACR1 to study cardiac electrophysiology in human tissue or hearts from larger mammals is limited by the restricted tissue penetration of green light needed for GtACR1 activation (maximal activation at ∼515 nm). This could be overcome by using flexible micro-LED systems for local light delivery (Ayub et al., 2017), or by replacing GtACR1 with a red-shifted ACR. Recent studies have identified ACR with action spectra shifted to longer wavelengths, both by protein engineering (Wietek et al., 2017) and genomic screening (Govorunova et al., 2017). The recently reported crystal structure of GtACR1 will facilitate further spectral tuning, e.g., by transferring mutations identified in the most red-shifted channelrhodopsin variant Chrimson S169A to GtACR1 and related ACR (Kim et al., 2018; Oda et al., 2018). Computational modeling has predicted that epicardial (and even pericardial) illumination will be sufficient for transmural activation of red-light gated channelrhodopsins in human hearts. This model considered the less light-sensitive ChR2, under the assumption of activation at 669 nm at an intensity of 10 $mW{\cdot}mm^{-2}$ (4.7-fold higher for pericardial light delivery) (Bruegmann et al., 2016). Thus, on the premise of further optimized means of light delivery and tuned rhodopsin variants, it should become feasible to use ACR for triggering transmural Cl^{-} currents in hearts from larger animals. Application to humans would require addressing a host of other issues, such as targeting specificity and avoidance of immunogenic responses. These aspects are the subject of ongoing studies in the field.

In summary, GtACR1 represents a potent tool for light-induced depolarization of defined cardiac cell populations. As is the case for ChR2, this can be used both to activate and to silence AP generation in cardiomyocytes. Compared to ChR2, ACR shows only weak intrinsic cation conductance, rendering ACR a superior tool for some applications, such as OP of myocardium. One has to keep in mind, however, that sustained membrane depolarization for cardiac silencing will give rise to secondary ion fluxes that may affect transmembrane ion distribution. This could increase arrhythmogenicity in myocardium, and be particularly counter-productive when using optogenetic approaches in ischemic myocardium where cardiomyocytes are already overloaded with Na^{+} and/or Ca^{2+}.

MATERIALS AND METHODS

If not stated otherwise chemicals were purchased from Sigma-Aldrich (St. Louis, MO, United States).

Molecular Biology

pUC57-GtACR1 was a kind gift from Dr. Jonas Wietek, Humboldt-Universität zu Berlin. The codon-optimized (mouse, human) sequence encoding for GtACR1 (*GenBank* accession

AKN63094.1) was subcloned into the peGFP-N1 vector (Clontech, Mountain View, CA, United States) using FastDigest NheI and AgeI (Thermo Fisher Scientific, Waltham, MA, USA).

For expression in cardiomyocytes, GtACR1-eGFP was cloned into pAdeno-CMV following the manufacturer's instructions (Adeno-X Adenoviral System, Clontech). Adenovirus was produced by the Viral Core Facility of the Charité—Universitätsmedizin Berlin, Germany.

HEK 293T Cell Culture

HEK 293T cells were seeded onto coverslips at a final density of 25,000 cells/mL. After 24h, jetPEI Transfection Reagent (Polyplus transfection, Illkirch, France) was used for transfecting GtACR1-eGFP into HEK 293T cells. HEK cells were measured 24–48 h post-transfection.

Cell Isolation and Culturing of Primary Cardiomyocytes

All rabbit experiments were carried out according to the guidelines stated in Directive 2010/63/EU of the European Parliament on the protection of animals used for scientific purposes and approved by the local authorities in Baden-Württemberg (X-16/10R). Culturing of isolated ventricular cells from rabbit hearts was performed as previously described (Bernal Sierra et al., 2018). Rabbits (9-10 weeks old of both sex [3 male, 4 female], total $N = 7$) were anesthetized via intramuscular injection of esketamine hydrochloride (Ketanest®S 25 mg/mL, Pfizer Pharma PFE GmbH, Berlin, Germany; 12.5 mg/kg body weight) and xylazine hydrochloride (Rompun® 2%, Bayer Vital GmbH, Leverkusen, Germany; 0.2 mL/kg body weight). During anesthesia 1,000 units heparin (Heparin-Sodium 5,000 I.E./mL, B. Braun Melsungen AG, Melsungen, Germany) and 5 mg esketamine hydrochloride were given intravenously. Thiopental (Thiopental Inresa 0.5 g, Inresa Arzneimittel GmbH, Freiburg, Germany; 12.5 mg/mL) was injected intravenously until apnea. The heart was excised and rinsed in normal Tyrode solution (**Table 2**). The aorta was cannulated, the heart was transferred to a Langendorff perfusion setup and perfused with normal Tyrode solution to wash out the blood. The heart was then perfused with Ca^{2+}-free cardioplegic solution (**Table 2**) for 3 more minutes after the heart had stopped beating, and it was then digested with enzyme solution (**Table 2**) until the tissue appeared soft (45–60 min). Left ventricle and septum were separated and cells were released by mechanical dissociation in blocking solution (**Table 2**).

After digestion cell suspensions were filtrated through a mesh (pore size [1 mm^2]) and centrifuged for 2 min at $22 \times g$ (gravitational acceleration). Fibroblasts remaining in the supernatant were removed and cardiomyocytes were resuspended in blocking solution. After cardiomyocytes settled, the supernatant was removed and cells were resuspended in plating medium (in mM: 5 creatine, 2 L-carnitine hydrochloride, 5 taurine, 1 sodium pyruvate, plus 0.25 U/L insulin, 10 µM cytosine-β-D-arabinofuranoside, 5% FCS, 0.05 mg/mL gentamycin [gibco®, Grand Island, NY, United States] in medium 199). Cardiomyocytes (17,500 cells/mL) were cultured on laminin (100 µg/mL) coated coverslips. Medium was exchanged 3–4 h after seeding cells, and cells were either measured after 48 h (control cells) or treated with adenovirus. Adenovirus (type 5) coding for GtACR1 was added immediately after the 3–4 h medium exchange (MOI75 for 48–72 h). Medium was renewed after 48–72 h of transduction immediately before cells were used for functional experiments.

Patch-Clamp Recordings

Whole-cell patch-clamp measurements on single isolated cardiomyocytes or HEK 293T cells were performed at room temperature using an inverted DMI 4000B microscope (Leica Microsystems, Wetzlar, Germany), an Axopatch 200B amplifier and an Axon Digidata 1550A (Molecular Devices, San José, CA, United States). Activation light was delivered by a 525-nm LED (Luminus Devices PT-120-G, Sunnyvale, CA, United States) using a 530/20x filter and controlled *via* custom-built hardware (Essel Research and Development, Toronto, Canada). Light intensity in the object plane was determined with an optical power meter (PM100D, Thorlabs; Newton, NJ, United States) and the illuminated area was determined using a stage micrometer ($A = 0.8$ mm^2). LED-input power was controlled via the custom-built LED control unit. If not specified otherwise, external (bath) and internal (pipette) standard solutions were used (**Tables 3**, **4**).

Photoinhibition Protocol

In current-clamp mode AP were triggered at 0.25 Hz by current injection of 50% more than the threshold to elicit an AP using a current ramp from 0 pA within 10 ms. Light (525 nm for 64, 32, or 16 s at 4 $mW{\cdot}mm^{-2}$ or 0.4 $mW{\cdot}mm^{-2}$) was applied after 15 electrically-triggered AP, and at least 15 AP were recorded after light exposure. AP durations were determined at the 20th or 90th percentile of signal amplitude above resting potential, as earlier described (Wang et al., 2015). Depolarizations with peak amplitudes below 0 mV were marked as inhibited.

Light Titration

Maximal amplitude of inward currents was measured at −60 mV after light application for 1, 10, 100, 300 ms at light intensities of 0.1, 0.2, 0.4, 0.7, 1, 2, 4, 7, 10, and 11 $mW{\cdot}mm^{-2}$. The dissociation constant K_d was calculated by fitting the titration curves with a Hill equation.

Ion Selectivity Measurements

Maximal amplitudes of in- and outward currents were measured at different holding potentials (cardiomyocytes: −100 mV to +60 mV in steps of 20 mV, HEK cells: −60 mV to +60 mV in steps of 20 mV) during light exposure (525 nm, 300 ms, 4 $mW{\cdot}mm^{-2}$).

For titration of the Cl^- concentration, different solutions (strongly reduced external Cl^-, moderately reduced external Cl^- and standard external) were used in combination with standard internal solution, and the reversal potential was determined from the IE curves. Different internal solutions (strongly reduced internal Cl^- and moderately reduced internal Cl^-) were tested in combination with standard external solution (**Table 2**).

TABLE 2 | Composition of solutions used for cell isolation.

	Normal Tyrode solution	Ca^{2+}- free cardioplegic solution	Enzyme solution	Blocking solution
NaCl [mM]	137	137	137	137
KCl (VWR International bvba, Leuven, Belgium) [mM]	4	14	14	14
HEPES [mM]	10	10	10	10
Creatine [mM]	10	10	10	10
Taurine [mM]	20	20	20	20
Glucose [mM]	10	10	10	10
$MgCl_2$ [mM]	1	1	1	1
Adenosine [mM]	5	5	5	5
L-carnitine [mM]	2	2	2	2
$CaCl_2$ (Honeywell Fluka™, Seelze, Germany) [mM]	1	-	0.1	0.1
Heparin-sodium [units/L]	5,000	-		
EGTA (Carl Roth GmbH, Karlsruhe, Germany) [mM]		0.096	0.096	0.096
Collagenase type 2, 315 U/mg (Worthington, Lakewood, NJ, USA) [g/L]			0.6	
Protease XIV [g/L]			0.03	
Bovine serum albumin [%]				0.5

All solutions were adjusted to pH 7.4 at 37°C.

TABLE 3 | Composition of bath solutions used in whole-cell patch-clamp experiments.

Components of external bath solution [mM]	Standard solution	Alkaline solution	Strongly reduced Na^+ concentration	Moderately reduced Na^+ concentration	Strongly reduced Cl^- concentration	Moderately reduced Cl^- concentration	Moderately increased K^+ concentration	Strongly increased K^+ concentration
NaCl	140	140	1	12	-	60	140	140
Na-aspartate	-	-	-	-	140	80	-	-
Tetraethyl-ammoniumchloride	-	-	139	127	-	-	-	-
K-aspartate	-	-	-	-	-	-	6.6	21.6
KCl	5.4	5.4	5.4	5.4	5.4	5.4	5.4	5.4
$CaCl_2$	1	1	1	1	1	1	1	1
$MgCl_2$	2	2	2	2	2	2	2	2
Glucose	10	10	10	10	10	10	10	10
HEPES/TRIS	10/-	-/10	10/-	10/-	10/-	10/-	10/-	10/-
pH	7.4	9	7.4	7.4	7.4	7.4	7.4	7.4

TABLE 4 | Composition of pipette solutions used in whole-cell patch-clamp experiments.

Components of internal (pipette) solutions [mM]	Standard solution	Strongly reduced Cl^- concentration	Moderately reduced Cl^- concentration
KCl	50	-	11
K-aspartate	80	130	119
$MgCl_2$	2	2	2
Mg-ATP	3	3	3
EGTA	10	10	10
HEPES	10	10	10

All solutions were adjusted to pH 7.2.

pH dependency experiments in standard external solution (pH = 7.4) were compared with external alkaline solution at pH 9.0 (**Table 3**).

For titration of Na^+ concentration effects, three external solutions (strongly reduced and moderately reduced Na^+ concentration, and standard external solution, **Table 3**) were

used in combination with standard internal solution (**Table 4**). Similarly, extracellular K^+ effects were assessed by exchanging the standard external solution by solutions with either strongly increased or moderately increased K^+ concentration (**Table 3**).

The osmolality of all solutions was determined using a semimicro osmometer K-7400 (Knauer AG, Berlin, Germany) and adjusted to 300 ± 5 mOsm with glucose.

Peak Current Recovery

Cardiomyocytes were clamped at −60 mV and peak current amplitudes were recorded while optically stimulating for 300 ms at 11 mW·mm^2. In dual-stimulation experiments peak recovery was probed by increasing dark intervals in-between stimuli from 1 to 20 s, in 1-s steps.

Optical Pacing

Cardiomyocyte membrane potential was recorded in current clamp mode at 0 pA. Myocytes were paced at 0.25 Hz with light pulses of 10 ms using either the threshold light intensity (P/A_{thr}, minimal light intensity for 100% capture) or twice the threshold light intensity ($P/A_{2\cdot\mathrm{thr}}$).

Sarcomere Length Measurements

Cardiomyocyte contractions were followed by detecting changes in sarcomere length as previously described (Peyronnet et al., 2017). Cardiomyocytes were imaged with a MyoCam-S camera (IonOptix, Dublin, Ireland) on an inverted microscope (DM IRBE, Leica Microsystems, Wetzlar, Germany). Sarcomere length was calculated in real time by a Fast Fourier Transform of the power spectrum of the striation pattern (IonWizard, IonOptix). Cells were field stimulated at 14–15 V/0.25 Hz with a Myopacer (IonOptix). For the contraction inhibition protocol, a light pulse of 525 nm was applied for 64 s. For OP, light pulses of 10 ms were applied at 0.25 Hz. Resting sarcomere length, time to peak, time to 90% relaxation, fractional sarcomere shortening, maximum velocity of contraction and relaxation were analyzed as described before (Peyronnet et al., 2017).

Confocal Microscopy of GtACR1-eGFP Expressing Cardiomyocytes

Transduced cardiomyocytes were washed two times with Dulbecco's Phosphate Buffered Saline (PBS). Ice-cold acetone was added, the samples were kept for 5 min at −20°C and washed again with PBS. Cells on coverslips were fixed with Mountant, Perma Fluor (Thermo Fisher Scientific) and flipped onto an object slide. The mounted samples were imaged with a confocal laser-scanning microscope (LSM 880; Carl Zeiss Microscopy, Oberkochen, Germany).

Generation of cmlc2:GtACR1-eGFP Transgenic Zebrafish

All experimental procedures in zebrafish were approved by the Dalhousie University Committee for Laboratory Animals and followed the guidelines of the Canadian Council on Animal Care. Details of experimental protocols are reported following the Minimum Information about a Cardiac Electrophysiology Experiment (MICEE) reporting standard (Quinn et al., 2011).

A cmlc2:GtACR1-eGFP plasmid was generated using standard cloning and microbiology techniques combined with the multisite Gateway system for Tol2 transposon transgenesis (Rafferty and Quinn, 2018). The 5′ entry plasmid p5E-cmlc2 and destination plasmid pDestTol2pA2 were obtained from Dr. Ian Scott (University of Toronto, Toronto, Canada). The donor plasmid pME-TA and 3′ entry plasmid p3E-polyA were obtained from Dr. Jason Berman (Dalhousie University, Halifax, Canada). To generate the middle entry plasmid, the sequence of the L13_CMV_GtACR1-eGFP plasmid was confirmed (using primers CMV_Forward: 5′-CGCAAATGGGCGGTAGGCGTG-3′ and EGFP-C-REV: 5′-GTTCAGGGGGAGGTGTG-3′) and then GtACR1-eGFP was amplified out of the plasmid using polymerase chain reaction (PCR) with primers GtACR1_for: 5′-GCCACCATGAGCAGCATTAC-3′ and EGFP-stop_rev: 5′-TTTACTTGTACAGCTCGTCCAT-3′. The GtACR1-eGFP PCR product, purified using a Gel Extraction Kit (QIAEX II, Qiagen; Hilden, Germany) and with the addition of a polyA (pA) tail was ligated into pME-TA to generate the middle entry plasmid pME-GtACR1-eGFP-pA, which was then subjected to restriction digest and sequencing (using primers M13F(-21): 5′-TGTAAAACGACGGCCAGT-3′, GtACR1, and EGFP_stop_rev). An expression plasmid was then generated by ligating p5E-cmlc2, pME-GtACR1-eGFP-pA, and p3E-polyA into pDestTol2pA2. Restriction digest and sequencing (using primers T7: 5′-TAATACGACTCACTATAGGG-3′ and EGFP-stop_rev) confirmed the sequence of isolated expression plasmid DNA. The cmlc2-GtACR1-eGFP-pA-pDestTol2pA2 DNA was purified with a PCR Purification Kit (QIAquick, Qiagen) before microinjection of 22.7 ng/μL DNA and 16 ng/μL Tol2 transposase mRNA into one-cell stage Casper zebrafish embryos. Injected fish were screened for successful gene transduction by eGFP expression using a fluorescent microscope (MZ16F, Leica; Wetzlar, Germany).

Zebrafish Isolated Heart Preparation

Hearts were isolated from 3-month post fertilization (mpf) zebrafish expressing GtACR1-eGFP as previously described (Stoyek et al., 2016, 2018; MacDonald et al., 2017). Fish were anesthetized in Tris-buffered (pH 7.4, BP152, Fisher Scientific; Hampton, United States) tricaine (1.5 mM MS-222) in room temperature tank water until opercular movements ceased and the animals lacked response to fin pinch with forceps. A midline incision was made through the ventral body wall and tissues of the ventral aorta, ventricle, atrium, and venous sinus were removed, pinned into a 15 mL dish lined with Sylgard (DC 170, Dow Corning; Midland, United States) containing Tyrode's solution (in mM: 142 NaCl, 4.7 KCl, 1 $MgCl_2$, 1.8 $CaCl_2$, 10 Glucose, 10 HEPES) of an osmolality of 300 ± 5 mOsm checked with an osmometer (Model 5004 μOsmette, Precision Systems; Natick, United States) and with pH titrated to 7.4 with NaOH. In addition, 10 μM (±)-blebbistatin (B592490, Toronto Research Chemicals; Toronto, Canada), a myosin inhibitor used for excitation-contraction uncoupling was added to the bath to eliminate contraction for stability of intracellular microelectrode recordings.

Intracellular Microelectrode Recordings of Zebrafish Ventricular Myocyte Membrane Potential

Intracellular microelectrode recordings were performed as previously described (Smith et al., 2016). Microelectrodes made from borosilicate glass tubing (0.5 mm inner diameter, 1.0 mm outer diameter, with internal filament; type BF/100/50/10, Sutter Instruments; Novato, United States) were pulled on a Brown/Flaming micropipette puller (Model P97, Sutter Instruments) to tip diameters resulting in a 40–60 MΩ resistance when filled with 3 M KCl. Electrodes were coupled to the headstage of an amplifier (Model 1600 Neuroprobe Amplifier, A/M Systems; Everett, United States) operated in current clamp mode with an electrode holder (ESW-M10N, Warner Instruments; Hamden, United States). Electrodes were advanced with a mechanical manipulator (MX/4, Narishige; Tokyo, Japan) into the ventricular epicardium. Before cell penetration, the tip potential of the electrode was nulled using the bridge controls of the intracellular amplifier with the electrode tip in the bath. At the end of a recording, the microelectrode was withdrawn from the cell, the null potential was checked, and the previous data adjusted if necessary. Transmembrane potential was taken as the difference between the potential measured in the bath with a silver/silver-chloride lead and the intracellular potential. Successful impalement was signaled by a sudden step of the electrode potential to a negative value. Criteria for accepting a cell were AP with a stable resting membrane potential (E_R) < -60 mV and an AP peak >0 mV that were maintained throughout the recording. Transmembrane potential was recorded at 10 kHz using a software-controlled data acquisition system (LabChart and PowerLab, ADInstruments; Sydney, Australia).

Activation of GtACR1 in Zebrafish Isolated Hearts

Experiments were performed in zebrafish isolated hearts and intact zebrafish larvae at room temperature using an upright microscope (BX51WI, Olympus; Shinjuku, Japan). Light for activation of GtACR1 was delivered by a white LED (CFT-90-W, Luminus Devices; Sunnyvale, USA) through a 531/22 nm filter (FF02-531/22, Semrock; Rochester, USA) focused on the ventricle with a 10X (for isolated hearts) or 20X (for zebrafish larvae) water-immersion objective (UMPLFLN 10XW or XLUMPLFLN 20XW, Olympus). The microscope field stop was set at the smallest aperture to produce a 0.16 mm^2 spot with an intensity of 1–5 mW/mm^2. Light application was either sustained for 15 s or pulsed for 10 ms at a rate 2× sinus heart rate (HR) in regions displaying high or no eGFP expression, checked with 466/40 nm excitation (FF01-466/40, Semrock), 495 nm dichroic (FF495-Di03, Semrock), and 525/50 nm (ET525/50m, Chroma Technology; Bellows Falls, United States) filters. OP was compared to EP at the same rate applied extracellularly by a pair of silver wire electrodes on either side of the heart coupled to a constant current stimulus isolation unit (PSIU6D, Grass Technologies; West Warwick, USA) driven by 10 ms rectangular pulses from a waveform generator (S44, Grass). Measurements of HR, E_R, upstroke velocity (dE/dt_{max}), AP amplitude (AP_{Amp}), APD_{50} and APD_{90} were averaged over three consecutive heart beats before and during light stimulation. Light intensity was measured at the end of the experiment using a USB power meter (PM16-120, Thorlabs; Newton, United States).

Confocal Microscopy of Ventricular cmlc2:GtACR1-eGFP Expression

GtACR1-eGFP expression in the ventricle was investigated in two subsets of zebrafish isolated hearts by confocal microscopy. The first subset included specimens from activation of GtACR1 in zebrafish isolated heart experiments. In this group immediately following the activation experiment isolated hearts were immersed in 2% methyl-cellulose on a depression slide, put under a cover slip, and GFP expression imaged. In the second subset, whole hearts were labeled with an antibody against GFP (1:100, PA1-980A, Thermo Fisher Scientific; Waltham, United States) to enhance the signal associated with the eGFP tagged to ACR1. Tissues were fixed overnight in 2% paraformaldehyde (RT-15710, Electron Microscopy Sciences; Hatfield, United States) with 1% dimethyl sulfoxide in phosphate-buffered saline (PBS, in mM): 140 NaCl, 50 Na_2HPO_4, with pH titrated to 7.2 with NaOH. Fixed tissues were rinsed in PBS, and then incubated with primary GFP-antibody diluted in a solution containing 0.1% Triton X-100 in PBS (PBS-T) for 36 h at room temperature with gentle agitation. Tissues were then rinsed and transferred to a solution of PBS-T containing anti-rabbit AlexaFluor 488 (1:200, A-21206, Life Technologies; Carlsbad, United States) for 24 h at room temperature with gentle agitation. Final rinsing was done with PBS and specimens were placed in Scale CUBIC-1 clearing solution (Susaki et al., 2014) overnight at room temperature with gentle agitation. Tissues were mounted on glass slides in CUBIC-1 for confocal microscopy.

In both subsets, processed specimens were examined as whole-mounts using an LSM 510 confocal microscope (Carl Zeiss Microscopy) with a 10×, 0.45 NA objective (Plan-Apochromat SF25, Carl Zeiss) or a 25×, 0.80 NA objective (LCI Plan-Neofluar, Carl Zeiss). Preparations were epi-illuminated with a 488 nm argon laser reflected by a 488 nm dichroic mirror (HFT 488; Carl Zeiss). Emitted fluorescence was collected using a 500–530 nm band-pass filter (Carl Zeiss AG). Confocal image Z-stacks ranging from 20 to 50 µm in depth, including a region of 2–5 µm above and below the region of interest (to ensure that all structures were captured, while limiting issues of light scattering) were acquired and processed using Zen2009 software (Carl Zeiss) from regions surrounding immunoreactive tissues.

Data Analysis

Data was analyzed with pClamp 11, IonWizard, OriginPro, and with custom routines in Matlab. For unpaired datasets the non-parametric Mann-Whitney-test was applied. The Wilcoxon-test and two-tailed paired Student's *t*-test were used to pair-wise compare two datasets. For more than two datasets ANOVA one-way repeated (*post-hoc* test: Tukey or Dunnett) was used. A $p < 0.05$ was taken to indicate a significant difference between means.

DATA AND MATERIAL AVAILABILITY

The raw data supporting the conclusions of this manuscript will be made available by the authors, without undue reservation, to any qualified researcher. DNA plasmids and established zebrafish lines will be provided upon request.

AUTHOR CONTRIBUTIONS

RK, TQ, PK and FS-W designed the experiments. RK, JB, SR, RM, CZ-J, SP, MS, FS, TQ and FS-W performed the experiments and analyzed the data. RK, CZ-J, FS, MS, TQ, PK and FS-W wrote the manuscript and designed the figures. All authors approved the final manuscript.

FUNDING

This project was funded by the European Research Council Advanced Grant CardioNECT (Project ID: 323099, to PK), the German Research Foundation (SPP1926, SCHN 1486/1-1, to FS-W), the Natural Sciences and Engineering Research Council of Canada (RGPIN-2016-04879 to TQ), the Heart and Stroke Foundation of Canada (G-18-0022185 to TQ), and the Canada Foundation for Innovation and Nova Scotia Research and Innovation Trust (32962 to TQ).

ACKNOWLEDGMENTS

We thank Dr. Remi Peyronnet (Institute for Experimental Cardiovascular Medicine, Freiburg, Germany) for help with the sarcomere length measurements and the Life Imaging Center of the University of Freiburg for help with confocal microscopy. We are thankful to Cinthia Buchmann and Stefanie Perez-Feliz for excellent technical assistance. We thank Dr. Jonas Wietek (Humboldt-University, Berlin, Germany) for providing the pUC57-GtACR1 plasmid. We thank the Zebrafish and Cellular and Molecular Digital Imaging Facilities at Dalhousie University for their support. We thank Dr. Ian Scott (University of Toronto, Toronto, Canada) for providing the 5′ entry plasmid p5E-cmlc2 and destination plasmid pDestTol2pA2 and Dr. Jason Berman (Dalhousie University, Halifax, Canada) for providing the donor plasmid pME-TA and 3′ entry plasmid p3E-polyA.

SUPPLEMENTARY MATERIAL

The Supplementary Material for this article can be found online at: https://www.frontiersin.org/articles/10.3389/fphys.2018.01806/full#supplementary-material

Supplementary Figure 1 | (A) *IE* relationship of GtACR1 currents at various internal chloride concentrations in HEK 293T cells ($n = 7$–12). **(B)** *IE* relationship of GtACR1 currents at various external K^+ concentrations in HEK 293T cells ($n = 7$–12). **(C)** *IE* relationship of GtACR1 currents at various internal chloride concentrations in cardiomyocytes ($n = 7$–17, $N = 4$). **(D)** *IE* relationship recorded at pH 7.4 and pH 9.0 ($n = 17$–20, $N = 4$). **(E)** Change of resting membrane potential during electrical and optical pacing of cardiomyocytes. Mann-Whitney test: $p > 0.05$ (n.s.), Wilcoxon test: $p < 0.01$ (**, $n = 10$, $N = 2$). **(F)** Change of resting membrane potential E_R during optical pacing (OP) at threshold light intensity and two times threshold intensity. Wilcoxon test: $p < 0.05$ (*). **(G)** Resting membrane potential and **(H)** APD_{90} in control wild-type cells during optical inhibition protocol ($n = 10$, $N = 1$). AP are not inhibited by light. ANOVA one-way repeated Dunnett test: n.s. **(I-N)** Quantification of key parameters of cellular contractions in sarcomere length measurements ($n = 12$–17, $N = 3$). **(I)** Resting sarcomere length (RSL, $p \leq 0.05$ [*]), **(J)** time to peak, a parameter for the active shortening, **(K)** time from peak to 90% relaxation, **(L)** fractional sarcomere shortening, the percentage of the peak amplitude in relation to the RSL, **(M)** maximum velocity of contraction and **(N)** relaxation were analyzed for 6 contractions before and after light exposure. Wilcoxon was used to compare paired data, Mann-Whitney for comparison of control cells vs. GtACR1-expressing cells before light.

Supplementary Figure 2 | Representative traces of cardiomyocyte membrane potential during electrical pacing (EP) at 0.25 Hz (current injections of 0.6 nA for 10 ms). AP generation is inhibited by green light application for 64 s **(A)**, 32 s **(B)** and 16 s **(C)**.

Supplementary Figure 3 | Confocal microscopy optical slice through the ventricular mid-wall of an immunohistochemically labeled zebrafish isolated heart. Anti-GFP reveals heterogeneous cellular expression of GtACR1-eGFP (indicated by areas of bright green; the duller green represents tissue autofluorescence). The region of high intensity at the apex illustrates epicardial expression (as the optical slice goes through the epicardium in this region), while the bright band in the center of the image represents high expression in trabecular muscle.

Supplementary Figure 4 | Comparison of OP and EP at the same rate shows no difference in the resulting AP morphology of a ventricular cell inside an isolated heart of zebrafish 3 mpf.

Supplementary Movie 1 | Inhibition of ventricular contraction by exposure of the entire ventricle to 1.7 $mW{\cdot}mm^{-2}$ light in an intact zebrafish larva 21 days post fertilization.

REFERENCES

Alfonsa, H., Merricks, E. M., Codadu, N. K., Cunningham, M. O., Deisseroth, K., Racca, C., et al. (2015). The contribution of raised intraneuronal chloride to epileptic network activity. *J. Neurosci.* 35, 7715–7726. doi: 10.1523/JNEUROSCI.4105-14.2015

Arrenberg, A. B., Del Bene, F., and Baier, H., (2009). Optical control of zebrafish behavior with halorhodopsin. *Proc. Natl. Acad. Sci. U.S.A.* 106, 17968–17973. doi: 10.1073/pnas.0906252106

Arrenberg, A. B., Stainier, D. Y. R., Baier, H., and Huisken, J., (2010). Optogenetic control of cardiac function. *Science* 330, 971–974. doi: 10.1126/science.1195929

Ayub, S., Gentet, L. J., Fiáth, R., Schwaerzle, M., Borel, M., David, F., et al. (2017). Hybrid intracerebral probe with integrated bare LED chips for optogenetic studies. *Biomed. Microdevices* 19:49. doi: 10.1007/s10544-017-0190-3

Baumgarten, C. M., Browe, D. M., and Ren, Z., (2005). "Swelling- and stretch-activated chloride channels in the heart: regulation and function," in *Mechanosensitivity in Cells and Tissues*, eds A. Kamkin, and I. Kiseleva (Moscow: Academia). Available online at: http://www.ncbi.nlm.nih.gov/pubmed/21290764 (Accessed August 23, 2018).

Bernal Sierra, Y. A., Rost, B. R., Pofahl, M., Fernandes, A. M., Kopton, R. A., Moser, S., et al. (2018). Potassium channel-based optogenetic silencing. *Nat. Commun.* 9:4611. doi: 10.1038/s41467-018-07038-8

Berndt, A., Lee, S. Y., Ramakrishnan, C., and Deisseroth, K., (2014). Structure-guided transformation of channelrhodopsin into a light-activated chloride channel. *Science* 344, 420–424. doi: 10.1126/science.1252367

Berndt, A., Lee, S. Y., Wietek, J., Ramakrishnan, C., Steinberg, E. E., Rashid, A. J., et al. (2016). Structural foundations of optogenetics: determinants of channelrhodopsin ion selectivity. *Proc. Natl. Acad. Sci. U.S.A.* 113, 822–829. doi: 10.1073/pnas.1523341113

Boyden, E. S., Zhang, F., Bamberg, E., Nagel, G., and Deisseroth, K., (2005). Millisecond-timescale, genetically targeted optical control of neural activity. *Nat. Neurosci.* 8, 1263–1268. doi: 10.1038/nn1525

Bruegmann, T., Boyle, P. M., Vogt, C. C., Karathanos, T. V., Arevalo, H. J., Fleischmann, B. K., et al. (2016). Optogenetic defibrillation terminates ventricular arrhythmia in mouse hearts and human simulations. *J. Clin. Invest.* 126, 3894–3904 doi: 10.1172/JCI88950

Bruegmann, T., Malan, D., Hesse, M., Beiert, T., Fuegemann, C. J., Fleischmann, B. K., et al. (2010). Optogenetic control of heart muscle *in vitro* and *in vivo*. *Nat. Methods* 7, 897–900. doi: 10.1038/nmeth.1512

Clemo, H. F., Stambler, B. S., and Baumgarten, C. M., (1999). Swelling-activated chloride current is persistently tachycardia-induced congestive heart failure. *Circ. Res.* 5, 157–165.

Deisseroth, K., Feng, G., Majewska, A. K., Miesenböck, G., Ting, A., and Schnitzer, M. J., (2006). Next-generation optical technologies for illuminating genetically targeted brain circuits. *J. Neurosci.* 26, 10380–10386. doi: 10.1523/JNEUROSCI.3863-06.2006

Duan, D. D., (2013). Phenomics of cardiac chloride channels. *Compr. Physiol.* 3, 667–692. doi: 10.1002/cphy.c110014

Forli, A., Vecchia, D., Binini, N., Succol, F., Bovetti, S., Moretti, C., et al. (2018). Two-photon bidirectional control and imaging of neuronal excitability with high spatial resolution *in vivo*. *Cell Rep.* 22, 3087–3098.

Govorunova, E. G., Cunha, S. R., Sineshchekov, O. A., and Spudich, J. L., (2016). Anion channelrhodopsins for inhibitory cardiac optogenetics. *Sci. Rep.* 6, 1–7. doi: 10.1038/srep33530

Govorunova, E. G., Sineshchekov, O. A., Janz, R., Liu, X., and Spudich, J. L., (2015a). NEUROSCIENCE. *Natural light-gated anion channels: a family of microbial rhodopsins for advanced optogenetics. Science* 349, 647–650. doi: 10.1126/science.aaa7484

Govorunova, E. G., Sineshchekov, O. A., Rodarte, E. M., Janz, R., Morelle, O., Melkonian, M., et al. (2017). The expanding family of natural anion channelrhodopsins reveals large variations in kinetics, conductance, and spectral sensitivity. *Sci. Rep.* 7:43358. doi: 10.1038/srep43358

Govorunova, E. G., Sineshchekov, O. A., and Spudich, J. L., (2015b). *Proteomonas sulcata* ACR1: a fast anion channelrhodopsin. *Photochem. Photobiol.* 92, 257–263. doi: 10.1111/php.12558

Gradinaru, V., Thompson, K. R., and Deisseroth, K., (2008). eNpHR: a *Natronomonas* halorhodopsin enhanced for optogenetic applications. *Brain Cell Biol.* 36, 129–139. doi: 10.1007/s11068-008-9027-6

Gradinaru, V., Zhang, F., Ramakrishnan, C., Mattis, J., Prakash, R., Diester, I., et al. (2010). Molecular and cellular approaches for diversifying and extending optogenetics. *Cell* 141, 154–165. doi: 10.1016/j.cell.2010.02.037

Grimm, C., Silapetere, A., Vogt, A., Bernal Sierra, Y. A., and Hegemann, P., (2018). Electrical properties, substrate specificity and optogenetic potential of the engineered light-driven sodium pump eKR2. *Sci. Rep.* 8:9316. doi: 10.1038/s41598-018-27690-w

Han, X., and Boyden, E. S., (2007). Multiple-color optical activation, silencing, and desynchronization of neural activity, with single-spike temporal resolution. *PLoS ONE* 2:e299. doi: 10.1371/journal.pone.0000299

Han, X., Chow, B. Y., Zhou, H., Klapoetke, N. C., Chuong, A., Rajimehr, R., et al. (2011). A high-light sensitivity optical neural silencer: development and application to optogenetic control of non-human primate cortex. *Front. Syst. Neurosci.* 5:18. doi: 10.3389/fnsys.2011.00018

Hulsmans, M., Clauss, S., Xiao, L., Aguirre, A. D., King, K. R., Hanley, A., et al. (2017). Macrophages facilitate electrical conduction in the heart. *Cell* 169, 510–522.e20. doi: 10.1016/j.cell.2017.03.050

Inoue, K., Ono, H., Abe-Yoshizumi, R., Yoshizawa, S., Ito, H., Kogure, K., et al. (2013). A light-driven sodium ion pump in marine bacteria. *Nat. Commun.* 4:1678. doi: 10.1038/ncomms2689

Johnston, C. M., Rog-Zielinska, E. A., Wülfers, E. M., Houwaart, T., Siedlecka, U., Naumann, A., et al. (2017). Optogenetic targeting of cardiac myocytes and non-myocytes: Tools, challenges and utility. *Prog. Biophys. Mol. Biol.* 130, 140–149. doi: 10.1016/j.pbiomolbio.2017.09.014

Kato, H. E., Inoue, K., Abe-Yoshizumi, R., Kato, Y., Ono, H., Konno, M., et al. (2015). Structural basis for Na+ transport mechanism by a light-driven Na+ pump. *Nature* 521, 48–53. doi: 10.1038/nature14322

Kim, Y. S., Kato, H. E., Yamashita, K., Ito, S., Inoue, K., Ramakrishnan, C., et al. (2018). Crystal structure of the natural anion- conducting channelrhodopsin Gt ACR1. *Nature* 561, 343–348. doi: 10.1038/s41586-018-0511-6

MacDonald, E. A., Stoyek, M. R., Rose, R. A., and Quinn, T. A., (2017). Intrinsic regulation of sinoatrial node function and the zebrafish as a model of stretch effects on pacemaking. *Prog. Biophys. Mol. Biol.* 130, 198–211. doi: 10.1016/j.pbiomolbio.2017.07.012

Mahn, M., Gibor, L., Patil, P., Cohen-Kashi Malina, K., Oring, S., Printz, Y., et al. (2018). High-efficiency optogenetic silencing with soma-targeted anion-conducting channelrhodopsins. *Nat. Commun.* 9:4125. doi: 10.1038/s41467-018-06511-8

Mahn, M., Prigge, M., Ron, S., Levy, R., and Yizhar, O., (2016). Biophysical constraints of optogenetic inhibition at presynaptic terminals. *Nat. Neurosci.* 19, 554–556. doi: 10.1038/nn.4266

Malyshev, A. Y., Roshchin, M. V., Smirnova, G. R., Dolgikh, D. A., Balaban, P. M., and Ostrovsky, M. A., (2017). Chloride conducting light activated channel GtACR2 can produce both cessation of firing and generation of action potentials in cortical neurons in response to light. *Neurosci. Lett.* 640, 76–80. doi: 10.1016/j.neulet.2017.01.026

Mattis, J., Tye, K. M., Ferenczi, E. A., Ramakrishnan, C., O'Shea, D. J., Prakash, R., et al. (2012). Principles for applying optogenetic tools derived from direct comparative analysis of microbial opsins. *Nat. Methods* 9, 159–172. doi: 10.1038/nmeth.1808

Mauss, A. S., Busch, C., and Borst, A., (2017). Optogenetic Neuronal silencing in drosophila during visual processing. *Sci. Rep.* 7:13823. doi: 10.1038/s41598-017-14076-7

Messier, J. E., Chen, H., Cai, Z.-L., and Xue, M., (2018). Targeting light-gated chloride channels to neuronal somatodendritic domain reduces their excitatory effect in the axon. *Elife* 7:e38506. doi: 10.7554/eLife.38506

Miesenböck, G., (2009). The optogenetic catechism. *Science* 326, 395–399. doi: 10.1126/science.1174520

Mohamed, G. A., Cheng, R.-K., Ho, J., Krishnan, S., Mohammad, F., Claridge-Chang, A., et al. (2017). Optical inhibition of larval zebrafish behaviour with anion channelrhodopsins. *BMC Biol.* 15:103. doi: 10.1186/s12915-017-0430-2

Oda, K., Vierock, J., Oishi, S., Rodriguez-Rozada, S., Taniguchi, R., Yamashita, K., et al. (2018). Crystal structure of the red light-activated channelrhodopsin Chrimson. *Nat. Commun.* 9:3949. doi: 10.1038/s41467-018-06421-9

Peyronnet, R., Bollensdorff, C., Capel, R. A., Rog-Zielinska, E. A., Woods, C. E., Charo, D. N., et al. (2017). Load-dependent effects of apelin on murine cardiomyocytes. *Prog. Biophys. Mol. Biol.* 130, 333–343. doi: 10.1016/j.pbiomolbio.2017.09.013

Quinn, T. A., Camelliti, P., Rog-Zielinska, E. A., Siedlecka, U., Poggioli, T., O'Toole, E. T., et al. (2016). Electrotonic coupling of excitable and nonexcitable cells in the heart revealed by optogenetics. *Proc. Natl. Acad. Sci. U.S.A.* 113, 14852–14857. doi: 10.1073/pnas.1611184114

Quinn, T. A., Granite, S., Allessie, M. A., Antzelevitch, C., Bollensdorff, C., Bub, G., et al. (2011). Minimum Information about a Cardiac Electrophysiology Experiment (MICEE): standardised reporting for model reproducibility, interoperability, and data sharing. *Prog. Biophys. Mol. Biol.* 107, 4–10. doi: 10.1016/j.pbiomolbio.2011.07.001

Rafferty, S. A., and Quinn, T. A., (2018). A beginner's guide to understanding and implementing the genetic modification of zebrafish. *Prog. Biophys. Mol. Biol.* 138, 3–19. doi: 10.1016/j.pbiomolbio.2018.07.005

Raimondo, J. V., Kay, L., Ellender, T. J., and Akerman, C. J., (2012). Optogenetic silencing strategies differ in their effects on inhibitory synaptic transmission. *Nat. Neurosci.* 15, 1102–1104. doi: 10.1038/nn.3143

Ravens, U., (2018). Ionic basis of cardiac electrophysiology in zebrafish compared to human hearts. *Prog. Biophys. Mol. Biol.* 138, 38–44. doi: 10.1016/j.pbiomolbio.2018.06.008

Schneider, F., Grimm, C., and Hegemann, P., (2015). Biophysics of Channelrhodopsin. *Annu. Rev. Biophys.* 44, 167–186. doi: 10.1146/annurev-biophys-060414-034014

Schneider-Warme, F., and Ravens, U., (2018). Using light to fight atrial fibrillation. *Cardiovasc. Res.* 114, 635–637. doi: 10.1093/cvr/cvy041

Sineshchekov, O. A., Govorunova, E. G., Li, H., and Spudich, J. L., (2015). Gating mechanisms of a natural anion channelrhodopsin. *Proc. Natl. Acad. Sci. U.S.A.* 112, 14236–14241. doi: 10.1073/pnas.1513602112

Smith, F. M., Vermeulen, M., and Cardinal, R., (2016). Long-term spinal cord stimulation modifies canine intrinsic cardiac neuronal properties and ganglionic transmission during high-frequency repetitive activation. *Physiol. Rep.* 4:e12855. doi: 10.14814/phy2.12855

Stoyek, M. R., Quinn, T. A., Croll, R. P., and Smith, F. M., (2016). Zebrafish heart as a model to study the integrative autonomic control of pacemaker function. *Am. J. Physiol. Circ. Physiol.* 311, H676–H688. doi: 10.1152/ajpheart.00330.2016

Stoyek, M. R., Rog-Zielinska, E. A., and Quinn, T. A., (2018). Age-associated changes in electrical function of the zebrafish heart. *Prog. Biophys. Mol. Biol.* 138, 91–104. doi: 10.1016/j.pbiomolbio.2018.07.014

Susaki, E. A., Tainaka, K., Perrin, D., Kishino, F., Tawara, T., Watanabe, T. M., et al. (2014). Whole-brain imaging with single-cell resolution using chemical cocktails and computational analysis. *Cell* 157, 726–739. doi: 10.1016/j.cell.2014.03.042

Wang, K., Lee, P., Mirams, G. R., Sarathchandra, P., Borg, T. K., Gavaghan, D. J., et al. (2015). Cardiac tissue slices: preparation, handling, and successful optical mapping. *Am. J. Physiol. Heart Circ. Physiol.* 308, H1112–H1125. doi: 10.1152/ajpheart.00556.2014

Wiegert, J. S., Mahn, M., Prigge, M., Printz, Y., and Yizhar, O., (2017). Silencing neurons: tools, applications, and experimental constraints. *Neuron* 95, 504–529. doi: 10.1016/j.neuron.2017.06.050

Wietek, J., Beltramo, R., Scanziani, M., Hegemann, P., Oertner, T. G., and Simon Wiegert, J., (2015). An improved chloride-conducting channelrhodopsin for light-induced inhibition of neuronal activity *in vivo*. *Sci. Rep.* 5:14807. doi: 10.1038/srep14807

Wietek, J., Broser, M., Krause, B. S., and Hegemann, P., (2016). Identification of a natural green light absorbing chloride conducting channelrhodopsin from *Proteomonas sulcata*. *J. Biol. Chem.* 291, 4121–4127. doi: 10.1074/jbc.M115.699637

Wietek, J., Rodriguez-Rozada, S., Tutas, J., Tenedini, F., Grimm, C., Oertner, T. G., et al. (2017). Anion-conducting channelrhodopsins with tuned spectra and modified kinetics engineered for optogenetic manipulation of behavior. *Sci. Rep.* 7:14957. doi: 10.1038/s41598-017-14330-y

Wietek, J., Wiegert, J. S., Adeishvili, N., Schneider, F., Watanabe, H., Tsunoda, S. P., et al. (2014). Conversion of channelrhodopsin into a light-gated chloride channel. *Science* 344, 409–412. doi: 10.1126/science.1249375

Zhang, F., Vierock, J., Yizhar, O., Fenno, L. E., Tsunoda, S., Kianianmomeni, A., et al. (2011). The microbial opsin family of optogenetic tools. *Cell* 147, 1446–1457. doi: 10.1016/j.cell.2011.12.004

Zhang, F., Wang, L.-P., Brauner, M., Liewald, J. F., Kay, K., Watzke, N., et al. (2007). Multimodal fast optical interrogation of neural circuitry. *Nature* 446, 633–639. doi: 10.1038/nature05744

Conflict of Interest Statement: The authors declare that the research was conducted in the absence of any commercial or financial relationships that could be construed as a potential conflict of interest.

The handling editor and reviewer CH declared their involvement as co-editors in the Research Topic, and confirm the absence of any other collaboration.

frontiers in Physiology

ORIGINAL RESEARCH
published: 27 November 2018
doi: 10.3389/fphys.2018.01651

Energy-Reduced Arrhythmia Termination Using Global Photostimulation in Optogenetic Murine Hearts

Raúl A. Quiñonez Uribe[1], *Stefan Luther*[1,2,3,4], *Laura Diaz-Maue*[1] *and Claudia Richter*[1,4,5]*

[1] RG Biomedical Physics, Max Planck Institute for Dynamics and Self-Organization, Göttingen, Germany, [2] Institute for Nonlinear Dynamics, Georg-August University, Göttingen, Germany, [3] Department of Pharmacology and Toxicology, University Medical Center, Göttingen, Germany, [4] German Center for Cardiovascular Research (DZHK e.V.), Partner Site Göttingen, Göttingen, Germany, [5] Department of Cardiology and Pneumology, University Medical Center, Göttingen, Germany

Complex spatiotemporal non-linearity as observed during cardiac arrhythmia strongly correlates with vortex-like excitation wavelengths and tissue characteristics. Therefore, the control of arrhythmic patterns requires fundamental understanding of dependencies between onset and perpetuation of arrhythmia and substrate instabilities. Available treatments, such as drug application or high-energy electrical shocks, are discussed for potential side effects resulting in prognosis worsening due to the lack of specificity and spatiotemporal precision. In contrast, cardiac optogenetics relies on light sensitive ion channels stimulated to trigger excitation of cardiomyocytes solely making use of the inner cell mechanisms. This enables low-energy, non-damaging optical control of cardiac excitation with high resolution. Recently, the capability of optogenetic cardioversion was shown in Channelrhodopsin-2 (ChR2) transgenic mice. But these studies used mainly structured and local illumination for cardiac stimulation. In addition, since optogenetic and electrical stimulus work on different principles to control the electrical activity of cardiac tissue, a better understanding of the phenomena behind optogenetic cardioversion is still needed. The present study aims to investigate global illumination with regard to parameter characterization and its potential for cardioversion. Our results show that by tuning the light intensity without exceeding 1.10 mW mm^{-2}, a single pulse in the range of 10–1,000 ms is sufficient to reliably reset the heart into sinus rhythm. The combination of our panoramic low-intensity photostimulation with optical mapping techniques visualized wave collision resulting in annihilation as well as propagation perturbations as mechanisms leading to optogenetic cardioversion, which seem to base on other processes than electrical defibrillation. This study contributes to the understanding of the roles played by epicardial illumination, pulse duration and light intensity in optogenetic cardioversion, which are the main variables influencing cardiac optogenetic control, highlighting the advantages and insights of global stimulation. Therefore, the presented results can be modules in the design of novel illumination technologies with specific energy requirements on the way toward tissue-protective defibrillation techniques.

Keywords: optogenetics, energy-reduced defibrillation, cardiac arrhythmia, channelrhodopsin-2, photostimulation, global illumination

OPEN ACCESS

Edited by:
Ming Lei,
University of Oxford, United Kingdom

Reviewed by:
Alexey V. Glukhov,
University of Wisconsin System, United States
Jason D. Bayer,
Université de Bordeaux, France

***Correspondence:**
Claudia Richter
claudia.richter@ds.mpg.de

Specialty section:
This article was submitted to Cardiac Electrophysiology, a section of the journal Frontiers in Physiology

Received: *13 August 2018*
Accepted: *02 November 2018*
Published: *27 November 2018*

Citation:
Quiñonez Uribe RA, Luther S, Diaz-Maue L and Richter C (2018) Energy-Reduced Arrhythmia Termination Using Global Photostimulation in Optogenetic Murine Hearts. Front. Physiol. 9:1651. doi: 10.3389/fphys.2018.01651

1. INTRODUCTION

Spatiotemporal dynamics in biological systems, particularly the control of complex excitation patterns, are a fundamental nonlinear problem with extensive potential in medical engineering and therapeutic application. Due to the intrinsic complexity of cardiac tissue, it is challenging to understand in detail the underlying biophysical mechanisms of arrhythmia. The normal sinus rhythm of the heart is triggered by regular, quasi-planar waves of electric depolarization. Spatiotemporally chaotic activation patterns have been identified, and are shown to be responsible for arrhythmic, life-threatening regimes (Davidenko et al., 1992; Luther et al., 2011; Christoph et al., 2018). The inferences of patterns in electrocardiograms (ECG), which showed up as irregular, sometimes aperiodic structures, gave the impulse to think of arrhythmia and especially of ventricular fibrillation as an uncontrolled, shivering activation of heart muscle. Thereby the underlying patterns are results of multiple erratic excitation waves changing in direction and shape. The complexity of wave patterns, leading to spatiotemporal chaotic regimes, is a consequence of the non-linearity. The dynamical processes are characterized by the annihilation of interacting waves, a mechanism also found in other physical systems (Panfilov and Holden, 1990; Jalifé et al., 1998). State-of-the-art therapies include high energy electrical shocks applied either external or internal to defibrillate the heart. These, for the patient mostly painful, shocks terminate the chaotic spreading activity almost certainly, but are suspected to worsen the existing tissue conditions mostly due to their potential electroporating effect on cardiomyocytes. Hence, they also serve as trigger for new arrhythmia with increasing probability over time. Much work has been devoted to the search for improved therapies (see e.g., Zipes and Jalife, 2009). Methods such as Anti-Tachycardia Pacing (ATP), already used in implantable devices, involve very small electrical currents delivered by a single electrode. Provided that the pacing frequency is high enough, ATP can terminate arrhythmia with a fairly high success rate (Wathen et al., 2004). Regardless, even with a high success rate the case of failure can never be disesteemed. Especially stationery vortex-activities are difficult to terminate with only one pacing electrode, which is not close enough to the pinning region. So it is not astonishing that several research groups are investigating advanced implementations of ATP compared to the traditional applied defibrillation shocks (Efimov et al., 2000; Exner, 2005). In addition to the ATP, the Low-Energy Anti-Fibrillation Pacing (LEAP) method was announced. It consists in pacing the tissue with an externally applied electric field. *In vitro* and *in vivo* experiments have provided ample evidence that LEAP significantly reduces the energy necessary to terminate atrial and ventricular fibrillation (Fenton et al., 2009; Luther et al., 2011) by using repeated stimulation with fields of lower amplitude. One crucial feature of LEAP is that it is based on multiple virtual electrodes induced by intrinsic obstacles. Referring to former *in vitro* and *in vivo* experiments (Exner, 2005), especially defibrillation approaches implementing multiple pacing sites have significant influence on arrhythmia specific excitation patterns resulting in rapid synchronization. Anyhow, in order to stimulate at multiple pacing sites either multiple implanted electrodes or specific electrical fields are necessary, which raises obvious translational hurdles. Also, all these valuable methods are still based on electrical shock application, which in turn can never be fully acquitted of potential worsening side effects. Consequentially, the evaluation of new cardiac treatments with side effect diminishing properties but fairly high success rates has to be brought into focus. At this point patterned light control of optogenetically modified cardiac tissue gives the opportunity to specifically stimulate well-defined tissue regions without critical Faraday reactions. Optogenetic photostimulation uses light of specific wavelengths to activate light-sensitive ion channels, which works without former electrically induced membrane potential changes (Bruegmann et al., 2011; Deisseroth, 2011). Recently, optogenetic cardioversion methods applying localized photostimulation were shown to be feasible (Zaglia et al., 2015; Bruegmann et al., 2016; Crocini et al., 2016; Nyns et al., 2016; Richter et al., 2016). Although much effort was put into the characterization of locally applied light intensity and energy (Bruegmann et al., 2010; Zaglia et al., 2015; Diaz-Maue et al., 2018) the underlying dependencies of light intensity, pulse duration and successful cardioversion remains somehow elusive.

However, recent studies showed that inducing multi-centered excitation within the arrhythmic tissue leads to a better control of spatiotemporal wave patterns, typical for fibrillation (Pumir et al., 2007; Luther et al., 2011; Janardhan et al., 2012). Having this in mind, successful global photostimulation would represent the maximum number of available pacing sites. In comparison with the conventional high-energetic electrotherapy, global photostimulation could overcome adverse side-effects like electroporation or unwanted co-stimulation of sensible neurons responsible for pain sensation during defibrillation. Indeed there still remain some questions to be solved before global illumination or multi-site photostimulation could count for reliable defibrillation. With regard to potential clinical translation especially the dependencies between the minimal required light intensity and pulse duration as well as the applied over-all energy are important for the design and optimization of implanteable light-emitting devices. Furthermore, the investigation of global photodefibrilation and the underlying spatiotemporal mechanisms could help to deepen our understanding of the mode of action of conventional electrotherapy.

In the present study, we determine the threshold value of the applied global photostimulation as a function of the intensity and pulse duration, and we compare our experimental results with other photostimulation data. Another main question is whether it is possible to terminate arrhythmia like patterns by light-induced excitation.

2. MATERIALS AND METHODS

All experiments were done in accordance with the current version of the German animal welfare law and were reported to our animal welfare representatives; the application for approval of animal experiments has been approved by the responsible animal welfare authority (Lower Saxony State Office

for Consumer protection and Food Safety). Humane welfare-oriented procedures were carried out in accordance with the Guide for the Care and Use of Laboratory Animals and done after recommendations of the Federation of Laboratory Animal Science Associations (FELASA).

2.1. Langendorff Perfusion

The presented experiments are based on retrograde Langendorff perfusion using a constitutive transgenic mouse model, α-MHC-ChR2, which restricts expression of channelrhodopsin-2 (ChR2) to cardiac tissue. The ChR2 expression was proven by biomolecular protocols. The perfusion protocol includes two different tyrode solutions, either for arrhythmia induction or maintenance. The maintenance tyrode composition was described elsewhere (Richter et al., 2016). Briefly, 130 mM NaCl, 4 mM KCl, 1 mM $MgCl_2$, 24 mM $NaHCO_3$, 1.8 mM $CaCl_2$, 1.2 mM KH_2PO_4, 5.6 mM glucose, 1 % albumin/BSA were aerated with carbogen (95 % oxygen and 5 % CO_2).

2.1.1. Arrhythmia Induction

In order to induce sustained arrhythmia we lowered the concentration of KCl to 2 mM, so that the arrhythmia induction tyrode contains 130 mM NaCl, 2 mM KCl, 1 mM $MgCl_2$, 24 mM $NaHCO_3$, 1.8 mM $CaCl_2$, 1.2 mM KH_2PO_4, 5.6 mM glucose, 1 % albumin/BSA were aerated with carbogen (95 % oxygen and 5 % CO_2). Because of a reduction in transmural dispersion of repolarization the so induced hypokalemia enhances arrhythmia induction (Killeen et al., 2007). In addition, 100 µM Pinacidil, which is a KATPchannel activator, was applied to shorten the action potential duration (Wilde, 1994; Glukhov et al., 2010). The combination of both factors has been successfully applied to induce long sustained ventricular arrhythmia in murine Langendorff-perfused hearts (Bruegmann et al., 2016). Sustained arrhythmia was induced by applying 30 electrical pulses with a needle electrode in the range of 30–50 Hz. To diminish motion artifacts in optical records, the contraction uncoupling reagent Blebbistatin ($c = 5$ µM, Thermo Fisher Scientific) was administrated. Potientiometric staining was achieved by the red-shifted dye Di-4-ANBDQPQ ($c = 50$ µM, Thermo Fisher Scientific) via bolus injection. All perfusion experiments were done at 37 °C.

2.1.2. Optical Mapping

A longpass 685 nm dichroic mirror (FF685-Di02-25x36, Semrock) was integrated to reflect the excitation light from a 625 nm mounted LED (M625L3, Thorlabs) after a bandpass filter (FF02-628/40-25, Semrock) onto the heart. The emission light was collected with a 775 ± 70 nm bandpass filter (FF01-775/140-25, Semrock) before reaching the camera (see **Figure 1**). Epicardial signal recording of the anterior wall was done with an electron multiplying charged coupled device (EMCCD, Cascade 128+, Photometrics) camera with a spatial resolution of 64×64 pixels (133 µm per pixel) at 1 kHz. Camera control was achieved using custom-made recording software and the electrical heart activity was recorded using a monophasic action potential (MAP) electrode (BIOPAC Systems, Inc.).

2.2. Optogenetic Illumination Strategies

We employed local and global illumination to stimulate the heart, whereby only global illumination was used for cardioversion. Local illumination was achieved by positioning the tip of an optical fiber of $\varnothing = 400$ µm in contact with the left ventricle. On the other hand, in order to achieve a consistent optogenetic stimulation of the whole heart surface and therewith global illumination, the hearts were vertically arranged surrounded by three blue-light emitting diodes (blue-LED, Thorlabs) with their wavelengths centered at 460 nm and limited by a 470 ± 20 nm bandpass filter (ET470/40x, Chroma) (see **Figure 1**). Synchronous millisecond control of LED at different intensities was conducted via a function generator (Arbitrary Function Generator A2230, Agilent Instruments). Intensity measurements were done using the PM100D optical power meter and the S120VC photodiode power sensor (Thorlabs). Since the experimental setup consists of three blue-LED spaced at 120°, the intensity was measured directly facing each LED from the heart position and the calculated mean was considered the overall light intensity during global illumination.

To minimize effects of potential edema as well as metabolic changes during repeated arrhythmia periods on the defibrillation success rate, we limited the experimental time to 2 h and a maximum number of defibrillation attempts of 50.

2.3. Data Analysis

The obtained fluorescent images were analyzed and processed using MatLab (MathWork, Inc.). Briefly, spatial and temporal smoothing filter were applied after pixelwise normalization. Overlapping of the blue light with the emission signal of the dye was removed by subtracting the average difference in intensities with and without blue light from each pixel over time (see **Figure S1**). The estimation of the total surface area of both ventricles and atria was achieved by reconstructing three-dimensional heart shapes from photographs using a shape from contour approach as previously described (Christoph et al., 2017). In total three hearts were used to calculate an average epicardiac surface area of 274 mm^2. Statistical analysis was done by Student's t-test (one-tailored and unequal variance) comparing each increasing step with the following value. Throughout the text results are indicated with $\pm$ standard deviation, unless otherwise noted.

Concerning local and global pacing experiments a train of 20 pulses was applied, whereby only the last 10 pulses were considered for the analysis. The minimum pulse lengths needed to reach 1:1 capture in all the tested hearts for different intensities were investigated. Each light intensity was tested in combination with maximal four different pulse duration values.

To determine the success rate of arrhythmia termination, we induced multiple arrhythmia in each heart and attempted termination 10 times with each light intensity-duration combination. To consider an arrhythmia as sustained we waited for 5 s after induction before attempting termination, which consisted of illuminating the whole heart by simultaneously turning on the three LED for the duration and intensity tested. If the arrhythmia stopped within maximum 1 s after the conclusion of stimulation, it was considered a successful attempt. In case

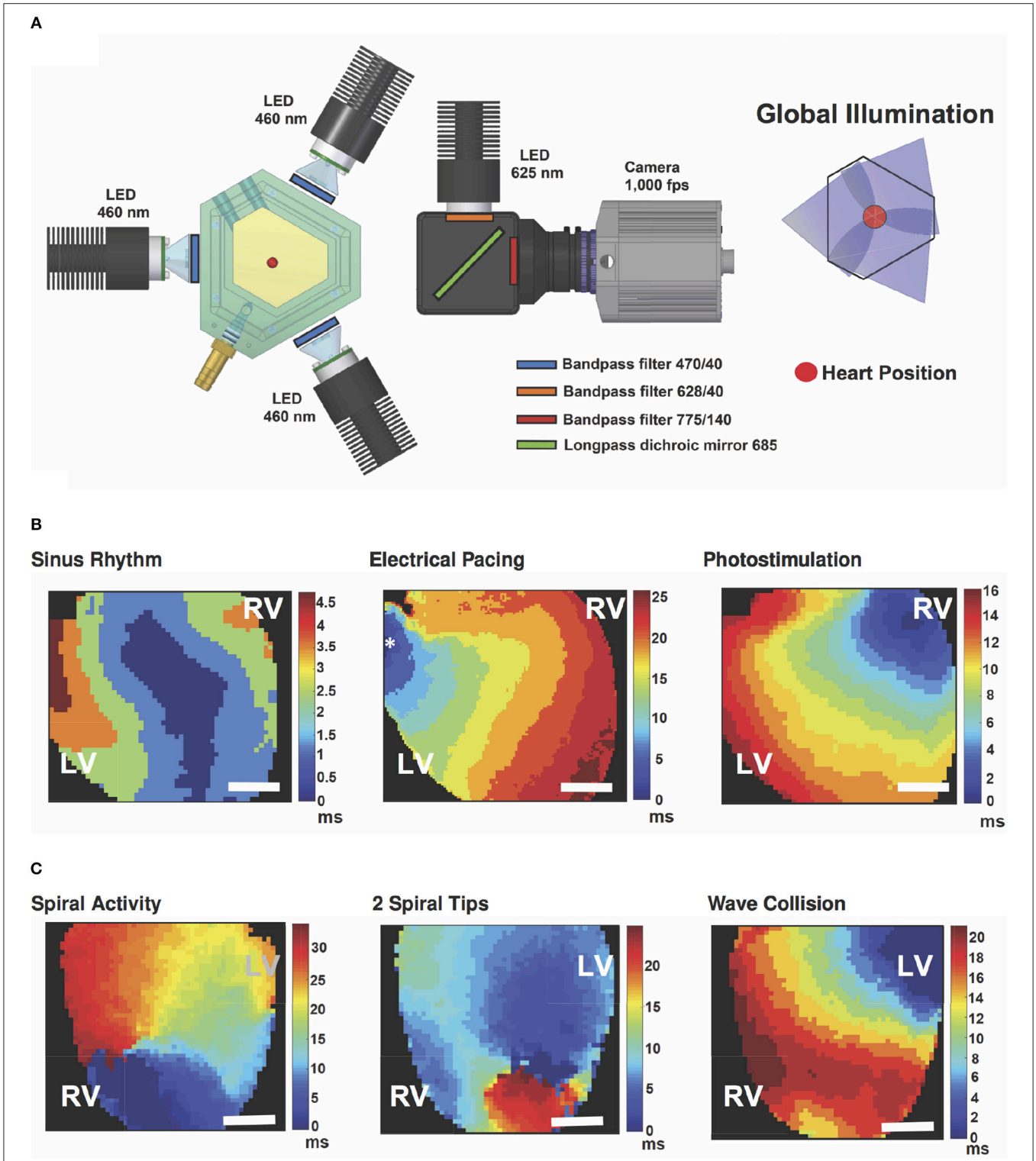

FIGURE 1 | Global illumination and optical mapping setup. **(A)** The heart is perfused in a bath surrounded by three blue-LED for panoramic photostimulation. Light of a 625 nm LED is reflected via a dichroic mirror onto the heart surface. Emission was recorded through a 775 ± 70 nm bandpass filter and an EMCCD camera at 1 kHz. Global illumination is reached via overlapping light cylinders. **(B)** Activation maps in posterior view of the heart of spontaneous sinus rhythm and stimulation examples electrically (electrode position is marked with an asterisk) as well as by global illumination. **(C)** Exemplary activation maps in anterior view of the heart of induced cardiac arrhythmia and collision of waves leading to annihilation of arrhythmic pattern. Color-bars indicate activation time in ms and the scale-bars mark 2 mm. A movie of the wave collision is available as (**Supplementary Material Movie 1**). LV - Left Ventricle, RV - Right Ventricle.

of failed termination, we applied backup defibrillation, which consisted on increasing the intensity and duration of the pulses. To support the defibrillation procedure the hearts were perfused with maintenance tyrode (as described in section 2.1 and 2.1.1). The parameter combination with the highest termination rate and the lowest pulse duration values were determined as the most efficient ones. They also served as a decision-critical point for parameter change.

3. RESULTS

3.1. Global vs. Local Optogenetic Pacing

To characterize successful cardiac photostimulation, we tested the necessary pacing parameters to achieve 1:1 capture with respect to different pulse durations and light intensities. In order to avoid potential photochemical reactions and other side-effects stimulation light was turned off after every pacing.

First, global pacing was applied. **Table 1** gives an overview of the step-wise measured intensities in relation to pulse duration and success rate. Our results prove that a shorter pulse duration correlates with higher intensities needed to gain 1:1 capture. The shortest pulse duration to successfully pace was $t_{gpacing} = 3$ ms applying an intensity of $I_{gpacing} = 113\,\mu W\,mm^{-2}$ ($N = 6$). For pacing with 20 ms pulses successful pacing required an intensity of $I_{gpacing} = 19.6\,\mu W\,mm^{-2}$. Thus, constituting the lowest intensity reported to pace an optogenetic murine heart by photostimulation so far. Pacing the heart with $I_{gpacing} = 140\,\mu W\,mm^{-2}$ was also tested for $t_{gpacing} = 2$ ms, but could only be considered successful in one heart. **Figure 2** shows the intensities and energies necessary to pace the heart with 1:1 capture at different pulse lengths using global stimulation. The graph shows that the energy necessary to pace at different intensity and duration combinations remained constant at an average of $E_{gpacing} = 98 \pm 5\,\mu J$.

For comparison, we also conducted local photostimulation. Considering an increase in intensity required to pace the heart when stimulating smaller areas, we measured the intensity necessary to achieve 1:1 capture using an optical fiber of $A_{fiber} = 0.126\,mm^2$ with a $t_{lpacing}$ of 3 ms, 7 ms, 9 ms and 15 ms. Compared to global pacing, all the intensity values required to obtain 1:1 capture were increased by minimum one order of magnitude with a maximum of $I_{lpacing} = 1.77\,mW\,mm^{-2}$.

In the course of these experiments, it could be observed that the average energy delivered to the epicardium is constant for both global and local illumination. In spite of the clear increase in intensity, it is in average 30-fold lower when pacing locally than globally, at $E_{lpacing} = 2.8 \pm 0.6\,\mu J$ and $E_{gpacing} = 98 \pm 5\,\mu J$, respectively.

3.2. Global Optogenetic Cardioversion

In order to find the optimal parameters for optical cardioversion, we induced cardiac tachyarrhythmia applying Pinacidil and rapid electrical pacing. Therewith 75 % of all arrhythmia lasted more than $t_{arr} = 5$ s (59 out of 79 induced arrhythmia). We considered the $t_{arr} = 5$ s duration as threshold for classification as sustained, since about 90 % lasted for $t_{arr} \geq 10$ s. Non-sustained arrhythmia shorter than the threshold lasted on average $t_{arr} = 1.5 \pm 1.0$ s (**Figure 3**). The average arrhythmia frequency was $f_{arr} = 24 \pm 5$ Hz, and one third of all induced arrhythmia lasted $t_{arr} \geq 60$ s. Optical Mapping data showed multiple vortex-like wave dynamics, hence proving the successful induction of ventricular arrhythmia (**Figure 1C**).

3.2.1. Optical Parameter Characterization

Our measurements concerning global optogenetic photo-defibrillation were triggered by Bruegmann et al. (2016), where local illumination cardioversion was first achieved by using an intensity of $I_{cv(Brueg.)} = 0.40\,mW\,mm^{-2}$ comprising a surface area of $A_{heart(Brueg.)} = 143\,mm^2$ with a 1 s pulse. In order to match the postulated amount of energy delivered by Bruegmann et al. [$E_{cv(Brueg.)} = 57.2$ mJ] with our global illumination, which spans a larger epicardial surface ($A_{heart} = 274\,mm^2$), we modulated the pulse duration by keeping the intensity constant at $I_{cv} = 0.42\,mW\,mm^{-2}$. **Figure 4** shows the main results of the photo-defibrillation attempts. One single long stimulation pulse led to a successful arrhythmia termination in 82 % of the experiments, which is comparable to the results obtained by Bruegmann et al.

Subsequently, we assessed the influence of light intensity by maintaining the pulse duration constant at $t_{cv} = 500$ ms. While all tested light intensities successfully terminated the arrhythmia, a decrease in light intensity correlated with a significant depression in cardioversion efficiency (**Figure 4B**). At the most efficient light intensity of $I_{cv} = 0.79\,mW\,mm^{-2}$, a success rate of 96 ± 2 % [mean $\pm$ standard error of the mean (SEM)] was achieved. However, a decrease in intensity by 40-fold still managed to revert the heart rhythm in more than 30 % of the attempts for the hearts tested ($N = 6$).

Afterwards, to evaluate the effect of pulse duration we kept the light intensity constant at $I_{cv} = 0.79\,mW\,mm^{-2}$ and applied pulses shorter than $t_{cv} = 500$ ms. However, no significant change in termination rate was found for pulse durations of 500, 250, 100, and 10 ms. A shortening of pulse duration from 500 to 10 ms resulted in a decline of 13 % of arrhythmia terminated (**Figure 4B**). Supposing the parameter combination of $t_{cv} = 10$ ms and $I_{cv} = 0.79\,mW\,mm^{-2}$ is as efficient as $t_{cv} = 500$ ms at the same light intensity, in the following we tested a constant pulse duration of $t_{cv} = 10$ ms while step-wise increasing light intensity from $I_{cv} = 0.08$ to $1.1\,mWmm^{-2}$. Thereby we obtained successful termination in 92 ± 4 % of the experiments. Pursuing a wider comprehension of the effects of intensity and duration on global light-induced arrhythmia termination, we then experimented with 1 s long pulses, where an efficiency of 96 ± 2 % was achieved with $I_{cv} = 0.56\,mW\,mm^{-2}$.

3.3. Effects of Global Illumination on Arrhythmia Patterns

Since the 1 s stimuli lasts multiple tachycardia and sinus rhythm cycles, we identified that the transition from an arrhythmic state to the natural sinus frequency took place at different time points from the onset of stimulation. The electrical signal shown in **Figures 4A,C** shows a clear sinus activity even before the photostimulation has ended. To estimate the time between the beginning of stimulation and the moment of optical cardioversion, we defined two characteristic points in time of

TABLE 1 | Measured pulse duration and light intensity combinations.

Pulse duration [ms]	Light intensity [μW mm^{-2}]							
	19.6	24.4	34	37	52	73	113	140
20	100 ± 0							
15	23 ± 11	100 ± 0						
12.5		40 ± 8.9	100 ± 0					
10			100 ± 0					
9			61 ± 8.8	100 ± 0				
8			14 ± 7.1	93 ± 5.2	100 ± 0			
7				20 ± 7.9	100 ± 0			
6				6.5 ± 3.6	90 ± 4.7	100 ± 0		
5					13 ± 7.2	100 ± 0		
4						86 ± 6.9	100 ± 0	
3							100 ± 0	
2							5.2 ± 2.3	57 ± 10

Inscribed is the averaged success rate [%] ± SEM of 1:1 capture during global illumination. The visible trend within the success rate regarding the dependency of light intensity and pulse duration is also mirrored in a constant energy level. Highlighted values indicate the most efficient pulse duration and light intensity combinations, which are drawn in ***Figure 2B*** *together with the corresponding energy values. The shown values are based on 23 measurements from N = 6 hearts.*

the MAP signal (**Figure 4C**). First we define t_{last} as the moment when the last peak of the arrhythmia occurred, and second t_{sin} as the time point when the sinus rhythm signal first appeared. These two values were calculated for all the successful arrhythmia terminations of different intensities for the 1 s pulses. **Figure 4D** illustrates the percentages of t_{last} and t_{sin} for four time lapses. it can be observed that t_{last} occurred at $\leq$ 60 ms of stimulus for 81 % of the cardioversions when triggered with $I_{cv} = 0.56\,\mathrm{mW\,mm^{-2}}$. However, this seems to depend on the light intensity, since cardioversions triggered with $I_{cv} = 0.25\,\mathrm{mW\,mm^{-2}}$ showed this phenomenon in 55 % of the cases and with an intensity of $I_{cv} = 0.08\,\mathrm{mW\,mm^{-2}}$ in only 30 %. Furthermore, t_{sin} $\leq$215 ms occurred in 76, 60, and 54% of the respective tested intensities.

3.3.1. Cardiac Dynamics During Global Illumination

The optical mapping analysis of the 10 ms as well as 1 s stimulation experiments combined with the analysis of t_{last} in 1 s pulse attempts led to identify two preferential mechanisms for global optical cardioversion. The first mechanism consists of a cardioversion that happens on the onset of illumination, mainly annihilating the spiral by the depolarization and following refractoriness of the cardiac tissue (**Figure 5**). While in the second mechanism, an unpinning and disturbance of the spiral can be observed (**Figure 6**), with the elimination of the spiral taking place at the mid and late stimulation period. Optical mapping data showing the two mechanisms could be found in the (**Supplementary Material Movies 2**, **3**). As the dominant mechanism the annihilation was observed for both pulse duration 10 ms and 1 s, and took place in 90 % of all cardioversions using 1 s pulses ($N = 120$). This mechanism included a $t_{last} = 58 \pm 19$ ms. In contrast, the second mechanism was only observed in the 1 s pulses with an averaged $t_{last} = 296 \pm 122$ ms. Analyzing the MAP recordings led to a clear distinction between the two mechanisms, whereby the number of arrhythmic excitation peaks during t_{last} was ≤ 2 for 86 % of all the annihilation observations, while all the unpinning cases presented > 4 arrhythmia cycles during t_{last}.

4. DISCUSSION

The control of spatiotemporal cardiac regimes and the influence of the thereto applied electrical pulses have been investigated extensively in theory and experiment in the last decades (see e.g., Pumir and Krinsky, 1999; Takagi et al., 2004). In consequence, especially the diminishment of adverse side effects of high-energy electrical shocks, like e.g., electroporatic cell membrane disturbances, while keeping a very high success rate has been highly prioritized. In this manner, Janardhan et al. introduced a low-energy defibrillation approach to successfully terminate ventricular tachycardia (VT) applying multistage organized shocks (Janardhan et al., 2012). Thereby they eliminated the phase dependence of shock application, which is crucial for single shock therapy in VT. Furthermore, the possibility to control cardiac excitation dynamics by applying multi-centered new activation origins was proposed as one auspicious approach (Pumir et al., 2007; Luther et al., 2011). Luther et al. impressively showed that recruiting multiple pacing sites has remarkable success in counter-steering arrhythmic regimes, which in return makes tissue protective defibrillation feasible. Against this background, non-electrical approaches would benefit both the development of tissue protective defibrillation and the investigation of mechanistic associations without unpredictable worsening side effects. Cardiac optogenetics with its light initiated depolarization and accordingly hyperpolarization fulfills this position as a suitable tool to characterize mechanisms underlying multi-site pacing. Considering the complex non-linear dynamics of cardiac arrhythmia, photostimulation convinces with the highly controllable temporal as well as spatial resolution. Compared to conventional electrical approaches, the direct interaction of

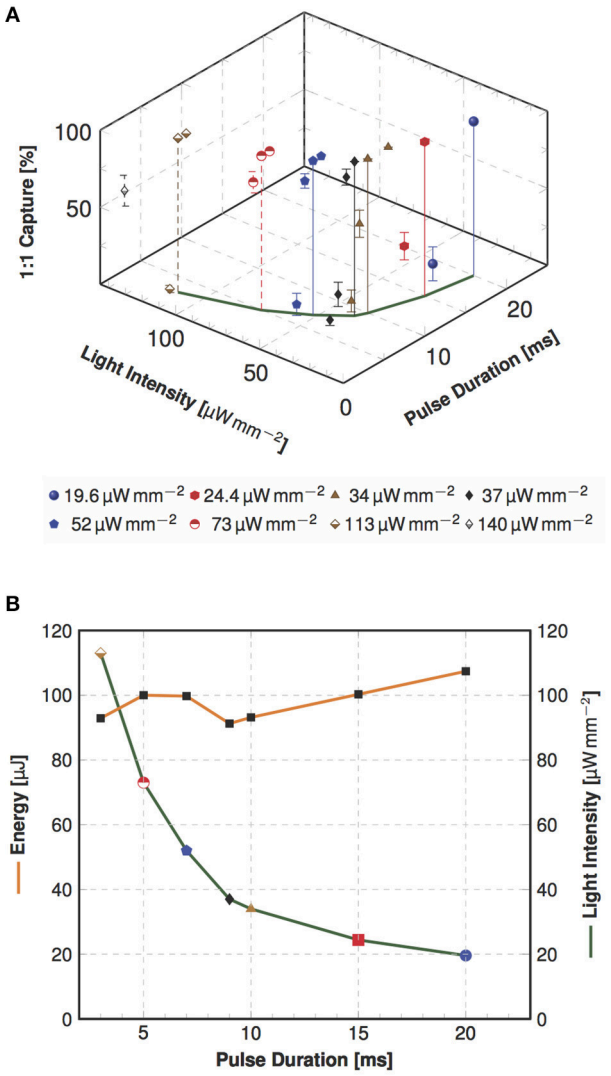

FIGURE 2 | Dependency of pulse duration and light intensity as well as pulse energy in global optogenetic pacing. **(A)** The three-dimensional plot illustrates the averaged success rate ± SEM of 1:1 capture in dependency of investigated combinations of light intensity and pulse duration (as indicated in **Table 1**). In this view the variation of measured capture rates is clearly visible, but still approving the dependency of successful 1:1 capture of light intensity and pulse duration. In the x-y section are the most efficient combinations marked, which is visualized in a plain view in the next panel. **(B)** Shown are the most efficient combinations of required light intensity and energy for different pulse duration values ($N = 6$). The analysis shows a nearly constant energy, but an increase in intensity when the pulse duration is shortened.

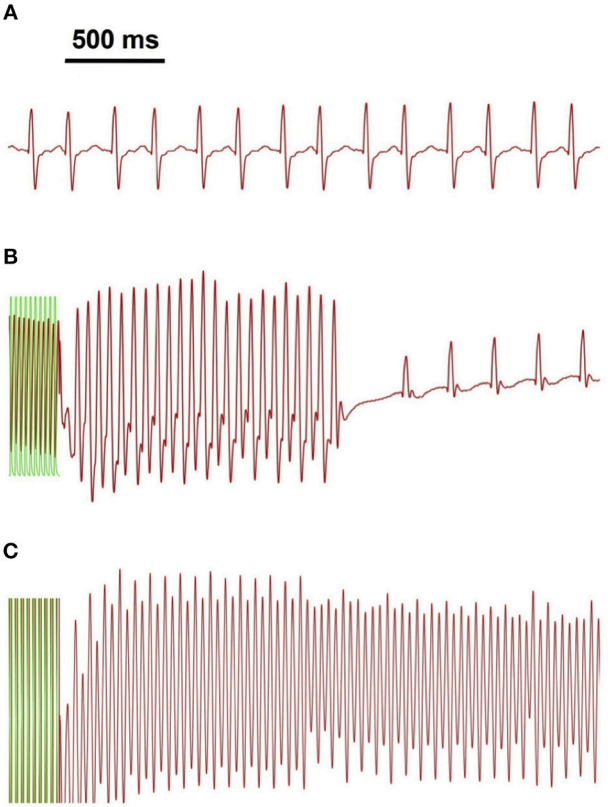

FIGURE 3 | Arrhythmia classification on the basis of electrical signal analysis. Shown are exemplary traces of MAP measurements (in red) for **(A)** sinus rhythm, **(B)** non-sustained and **(C)** sustained arrhythmia. Green overlay indicates part of the electrical pacing used to induce arrhythmia.

light with optogenetic cardiac tissue can trigger excitation in single cardiomyocytes or united cell structures without activating the surrounding tissue structures or inducing critical Faraday reactions (Ambrosi and Entcheva, 2014). Here, we presented a setup to investigate arrhythmia termination using global illumination. The feasibility of photon initiated cardioversion was shown recently by Bruegmann et al. (2016), Crocini et al. (2016), and Nyns et al. (2016). Concentrating mainly on low-numbered multi-site pacing Crocini et al. implemented a mechanistic approach using pulse series of an arrhythmia-specific light pattern that enabled cardioversion using a total amount of 1.8 mJ. In comparison the required light intensities up to 40 mW mm^{-2} exceeded the highest intensity implemented in our experiments by more than the 30-fold. Furthermore, Bruegmann et al. described an illumination protocol applying 1 % of the light intensity used by Crocini et al., but with a highly increased pulse duration of four pulses of 1 s with 1–5 s in-between accounting for a total amount of energy of 228.8 mJ. Having this in mind, in our experiments we concentrated on the characterization of the separate parameter combinations. In order to do so, the global stimulation of the whole cardiac tissue represents the maximum number of pacing sites available and thus it is comparable to conventional high-energy electrical defibrillation approaches. We showed the impact of illuminating the epicardial surface by pacing with the lowest intensities published so far. An interesting result is that the energy required to pace both globally and locally remained constant for each of the methods (98 ± 5 μJ and 2.8 ± 0.6 μJ, respectively) and increased with a growing stimulation area. Certainly, the excitation origin depends on different factors such as wavelength or light propagation characteristics. An interesting observation

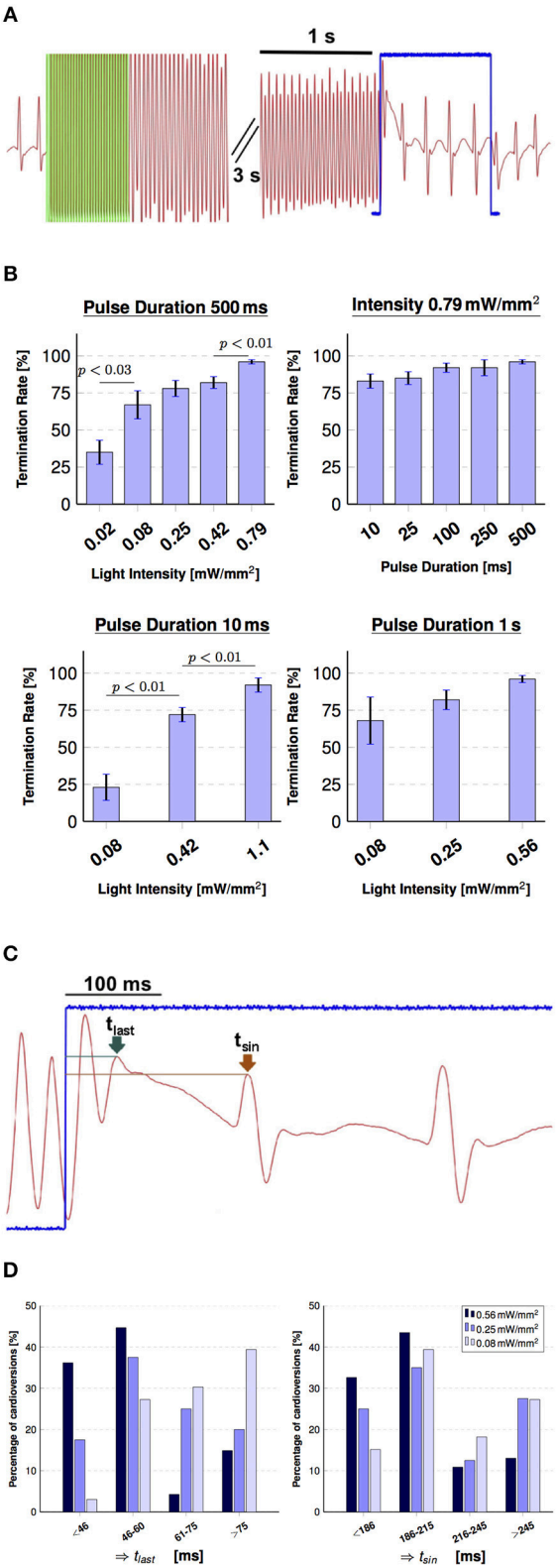

FIGURE 4 | Global illumination for cardioversion. **(A)** Shows the pseudoECG signal during arrhythmia evocation via electrical pacing and termination using global illumination (green overlay indicates electrical pacing at 50 Hz, 30 pulse). The arrhythmic conditions were terminated with a 1 s stimulation pulse (indicated in blue), during which the normal sinus rhythm already returned. **(B)** Summary of the influence of intensity and pulse duration on cardioversion attempts. Successful optogenetic defibrillation rates (percentage of successful attempts reported as mean ± SEM, $N = 6$). **(C)** Visualizes the effect of the termination pulse shown in **(A)** in more detail. Two time points were defined in order to characterize the moment of arrhythmia termination for the 1 s pulses: t_{last} (green arrow), which denotes the last peak of the arrhythmia and t_{sin} (brown arrow), which denotes the first peak of the sinus rhythm during optogenetic stimulation. **(D)** Charts indicating the effect of intensity on cardioversion times in percentage of arrhythmia terminated in those periods of t_{last} (left) and t_{sin} (right) for 0.56 mW mm^{-2} ($N = 47$), 0.25 mW mm^{-2} ($N = 40$), 0.08 mW mm^{-2} ($N = 33$).

(Continued)

during global photostimulation is the correlation between increasing light intensity and rising efficiency of cardioversion. Lilienkamp et al. introduced *in silico* results similar to our experimental findings, which can give hints that the overall size of an excitable medium has a direct effect on the lifetime of chaotic spatiotemporal dynamics, like the ones seen during arrhythmia (Lilienkamp et al., 2017). One possible explanation could be the change in penetration depth when using higher light intensities for photostimulation, hence depolarizing a greater number of cells and creating a thicker reversible conduction pattern. This was also described by Watanabe et al. in experiments with ventricular slices, where they showed a temporal decrease on the effective size available for the arrhythmia to wander (Watanabe et al., 2017). In their work, Watanabe et al. proved that by increasing the transmurality of illumination, the chances of terminating an anatomical re-entry on the slices increased. This effect could be lead back to the indispensable fact of reaching the critical cell number for excitation evocation (Zipes et al., 1975). In contrast, a varied pulse duration at constant light intensity might prolong the depolarization of the stimulated layers of cardiac tissue without effectively changing the size of the stimulated cardiac tissue (Bruegmann et al., 2010).

Optogenetic intensity-dependent effects have been recorded at the level of single cells, quasi-two dimensional cell cultures and organs (Bruegmann et al., 2010; Nussinovitch et al., 2014; Burton et al., 2015; Nussinovitch and Gepstein, 2015; Zaglia et al., 2015). Accordingly, the effect of light intensity as described by t_{last} for the 1 s pulses could be explained by a theoretical combination of the amount of cells excited, the applied photocurrents and the conduction velocity of a generated excitation wave (Bruegmann et al., 2010; Burton et al., 2015; Zaglia et al., 2015). Moreover, the evidence showing that the majority of defibrillations took place during the onset of stimulation could be explained by the Channelrhodopsin-2 kinetics, since its photo-current reaches a peak during the first milliseconds of activation before dropping to a smaller current during continuous illumination (Nagel et al., 2003; Bruegmann et al., 2010). Yet, the difference on t_{sin} for each intensity is not likewise obvious, since it could be more related to the intrinsic sinus period of the heart than to the light induced effect on cardioversion. On the other hand, the effect of the pulse duration, even when the difference seems not to be significant might lead to diverse

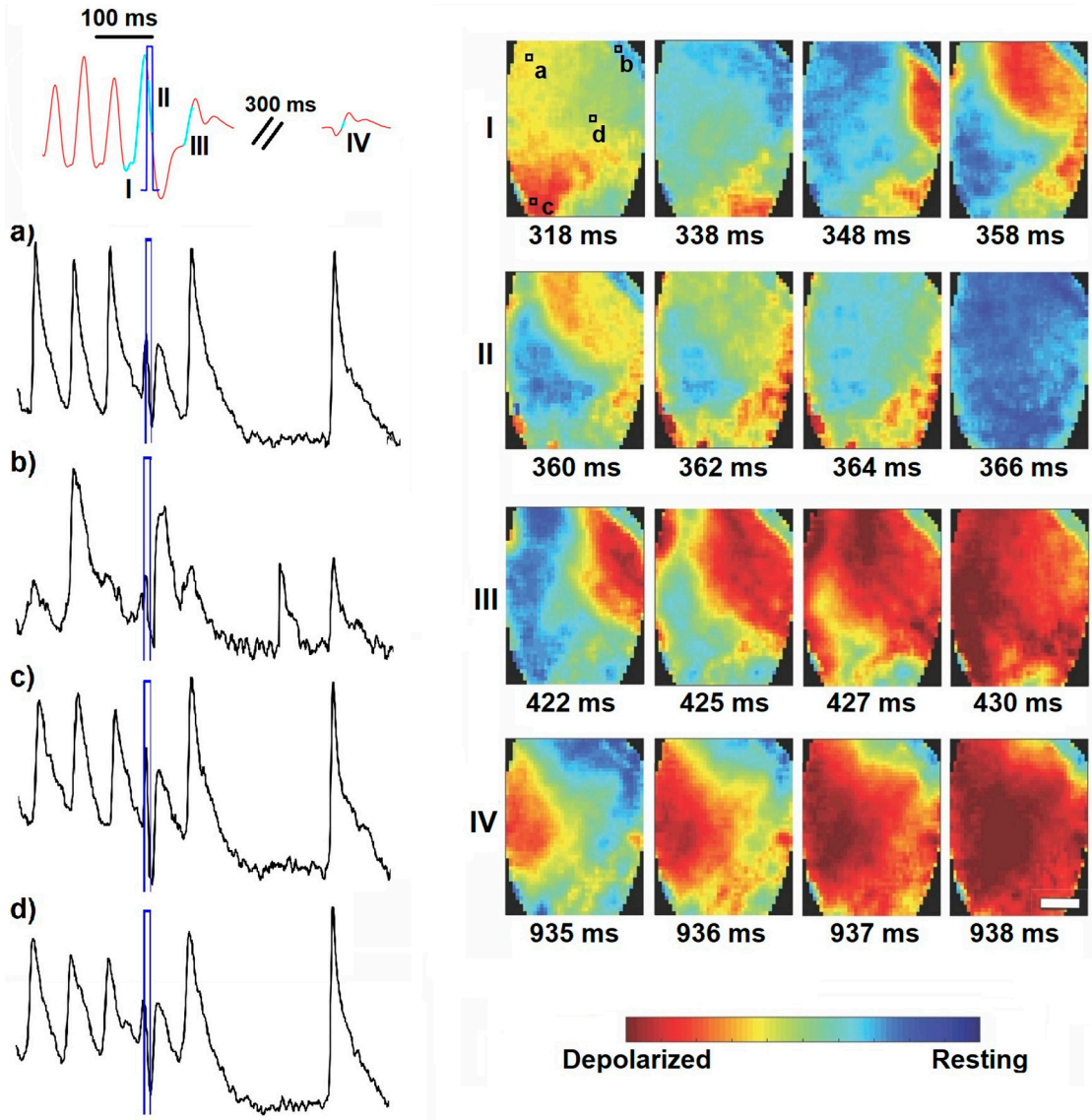

FIGURE 5 | Wave dynamics during short global light pulse (10 ms, 0.25 mW mm^{-2}, highlighted in blue). Shown are the MAP recording (in red) and optical traces of several local spots on the ventricles (in black, as indicated in panel I). Optical mapping analysis revealed vortex-like electrical activity on the heart surface (image sequence I), which is disturbed by global illumination (image sequence II) and thus provoking wave collision resulting in annihilation (image sequence III). Sinus activity follows after a peak corresponding to depolarization of the whole heart (image sequence IV). The corresponding movie is available as (**Supplementary Material Movie 2**).

mechanisms of termination. Presumably, spiral disturbance is unlikely to happen during short pulses of 10 and 25 ms. Nevertheless, a longer pulse duration such as 500 ms or 1 s can still disrupt the tachycardia even after the onset of the stimulus, leading to a higher success rate. According to the biophysics of ChR2, these light-activated channelrhodopsins are un-selective for different cations like Ca^{2+} or Na^{+} (Schneider et al., 2015). Due to that fact, long photostimulation pulses probably lead to an accumulation of action potential relevant cations causing continuous depolarization to less negative membrane voltages. This assumption is supported by the fact that 10 % of cardioversions for 1 s stimulus occurred during mid-late stimulation.

However, the results presented here strengthen the application of cardiac optogenetics, although some underlying mechanisms still remain to be part of ongoing research. Especially the investigation of defibrillation protocols consisting of multistage anti-fibrillation pacing as well as multi-site pacing strategies have to be addressed, since such experiments would help to understand the dependencies of phase-specific pacing and success rate of arrhythmia termination. Therefore, all *ex vivo* experiments and the basic classification of photostimulation

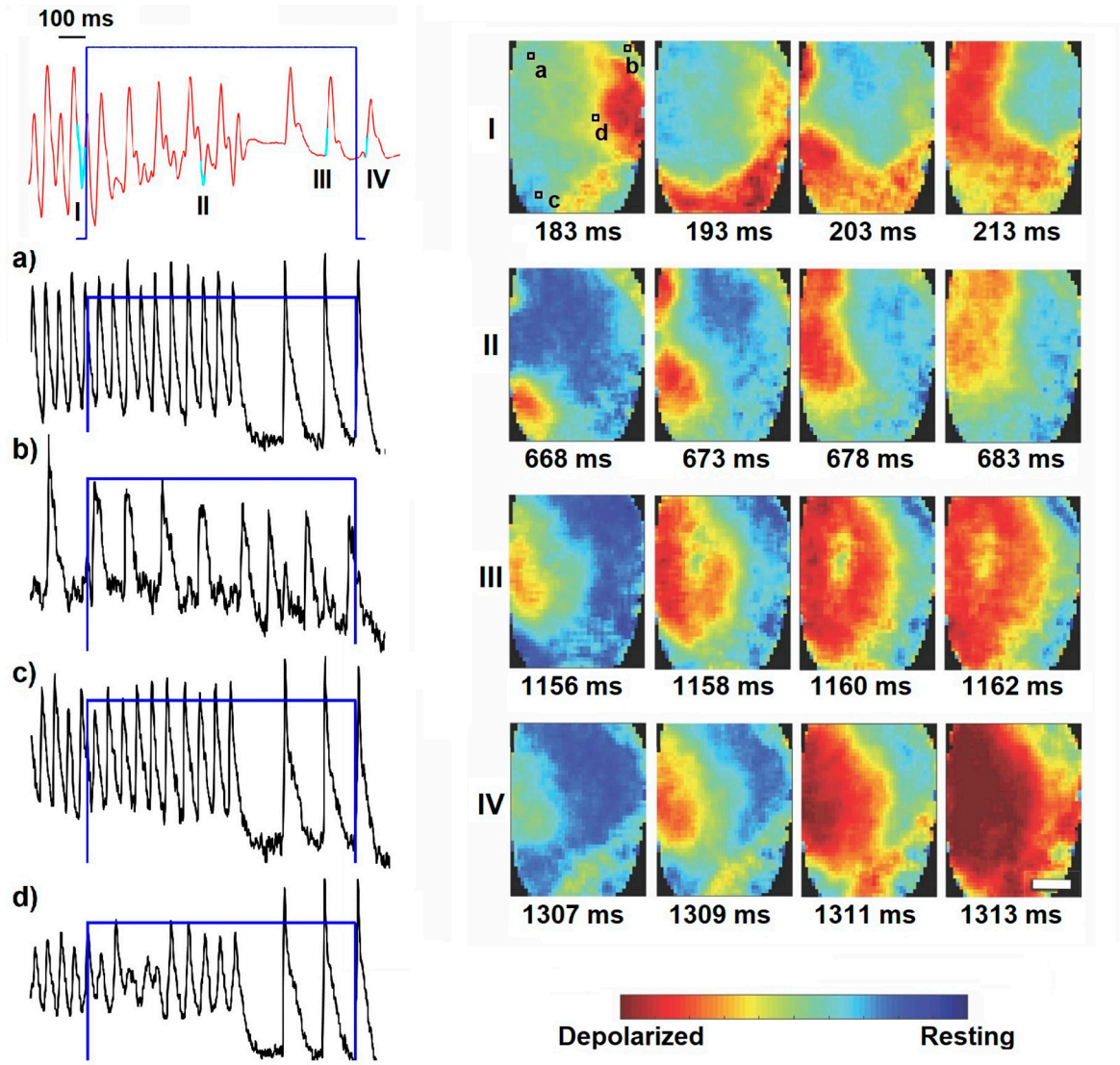

FIGURE 6 | Optical determination of the second identified mechanism, which was only observed in 1 s pulses (0.25 mW mm^{-2}, highlighted in blue). Here the locally stable spiral activity (image sequence I) is disrupted by the illumination resulting in extrusion of the arrhythmic wave pattern to the boundaries (image sequence II). Already during photostimulation the sinus rhythm resets (image sequence III) and continues after switching off (image sequence IV). The scale-bars indicate 2 mm and are equal for all images in the corresponding panel. Shown are the MAP recording (in red) and optical traces of several local spots on the ventricles (in black, as indicated in panel I). The corresponding movie is available as (**Supplementary Material Movie 3**).

parameter function as a trigger for development, optimization and evaluation of a controllable as well as flexible light induced cardiac rhythm management. As a positive effect also the design of new non-electrical multi-site pacing methods with high potential of translation into clinically relevant approaches comes within reach.

4.1. Limitations

With the translation into *in vivo* conditions in mind, one has to mention that the *ex vivo* measurements lack the interference of blood specific absorption of ChR2 exciting wavelengths. Consequently, any effects during blue-light photostimulation *in vivo* would represent only a superficial excitation. Certainly, the cardiac excitation conduction is not restricted to epicardial phenomena but also connected to complex transmural wave propagation (Christoph et al., 2018). Therefore, near infrared modulated opsins would support the translation of *ex vivo* experimental results into clinically relevant *in vivo* attempts (Karathanos et al., 2016). Here we successfully achieved cardioversion using single pulses of divers pulse duration by tuning light intensities between 0.56 and 1.1 mWmm^{-2}, delivering total energies 3–153.6 mJ to the epicardium. The importance of this low-intensity, pulse duration versatility relies on the fast spatiotemporal dynamics of arrhythmia, where the optimal duration of the stimulus could be arrhythmia-specific dependent. That would also result in a smaller amount of light

being delivered to the cardiomyocytes located transmurally. The more precise estimation of excited cells within the ventricular wall and the characterization of light propagation through cardiac tissue are subject of current research projects. In the presented study we only examined murine hearts, for which reason the presented parameter findings can solely be considered as species specific. For larger species with much thicker ventricular walls or fatty epicardial regions the light intensity actually impacting light-sensitive cardiomyocytes will differ significantly. However, the gotten insights and general conclusions, like the fact that illuminating the whole epicardial surface will result in a decrease of minimum light intensity should be accountable also for larger species.

Furthermore, induced photochemical reactions during illumination are possible sources of direct cell response (Lubart et al., 2007). Lubart et al. showed that especially visible light (400 nm to 700 nm) could stimulate photobiomodulation and photosensitization in cardiomyocytes. These processes are inter alia initiated by generation of reactive oxygen species, which in return can lead to a change of the redox state of the cardiac cell and thus have indirect influence on the calcium induced calcium release (CICR) via redox sensitive L-type calcium channels. Although, compared to the energy used by Lubart et al. with 3.6 J cm^{-2} the total energy applied for global illumination in this study was 0.01–0.61 Jcm^{-2}, which may have alleviated photochemical effects. Hence, the measurement and characterization of potential photobiomodulation with regard to repeated rapid photostimulation are considered for ongoing projects.

Experiments including optical mapping were done with Blebbistatin, which reduces motion artifacts due to its electromechanical uncoupling function. Since we used stimulation light of a blue wavelength (470 nm) it is important to mention, that the uncoupling effects of Blebbistatin could be reversed by blue light illumination (Fedorov et al., 2012). In our experiments we did not observe such light induced effects on the motion inhibition, which could be related to the fact that Fedorov et al. used much shorter wavelengths for illumination than we applied. This observation was also published by Swift et al. (2012). Nevertheless, it should be emphasized that Blebbistatin does possibly alter the metabolic state of ischemic cardiomyocytes (Swift et al., 2012).

5. CONCLUSION

According to recent cardiac optogenetic studies the usage of photodefibrillation seems to be feasible (Bruegmann et al., 2016, Crocini et al., 2016; Richter et al., 2016). Here we investigated for the first time the effects of global optogenetic epicardial illumination which benefits from the larger area covered to decrease the intensity required to stimulate the heart. In consequence, we managed to terminate arrhythmic excitation patterns using pulse lengths spanning three orders of magnitude, demonstrating an efficient and versatile low-intensity and low-energy method to investigate arrhythmia dynamics and manipulation. Besides, we observed two different mechanisms leading to optogenetic cardioversion, which exhibit not the same behavior than electrical cardioversion.

AUTHOR CONTRIBUTIONS

RQ performed the experiments and analyzed the data. RQ and CR designed research, experiments and wrote the paper. SL and LD-M contributed to the discussion and edited the manuscript. All authors read and approved the manuscript.

FUNDING

This project has received funding from the European Union's Horizon 2020 Programme through the project Advanced BiomEdical OPTICAL Imaging and Data Analysis (BE-OPTICAL) under grant agreement number 675512. The research leading to these results received funding by the European Community's Seventh Framework Programme FP7/2007-2013 under grant agreement number HEALTH-F2-2009-241526. Additional support was provided by the DZHK e.V., the German Federal Ministry of Education and Research (BMBF, project FKZ 031A147, Go-Bio), the German Research Foundation (DFG, Collaborative Research Centers SFB 1002, Projects B05 and C03 and SFB 937, Project A18) and the Max Planck Society.

ACKNOWLEDGMENTS

We want to thank Marion Kunze and Tina Althaus for their excellent technical assistance during experimental setup and experiment conduction. Many thanks to Thomas Lilienkamp and Ulrich Parlitz for fruitful discussions and their thought-provoking impulses.

SUPPLEMENTARY MATERIAL

The Supplementary Material for this article can be found online at: https://www.frontiersin.org/articles/10.3389/fphys.2018.01651/full#supplementary-material

REFERENCES

Ambrosi, C., and Entcheva, E. (2014). Optogenetics' promise: pacing and cardioversion by light? *Future Cardiol.* 10, 1–4. doi: 10.2217/fca.13.89

Bruegmann, T., Boyle, P. M., Vogt, C. C., Karathanos, T. V., Arevalo, H. J., Fleischmann, B. K., et al. (2016). Optogenetic defibrillation terminates ventricular arrhythmia in mouse hearts and human simulations. *J. Clin. Invest.* 126, 3894–3904. doi: 10.1172/JCI88950

Bruegmann, T., Malan, D., Hesse, M., Beiert, T., Fuegemann, C., Fleischmann, B., et al. (2011). Channelrhodopsin2 expression in cardiomyocytes: a new tool for light-induced depolarization with high spatio-temporal resolution *in vitro* and *in vivo*. *Thorac. Cardiovasc. Surg.* 59:MO19. doi: 10.1055/s-0030-1269109

Bruegmann, T., Malan, D., Hesse, M., Beiert, T., Fuegemann, C. J., Fleischmann, B. K., et al. (2010). Optogenetic control of heart muscle *in vitro* and *in vivo*. *Nat. Methods* 7, 897–900. doi: 10.1038/nmeth.1512

Burton, R. A. B., Klimas, A., Ambrosi, C. M., Tomek, J., Corbett, A., Entcheva, E., et al. (2015). Optical control of excitation waves in cardiac tissue. *Nat. Photonics* 9, 813–816. doi: 10.1038/nphoton.2015.196

Christoph, J., Chebbok, M., Richter, C., Schrder-Schetelig, J., Bittihn, P., Stein, S., et al. (2018). Electromechanical vortex filaments during cardiac fibrillation. *Nature* 555:667 EP. doi: 10.1038/nature26001

Christoph, J., Schröder-Schetelig, J., and Luther, S. (2017). Electromechanical optical mapping. *Prog. Biophys. Mol. Biol.* 130, 150–169. doi: 10.1016/j.pbiomolbio.2017.09.015

Crocini, C., Ferrantini, C., Coppini, R., Scardigli, M., Yan, P., Loew, L. M., et al. (2016). Optogenetics design of mechanistically-based stimulation patterns for cardiac defibrillation. *Sci. Rep.* 6:35628EP. doi: 10.1038/srep35628

Davidenko, J., Pertsov, A., Salamonsz, R., Baxter, W., and Jalif, J. (1992). Stationary and drifting spiral waves of excitation in isolated cardiac muscle. *Nature* 355, 349–351. doi: 10.1038/355349a0

Deisseroth, K. (2011). Optogenetics. *Nat. Methods* 8, 26–29. doi: 10.1038/nmeth.f.324

Diaz-Maue, L., Luther, S., and Richter, C. (2018). "Towards optogenetic control of spatiotemporal cardiac dynamics," in *Proceedings SPIE–Optogenetics and Optical Manipulation 2018* (San Francisco, CA: SPIE), 1482G.

Efimov, I. R., Aguel, F., Cheng, Y., Wollenzier, B., and Trayanova, N. (2000). Virtual electrode polarization in the far field: implications for external defibrillation. *Am. J. Physiol. Heart Circ.* 279, H1055–H1070. doi: 10.1152/ajpheart.2000.279.3.H1055

Exner, D. (2005). Is antitachycardia pacing a safe and efficacious alternative to shocks for fast ventricular tachyarrhythmia treatment? *Nat. Clin. Pract. Cardiovasc. Med.* 2:68. doi: 10.1038/ncpcardio0116

Fedorov, V., Lozinsky, I., Sosunov, E., Anyukhovsky, E., Rosen, M., Balke, C., et al. (2012). Application of blebbistatin as an excitation-contraction uncoupler for electrophysiologic study of rat and rabbit hearts. *Heart Rhythm.* 4, 619–626. doi: 10.1016/j.hrthm.2006.12.047

Fenton, F., Luther, S., Cherry, E., Otani, N., Krinsky, V., Pumir, A., et al. (2009). Termination of atrial fibrillation using pulsed low-energy far-field stimulation. *Circulation* 120, 467–476. doi: 10.1161/CIRCULATIONAHA.108.825091

Glukhov, A. V., Flagg, T. P., Fedorov, V. V., Igor, R. E., and Nichols, C. G. (2010). Differential katp channel pharmacology in intact mouse heart. *J. Mol. Cell. Cardiol.* 48, 152–160. doi: 10.1016/j.yjmcc.2009.08.026

Jalifé, J., Gray, R., Morley, G., and Davidenko, J. (1998). Self-organization and the dynamical nature of ventricular fibrillation. *Chaos* 8, 79–93. doi: 10.1063/1.166289

Janardhan, A., Li, W., Fedorov, V., Yeung, M., Wallendorf, M., Schuessler, R., et al. (2012). A novel low-energy electrotherapy that terminates ventricular tachycardia with lower energy than a biphasic shock when antitachycardia pacing fails. *JACC* 60, 2393–2398. doi: 10.1016/j.jacc.2012.08.1001

Karathanos, T., Bayer, J., Wang, D., Boyle, P., and Trayanova, N. (2016). Opsin spectral sensitivity determines the effectiveness of optogenetic termination of ventricular fibrillation in the human heart: a simulation study. *J. Physiol.* 594, 6879–6891. doi: 10.1113/JP271739

Killeen, M., Thomas, G., Gurung, I., Goddard, C., Fraser, J., Mahaut-Smith, M., et al. (2007). Arrhythmogenic mechanisms in the isolated perfused hypokalaemic murine heart. *Acta Physiol.* 189, 33–46. doi: 10.1111/j.1748-1716.2006.01643.x

Lilienkamp, T., Christoph, J., and Parlitz, U. (2017). Features of chaotic transients in excitable media governed by spiral and scroll waves. *Phys. Rev. Lett.* 119, 1–5. doi: 10.1103/PhysRevLett.119.054101

Lubart, R., Lavi, R., Friedmann, H., and Rochkind, S. (2007). Photochemistry and photobiology of light absorption by living cells. *Photomed. Laser Surg.* 24, 179–185. doi: 10.1089/pho.2006.24.179

Luther, S., Fenton, F. H., Kornreich, B. G., Squires, A., Bittihn, P., Hornung, D., et al. (2011). Low-energy control of electrical turbulence in the heart. *Nature* 475, 235–239. doi: 10.1038/nature10216

Nagel, G., Szellas, T., Huhn, W., Kateriya, S., Adeishvili, N., Berthold, P., et al. (2003). Channelrhodopsin-2, a directly light-gated cation-selective membrane channel. *Proc. Natl. Acad. Sci. U.S.A.* 100, 13940–13945. doi: 10.1073/pnas.1936192100

Nussinovitch, U., and Gepstein, L. (2015). Optogenetics for *in vivo* cardiac pacing and resynchronization therapies. *Nat. Biotechnol.* 33, 750–754. doi: 10.1038/nbt.3268

Nussinovitch, U., Shinnawi, R., and Gepstein, L. (2014). Modulation of cardiac tissue electrophysiological properties with light-sensitive proteins. *Cardiovasc. Res.* 102, 176–187. doi: 10.1093/cvr/cvu037

Nyns, E. C., Kip, A., Bart, C. I., Plomp, J. J., Zeppenfeld, K., Schalij, M. J., et al. (2016). Optogenetic termination of ventricular arrhythmias in the whole heart: towards biological cardiac rhythm management. *Eur. Heart J.* 38:ehw574. doi: 10.1093/eurheartj/ehw574

Panfilov, A., and Holden, A. (1990). Self-generation of turbulent vortices in a two-dimensional model of cardiac tissue. *Phys. Lett. A* 151, 23–26. doi: 10.1016/0375-9601(90)90840-K

Pumir, A., and Krinsky, V. (1999). Unpinning of a rotating wave in cardiac muscle by an electric field. *J. Theoret. Biol.* 199, 311–319. doi: 10.1006/jtbi.1999.0957

Pumir, A., Nikolsky, V., Hoerning, M., Isomura, A., Agladze, K., Yoshikawa, K., et al. (2007). Wave emission from heterogeneities opens a way to controlling chaos in the heart. *Phys. Rev. Lett.* 99:208101. doi: 10.1103/PhysRevLett.99.208101

Richter, C., Christoph, J., Lehnart, S. E., and Luther, S. (2016). "Optogenetic light crafting tools for the control of cardiac arrhythmias," in *Optogenetics – Methods and Protocols*, Vol. 1408, ed A. Kianianmomeni (New York, NY: Springer Science+Business Media), 293–302.

Schneider, F., Grimm, C., and Hegemann, P. (2015). Biophysics of channelrhodopsin. *Annu. Rev. Biophys.* 44, 167–86. doi: 10.1146/annurev-biophys-060414-034014

Swift, L., Asfour, H., Posnack, N., Arutunyan, A., Kay, M., and Sarvazyan, N. (2012). Properties of blebbistatin for cardiac optical mapping and other imaging applications. *Pflugers Arch. Eur. J. Physiol.* 464, 503–512. doi: 10.1007/s00424-012-1147-2

Takagi, S., Pumir, A., Pazó, D., Efimov, I., Nikolski, V., and Krinsky, V. (2004). Unpinning and removal of rotating wave in cardiac muscle. *Phys. Rev. Lett.* 93:058101. doi: 10.1103/PhysRevLett.93.058101

Watanabe, M., Feola, I., Majumder, R., Jangsangthong, W., Teplenin, A. S., Ypey, D. L., et al. (2017). Optogenetic manipulation of anatomical re-entry by light-guided generation of a reversible local conduction block. *Cardiovasc. Res.* 113, 354–366. doi: 10.1093/cvr/cvx003

Wathen, M. S., DeGroot, P. J., Sweeney, M. O., Stark, A. J., Otterness, M. F., Adkisson, W. O., et al. (2004). Prospective randomized multicenter trial of empirical antitachycardia pacing versus shocks for spontaneous rapid ventricular tachycardia in patients with implantable cardioverter-defibrillators: Pacing fast ventricular tachycardia reduces shock therapies. *Circulation* 110, 2591–2596. doi: 10.1161/01.CIR.0000145610.64014.E4

Wilde, A. (1994). K+atp channel opening and arrhythmogenesis. *J. Cardiovasc. Pharmacol.* 24(Suppl. 4), S35–S40.

Zaglia, T., Pianca, N., Borile, G., Da Broi, F., Richter, C., Campione, M., et al. (2015). Optogenetic determination of the myocardial requirements for extrasystoles by cell type-specific targeting of ChannelRhodopsin-2. *Proc. Natl. Acad. Sci. U.S.A.* 112:1509380112. doi: 10.1073/pnas.1509380112

Zipes, D. P., Fischer, J., King, R. M., Nicoll, A. d., and Jolly, W. W. (1975). Termination of ventricular fibrillation in dogs by depolarizing a critical amount of myocardium. *Am. J. Cardiol.* 36, 37–44. doi: 10.1016/0002-9149(75)90865-6

Zipes, D. P., and Jalife, J. (2009). *Cardiac Electrophysiology: From Cell to Bedside*. Philadelphia, PA: Saunders; Elsevier.

Conflict of Interest Statement: The authors declare that the research was conducted in the absence of any commercial or financial relationships that could be construed as a potential conflict of interest.

Advantages of publishing in Frontiers

OPEN ACCESS
Articles are free to read for greatest visibility and readership

FAST PUBLICATION
Around 90 days from submission to decision

HIGH QUALITY PEER-REVIEW
Rigorous, collaborative, and constructive peer-review

TRANSPARENT PEER-REVIEW
Editors and reviewers acknowledged by name on published articles

Frontiers
Avenue du Tribunal-Fédéral 34
1005 Lausanne | Switzerland

Visit us: www.frontiersin.org
Contact us: info@frontiersin.org | +41 21 510 17 00

REPRODUCIBILITY OF RESEARCH
Support open data and methods to enhance research reproducibility

DIGITAL PUBLISHING
Articles designed for optimal readership across devices

FOLLOW US
@frontiersin

IMPACT METRICS
Advanced article metrics track visibility across digital media

EXTENSIVE PROMOTION
Marketing and promotion of impactful research

LOOP RESEARCH NETWORK
Our network increases your article's readership